



# **Machine Learning Model for the Prediction of Human Movement Biomechanics**

**Abdelrahman Zaroug**

BEng, MEng

Submitted in fulfilment of the requirement for the degree of

**Doctor of philosophy**

Principal Supervisor: Professor Rezaul Begg

Associate Supervisor: Assoc. Prof. Daniel Lai

External Associate Supervisor: Dr Kurt Mudie

(Defence Science and Technology Group)

February, 2021

## ABSTRACT

An increasingly useful application of machine learning (ML) is in predicting features of human actions. If it can be shown that algorithm inputs related to actual movement mechanics can predict a limb or limb segment's future trajectory, a range of apparently intractable problems in movement science could be solved. The forecasting of lower limb trajectories can anticipate movement characteristics that may predict the risk of tripping, slipping or balance loss. Particularly in the design of human augmentation technology such as the exoskeleton, human movement prediction will improve the synchronisation between the user and the device greatly enhancing its efficacy.

Long Short Term Memory (LSTM) neural networks are a subset of ML algorithms that proven a wide success in modelling the human movement data. The aim of this thesis was to examine four LSTM neural network architectures (Vanilla, Stacked, Bidirectional and Autoencoders) in predicting the future trajectories of lower limb kinematics, i.e. Angular Velocity (AV) and Linear Acceleration (LA). This work also aims to investigate whether linear statistical methods such as the Linear Regression (LR) is enough to predict the trajectories of lower limb kinematics. Kinematics data (LA and AV) of foot, shank and thigh were collected from 13 male and 3 female participants ( $28 \pm 4$  years old,  $1.72 \pm 0.07$  m in height,  $66 \pm 10$  kg in mass) who walked for 10 minutes at 4 different walking speeds on a 0% gradient treadmill. Walking speeds included preferred walking speed (PWS  $4.34 \pm 0.43$  km.h<sup>-1</sup>), imposed speed (5km.h<sup>-1</sup>,  $15.4\% \pm 7.6\%$  faster), slower speed (-20% PWS  $3.59 \pm 0.47$  km.h<sup>-1</sup>) and faster speed (+20% PWS  $5.26 \pm 0.53$  km.h<sup>-1</sup>). The sliding window technique was adopted for training and testing the LSTM models with total kinematics time-series data of 17,638 strides for all trials.

The aim and findings of this work were carried out in 3 studies. Study 1 confirmed the possibility of predicting the future trajectories of human lower limb kinematics using LSTM autoencoders (ED-LSTM) and the LR during an imposed walking speed (5km.h<sup>-1</sup>). Both models achieved satisfactory predicted trajectories up to 0.06s. A prediction horizon of 0.06s can be used to compensate for delays in an exoskeleton's feed-forward controller to better estimate the human motions and synchronise with intended movement trajectories. Study 2 (Chapter 4) indicated that the LR model is not suitable for the prediction of future lower limb kinematics at PWS. The LSTM performance results suggested that the ED-LSTM and the Stacked LSTM are more accurate to predict the future lower limb kinematics up to 0.1s at PWS

and imposed walking speed ( $5\text{km}\cdot\text{h}^{-1}$ ). The average duration for a gait cycle ranges between 0.98-1.07s, and a prediction horizon of 0.1 accounts for about 10% of the gait cycle. Such a forecast may assist users in anticipating a low foot clearance to develop early countermeasures such as slowing down or stopping. Study 3 (Chapter 5) have shown that at +20% PWS the LSTM models' performance obtained better predictions compared to all tested walking speed conditions (i.e. PWS, -20% PWS and  $5\text{km}\cdot\text{h}^{-1}$ ). While at -20% PWS, results indicated that at slower walking speeds all of the LSTM architectures obtained weaker predictions compared to all tested walking speeds (i.e. PWS, +20% PWS and  $5\text{km}\cdot\text{h}^{-1}$ ). In addition to the applications of a known future trajectories at the PWS mentioned in study 1 and 2, the prediction at fast and slow walking speeds familiarise the developed ML models with changes in human walking speed which are known to have large effects on lower limb kinematics. When intelligent ML methods are familiarised with the degree of kinematic changes due to speed variations, it could be used to improve human-machine interface in bionics design for various walking speeds

The key finding of the three studies is that the ED-LSTM was found to be the most accurate model to predict and adapt to the human motion kinematics at PWS,  $\pm 20\%$  PWS and  $5\text{km}\cdot\text{h}^{-1}$ , up to 0.1s. The ability to predict future lower limb motions may have a wide range of applications including the design and control of bionics allowing better human-machine interface and mitigating the risk of tripping and balance loss.

## DECLARATION

“I, Abdelrahman Zaroug, declare that the PhD thesis entitled *Machine Learning Model for the Prediction of Human Movement Biomechanics* is no more than 80,000 words in length including quotes and exclusive of tables, figures, appendices, bibliography, references and footnotes. This thesis contains no material that has been submitted previously, in whole or in part, for the award of any other academic degree or diploma. Except where otherwise indicated, this thesis is my own work”.

“I have conducted my research in alignment with the Australian Code for the Responsible Conduct of Research and Victoria University’s Higher Degree by Research Policy and Procedures”.

Signature

19<sup>th</sup> February 2021



# **DEDICATION**

*Especially dedicated to my beloved family.*

## ACKNOWLEDGMENT

*Alhamdulillah* for bounding me by fortitude and resilience to carry out this work.  
*Alhamdulillah* for everything.

I have to admit that my doctoral years were the most intensive years of my life, packed with both joyful and challenging moments. The whole last year of my PhD was completed from home under covid-restrictions and lockdowns. To my family, I can't thank you enough. You kept me tenacious, motivated and perseverant. I miss you all.

During the course of my PhD journey, I was working with such deferential and positive supervisors. Unequivocally, this would have been a difficult journey without their guidance and support. To my supervisors Prof. Rezaul Begg and Assoc. Prof. Daniel Lai, thank you. You were continuously helpful when perplexing issues arise, when my learning curve was steep and when my vision needed an insight. Consistently benevolent and tolerant. Working with you was so wonderful and brilliant. Appreciate it.

I acknowledge the top-up funding of this research by the Defence Science and Technology Group, Melbourne. That helped. Thanks to Dr. Kurt Mudie for facilitating the data collection and the application of this research.

Special thanks to my dear friend and colleague Dr. Alessandro Garofolini. You were remarkably keen to step up and help out. Particularly the biomechanics data collection and processing, you have made it so easy for me.

Thanks to Mrs. Jasmine Proud. You were a cooperative peer and you will get yours done soon!

Cheers to you all.

## **PUBLICATIONS AND CONFERENCES**

This thesis includes chapters that have been published and submitted to journals as follows:

### **Chapter 2:**

**Zaroug, A.,** Proud, J. K., Lai, D. T. H., Mudie, K., Billing, D., & Begg, R. (2019). Overview of Computational Intelligence (CI) Techniques for Powered Exoskeletons. Published in *Computational Intelligence in Sensor Networks*: Springer.

### **Chapter 3:**

**Zaroug, A.,** Lai, D. T. H., Mudie, K., & Begg, R. (2020). Lower Limb Kinematics Trajectory Prediction Using Long Short-Term Memory Neural Networks. Published at the *Frontiers in Bioengineering and Biotechnology*, 8, *Machine Learning Approaches to Human Movement Analysis*.

### **Refereed conference paper**

**Zaroug, A.,** Lai, D. T. H., Mudie, K., Billing, D., & Begg, R. (2019). Prediction of Gait Events from Lower Limb Kinematics during Loaded Marching using Deep Learning. Submitted and presented to the *41<sup>st</sup> Annual international IEEE Engineering in Medicine and Biology Conference (EMBC)*.

### **Refereed conference abstract**

**Zaroug, A.,** Lai, D. T. H., Mudie, K., Billing, D., & Begg, R. (2020). A Comparison of Multiple Machine Learning Algorithms on the Prediction of Gait Events during Load Carriage. Presented on February 2020 at the *5<sup>th</sup> International Congress on Soldiers' Physical Performance*.

# TABLE OF CONTENTS

|          |   |           |
|----------|---|-----------|
| <b>1</b> | <b>CHAPTER ONE: INTRODUCTION.....</b>   | <b>1</b>  |
| 1.1      | Background .....  | 1         |
| 1.2      | Changes of kinematic characteristics with gait speed.....   | 2         |
| 1.3      | Statistical methods for gait inference .....  | 3         |
| 1.4      | The Measurement and prediction of gait biomechanics.....  | 4         |
| 1.4.1    | Motion capture systems .....  | 5         |
| 1.4.2    | The Inertial Measurement Units (IMUs) .....   | 7         |
| 1.4.3    | The Electroencephalography (EEG) .....  | 9         |
| 1.4.4    | The surface Electromyography (sEMG).....  | 10        |
| 1.5      | Motivation of the research.....   | 11        |
| 1.6      | Research aims.....  | 12        |
| 1.7      | Significance.....   | 13        |
| <b>2</b> | <b>CHAPTER TWO: OVERVIEW OF ML TECHNIQUES FOR THE PREDICTION OF HUMAN MOVEMENT BIOMECHANICS .....</b> | <b>15</b> |
| 2.1      | Overview .....  | 15        |
| 2.2      | Predictive modelling and statistical learning .....   | 15        |
| 2.3      | Machine Learning (ML).....  | 16        |
| 2.3.1    | Dataset.....  | 17        |
| 2.3.2    | Features Engineering .....  | 17        |
| 2.3.3    | The learning process .....  | 18        |
| 2.3.4    | Evaluation .....  | 20        |
| 2.3.5    | Parametric and non-parametric ML algorithms.....  | 21        |
| 2.4      | ML models for the human movement prediction.....  | 21        |
| 2.4.1    | Linear Regression (LR).....   | 21        |
| 2.4.2    | Logistic Regression.....  | 23        |
| 2.4.3    | Fisher's Discriminant Analysis (FDA) .....  | 24        |
| 2.4.4    | Hidden Markov Model (HMM).....  | 25        |
| 2.4.5    | Gaussian Mixture Model (GMM).....   | 28        |
| 2.4.6    | Support Vector Machines (SVM).....  | 29        |
| 2.4.7    | Artificial Neural Networks (ANN).....   | 31        |
| 2.5      | Applications of ML in assistive devices .....   | 34        |

|          |  |           |
|----------|--|-----------|
| 2.6      | Applications of ML in falls prevention .....   | 36        |
| 2.7      | Summary and thesis scope .....   | 37        |
| <b>3</b> | <b>CHAPTER THREE: PREDICTION OF LOWER LIMB KINEMATICS AT<br/>IMPOSED WALKING SPEED– Study 1.....</b>   | <b>39</b> |
| 3.1      | Overview .....   | 39        |
| 3.2      | Introduction .....   | 40        |
| 3.3      | Materials and Methods .....  | 42        |
| 3.3.1    | Collection protocol.....   | 42        |
| 3.3.2    | Dataset Processing .....   | 42        |
| 3.3.3    | Dataset Description.....   | 44        |
| 3.3.4    | Time Series Transformation to a Supervised Learning Problem.....                                       | 44        |
| 3.3.5    | Linear Regression (LR).....  | 45        |
| 3.3.6    | Recurrent Neural Networks (RNN) .....  | 46        |
| 3.3.7    | Long Short Term Memory (LSTM) Networks .....   | 47        |
| 3.3.8    | Design of the LSTM model .....   | 49        |
| 3.3.9    | Evaluation metrics .....   | 49        |
| 3.4      | Results .....  | 50        |
| 3.4.1    | ED-LSTM performance with different input window sizes .....  | 50        |
| 3.4.2    | ED-LSTM performance with 5 timesteps prediction window.....  | 51        |
| 3.4.3    | ED-LSTM performance with 10 timesteps prediction window.....   | 53        |
| 3.4.4    | The LR prediction performance.....   | 55        |
| 3.5      | Discussion .....   | 58        |
| 3.6      | Conclusion.....  | 60        |
| <b>4</b> | <b>CHAPTER FOUR: PREDICTION OF LOWER LIMB KINEMATICS AT<br/>PREFERRED WALKING SPEED – Study 2.....</b> | <b>62</b> |
| 4.1      | Overview .....   | 62        |
| 4.2      | Introduction .....   | 62        |
| 4.3      | Methods.....   | 65        |
| 4.3.1    | Study participants.....  | 65        |
| 4.3.2    | Gait analysis.....   | 66        |
| 4.3.3    | Kinematic walking profiles.....  | 67        |
| 4.3.4    | Datasets .....   | 69        |
| 4.3.5    | Time Series transformation to a supervised Learning problem .....                                      | 70        |
| 4.3.6    | Implemented LSTM model architectures .....   | 71        |
| 4.3.7    | Vanilla LSTM neural network.....   | 72        |

|          |   |            |
|----------|---|------------|
| 4.3.8    | Stacked LSTM neural network .....   | 72         |
| 4.3.9    | Bidirectional LSTM (Bi-LSTM) neural network .....   | 73         |
| 4.3.10   | LSTM autoencoder (ED-LSTM) neural network .....   | 74         |
| 4.3.11   | Evaluation and performance metrics .....  | 75         |
| 4.4      | Results .....   | 76         |
| 4.4.1    | LSTM models .....   | 76         |
| 4.4.2    | The LR prediction performance .....   | 81         |
| 4.5      | Discussion .....  | 83         |
| 4.6      | Conclusion.....   | 89         |
| <b>5</b> | <b>CHAPTER FIVE: PREDICTION OF LOWER LIMB KINEMATICS AT SLOWER AND FASTER WALKING SPEEDS – Study 3.</b> ..... | <b>91</b>  |
| 5.1      | Overview .....  | 91         |
| 5.2      | Introduction .....  | 91         |
| 5.3      | Methods.....  | 92         |
| 5.3.1    | Datasets .....  | 92         |
| 5.3.2    | Evaluation and performance metrics .....  | 95         |
| 5.4      | Results for faster walking speed (+20% PWS).....  | 95         |
| 5.4.1    | Leave-one-out cross validation test results for +20% PWS .....  | 99         |
| 5.5      | Results for slower walking speeds (-20% PWS).....   | 103        |
| 5.5.1    | Leave-one-out cross validation test results for -20% PWS .....  | 106        |
| 5.6      | Performance comparison between the developed LSTM models in Study 2 and Study 3.....                          | 110        |
| 5.7      | Discussion .....  | 111        |
| 5.8      | Conclusion.....   | 116        |
| <b>6</b> | <b>CHAPTER SIX: CONCLUSION AND FUTURE DIRECTIONS</b> .....  | <b>117</b> |
| 6.1      | Summary .....   | 117        |
| 6.2      | Limitations and future directions .....   | 119        |
| 6.3      | Practical ML-based applications of a known human movement biomechanics .....                                  | 120        |
| <b>7</b> | <b>REFERENCES</b> .....   | <b>123</b> |
| <b>8</b> | <b>APPENDIX A</b> .....   | <b>149</b> |
| <b>9</b> | <b>APPENDIX B</b> .....   | <b>150</b> |

## LIST OF FIGURES

|  |    |
|--|----|
| <b>Figure 1-1:</b> Illustration of different gait events during the walking gait cycle (Papavasileiou, Zhang, & Han, 2017; Rueterbories et al., 2010).....   | 2  |
| <b>Figure 1-2:</b> Vicon motion capture system at the Victoria University, Biomechanics laboratory. ....   | 6  |
| <b>Figure 1-3:</b> The Vicon motion capture system (14-cameras) and the force-plates instrumented treadmill setup at the Victoria University biomechanics laboratory. In the middle is the human skeletal model inter-linking body segments (i.e. lower limbs, pelvis and trunk) designed to represent the motion of the underlying bone (Garofolini, 2019; Taylor, 2012). Red markers refer to the left limb. Green markers refer to the right limb. Middle yellow markers refer to the pelvis. Upper yellow markers refer to trunk.....                      | 6  |
| <b>Figure 1-4:</b> Schematic diagram of the research questions addressed in this thesis. ....  | 13 |
| <b>Figure 2-1:</b> General ML design process (Mason et al., 2016). ....  | 17 |
| <b>Figure 2-2:</b> Classifier development (Kubat, 2015). ....  | 19 |
| <b>Figure 2-3:</b> The logistic function. ....   | 23 |
| <b>Figure 2-4:</b> GMM adaptation method (Allen et al., 2006).....   | 28 |
| <b>Figure 2-5:</b> Linear (a) and non-linear (b) SVM to find optimum possible planes to divide the data into two classes (R. Begg & Kamruzzaman, 2005; Nakano et al., 2016). ....  | 30 |
| <b>Figure 2-6:</b> The classification accuracy of SVM against the number of features in (R. Begg & Kamruzzaman, 2005).....   | 31 |
| <b>Figure 2-7:</b> The architecture of artificial neuron (Da Silva et al., 2017). ....   | 32 |
| <b>Figure 2-8:</b> The general structure of ANN (Kim, 2017).....   | 33 |
| <b>Figure 3-1:</b> The skeletal model along with the components (X,Y,Z) definition and the markers setup. Grey balls are the retroreflective markers. The Turquoise ball is a virtual marker refers to the participant’s centre of mass. ....  | 43 |
| <b>Figure 3-2:</b> Average thigh and shank LA and AV within a stride. A stride was defined as the interval between two successive heel strikes of the same foot (Soutas-Little, 1998). A) Thigh three dimensional AV (Direction of rotation around the X-axis). B) Shank three dimensional AV (Direction of rotation around the X-axis). C) Thigh three dimensional LA (direction of progression along the Y-axis). D) Shank three dimensional LA (direction of progression along the Y-axis). Red is the X-axis. Green is the Y-axis. Blue is the Z-axis..... | 44 |
| <b>Figure 3-3:</b> Sliding window illustration example using the normalised shank angular velocity X-axis component (1 feature). The window in this model is 25 timesteps and 4 features and the prediction output is 5 timesteps of 4 features. ....  | 45 |
| <b>Figure 3-4:</b> Unfolded structure of the Recurrent Neural Network.....   | 46 |
| <b>Figure 3-5:</b> Standard LSTM memory cell with peephole connections. ....   | 47 |
| <b>Figure 3-6:</b> Structure of the implemented Encoder-Decoder LSTM architecture given 1 input window. The adapter converts the 2D encoded features into 3D output to be adopted by LSTM. The last layer is a fully connected dense layer for outputting 1 window predictions. 49   | 49 |

|  |    |
|--|----|
| <b>Figure 3-7:</b> Model performance with different input window sizes. Red is MAE. Blue is MSE. A) Thigh LA (Y1). B) Shank LA (Y2). C) Thigh AV (X3). D) Shank AV (X4).   | 51 |
| <b>Figure 3-8:</b> The ED-LSTM performance for the first window, showing predicted trajectories (green) and actual trajectories (red). Columns represent the Absolute Error (AE) for the 5 predicted timesteps. (a) Thigh LA Y1. (b) Shank LA Y2. (c) Thigh AV X3. (d) Shank AV X4   | 52 |
| <b>Figure 3-9:</b> The ED-LSTM performance over the entire gait cycle when 5 timesteps prediction window is used. The figure shows predicted trajectories (orange) and actual trajectories (blue). (A) Thigh LA Y1. (B) Shank LA Y2. (C) Thigh AV X3. (D) Shank AV X4.   | 53 |
| <b>Figure 3-10:</b> The ED-LSTM performance for the first window, showing predicted trajectories (green) and actual trajectories (red). Columns represent the Absolute Error (AE) for the 10 predicted timesteps. (a) Thigh LA Y1. (b) Shank LA Y2. (c) Thigh AV X3. (d) Shank AV X4.  | 54 |
| <b>Figure 3-11:</b> The ED-LSTM performance over the entire gait cycle when 10 timesteps prediction window is used. The figure shows predicted trajectories (orange) and actual trajectories (blue). (A) Thigh LA Y1. (B) Shank LA Y2. (C) Thigh AV X3. (D) Shank AV X4.   | 55 |
| <b>Figure 3-12:</b> The LR prediction performance over the gait cycle when 5 timesteps output prediction window is used. The figure shows predicted trajectories (Magenta) and actual trajectories (black). (a) Thigh LA Y1. (b) Shank LA Y2. (c) Thigh AV X3. (d) Shank AV X4.  | 56 |
| <b>Figure 3-13:</b> The LR prediction performance over the gait cycle when 10 timesteps output prediction window is used. The figure shows predicted trajectories (Magenta) and actual trajectories (black). (a) Thigh LA Y1. (b) Shank LA Y2. (c) Thigh AV X3. (d) Shank AV X4.   | 57 |
| <b>Figure 4-1:</b> The skeletal model along with the components (X,Y,Z) definition and the markers setup. Grey balls are the retroreflective markers. The turquoise ball is a virtual marker refers to the centre of mass.   | 66 |
| <b>Figure 4-2:</b> Definition of sagittal plane movements as well as the (X,Y) coordinates. Sagittal plane movements included the rotation around the X-axis (i.e., AV) and the translation along the Y-axis (i.e., LA).   | 68 |
| <b>Figure 4-3:</b> Foot, shank and thigh Sagittal plane AV and LA. Those were selected as the model's independent variables predominantly because primary motions of the human movement are flexion and extension in the sagittal plane (Srinivasan et al., 2008). (a) Foot (X1), shank (X2) and thigh (X3) AV. (b) Foot (Y1), shank (Y2) and thigh (Y3) LA. | 69 |
| <b>Figure 4-4:</b> Sliding window demonstration on 1 feature. The graph shows the sliding window operation on the foot angular velocity (X1). In this work, the input/output window comprises of 6 features.   | 71 |
| <b>Figure 4-7:</b> Vanilla LSTM neural networks (Y. Wu et al., 2018).  | 72 |
| <b>Figure 4-8:</b> Stacked LSTM neural networks (Graves, 2013).  | 73 |
| <b>Figure 4-9:</b> Bi-LSTM neural networks with a BN input layer (Schuster & Paliwal, 1997).   | 74 |

**Figure 4-10:** ED-LSTM neural networks architecture (Sagheer & Kotb, 2019b; Zaroug et al., 2020). ..... 75

**Figure 4-11:** LSTM models prediction performance based on the inter-subject test for each feature vector at PWS only. Models were tested with 75 timesteps (i.e. 1.5s) and the same participant was tested across LSTM models. Black is the actual trajectory. Brown is the Vanilla LSTM predicted trajectory. Red is the Stacked LSTM predicted trajectory. Green is the Bi-LSTM predicted trajectory. Blue is the ED-LSTM predicted trajectory. (a) Foot AV (X1). (b) Foot LA (Y4). (c) Shank AV (X2). (d) Shank LA (Y5). (e) Thigh AV (X3). (f) Thigh LA (Y6). ..... 77

**Figure 4-12:** Performance comparison between LSTM models based on leave-one-out cross validation at PWS and 5km.h<sup>-1</sup> for each feature vector. Red is the RMSE (Left Y-axis). Black is the CC (Right Y-axis). Wider gaps between the two error lines (CC and RMSE) means better prediction quality for the related feature vector. The Stacked and ED LSTM maintained the gap for all feature vectors. (a) Foot AV (X1). (b) Foot LA (Y4). (c) Shank AV (X2). (d) Shank LA (Y5). (e) Thigh AV (X3). (f) Thigh LA (Y6). ..... 80

**Figure 4-13:** Performance comparison between LSTM models based on leave-one-out cross validation at PWS and 5km.h<sup>-1</sup> for each feature vector. Green is the RMSE (Left Y-axis). Blue is the NRMSE (Right Y-axis). Lower error points for the MAE and NRMSE means a better predictive model for the related feature vector. (a) Foot AV (X1). (b) Foot LA (Y4). (c) Shank AV (X2). (d) Shank LA (Y5). (e) Thigh AV (X3). (f) Thigh LA (Y6). ..... 81

**Figure 4-14:** The LR prediction performance with 75 timesteps (i.e. 1.5s) based on the inter-subject test for each feature vector at PWS only. Black is the actual trajectory. Magenta is the LR predicted trajectory. (a) Foot AV (X1). (b) Foot LA (Y4). (c) Shank AV (X2). (d) Shank LA (Y5). (e) Thigh AV (X3). (f) Thigh LA (Y6). ..... 82

**Figure 5-1:** The phase shift difference between the slower (-20% PWS) and faster (+20% PWS) walking speeds, and the normal (PWS) and 5km.h<sup>-1</sup> walking conditions at 75 timesteps (1.5s) of the gait cycle starting from the right foot strike. In this chapter, the LSTM models are tested to predict the kinematics of slower and faster walking speeds only. Magenta is the slower walking speed. Blue is the faster walking speed. Black is the PWS. Grey is the 5km.h<sup>-1</sup>. (a) Foot AV (X1). (b) Foot LA (Y4). (c) Shank AV (X2). (d) Shank LA (Y5). (e) Thigh AV (X3). (f) Thigh LA (Y6). This dataset is a superimposed signals of all test sets related to the same participant evaluated before the cross validations in Chapter 4 and 5. ..... 94

**Figure 5-2:** LSTM models prediction performance based on the inter-subject test for each feature vector at +20% PWS only. Models were tested with 75 timesteps and the same participant was tested across LSTM models. Black is the actual trajectory. Brown is the Vanilla LSTM predicted trajectory. Red is the Stacked LSTM predicted trajectory. Green is the Bi-LSTM predicted trajectory. Blue is the ED-LSTM predicted trajectory. (a) Foot AV (X1). (b) Foot LA (Y4). (c) Shank AV (X2). (d) Shank LA (Y5). (e) Thigh AV (X3). (f) Thigh LA (Y6). ..... 97

**Figure 5-3:** Performance comparison between LSTM models based on leave-one-out cross validation at +20% PWS for each feature vector. Green is the RMSE (Left Y-axis). Blue is the NRMSE (Right Y-axis). Lower error points for the MAE and NRMSE means a better predictive model for the related feature vector. (a) Foot AV (X1). (b) Foot LA (Y4). (c) Shank AV (X2). (d) Shank LA (Y5). (e) Thigh AV (X3). (f) Thigh LA (Y6)..... 101

**Figure 5-4:** Performance comparison between LSTM models based on the leave-one-out cross validation at +20% PWS for each feature vector. Red is the RMSE (Left Y-axis). Black

is the CC (Right Y-axis). Wider gaps between the two error lines (CC and RMSE) means better prediction quality for the related feature vector. (a) Foot AV (X1). (b) Foot LA (Y4). (c) Shank AV (X2). (d) Shank LA (Y5). (e) Thigh AV (X3). (f) Thigh LA (Y6). ..... 102

**Figure 5-5:** Predicted versus actual trajectories for the Vanilla (brown), Stacked (red), Bi (green) and ED (blue) LSTM at -20% PWS. All models were tested on the same participant at the same speed. Each single predicted output window was 5 timesteps (0.1s). (a) Foot AV (X1). (b) Foot LA (Y4). (c) Shank AV (X2). (d) Shank LA (Y5). (e) Thigh AV (X3). (f) Thigh LA (Y6). ..... 104

**Figure 5-6:** Performance comparison between LSTM models based on leave-one-out cross validation at +20% PWS for each feature vector. Green is the RMSE (Left Y-axis). Blue is the NRMSE (Right Y-axis). Lower error points for the MAE and NRMSE means a better predictive model for the related feature vector. (a) Foot AV (X1). (b) Foot LA (Y4). (c) Shank AV (X2). (d) Shank LA (Y5). (e) Thigh AV (X3). (f) Thigh LA (Y6). ..... 108

**Figure 5-7:** Performance comparison between LSTM models based on leave-one-out cross validation at +20% PWS for each feature vector. Red is the RMSE (Left Y-axis). Black is the CC (Right Y-axis). Wider gaps between the two error lines (CC and RMSE) means better prediction quality for the related feature vector. (a) Foot AV (X1). (b) Foot LA (Y4). (c) Shank AV (X2). (d) Shank LA (Y5). (e) Thigh AV (X3). (f) Thigh LA (Y6). ..... 109

**Figure 5-8:** Leave-one-out cross validation error (%) summary for the cross validated LSTM models in study 1 (PWS and 5km.h<sup>-1</sup>) and study 2 ( $\pm 20\%$  PWS). Brown is the Vanilla LSTM. Lower error point indicates better performing model for the relevant speed. Red is the Stacked LSTM. Green is the Bi-LSTM. Blue is the ED-LSTM. (a) Foot AV (X1). (b) Foot LA (Y4). (c) Shank AV (X2). (d) Shank LA (Y5). (e) Thigh AV (X3). (f) Thigh LA (Y6). 111

## LIST OF TABLES

|   |    |
|---|----|
| <b>Table 2-1:</b> Glossary maps common terms used in the field of ML and statistics. ....   | 16 |
| <b>Table 3-1:</b> ED-LSTM performance for predicting the first 5 predicted timesteps. ....  | 52 |
| <b>Table 3-2:</b> The ED-LSTM performance for predicting the complete stride using an input window size of 25 timesteps and an output window size of 5 timesteps.....   | 53 |
| <b>Table 3-3:</b> The ED-LSTM performance for predicting the first 10 predicted timesteps. ....   | 54 |
| <b>Table 3-4:</b> The ED-LSTM performance for predicting the complete stride using an input window size of 25 timesteps and an output window size of 10 timesteps.....  | 55 |
| <b>Table 3-5:</b> The LR average model performance for all output prediction windows using an input window size of 25 timesteps and an output window size of 5 timesteps. ....  | 56 |
| <b>Table 3-6:</b> The LR average model performance for all output prediction windows using an input window size of 25 timesteps and an output window size of 10 timesteps. ....   | 57 |
| <b>Table 4-1:</b> Train-test split datasets. The model was trained and tested using leave-one-out cross validation. At each epoch, the training set doesn't contain all trials of the tested participant. ....  | 70 |
| <b>Table 4-2:</b> Models' configuration for inter-subject leave-one-out cross validation test. The number of epochs is the starting point for testing the first participant. Using TL, subsequent participants were tested after 10 epochs each. ....               | 76 |
| <b>Table 4-3:</b> Leave-one-out cross validation test error based on the MAE, MSE and the RMSE at the PWS and 5km.h <sup>-1</sup> combined. Each of the predicted variables (i.e. $X_1, X_2, \dots, Y_6$ ) was evaluated for the 4 trained LSTM architectures. .... | 78 |
| <b>Table 4-4:</b> Leave-one-out cross validation test error based on the NRMSE (%) at the PWS and 5km.h <sup>-1</sup> combined. Each of the predicted variables (i.e. $X_1, X_2, \dots, Y_6$ ) was evaluated for the 4 trained LSTM architectures.....              | 79 |
| <b>Table 4-5:</b> Leave-one-out cross validation test evaluation based on the CC at the PWS and 5km.h <sup>-1</sup> combined. Each of the predicted variables (i.e. $X_1, X_2, \dots, Y_6$ ) was evaluated for the 4 trained LSTM architectures. ....               | 79 |
| <b>Table 4-6:</b> The LR performance results across 75 timesteps of walking on an unseen participant prior to TL. All participant's associated trials (e.g. 5k) were removed from the training set.....   | 82 |
| <b>Table 4-7:</b> The LR leave-one-out cross validation test among 15 participants across 75 timesteps. When a participant's data are used for testing, all their associated trials are removed from the training set. ....   | 83 |
| <b>Table 4-8:</b> ML-based methods for lower limb kinematics estimation (inter-subject test).....   | 87 |
| <b>Table 5-1:</b> Description of training and testing datasets.....   | 95 |
| <b>Table 5-2:</b> Models training process. The number of epochs is the starting point for testing the first participant. Using TL, subsequent participants were tested after 10 epochs each. ....   | 95 |
| <b>Table 5-3:</b> All LSTM models performance evaluation results based on the MAE, MSE and the RMSE. Each of the predicted independent variables (i.e. $X_1, X_2, \dots, Y_6$ ) was tested at   |    |

|  |     |
|--|-----|
| +20% PWS. The tested dataset comprised of 75 timesteps and is related to the first participant. Results were obtained after training the model with TL at 50 epochs. ....  | 98  |
| <b>Table 5-4:</b> All LSTM models performance evaluation results based on the NRMSE (%). Each of the predicted independent variables (i.e. $X_1, X_2, \dots, Y_6$ ) was tested at +20% PWS. The tested dataset comprised of 75 timesteps and is related to the first participant. Results were obtained after training the model with TL at 50 epochs. ....            | 98  |
| <b>Table 5-5:</b> All LSTM models performance evaluation results based on the CC. Each of the predicted independent variables (i.e. $X_1, X_2, \dots, Y_6$ ) was tested at +20% PWS. The tested dataset comprised of 75 timesteps and is related to the first participant. Results were obtained after training the model with TL at 50 epochs. ....                   | 99  |
| <b>Table 5-6:</b> Leave-one-out cross validation (9 participants) test for the faster walking speed (+20% PWS) based on the MAE, MSE and the RMSE for all the LSTM architectures.....  | 100 |
| <b>Table 5-7:</b> Leave-one-out cross validation (9 participants) test for the faster walking speed (+20% PWS) based on the NRMSE (%) for all LSTM architectures.....  | 100 |
| <b>Table 5-8:</b> Leave-one-out cross validation (9 participants) test for the faster walking speed (+20% PWS) based on the CC for all LSTM architectures. ....  | 100 |
| <b>Table 5-9:</b> All LSTM models performance evaluation results based on the MAE, MSE and the RMSE. Each of the predicted independent variables (i.e. $X_1, X_2, \dots, Y_6$ ) was tested at -20% PWS. The tested dataset comprised of 75 timesteps and is related to the first participant. Results were obtained after training the model with TL at 50 epochs..... | 105 |
| <b>Table 5-10:</b> All LSTM models performance evaluation results based on the NRMSE (%). Each of the predicted independent variables (i.e. $X_1, X_1, \dots, Y_6$ ) was tested at -20% PWS. The tested dataset comprised of 75 timesteps and is related to the first participant. Results were obtained after training the model with TL at 50 epochs. ....           | 105 |
| <b>Table 5-11:</b> All LSTM models performance evaluation results based on the CC. Each of the predicted independent variables (i.e. $X_1, X_2, \dots, Y_6$ ) was tested at -20% PWS. The tested dataset comprised of 75 timesteps and is related to the first participant. Results were obtained after training the model with TL at 50 epochs.....                   | 106 |
| <b>Table 5-12:</b> Leave-one-out cross validation (9 participants) test for the faster walking speed (-20% PWS) based on the MAE, MSE and th RMSE for all the LSTM architectures .....   | 107 |
| <b>Table 5-13:</b> Leave-one-out cross validation (9 participants) test for the faster walking speed (-20% PWS) based on the NRMSE (%) for all LSTM architectures. ....  | 107 |
| <b>Table 5-14:</b> Leave-one-out cross validation (9 participants) test for the faster walking speed (-20% PWS) based on the CC for all LSTM architectures.....  | 107 |

## LIST OF ABBREVIATIONS

|                |   |
|----------------|---|
| <b>ANOVA</b>   | Analysis of Variance                            |
| <b>AI</b>      | Artificial Intelligence                         |
| <b>ANN</b>     | Artificial Neural Networks                      |
| <b>AUC</b>     | Area Under the ROC curve                        |
| <b>AV</b>      | Angular Velocity                                |
| <b>AWS</b>     | Amazon Web Services                             |
| <b>Bi-LSTM</b> | Bidirectional LSTM                              |
| <b>BMI</b>     | Brain-Machine Interface                         |
| <b>BN</b>      | Batch Normalisation                             |
| <b>BP</b>      | Bereitschafts Potential                         |
| <b>CART</b>    | Classification and Regression Trees             |
| <b>CC</b>      | Correlation Coefficient                         |
| <b>CNN</b>     | Convolutional Neural Network                    |
| <b>CoM</b>     | Centre of Mass                                  |
| <b>DL</b>      | Deep Learning                                   |
| <b>DM</b>      | Data Modelling                                  |
| <b>ED-LSTM</b> | LSTM autoencoder, Encoder-Decoder LSTM          |
| <b>EEG</b>     | Electroencephalography                          |
| <b>EMG</b>     | Electromyography                                |
| <b>ERS/ERD</b> | Event-Related Synchronisation/Desynchronization |
| <b>EM</b>      | Expectation Maximisation                        |
| <b>FNN</b>     | Feedforward Neural Networks                     |
| <b>GMM</b>     | Gaussian Mixture Model                          |

|              |   |
|--------------|---|
| <b>GRNN</b>  | Generalised Regression Neural Networks        |
| <b>HAL</b>   | Hybrid Assistive Limb                         |
| <b>HMM</b>   | Hidden Markov Model                           |
| <b>IMU</b>   | Inertial Measurement Unit                     |
| <b>IoT</b>   | Internet of Things                            |
| <b>LA</b>    | Linear Acceleration                           |
| <b>LDA</b>   | Linear Discriminant Analysis                  |
| <b>LOPES</b> | Lower Extremity Powered Exoskeleton           |
| <b>LR</b>    | Linear Regression                             |
| <b>LSTM</b>  | Long Short Term Memory                        |
| <b>MAE</b>   | Mean Absolute Error                           |
| <b>MEMs</b>  | Micro-Electro-Mechanical systems              |
| <b>ML</b>    | Machine Learning                              |
| <b>MLP</b>   | Multiple Layer Perceptron                     |
| <b>MRCP</b>  | Movement-Related Cortical Potential           |
| <b>MSE</b>   | Mean Squared Error                            |
| <b>NARX</b>  | Nonlinear Autoregressive with External Inputs |
| <b>NB</b>    | Naïve Bayes                                   |
| <b>NRMSE</b> | Normalised RMSE                               |
| <b>PCA</b>   | Principal Component Analysis                  |
| <b>PDFs</b>  | Probability Density Functions                 |
| <b>PPCA</b>  | Probabilistic Principal Component Analysis    |
| <b>PWS</b>   | Preferred Walking Speed                       |
| <b>ReLU</b>  | Rectified Rectilinear Unit                    |

|             |                                   |
|-------------|-----------------------------------|
| <b>RMSE</b> | Root Mean Square Error            |
| <b>RNN</b>  | Recurrent Neural Networks         |
| <b>ROC</b>  | Receiver Operating Characteristic |
| <b>sEMG</b> | surface Electromyography          |
| <b>SGD</b>  | Stochastic Gradient Descent       |
| <b>SVM</b>  | Support Vector Machines           |
| <b>TL</b>   | Transfer Learning                 |



# 1 CHAPTER ONE: INTRODUCTION

## 1.1 Background

Mechanics is one of the oldest divisions of physics that describes bodies at rest or in motions state subjected to force actions (Hibbeler, 2007). When those bodies are living things, it is referred to as Bio-Mechanics (Knudson, 2007). Biomechanics is an interdisciplinary field that describes, analyses and evaluates the human movement (Winter, 2009). The understanding of gait biomechanics was found to be a useful tool to reduce the risk of slipping (Sundaram et al., 2020) and to investigate the assistance of wearable assistive devices (Madinei, Alemi, Kim, Srinivasan, & Nussbaum, 2020; Mudie et al., 2018).

Gait analysis is a biomechanics branch that started to surface since late 1900s, devoted to the motions of the human limbs (DeLisa, 1998). The walking gait cycle can be considered as the cyclic rotation of the human limbs or the body segments (Baker, 2007). Walking is an oscillating process that obeys Newton's laws of motion (Inman & Eberhart, 1953). It consists of a repetitive cycle that is generated from either a peripheral or a central origin (Brenière, 1996). A single gait cycle can be defined as the period of time between the heel strike event of a particular foot to the next heel strike event of the same foot (DeLisa, 1998). The gait cycle (**Figure 1-1**) is also divided into dual phases, the stance phase and the swing phase. The approximate time for the walking gait cycle is 1 second with a stance phase that accounts for 60% and a swing phase about 40% of the gait cycle.

The stance phase starts from the heel strike which also marks the start of the loading response where the entire foot is placed on the ground and absorbing the full body weight (Rueterbories, Spaich, Larsen, & Andersen, 2010). Then, is the double stance where both feet are on the ground. At the mid-stance phase, the body is moved forward and the contralateral limb is in the swing phase. The body in this phase is at the minimum stability, as the body is relying on one limb only. The occurrence of heel off marks the transition from the mid-stance to the terminal stance. That causes the body to move forward, leading to the beginning of the pre-swig phase which ends with toe off. Toe off is when the foot starts leaving the ground. Hence, the swing phase starts. The swing phase is divided into three sub-events which are; the initial swing, mid-swing, and the terminal swing. Firstly, at the initial swing the foot starts accelerating forward. Then at the mid-swing, the swinging limb starts to lead the contralateral limb. Finally at the terminal swing, the foot deaccelerates in preparation to land on heels (i.e.

heel strike) (see **Figure 1-1**). Two subsequent heel strikes of the opposite limb is known as a step, while two subsequent steps constitute a stride (Tesio & Rota, 2019).

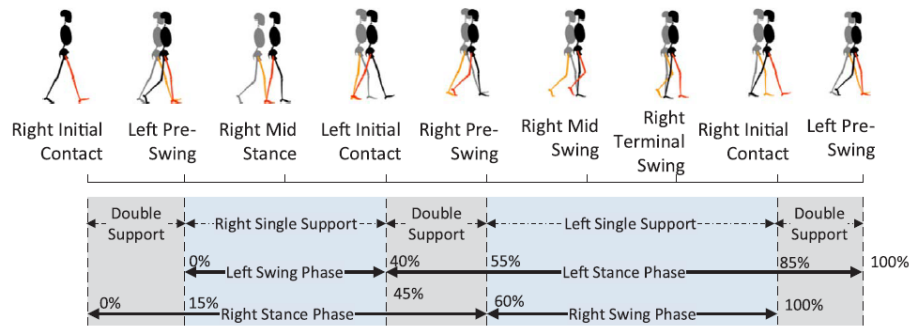


**Figure 1-1:** Illustration of different gait events during the walking gait cycle (Papavasileiou, Zhang, & Han, 2017; Rueterbories et al., 2010).

## 1.2 Changes of kinematic characteristics with gait speed

The kinematics of the human movement are the linear and the angular displacements, velocities and accelerations that describe the spatial movement of a rigid body (i.e. foot). While kinetics are the forces, powers and energetics that caused the movement of a rigid body (Winter, 1991). According to Newton’s second law of motion, when the body centre of mass accelerates or deaccelerates, its linear acceleration is determined by the forces acting on the body system as a whole (Goldstein, Poole, & Safko, 2002). This constitutes the concept that body segments (i.e. foot, thigh, shank, etc) are responsible for the displacement of the body centre of mass which may sometimes be outside the body system (Tesio & Rota, 2019).

The changes of speed in body segments are known to have substantial impacts on the spatiotemporal as well as the kinematic and kinetic patterns of the gait cycle among different age groups; children, young and older adults (Claudiane Arakaki Fukuchi, Fukuchi, & Duarte, 2019; Grant & Chester, 2015). The walking speed was the most influential variable amongst sex, age and body mass index on the ambulatory kinematic and kinetic profiles (Chehab, Andriacchi, & Favre, 2017). Normal (comfortable or preferred) walking speed reported in the literature had averages ranging from  $1.05 \text{ m}\cdot\text{s}^{-1}$  to  $1.43 \text{ m}\cdot\text{s}^{-1}$  (or 101 to 122 steps/min, cadence) (Kwon, Son, & Lee, 2015; Winter, 1991). Reported faster and slower walking speeds were an increment of 10.45% to 58.06% ( $1.25 \text{ m}\cdot\text{s}^{-1}$  to  $2 \text{ m}\cdot\text{s}^{-1}$ ) and a decrement of 9.70% to 56.99% ( $0.4 \text{ m}\cdot\text{s}^{-1}$  to  $1.61 \text{ m}\cdot\text{s}^{-1}$ ). Changes in walking speed largely affects the sagittal plane kinematics (Sun, Fekete, Mei, & Gu, 2018). Significant differences were found at the foot angles as well as the ankle kinematics (Dubbeldam et al., 2010; Grant & Chester, 2015; Tulchin, Orendurff,

Adolfson, & Karol, 2009). Large differences were found in step length and velocity between old (64 to 86 years) and younger group of women, 1.57 mph for the older group versus 1.83 mph for the younger group of women (Finley, 1969). Oliveira *et al.* investigated the kinematic impacts over time during fast walking on older ( $71.0 \pm 5.6$  years) and younger populations ( $26.6 \pm 6.0$  years) and found gradual increase in ankle plantarflexion and decreased hip extension at the toe off for the older population, while younger adults had a progressive decrease in ankle dorsiflexion at the heel contact (Oliveira, Vieira, Machado Sousa, & Vilas-Boas, 2017). Both groups have shown continuing increase in step-width and high coordination of the lower limb joint angles. In a systematic review for gait speed-related studies (218 articles) by Fukuchi *et al.*, a comparison was conducted between fast (fast>comfortable) and slow (slow<comfortable) walking speeds across children (4 to 17 years old) as well as younger (18 to 59 years old) and older adults (60 to 85 years old). In children, there were large effect sizes found at the knee and hip flexion and ankle plantarflexion angles during slow walking (Claudiane Arakaki Fukuchi et al., 2019). For young adults walking at slower speed, there were small effect sizes for hip flexion and extension angles and large for the knee flexion angle. While at faster speed, there were small effect sizes at the hip flexion and ankle plantarflexion angles. Large effect sizes were found during faster speeds only, for the older adults. Walking speed was also found to be different between male and female participants. At natural cadence, females were found to have higher natural cadence than males (Finley & Cody, 1970). Females were also found to have 6 to 9 higher cadence than males (Winter, 1991).

Statistical methods such as the effect size, are amongst several other methods (i.e. analysis of variance, t-test, etc.) have been widely implemented in the literature to observe changes in walking kinematics between different conditions (i.e. fast vs. comfortable walking). Those methods maintained their importance across biomechanics researchers by reliably conveying the significance of different kinematic changes between the walking conditions.

### **1.3 Statistical methods for gait inference**

For the most of the last century, the interpretations and the deductions drawn from the human movement data were at most based on statistical assumptions or estimators (i.e. goodness-of-fit) that were highly relying on fixed parameters such as the Student's t-test, regression analysis and the Analysis of Variance (ANOVA) (Bohannon, 1997; Hageman & Blanke, 1986; Lage, White, & Yack, 1995; Mullineaux, Bartlett, & Bennett, 2001; Tinetti, Speechley, & Ginter, 1988). They were also referred to as Data Modelling (DM) approaches,

in which a stochastic data model is assumed and then its parameters are estimated from the data as well as the model to be used for prediction (Breiman, 2001). Those methods however were found to be not capable enough to cope with the ascending growth (i.e. volume and dimensionality) of human movement data such that the relationship between several heterogeneous biomechanical or clinical variables were loosely captured (Phinyomark, Hettinga, Osis, & Ferber, 2015; Phinyomark, Hettinga, Osis, & Ferber, 2014; Phinyomark, Petri, Ibáñez-Marcelo, Osis, & Ferber, 2018). Particularly, the rise of wearable sensors such as the Inertial Measurement Unit (IMU) (Sabatini, 2011; Vargas-Valencia, Elias, Rocon, Bastos-Filho, & Frizera, 2016), Electromyography (EMG) and the Electroencephalogram (EEG) sensors (Kawamoto & Sankai, 2002; S. Wang et al., 2015), have posed new challenges and opportunities to the analysis of human movement data (Halilaj et al., 2018).

In response to these limitations and to rejuvenate applied inference methods, a new set of algorithmic models related to the field of computer science have been widely adopted by biomechanist researchers called Machine Learning (ML) algorithms (Halilaj et al., 2018; Phinyomark et al., 2018). ML is a subfield of Artificial Intelligence (AI) concerned with the establishment of computer programs that automatically learn with experience (Mitchell, 1997). They are a set of algorithms that are able to categorise large datasets by observing their regularities and recognising their patterns (Bishop, 2006). In contrast to DM approaches where the model validation is simply a yes or no using goodness-of-fit tests, a ML algorithm relies on its predictive accuracy to optimise and fine-tune its parameters (Breiman, 2001).

#### **1.4 The Measurement and prediction of gait biomechanics**

The understanding of the human movement voluntariness has long been addressed over the centuries within the scope of philosophy until recently it became one of the core research areas in physiology (Ingram, Sadeghi, Flanagan, & Wolpert, 2017; Rothwell, 2012; Schmidt, Lee, Winstein, Wulf, & Zelaznik, 2018). The willingness to move and the movement initiation process are not intertwined and can be separated (Hallett, 2007; Zeman, 2002, 2005). That means the human movement starts subconsciously and then the volitional awareness for the movement becomes sensible later in time (Hallett, 2007). Scientific efforts to detect the human movement intention before it is occurrence have been successful with the aid of ML and accurate movement measurements (W. Tao, Liu, Zheng, & Feng, 2012). Commonly implemented measurement techniques for gait analysis are the motion capture systems (i.e. gold standards) (Komnik, Weiss, Pagani, & Potthast, 2015; Tong & Granat, 1999), gyroscopes (Abaid, Cappa,

Palermo, Petrarca, & Porfiri, 2013; Goršič et al., 2014), accelerometers (González, López, Rodriguez-Uría, Álvarez, & Alvarez, 2010), IMU devices (Nogueira, Siqueira, Inoue, & Terra, 2014), EEG and surface EMG sensors (Joshi, Lahiri, & Thakor, 2013; J. Li et al., 2016).

#### **1.4.1 Motion capture systems**

The motion capture systems are predominantly consist of 3D optoelectronic systems (Komnik et al., 2015) with integrated force platforms (Rueterbories, Spaich, & Andersen, 2014) (see **Figure 1-2**). The Optoelectronic systems are electronic devices that triangulate the 3D position of human motion between 2 or more cameras by sourcing, detecting and controlling of light (Hanley, Tucker, & Bissas, 2018; Rosencher & Vinter, 2002). The force platforms measure the 3D kinetic gait parameters and are commonly found as a force-plate or as a force-plate instrumented treadmill (Garofolini, Taylor, & Lepine, 2019; Yanxin Zhang & Ma, 2019). The motion capture systems offer a high quality motion tracking and are considered the top golden standards for gait data collection and analysis (Albert et al., 2020; do Carmo Vilas-Boas, Choupina, Rocha, Fernandes, & Cunha, 2019; Stone, Sarangi, & Pelah, 2019). Different motion capture systems have been extensively utilised to collect human motions such as the Qualisys (Baskwill, Belli, & Kelleher, 2017), OptoTrack (D. T. Lai, Taylor, & Begg, 2012) and Vicon (Best & Begg, 2008; Ewing, Fernandez, Begg, Galea, & Lee, 2016). The Qualisys and Vicon systems are both based on a passive (i.e. reflective) marker setup while the OptoTrack is based on active (i.e. connected back to the system) marker setup. Passive markers are coated with a retroreflective material and are tracked by reflecting the infrared light emitted generated from the motion cameras. While the active markers are powered to generate to generate the infrared light which enable the motion cameras to track the markers by their relative position. Normally at the beginning of any trial the group of cameras are calibrated to provide overlapping projections and the tracking of each of each on-body marker is verified (**Figure 1-3**).



**Figure 1-2:** Vicon motion capture system at the Victoria University, Biomechanics laboratory.

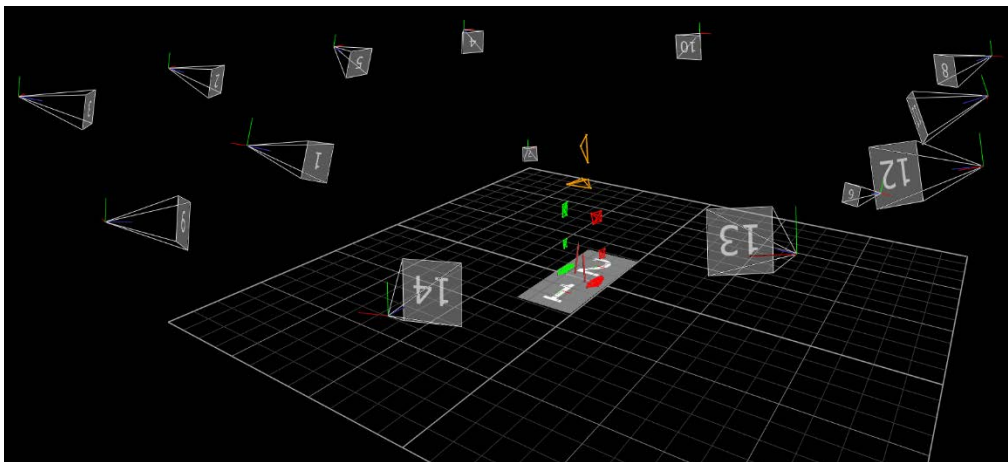


**Figure 1-3:** The Vicon motion capture system (14-cameras) and the force-plates instrumented treadmill setup at the Victoria University biomechanics laboratory. In the middle is the human skeletal model inter-linking body segments (i.e. lower limbs, pelvis and trunk) designed to represent the motion of the underlying bone (Garofolini, 2019; Taylor, 2012). Red markers refer to the left limb. Green markers refer to the right limb. Middle yellow markers refer to the pelvis. Upper yellow markers refer to trunk.

Studies have utilised ML to predict the gait kinematics and kinetics of the human movement for various motivations based on motion capture data. For instance, developing ML models based on motion capture data may help assisting clinicians to automate and expedite

the process of gait assessment and evaluation. Zhang and Ma compared the performance of 7 different supervised ML algorithms for the classification of gait patterns of children with cerebral palsy (Yanxin Zhang & Ma, 2019). Pogorelc *et al.* developed a ML model to identify Parkinson's disease along with other pathological gait based on the motion capture data (Pogorelc, Bosnić, & Gams, 2012). The motion capture data have also been utilised to test the possibility of using ML to predict kinematic and kinetic variables to be used outside the laboratory settings (i.e. ambient assisted living). For instance, Lai *et al.* developed a ML algorithm based on the motion capture system to estimate gait features during the swing phase that are directly related to predicting the risk of tripping and falling which can potentially transcended to elderly users (D. T. Lai et al., 2012).

The motion capture systems however are very costly and normally installed in large laboratories (Baskwill et al., 2017). Those factors suggested that collected data from the motion capture systems should be considered only as the baseline for studies that aim to transcend it is findings outside the laboratory settings.

#### **1.4.2 The Inertial Measurement Units (IMUs)**

The term “inertial” refers to the combination of 3-axis accelerometer and 3-axis gyroscope sensors (Tinder, 2006). Devices that are composed of those sensors are frequently denoted as IMUs. The gyroscope measures the sensor's angular velocity while the accelerometer measures the specific force which includes the earth's gravity and the linear acceleration (Titterton, Weston, & Weston, 2004). The main function of IMUs is the measurement of position and orientation tracking of the bodies onto which they are attached to (Cuesta-Vargas, Galán-Mercant, & Williams, 2010). The latest developments in the area of micro-electro-mechanical systems (MEMs) has made the IMUs more miniaturised and low in both cost as well as power consumption (Kok, Hol, & Schön, 2017). As a result, magnetic sensors have been integrated into IMUs. Although, they require a magnetic field for their operation, the entire earth offers abundant external magnetic source. They are sensitive to electromagnetic interference, however, they have zero drifts over time. (Sabatini, 2011). The combination of magnetic and IMU sensors has shown a viable solution in studies that require three-dimensional position tracking such as in gait analysis and clinical studies (Bergamini et al., 2014). This is done by integrating the gyroscopic signal from a known starting point given by magnetometers and accelerometers (Sabatini, 2011).

The IMUs have been widely implemented in human motion analysis studies and assistive devices and were found to be accurate, practical and easy to initialise (Beravs, Reberšek, Novak, Podobnik, & Munih, 2011; Cuesta-Vargas et al., 2010; Elliott, Marecki, & Herr, 2014). O'Reilly *et al.* developed a classifier to obtain different types of deadlift biomechanics based on a lumbar-worn IMU data (O'Reilly, Whelan, Ward, Delahunt, & Caulfield, 2017). Recently however with the aid of ML, several studies have shown the potential to predict the gait kinematics (i.e. joint angles) and kinetics (i.e. ground reaction forces) based on IMU data (Dehzangi, Taherisadr, & ChangalVala, 2017; Gholami, Napier, & Menon, 2020; Lim, Kim, & Park, 2020; Nogueira et al., 2017). Using ML techniques, Vu *et al.* were able to obtain the percentage of the gait cycle in a powered prosthetic device based on a shank-mounted IMU (Vu et al., 2018). Gholami *et al.* predicted the lower limb joint angles using ML model based on show-mounted accelerometer data (Gholami et al., 2020).

The IMU sensors are multidimensional, low in cost, ease to use, non-invasive and immune to interference (Mannini & Sabatini, 2010). They do not require external sources (e.g. electromagnetic signal) which may restrict their sensing range compared to optical tracking systems (Sabatini, 2011). These factors and the growing studies in human motion analysis based on IMU data have motivated many researchers to consider simulated IMU data when using the gold standard data collection approach (i.e. motion capture systems). Collecting biomechanical data with motion capture systems as well as force platforms is considered the benchmark and has been widely adopted in the literature for experimental purposes and in gait detection studies (R. Begg & Kamruzzaman, 2005; O'Connor, Thorpe, O'Malley, & Vaughan, 2007). The motion capture systems however are costly and impractical for outdoor use (Jung, Heo, Yang, & Park, 2015). Therefore, for use in outdoor environments, wearable sensors such as gyroscopes, accelerometers and IMUs are becoming prevalent in human movement studies (Hanlon & Anderson, 2009; Preece et al., 2011).

Simulated IMU data that included the linear acceleration (LA) and the angular velocity (AV) have been collected from the motion capture systems and was successfully modelled with ML algorithms in several studies for gait kinematics prediction (Dorschky et al., 2020; Mundt et al., 2020; Ross, Dowling, Troje, Fischer, & Graham, 2020; Zaroug, Lai, Mudie, & Begg, 2020). Clouthier *et al.* used simulated IMU data to train and develop ML model to classify athletic movements (Clouthier, Ross, & Graham, 2020). The utilisation of simulated IMU data such as the kinematics output from IMU sensors (i.e. LA and AV) have brought promising

results and may offer the opportunity to transcend predictive ML models outside the laboratory settings (De Brabandere et al., 2020; Preatoni, Nodari, & Lopomo, 2020).

### 1.4.3 The Electroencephalography (EEG)

The EEG is a wearable sensor discovered in 1929 by Hans Burger, that is worn around the scalp to measure the electrical activity of the brain (Binnie & Prior, 1994; Gloor, 1969). The EEG metal discs (i.e. electrodes) scan for voltage changes coming from the ionic current produced by some of the brain cells (Biasiucci, Franceschiello, & Murray, 2019; Davidson, Jackson, & Larson, 2000). Reported neural features related to the EEG signal were the Movement-Related Cortical Potential (MRCP) (H.-H. Kornhuber, 1965; Shakeel et al., 2015; Shibasaki & Hallett, 2006) and the Event-Related Synchronisation/Desynchronisation (ERS/ERD) (Pfurtscheller & Aranibar, 1979; Pfurtscheller & Neuper, 1994). The MRCP feature also known as the Bereitschafts Potential (BP), is the slow decrease in the EEG amplitude 0.5s before a self-paced movement initiation. While the ERD is the decrease in the frequency power 0.5-2s before the voluntary movement (Pfurtscheller, 1981). The spectral power were predominantly reported in the frequency bands mu (8-12 Hz) and beta (12-30 Hz) of the brain wave (Chéron et al., 2012; Pfurtscheller & Da Silva, 1999; Severens, Nienhuis, Desain, & Duysens, 2012).

The EEG was implemented by Kornhuber and Deecke to record EEG signals related to the voluntary finger movement and found a slow increasing surface-negative potential that takes place up to 1.5s before the physical movement (H. H. Kornhuber & Deecke, 1965). Bai *et al.* monitored self-paced wrist extension with the EEG and found an average time  $0.62 \pm 0.25$  s before the physical voluntary movement (Bai et al., 2011). Such scientific findings accelerated the development of Brain-Machine Interface (BMI) in assistive devices for patients with neurological injuries (Carvalho, Dias, & Cerqueira, 2019; Tahernezhad-Javazm, Azimirad, & Shoaran, 2018; Wolpaw & McFarland, 2004; Wolpaw, McFarland, Neat, & Forneris, 1991). The BMI (based on EEG) is a direct communication method between the user brain and the assistive device (i.e. powered exoskeleton). While the BMI is still being researched, the MRCP requires substantial initialisation time (i.e. several repetitions of the same trial) in order to extract good and reliable features (J. Li et al., 2016; Savić et al., 2014; S. Wang et al., 2015). The mobility sources were also found to be difficult to record from the brain cortex (Petersen, Willerslev-Olsen, Conway, & Nielsen, 2012) due to the low signal-to-noise ratio and the low amplitude (8-10  $\mu$ V) related to the MRCP (Bai et al., 2011). The ERD

feature also requires a steady state baseline for the voluntary movement in order to correctly detect the frequency power related to the movement (Sburlea, Montesano, de la Cuerda, et al., 2015; Sburlea, Montesano, & Minguez, 2015). Hasan *et al.* utilised ML algorithms to overcome some of the aforementioned EEG signal problems in two studies by implementing a discrete wavelet transform to extract features from pre-movement EEG data and classify the rest versus start and the stop versus walking movements (Hasan, Siddiquee, & Bai, 2020; Shafiul Hasan et al., 2020). The classification of pre-movement EEG data was possible with average accuracy of 76.41% for the rest vs. start and 74.12% for the walk vs. stop movements (Shafiul Hasan et al., 2020). The studies recommended further research into the reliability of real-time EEG intention detection (Hasan et al., 2020) due to the very noisy and non-stationary EEG data and the subjective differences of gait preparation which may increase the uncertainty of the EEG-based intention detection problem (Shafiul Hasan et al., 2020).

#### **1.4.4 The surface Electromyography (sEMG)**

The sEMG are wearable sensors that directly reflect the human muscle activities (Hakonen, Piitulainen, & Visala, 2015). The EMG sensor measures the muscles electrical response to nerve stimulation and has been used as a method for powered assistive devices control (Bi & Guan, 2019). Surface sEMG uses electrodes placed on the skin and has the benefit of being non-invasive. Several works in the literature have considered the detection of muscles' electric signals, as a mean for the assistive device to comprehend human intentions, such as in Hybrid Assistive Limb (HAL) exoskeleton (Kawamoto & Sankai, 2002), and the NEUROExos (Lenzi, De Rossi, Vitiello, & Carrozza, 2012). Fleischer *et al.* utilised the sEMG sensor in a lower limb exoskeleton calibrated with pose sensors (Hall sensors, accelerometers, and floor contact sensors) (Fleischer, Reinicke, & Hommel, 2005). Results have shown the possibility of measuring one muscle to represent a group of neighbouring muscles on healthy which indicate that further research is needed to observe whether this works in other motions (i.e. different muscle group). Chen *et al.* implemented the sEMG sensor integrated with computational algorithms in a knee exoskeleton and was able to predict human motor intent in real-time (X. Chen, Zeng, & Yin, 2017). The sEMG signal was treated as a harmonic oscillator using the energy kernel method (X. Chen, Yin, & Fan, 2014). Morbidoni *et al.* identified stance/swing phases based on sEMG lower limb signals (Morbidoni, Cucchiarelli, Fioretti, & Di Nardo, 2019). The sEMG was also able to detect gait events in children with Cerebral Palsy based on control algorithms. (Lauer, Smith, & Betz, 2005). In upper limb movements, the sEMG was utilised to compute the elbow torque (L. Wang & Buchanan, 2002) and to improve

the collaboration between the human arm and the robotic hand (i.e. pick and place robot) (Bi & Guan, 2019).

Nonetheless, the sEMG signals are difficult to interpret due to the unclear relationship between the muscle activations and the sEMG voltage response (L. Wang & Buchanan, 2002). The sEMGs are very sensitive to electrode placement, noise from neighbouring muscles and the influence of the human sweat. They are deemed unreliable for prolonged use, as they require calibration for inter-subject variability in rehabilitative devices (G. Chen, Chan, Guo, & Yu, 2013). Problems arise in its use for intended hand movement detection as the slender muscles controlling the individual finger overlap those of the arm and precise electrode placement is needed (Biggar & Yao, 2016).

## **1.5 Motivation of the research**

The nature of the human gait cycles have shown to be resembling the oscillating movements of the pendulum (i.e. stance phase) and the inverted pendulum (i.e. swing phase) (Kuo & Donelan, 2010). The cyclic and monotonous attributes of the human gait has paved the way for several mathematical modelling approaches such as ML algorithms to capture the movement patterns and provide insightful gait (R. Begg & Kamruzzaman, 2005; Halilaj et al., 2018; Mannini, Trojaniello, Cereatti, & Sabatini, 2016; Zaroug et al., 2019; C.-y. Zhao, Zhang, & Guo, 2012).

Machine Learning methods for gait classification and assessments have been satisfactory implemented based on various biomechanical measurements (Di Nardo, Morbidoni, Cucchiarelli, & Fioretti, 2021). The gait regression problems however were identified as the most challenging tasks for ML algorithms to solve (Sagheer & Kotb, 2019b). The developed ML classifiers for the human movement biomechanics (i.e. identifying abnormal patterns) account for 80.6% of the published literature (Halilaj et al., 2018). This resulted in a limited research on regression ML models that may be able to anticipate gait movements before its occurrence. Predicting the future motion trajectories has the potential to anticipate human movements and give more room to take action. This includes balance control (Fuschillo, Bagalà, Chiari, & Cappello, 2012), falls prevention (R. K. Begg et al., 2014; Nait Aicha, Englebienne, van Schooten, Pijnappels, & Kröse, 2018), Internet of Things (IoT) (X. Tao & Yun, 2017), robotics (Rudenko, Palmieri, Lilienthal, & Arras, 2018) and human- machine (i.e. assistive devices) interaction (G. Lee et al., 2017). Assistive devices in particular (i.e. exoskeletons, prosthetics, etc.) are highly coupled to the human body and hence, its operation

needs to be constantly compliant and flexible with human intention (C.-y. Zhao et al., 2012). There exist dynamic differences between these devices and the user. Differences including the nonlinear kinematics and kinetics that may result in an inaccurate movement synchronization and an unnatural interaction between the user and the device (Rupal et al., 2017; Torricelli et al., 2018). Such issues necessitate the need to synchronise wearable function with user intention as many lower limb assistive devices reported in current literature have limited capability to predict the user movements (Akyildiz, Su, Sankarasubramaniam, & Cayirci, 2002). A known future lower limb movements add a feedforward term to an assistive device controller rather than being re-active and predominantly rely on feedback terms (i.e. sensory information) (Shafiul Hasan et al., 2020; Tanghe, De Groote, Lefeber, De Schutter, & Aertbeliën, 2019).

Given the potential of lower limb movement prediction, no previous work was found that utilised ML techniques to predict the future lower limb trajectories based on simulated IMU data. The utilisation of simulated IMU data such as the kinematics output from wearable IMU sensors (i.e. LA and AV) have brought promising results and may offer the opportunity to transcend predictive ML models outside the laboratory settings (De Brabandere et al., 2020; Preatoni et al., 2020). The objective of this research is to investigate ML models that are satisfactory to predict the future lower limb trajectories at various walking speeds.

## **1.6 Research aims**

The overall aim of this research is to predict lower limb trajectories in walking based on simulated IMU data modelled with ML algorithms. The structure of this thesis research is demonstrated in **Figure 1-4**. The specific research objectives are:

1. To investigate the possibility of predicting the future lower limb kinematics with ML and a statistical model at an imposed walking speed (Study 1).
2. To develop and generalise ML models and a statistical model to be able to predict the future lower limb kinematics at a preferred walking speed (Study 2).
3. To finalise and observe the effects of speed variation on the developed models' performance (Study 3).

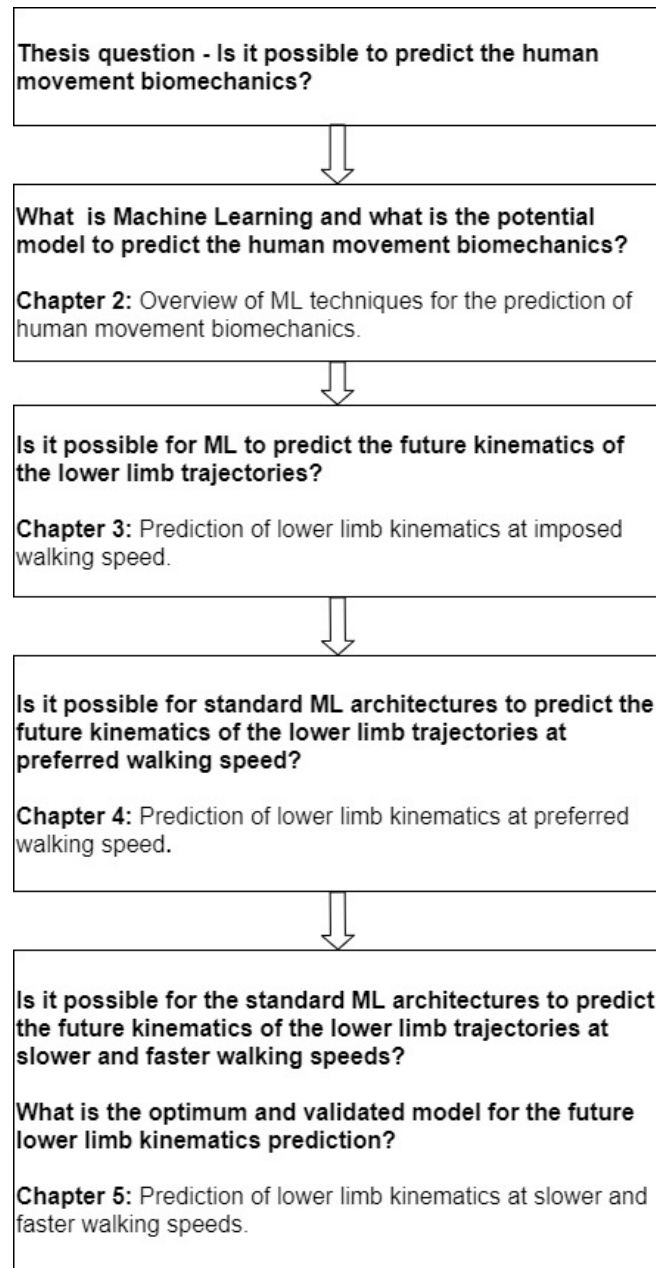


**Figure 1-4:** Schematic diagram of the research questions addressed in this thesis.

## 1.7 Significance

The prediction of future lower limb trajectories based on historical gait trajectories could have a profound impact on the human movement science. There is an emerging need to synchronize wearable function with user intention due to engagement delays found in assistive devices controller operation (Elliott et al., 2014; Shamaei, Napolitano, & Dollar, 2013). A known future lower limb trajectories add a feedforward term to an assistive device controller rather than being re-active and predominantly rely on feedback terms (i.e. sensory information)

(Shafiul Hasan et al., 2020; Tanghe et al., 2019). This enables the assistive device (i.e. exoskeleton, prosthesis) to adapt its controlling parameters according to changes in the human gait, allowing smoother synchronization with user intentions and minimize interruptions when the user changes their movement pattern (Ding, Kim, Kuindersma, & Walsh, 2018; Elliott et al., 2014; Zaroug et al., 2019; J. Zhang et al., 2017). An example of that is when the assistive device smoothly aligns its controlling modes with the ankle angle between the stance and the swing phase. The ankle joint is required to deliver higher torques in the stance phase to lift the human body and the assistive device. It is essential for the assistive device to smoothly deliver torque changes for each controlling mode rather than discrete torque adjustments (i.e. swing vs. stance). This necessitate the availability of future trajectories to smoothly regulate the device controlling parameters and deliver seamless transitions between gait phases.

Falling accounts for 9.7% of hospital emergency attendance in the state of Victoria, Australia (Cox, Roggenkamp, Bernard, & Smith, 2018; Rowbotham & Blau, 2017). More than 50% of falling incidents are due to tripping while walking in healthy older adults (Santhiranayagam, Lai, Sparrow, & Begg, 2015). A leading cause of falls is tripping and the Minimum Toe Clearance (MTC) is a critical tripping risk feature (Gillain et al., 2019; D. T. Lai, Shilton, Charry, Begg, & Palaniswami, 2009; Santhiranayagam et al., 2015). The MTC describes the minimum toe height during the mid-swing phase (Caldas, Mundt, Potthast, de Lima Neto, & Markert, 2017). A known future foot trajectory based on historical gait trajectory might assist in monitoring the MTC to minimise the risk of balance loss, tripping and falling. The MTC could be addressed early on time with volitional countermeasures such as slowing down or stopping and impending incidents can be remotely reported for early interventions (R. Begg, Best, Dell'Oro, & Taylor, 2007; R. Begg & Kamruzzaman, 2006; Hemmatpour, Ferrero, Montrucchio, & Rebaudengo, 2019; Naghavi, Miller, & Wade, 2019; Nait Aicha et al., 2018).

## **2 CHAPTER TWO: OVERVIEW OF ML TECHNIQUES FOR THE PREDICTION OF HUMAN MOVEMENT BIOMECHANICS**

### **2.1 Overview**

Biomechanics laboratory experiments, clinical gait assessments and wearable sensors are exponentially creating human movement data more than before. In order to capture the growth in volume and the dimensionality of the collected data, ML techniques are rapidly complementing traditional statistical methods to better recognise and analyse the human movements. This chapter briefly surveys ML techniques that have been widely implemented across biomechanics research for classification and regression tasks. The review indicated that sequential ML algorithms such as the Recurrent Neural Networks (RNN) architectures are reliable to model time series data such as the kinematics and kinetics of the human locomotion. Regression ML tasks were found to be the least investigated in biomechanics research which might be a powerful tool to improve powered assistive technologies and mitigate the risk of falls or balance loss. Part of this chapter was published as a book chapter in Computational Intelligence (CI) Techniques for Powered Exoskeletons, pp 353-383 (Zaroug et al., 2019).

### **2.2 Predictive modelling and statistical learning**

Predictive modelling is an approach that is highly focused on developing models to attain the most possible accurate predictions on a yet to be seen dataset (Kuhn & Johnson, 2013). It carries associations with pattern recognition, data mining and ML which are the integral process of predictive modelling. However, it slightly disregards the broader objective of ML (establishing computer based learning tools) and statistics (understanding data) and concerns it-self on making the minimum error with some degree of model skill measurement.

On the other hand, the statistics equivalent of predictive modelling is called the statistical learning where the focus on model interpretability outweighs the model skill behaviour. Statistical learning is a subfield of applied statistics where the emphasis is to apply statistical tools to model and understand complex datasets (Gareth, Daniela, Trevor, & Robert, 2013). In the statistics course by Rob Tibshirani, common terms used in the field of statistics and ML are mapped together in **Table 2-1** (Rob Tibshirani, 2018).

**Table 2-1:** Glossary maps common terms used in the field of ML and statistics.

| <b>Glossary</b>       |                                |
|-----------------------|--------------------------------|
| <b>ML</b>             | <b>Statistics</b>              |
| Network, graphs       | model                          |
| weights               | parameters                     |
| learning              | fitting                        |
| generalization        | test set performance           |
| supervised learning   | regression/classification      |
| unsupervised learning | density estimation, clustering |

### 2.3 Machine Learning (ML)

Gait data representation tends to be enormous in size and variability which may be tedious to understand and categorise. ML algorithms are able to learn from past and present motions and adapt to the environment, regardless of human interventions (Mason, Traoré, & Woungang, 2016). Each algorithm has a different method of learning such as Support Vector Machines (SVM) (R. Begg & Kamruzzaman, 2005), decision trees (M.-C. Su, Chen, Wang, Tew, & Huang, 2000), Linear Regression (LR) (T. H. Lee, Tsuchida, Kitahara, & Moriya, 1999) and neural nets (Paluszek & Thomas, 2017). **Figure 2-1** shows the design process of a typical ML model framework. The major elements amongst ML models are the datasets, features selection, model selection and evaluation.

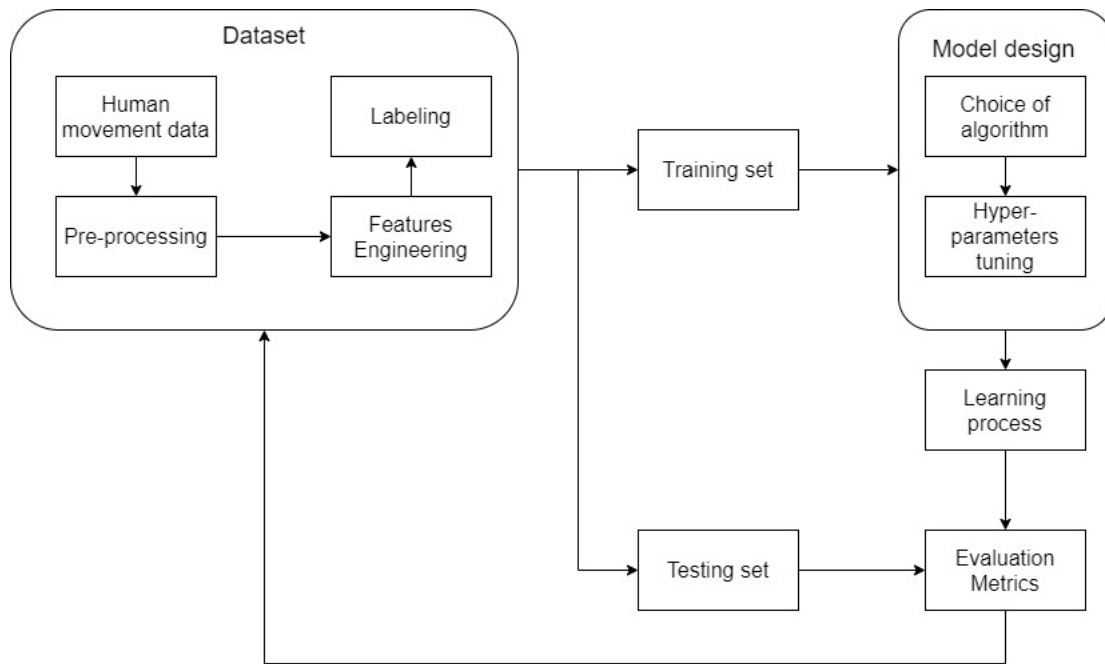


**Figure 2-1:** General ML design process (Mason et al., 2016).

### 2.3.1 Dataset

The Datasets are the starting point or the input to the ML model. The datasets are predominantly divided into two types; the training and the testing datasets. The training dataset is a correctly labelled data required to train and teach the algorithm how to obtain the correct predictions. The testing dataset is a correctly labelled data used to evaluate the ML algorithm skill in obtaining the correct labels and to approximate the algorithm error rate. Due to the irregularity or sometimes deficiency in datasets, this step might require a pre-processing afore getting into the learning algorithm, such as data normalization (Karvanen, 2003), scaling and cleaning (Chapman, 2005).

### 2.3.2 Features Engineering

Features engineering is considered a pre-processing step or a sub-algorithm computed within the ML model such as the Principal Component Analysis (PCA) (Isabelle, 2006; Witte, Ganter, Baumgart, & Peham, 2010). The PCA is a multivariate statistical technique developed by Hotelling (Hotelling, 1933) and it was proven effective in analysing large datasets of kinematic and kinetic waveform patterns to identify features that could potentially be highly relevant to the movement task (Astphen & Deluzio, 2005; Deluzio, Wyss, Zee, Costigan, & Serbie, 1997; Hubley-Kozey & Vezina, 2002). The PCA was found to be objectively

identifying discrete parameters such as peaks or ranges in a signal to facilitate comparisons between biomechanical variables (Chau, 2001).

The objective of features engineering is to clear the dataset from any redundant or irrelevant information. Therefore, it largely contributes to the accuracy of the learning model. It is beneficial in the case where the data size is multidimensional. It also expedites the process of learning because it allows the only important features to be considered (Bishop, 2006). However, precautions must be taken as crucial information might be discarded if poor features engineering is performed. Features engineering can be divided into two main techniques; Feature selection and feature extraction (Phinyomark et al., 2018). Features Selection aims at searching for the most relevant input features and minimizing features redundancy using filter and wrapper methods (Bishop, 2006; Isabelle, 2006). Filter methods uses similarity or distance measurements such as the t-tests, chi-squared (Manning, Raghavan, & Schütze, 2008) or the effect size (Potdevin, Femery, Decatoire, & Bosquet, 2007). While wrapper methods evaluates each feature with a cross-validation approach using a particular classifier such as the Linear Discriminant Analysis (LDA) (D.-X. Liu, Wu, Du, Wang, & Xu, 2016) and the SVM (R. K. Fukuchi, Eskofier, Duarte, & Ferber, 2011). On the other hand, a feature extractor works by transforming the original input feature space into a lower-dimensional feature space such as the PCA (Isabelle, 2006; Witte et al., 2010).

Feature selection should not be conflated with dimensionality reduction methods. Albeit, it seems counter-intuitive to discriminate between both terms, feature selection ultimately leads to reduction in data dimension. In dimensionality reduction, the goal is to build new combination of attributes or features and therefore it includes transformational techniques (Japkowicz & Shah, 2011). However, feature selection methods add or discard attributes without changing them, this means that it preserves the original-axis of this information (Guyon & Elisseeff, 2003). Common dimensionality reduction techniques are; the PCA and Linear Discriminant Analysis (LDA).

### **2.3.3 The learning process**

The learning model is the mathematical framework for the selected learning algorithm (Paluszek & Thomas, 2017). The model selection largely depends on the model that offers the best description or prediction for the presented data (Guyon, Saffari, Dror, & Cawley, 2010). It is how the algorithm models the problem and generates a classifier or a regression method.

A classifier (see **Figure 2-2**) is defined as a system that takes a vector of feature values and generates a single output vector. For example, in the following training set D:

$$D = \{d_1 = (x_1, y_1), d_2 = (x_2, y_2) \dots, d_n = (x_n, y_n)\} \quad (2 - 1)$$

The ML system then tries to find out the best possible mapping function between the input ( $x_k$ ), and its corresponding output ( $y_k$ ), until it reaches generalisation.

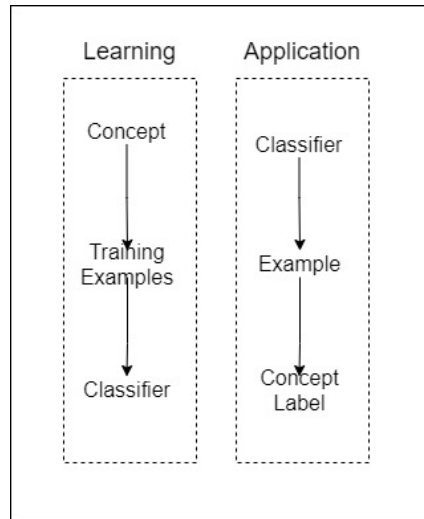


**Figure 2-2:** Classifier development (Kubat, 2015).

There are numerous ML models in the literature (Witten, Frank, Hall, & Pal, 2016). Nonetheless, the way they have been grouped is distinctive among authors. For example in (Mason et al., 2016), algorithms have been classified according to their mathematical model; learning style algorithms (e.g. supervised learning), algorithms that classify data based on similarities (e.g. LDA), and other measures. However, in (Paluszek & Thomas, 2017), and (Bishop, 2006), algorithms were classified according to their interaction with the input data; supervised learning, unsupervised learning, and reinforcement learning. In supervised learning, the machine is presented with a set of input vectors along with its corresponding output/outcome vectors which are referred to as labelled training data. The machine is directly told which outputs are true for each set of inputs. However, for the unsupervised learning, there are no set of target values for each set of input vectors. The machine is not told what the correct answer is and is set to discover patterns in data and to group each similar data point using clustering techniques.

Reinforcement learning is a decision-making problem where the machine tries to seek out the appropriate actions in a given situation. The goal here is to get the most out of a reward, which is essentially a feedback mechanism or rather the reinforcement of the learning process (Wiering & Van Otterlo, 2012). Typically, the machine interacts with its environment by forming a sequential state, and all the past and current states have a direct impact on the reward. Consequently, the machine keeps on amending its learning model.

### **2.3.3.1 Classification and regression problems**

In supervised learning the answers are known and the algorithm repeatedly makes predictions on the training data. Predictions are corrected when error updates are performed. Supervised learning can further be grouped into classification and regression problems (LeCun, Bengio, & Hinton, 2015). In classification problems, the algorithm is taught to predict a categorical output or a label such as normal or abnormal (i.e. Parkinsonian) gait (Ricciardi et al., 2019). While in regression, the algorithm is taught to predict a value such as the knee angle (Luu, Low, Qu, Lim, & Hoon, 2014). The value can be a future value (Tanghe et al., 2019) or a value that corresponds to certain movement dynamics (Findlow, Goulermas, Nester, Howard, & Kenney, 2008).

### **2.3.4 Evaluation**

The purpose of this step varies according to the performance criteria. The common goal however is to measure the model performance or what has been learned from the training dataset (Kubat, 2015; Witten et al., 2016). Other goals are to compare different learning algorithms against different classifiers on a specific problem, compare different classifiers within the same learning algorithm, or to create a set of generic classifiers for a specific problem (Bishop, 2006). The evaluation stage is an estimate of how well the model performs over the testing dataset. Commonly implemented statistical approaches are the resampling techniques, in which a population parameter is estimated from an available data (Good, 2006). The most basic resampling approach is the train-test splits, where the original dataset is split into training and testing datasets. This testing dataset can be part of the training data (intra-subject) or an unseen (inter-subject) dataset (**Figure 2-1**). Other more accurate approaches include; *k*-fold cross-validation, leave one out cross-validation and repeated random test-train splits (Brownlee, 2014; Salvador et al., 2017).

The selection of performance metrics is largely dependent on the ML task; classification or regression. Common metrics for classification task are; accuracy, logarithmic

loss, confusion matrix, sensitivity and specificity analysis, F score, Receiver Operating Characteristic (ROC) curve and the Area Under the ROC curve (AUC) (Fawcett, 2006; Kubat, 2015; Sokolova & Lapalme, 2009). Regression metrics are generally; Mean Absolute Error (MAE), Mean Squared Error (MSE) and  $R^2$  (Botchkarev, 2018).

### 2.3.5 Parametric and non-parametric ML algorithms

Based on the assumptions made during the learning process, ML algorithms can be classified into parametric and non-parametric algorithms. Parametric algorithms simplify the problem with a set of fixed parameters learned from the training data. The number of parameters within the mapping function cannot be changed. Therefore they are easier to understand and interpret their results, faster to learn and require less data to optimise. However, they have limited functional form and learning complexity. Examples of parametric models include; Logistic Regression (LR), LDA and the Perceptron.

On the other hand, non-parametric algorithms build loose assumptions during the learning process and therefore, they are free to learn any functional form. They are flexible (easier to generalise), capable of learning large set of features and able to produce higher performance models for prediction. However, they require larger set of data to optimise, slower to train and highly vulnerable to the overfitting problem. Examples of non-parametric models include; Artificial Neural Networks (ANN), Support Vector Machines (SVM), Naïve Bayes (NB) and the Classification and Regression Trees (CART) also called Decision Trees (Brownlee, 2019).

## 2.4 ML models for the human movement prediction

### 2.4.1 Linear Regression (LR)

The LR (i.e. also called Linear Basis Function) is one of the most well studied models in statistics and ML due to its existence for more than 200 years (Bishop, 2006; Brownlee, 2019). It basically assumes a linear relationship between the input (independent) variable ( $x$ ) and the output (dependent) variable ( $y$ ). When there is a single input attribute ( $x$ ) it is called a Simple LR and when there are multiple input variables  $x = (x_1, \dots, x_D)^T$  it is referred to as Multiple LR. The most basic expression of LR is the linear combination of input variables:

$$y(x, w) = w_0 + w_1x_1 + \dots + w_Dx_D \quad (2 - 2)$$

The unknown coefficients  $w_0, \dots, w_D$  are the training parameters of the LR model, commonly estimated using Ordinary Least Squares or the Gradient Descent (Bishop, 2006; Draper & Smith, 1998). Other methods for training the linear model are called regularisation methods, in which the squared error is minimised while the complexity of the model is reduced (i.e. number of coefficients). Popular regularization methods are the Lasso Regression (L1 regularisation) (Robert Tibshirani, 1996) and the Ridge Regression (L2 regularisation) (Hoerl & Kennard, 1970) which is known as weight decay in the context of neural networks (Bishop, 2006).

Major uses of LR was to predict gait signals (i.e. ground reaction force) based on the effect other gait features (i.e. walking speed) and determine the strength (i.e. collinearity) of a gait feature. For the first application, the LR was utilised as a method to predict the gait kinematics and kinetics from highly correlated gait parameters such as the walking speed (Chehab et al., 2017). Using the LR, sagittal plane joint angles for the hip, knee and ankle were reconstructed based on walking speed, gender, age and body mass index, and it achieved a root mean square of  $0.78 \pm 0.48^\circ$ ,  $0.86 \pm 0.78^\circ$ , and  $1.48 \pm 0.91^\circ$  for each of the joints respectively (Moissenet, Leboeuf, & Armand, 2019). Similar work was published by Fukuchi and Duarte in which the gait speed was found to be the reference to predict sagittal angles and moments for the lower limb joints (Claudiane A Fukuchi & Duarte, 2019).

For the second application, the LR was predominantly implemented to check for high collinearity amongst gait independent variables by finding the least room mean square error for all independent variables (Mikos et al., 2018). The resulting model can then be used as a normalisation technique to de-correlate anthropometric measurements from gait data (Wahid et al., 2016). Slow walking speeds were found linearly correlated to stride-length, step-length and step-frequency using LR  $R^2$  drop below 0.9 (Smith & Lemaire, 2018).

Limitations of the LR include:

1. High sensitivity to outliers, which impedes interpretability of output coefficients.
2. Assumes a linear relationship between dependent and independent variables.
3. Considers the mean as the dominant description of dependent and independent variables.

## 2.4.2 Logistic Regression

The theoretical underpinning principle in which logistic regression operates is the natural logarithm on odds ratio (Peng, Lee, & Ingersoll, 2002). The odds ratio can be used to identify the relationship between certain gait features (Punt et al., 2016). The logistic regression is a linear classification method that is mostly used to classify dichotomous (i.e. binary) or sometimes polytomous outcome classes based on the logistic function or the sigmoid function (Kleinbaum, Dietz, Gail, Klein, & Klein, 2002). The logistic regression takes any real number and maps it into a real value between 0 and 1 (see **Figure 2-3**). The logistic regression can be expressed as follows (Peng et al., 2002):

$$P(y = 1 | x_1, x_2, \dots, x_k) = P(X) = \frac{1}{1 + e^{-(\beta_0 + \sum \beta_i x_i)}} \quad (2-3)$$

Where  $P(X)$  is the probability of a binary class  $y = 0$  or  $1$  given the independent variables (i.e. age)  $x_1$  to  $x_k$  measured from a group of participants at time  $T_0$ . The Euler's number  $e$  is the base of the natural logarithm and  $\beta_0, \dots, \beta_i$  are the constant coefficients estimated using a Maximum-Likelihood algorithm such as the Stochastic Gradient Descent (SGD) or the Quasi-newton method (Bottou, 2010; Schraudolph, Yu, & Günter, 2007).

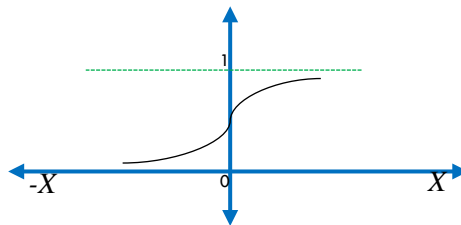


**Figure 2-3:** The logistic function.

Using the logistic regression it was found that increments in step lengths and decrements in cadence are highly associated with slip severity (Moyer, Chambers, Redfern, & Cham, 2006). Based on step time as well as step lengths, logistic regression was able to accurately classify 89.8% of trip outcomes (Pavol, Owings, Foley, & Grabiner, 1999). Participants with and without the Parkinson's disease were detected using logistic regression based on 16 gait characteristics (Rehman et al., 2019). In multiclass classification problems, multivariate logistic regression was able to classify 4 stages of dementia (i.e. cognitive status) using spatio-temporal gait parameters at 89% classification rate (De Cock et al., 2017).

Major limitations of logistic regression are the assumptions about the input/output data. The logistic regression assumes the following (Kleinbaum et al., 2002; Peng et al., 2002):

1. The relationship between the input and output variables is linear.
2. No error in the output variable or the class outcome.
3. The logistic regression model can easily overfit if there are many highly correlated input variables. Highly correlated variables could also result in a model that fails to converge.

### 2.4.3 Fisher's Discriminant Analysis (FDA)

The FDA also known as Linear Discriminant Analysis (LDA) is a multi-class classifier that searches for the maximum statistical differences between classes by creating the best linear combination of independent features (Fisher, 1936). The LDA evaluates the average  $mean_k$  value of each measurement ( $x$ ) for each class ( $k$ ) as well as the variance  $sigma^2$  across all measurements ( $x$ ) for the class ( $k$ ) (Fukunaga, 2013). Then it minimizes the measurements within a class and maximizes measurements between classes (Martínez & Kak, 2001). Based on Bayes theorem as well as the Gaussian distribution function (Bishop, 2006), the discriminant function is given as (Brownlee, 2019):

$$D_k(x) = x * \frac{mean_k}{sigma^2} - \frac{mean_k^2}{2*sigma^2} + \ln(P(k)) \quad (2 - 4)$$

Where  $D_k(x)$  is the discriminant function for class  $k$  given measurement  $x$  and  $P(k)$  is the probability of class  $k$ . The  $\ln()$  function is the natural logarithm.

In human movement research, the LDA was implemented as a movement classifier (Chavarriaga et al., 2013) as well as a feature extraction technique (J. Han & Bhanu, 2005). In feature related problems, LDA assisted in transforming the original dataset into subsets that carry the most discriminative features (Boulgouris & Chi, 2007). The distances between 4 lower limb joint angles measured with an active exoskeleton were adjusted based on LDA afore feeding it into an ANN model for gait phase recognition (D.-X. Liu et al., 2016). In classification problems, LDA was able to classify 7 walking modes in transtibial amputee and non-amputee participants from myoelectric signals and achieved a classification rate between 97.9% to 94.7% respectively (Miller, Beazer, & Hahn, 2013). Among 23 participants, LDA was able to classify up to 92.5% loaded (12.5kg) versus unloaded conditions based on 6 lower limb kinematics such as the range of motions (M. Lee, Roan, Smith, & Lockhart, 2009).

The LDA may not perform well on problems that are complex or linearly non-separable (R. Begg & Kamruzzaman, 2006). The LDA highly relies on descriptive statistics (i.e. mean and variance) to discriminate between classes in the feature space. This made LDA quite limited to Gaussian-looking data and sensitive to the outliers which can easily skew the independent variables. Data standardisation maybe need due LDA's assumption that all input variables have the same variance. Nonetheless, LDA is a well understood classification method and it was extended to Quadratic Discriminant Analysis, Flexible Discriminant Analysis and Regularised Discriminant Analysis (Brownlee, 2019).

#### 2.4.4 Hidden Markov Model (HMM)

The generation of natural analogue signals (e.g. speech samples, measured temperatures, etc.) can be characterised by signal models (Dugad & Desai, 1996). The most commonly used signal models are statistical models that are generally classified into deterministic models as well as stochastic models. For deterministic models, the model's behavioural properties are known, such as sine wave and exponential function. However, in stochastic models the signal's behaviour is inconsistent. Hidden Markov Model (HMM) is a double stochastic process in which the first process (hidden) is the Markov property which describes how the system may transition from one state to another. The second stochastic process (observable) gives the statistical description of the emissions from each state (the sensor readings or the feature vectors constructed from them), in terms of either discrete probabilities or continuous probabilities represented in Probability Density Functions (PDFs) (Dugad & Desai, 1996; Fink, 2014).

A stochastic process can be represented as a sequence of random variables

$$S = (S_1, S_2, \dots, S_N) \quad (2 - 5)$$

from a discrete or continuous domains (Fink, 2014). Markov chain is a type of stochastic modelling. It defines a series of random variables, in which the current state depends on the past states. The HMM is a double stochastic process in which the first process (hidden) is the Markov property which describes how the system may transition from one state to another. The second stochastic process (observable) gives the statistical description of the emissions from each state (the sensor readings or the feature vectors constructed from them), in terms of either discrete probabilities or continuous probabilities represented in PDFs (Dugad & Desai, 1996; Fink, 2014).

Major elements of HMM includes the following (Ching, Huang, Ng, & Siu, 2013; Dugad & Desai, 1996; Fink, 2014):

1.  $N$ , is the number of hidden states in the model (e.q. 2). However, The actual state at time  $t$  is denoted as  $q_t$ , where  $t = 1, 2, \dots$
2.  $M$ , is the number of distinct observation symbol for each hidden states. Denoted as follows:

$$V = (v_1, v_2, \dots, v_M) \quad (2-6)$$

and the actual state at time  $t$  is denoted as  $O_t$

3.  $A = (a_{ij})$ , is the state transition probability matrix, where:

$$a_{ij} = P(q_{t+1} = s_i | q_t = s_j) \quad 1 \leq i, j \leq N \quad (2-7)$$

4.  $B = (b_j(v_k))$ , is the probability distribution of an observable hidden state  $j$ , where:

$$b_j(v_k) = P(O_t = v_k | q_t = s_j), \quad 1 \leq j \leq N, 1 \leq k \leq M \quad (2-8)$$

5.  $\pi = (\pi_i)$ , is the initial state distribution, where:

$$\pi_i = P(Q_1 = s_i), \quad 1 \leq i \leq N \quad (2-9)$$

Given the appropriate values of  $N$ ,  $M$ ,  $A$ ,  $B$  and  $\pi$ , the HMM can be used as a generator to give an observation sequence

$$O = (O_1 O_2 O_3 \dots O_T) \quad (2-10)$$

Where,  $T$  is the number of observation in the sequence, and for simplicity, the following is the compact notation

$$\lambda = (A, B, \pi) \quad (2-11)$$

There are a number of other algorithms associated with HMM, that are concerned with computing the parameters mentioned in **2 – 11**:

1. The forward-backward algorithm (Jurafsky & Martin, 2014), which efficiently computes the observation sequence probability,  $O = (O_1 O_2 O_3 \dots O_T)$ .

2. The Viterbi algorithm (Jurafsky & Martin, 2014), which finds the optimal state sequence  $Q = (Q_1, Q_2, \dots, Q_T)$  within the hidden part, given the observation sequence in 1.
3. The Expectation Maximisation (EM) technique (Bishop, 2006) or the Baum-Welch algorithm (Dugad & Desai, 1996), which obtain the maximum probabilities for the model parameters  $\lambda$ .

The HMM has been implemented in the recognition of human physical activities, which became attractive in the area of healthcare monitoring (Mannini & Sabatini, 2010) and other applications such as bioinformatics (Yoon, 2009) and gesture recognition (Wilson & Bobick, 1999). It is a valid tool for gait analysis as well as gait events detection. It has also been compared against other basic algorithms (e.g. threshold, rule-based), and it is found to be having great performance (Goršič et al., 2014). In the area of wearable robotics, exoskeletons and biomechanics there have been few studies to implement HMM within gait phase detection using data obtained from wearable sensors. The HMM was able to discriminate between two pathological gaits in typical developing children as well as children suffering from Hemiplegia (Abaid et al., 2013). It was trained using a single-axis gyroscope embedded within an IMU on each foot HMM. Results were compared against FSR mounted on the foot and the algorithm found to be producing high sensitivity as well as specificity results. Additionally, two HMMs were used to detect gait phases as well as walking and jogging activities, using gyroscopic data obtained from an IMU mounted on the navicular space of the left foot (Mannini & Sabatini, 2012). In which, HMM outperformed threshold results obtaining more than 94% and 98% for specificity and sensitivity analysis respectively, which is a good generalisation. Using data from shoe insoles HMM achieved 96% success on walking phase detection in Crea *et al.* (Crea et al., 2012). A novel HMM distributed classifier based on hierarchical weighted decision and the results showed high specificity and sensitivity values of more than 0.98 (Banos et al., 2013; Taborri, Rossi, Palermo, Patanè, & Cappa, 2014). The HMM was also implemented in prosthetic devices. For example, the HMM was able to detect different steady-state gait phases of amputee walking using data acquired from seven IMUs mounted on different body segments (Goršič et al., 2014). The HMM performance was compared to a rule-based algorithm, and the results were approximately 97% success rate. For the upper extremities, an average accuracy of 94.63% is attained using HMM using data from EMGs to classify six different static limb motions; hand open and close, pronation, supination, wrist flexion and extension (A. D. Chan & Englehart, 2005).

### 2.4.5 Gaussian Mixture Model (GMM)

The GMM is a probabilistic density function characterized as a weighted sum of  $M$  component Gaussian densities (McLachlan & Peel, 2004; Reynolds, 2009), given by:

$$p(x|\lambda) = \sum_{i=1}^M \omega_i g(x|u_i, \Sigma_i) \quad (2-12)$$

$$g(x|u_i, \Sigma_i) = \frac{1}{(2\pi)^{D/2} |\Sigma_i|^{1/2}} \exp\left\{-\frac{1}{2}(x - \mu_i)' \Sigma_i^{-1}(x - \mu_i)\right\} \quad (2-13)$$

$$\lambda = \{\omega_i, \mu_i, \Sigma_i\} \quad i = 1, \dots, M. \quad (2-14)$$

Where  $x$  is the D-dimensional gait features,  $\omega_i$  is the mixture weights which should satisfy the condition that  $\sum_i^M \omega_i = 1$ .  $u_i$  is the mean vector,  $\Sigma_i$  is the covariance matrix,  $g(x|u_i, \Sigma_i)$  are the Gaussian component densities. Overall, the GMM is a parametric model characterised by the notation  $\lambda$  which is the combination of feature vector means ( $\mu_i$ ), the covariance matrices ( $\Sigma_i$ ) and the mixture weights ( $\omega_i$ ) (Reynolds, 2009).

The GMM applications include; forecast verification (Lakshmanan & Kain, 2010), market studies (M.-H. Zhang & Cheng, 2003), physics (Stepanek, Kus, & Franc, 2015), robotics (S. Park, Mustafa, & Shimada, 2013), and biomechanics (Allen, Ambikairajah, Lovell, & Celler, 2006; Vögele, Zsoldos, Krüger, & Licka, 2016). In Allen *et al.* (Allen et al., 2006), the GMM was used along with Bayesian adaptation to compensate for subject specific training (see **Figure 2-4**) in recognition of three postures (sitting, standing and lying) as well as five physical movements (sit to stand, stand to sit, lie to stand, stand to lie and walking). Thirty-two GMMs were trained from multiple users for each movement type using the EM algorithm, and then adopted to specific participants using the bayesian adaptation. Data was self-collected at home (unsupervised pilot study) using a tri axial accelerometer from six healthy users, and it was divided into approximately 60-40% as a training and testing sets.

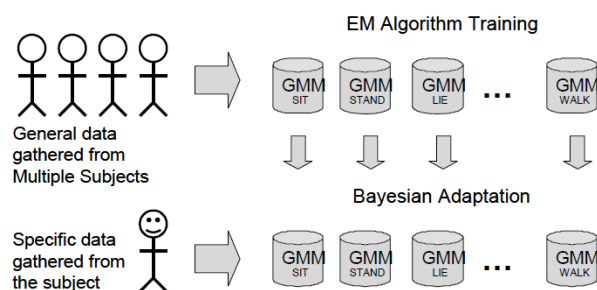


**Figure 2-4:** GMM adaptation method (Allen et al., 2006).

Adopting GMM improved the classification accuracy of time domain features (92.2%), which obtained better performance compared to frequency domain features (79.2%). However, as there was a single accelerometer there was challenges in distinguishing between sitting and standing. Also in Papavasileiou, (Papavasileiou, Zhang, & Han, 2016), Infinite GMM (IGMM) was fused with a Parallel Practile Filter in order to attain real-time gait phase recognition, which is a vital tool for patients to identify their walking patterns and update the parameters used for clinical rehabilitation. Hence, the IGMM was used to classify walking gait phases based on ground contact forces acquired from a barometric sensor, while model parameters were estimated and updated using the PPF. With the aid of a proportional-integral-deferential controller, a sparse Gaussian Process (GP) is used in (Long, Du, Dong, & Wang, 2017) to learn the human trajectory through torque sensors installed on the knee joint. The study aimed at improving the human-robot interaction mechanism by allowing the exoskeleton to track the joints angular motion. Data was collected while wearing the exoskeleton without operating the hydraulic actuators and then analysed offline using MATLAB. Results suggested the possibility of using GMM in intention recognition with physical HRI. For the upper extremity an implementation of both HMM and GMM (obtaining emission probabilities) was reported in (Siu, Shah, & Stirling, 2016) for object “grasp” and “release” tasks, using data from EMGs instrumented in a band around the forearm as well as a motion capture system. A comparison result between n-gram HMM and GMM with a different number of mixture components based on inter-subject training and testing yielded mean accuracy of 75.96% with 5 mixtures attained using the unigram (i.e. a single sequence) HMM.

#### **2.4.6 Support Vector Machines (SVM)**

The SVM also called support-vector network is a supervised learning method proposed by Vapnik and colleagues in 1995 (Cortes & Vapnik, 1995; Vapnik, 2013). The SVM is perhaps the most popular tool for pattern recognition and to solve classification, clustering and recently regression (i.e. support-vector regression) problems. Given its simplicity and easy implementation it requires few parameters to be tuned and it provides good generalisation in many data classification problems (Le Borgne & O’Connor, 2005). The SVM function can be explained over 3 major concepts; the maximum margin hyperplane, the soft margin classifier and the kernel function (Noble, 2006). The maximum margin hyperplane is a linear classifier (**Figure 2-5**) that can be described as a straight line selected to best separate two gait features  $X_1$  and  $X_2$  as:  $B_0 + (B_1 * X_1) + (B_2 * X_2) = 0$ . Where the intercept  $B_0$  and the coefficients  $B_1$  and  $B_2$  determine the slope of the line and can be optimised with the sub-gradient descent or

with quadratic programming such as the sequential minimal optimisation (Platt, 1998; Tobias, 1995). The soft margin classifier however extends the SVM to classify non-linearly separable data points. The soft margin relaxes the conditions of the maximum margin hyperplane and allows some of the feature points to violate the separating line (Noble, 2006). The complexity of the model is increased and a tuning variable  $C$  is introduced to define the amount of violation allowed (Mangasarian, 1998; Noble, 2006). The kernel function is a mathematical trick that basically extends the feature space from low-dimensional to highly dimensional space. The kernel function can be divided into 3 major classes: (1) the linear kernel, (2) the polynomial kernel and (2) the radial kernel (Cortes & Vapnik, 1995).

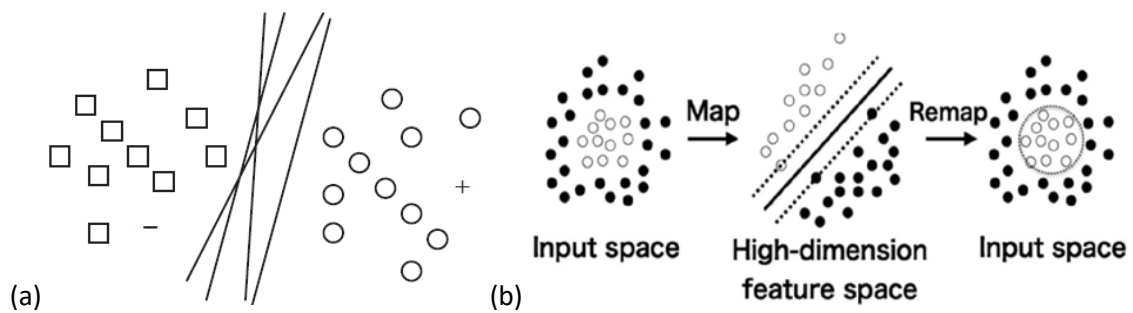


**Figure 2-5:** Linear (a) and non-linear (b) SVM to find optimum possible planes to divide the data into two classes (R. Begg & Kamruzzaman, 2005; Nakano et al., 2016).

In gait analysis, the SVM has been widely adopted for binary classification problems (R. Begg & Kamruzzaman, 2005; R. K. Begg, Palaniswami, & Owen, 2005; Nakano et al., 2016), where it finds the optimal separating hyperplane (see **Figure 2-5**). There are a number of applications where SVM is found to be contributing, amongst those are; face detection (Jee, Lee, & Pan, 2004), text recognition (Rajnoha, Burget, & Dutta, 2017), protein classification (Cai, Han, Ji, Chen, & Chen, 2003), and gait recognition (R. Begg & Kamruzzaman, 2005; R. K. Begg et al., 2005; X. Liu, Zhou, Mai, & Wang, 2017; Nukala et al., 2014; Yoo, Hwang, & Nixon, 2005).

In (Nakano et al., 2016), four types of SVM were used including; Linear SVM, Quadratic SVM, Cubic SVM, and Gaussian SVM to differentiate walking patterns between normal and patient users, using data obtained from a custom designed wireless gait sensor installed on 7 users (3 normal and 4 patients). The wireless gait sensor is a multi-dimensional kit that combines 3 MEMS chips including; a single axis gyroscope, a dual axis gyroscope, and a 3-axis linear accelerometer. Linear, Quadratic, and Cubic SVM obtained high specificity and sensitivity values of 100% and 95.2% respectively, as well as 98% accuracy. While Gaussian attained 87.8% accuracy, 71.7% sensitivity, and 100% specificity. Also in (R. Begg &

Kamruzzaman, 2005), SVM was used to discriminate the walking patterns between elderly and young populations using basic spatial/temporal, kinetic and kinematic data obtained from a force platform as well as a 3D motion analysis system. With gait data obtained from 24 users (12 youths and 12 elderly), results suggested better performance was achieved when combining more than a single type of data. That is, analysing the kinetic data alone obtained up to 83.3% of accuracy, while the combination of kinetic and kinematic data achieved up to 91.7% of accuracy. It was also found that not all features help in improving the classification accuracy. In **Figure 2-6**, only 3 features were required to attain the optimum accuracy and accuracy started to decrease after inclusion of features.

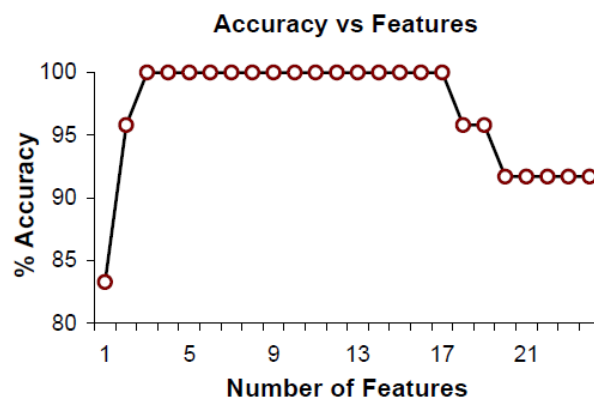


**Figure 2-6:** The classification accuracy of SVM against the number of features in (R. Begg & Kamruzzaman, 2005).

Overall, SVM is a powerful tool for binary discrimination problems, however, it is yet to be applied in active exoskeletons that are generally multiclass problems (Mai, Zhang, & Wang, 2017).

#### 2.4.7 Artificial Neural Networks (ANN)

The ANN is a mathematical model that emulates the structure as well as the function of the biological Neural Networks (Schmidhuber, 2015). The work in Silva et al and Kim provides a comprehensive discussion on the ANN working principles (Da Silva, Spatti, Flauzino, Liboni, & dos Reis Alves, 2017; Kim, 2017). Main architectures of ANN implemented in gait analysis are; the Feedforward Neural Networks (FNN), Recurrent Neural Networks (RNN), Convolutional Neural Network (CNN) and the Self Organizing neural maps (Barton, Lees, Lisboa, & Attfield, 2006; Kaczmarczyk, Wit, Krawczyk, Zaborski, & Piłsudski, 2011; Ordóñez & Roggen, 2016).

Deep learning (DL) is another type of ML and an extension of ANN, with a multiple layer NN (D. Xie, Zhang, & Bai, 2017). The DL ameliorated the deep NN by resolving the problems of back-propagation which are mainly; a vanishing gradient, overfitting, and the computational capacity (Kim, 2017). **Figure 2-7** shows the major elements of an artificial neuron. It is composed of 7 elements as follows:

1. Input signals ( $x_1, x_2, \dots, x_n$ ), are the input data from the environment
2. Synaptic weights ( $w_1, w_2, \dots, w_n$ ), are the inputs' weights which decides the relevance of input data according to the neuron function.
3. Linear aggregator ( $\Sigma$ ), sums up all the weighted input signals and produces the activation voltage.
4. Bias or activation threshold ( $\theta$ ), is a value that's added to sums at each node, they are special weight for the node.
5. Activation potential ( $u$ ), is the difference between the bias and the linear aggregator. It determines the behaviour of the node. If the resultant value is positive  $u \geq \theta$ , then the neuron generates an excitation signal, otherwise it supresses the output.
6. Activation function ( $g$ ), restricts the neuron's output within a reasonable range according to the neuron's function.
7. Output signal ( $y$ ), is the final value generated by the neuron and it can be used as input for other successive neurons.

The general structure of ANN consists of multiple versions of artificial neurons (see **Figure 2-8**). Hence, it forms three major layers:

1. The input layer which receives the input data.
2. The hidden layers which process and classify the data.
3. The output player which obtain the classification result(s).

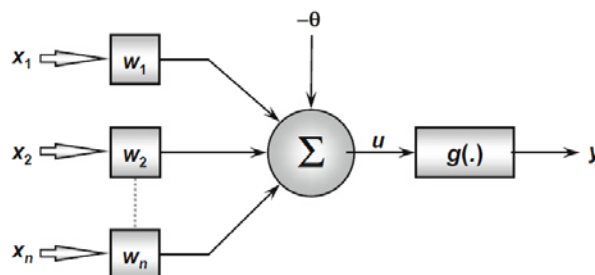


**Figure 2-7:** The architecture of artificial neuron (Da Silva et al., 2017).

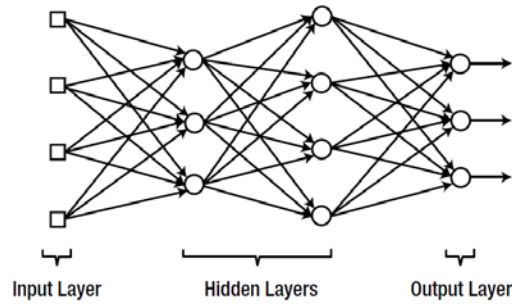


**Figure 2-8:** The general structure of ANN (Kim, 2017).

The first existence of ANN was decades ago. However, the DL appeared recently for a couple of reasons. Firstly, it took 30 years to come up with a learning rule (back-propagation) to solve the problem of a single layer ANN. Secondly, the back-propagation learning rule resulted in a poor performance for the single layer ANN, which is solved few decades later using the DL algorithm. The DL ameliorated the deep ANN by resolving the problems of back-propagation which are mainly; a Vanishing gradient, overfitting, and the computational capacity (Kim, 2017).

To date there is a large opportunity to use ANN for gait analysis. Among these is Jung *et al.* in which multiple layer perceptron (MLP) and the nonlinear autoregressive with external inputs (NARX) were implemented to classify gait phases (stance vs. swing) based on lower limb kinematics measured through the Robin-H exoskeleton (Jung et al., 2015). Results showed that MLP as well as NARX obtained a very similar outcome of approximately 2% error rate. Also, Liu et al validated a gait recognition model for multi-class classification using MLP for lower limb exoskeletons with joint angular sensors (D.-X. Liu et al., 2016). The study classified multiple gait phases in the swing and the stance phase started by dividing the swing phase into the initial, middle and terminal swing phase. The stance phase was divided into the initial contact, loading response, mid-stance, terminal stance, and pre-swing phases. Using cross-validation, MLP showed a correct detection rate for sample points in the training or testing sets of 94.45% and correct detection rate for sample points in a single phase of 87.22%.

The CNN was implemented as a human movement classifier and to extract features (i.e. Heel strike) from raw data (Ordóñez & Roggen, 2016). Gait parameters such as stride length, width and swing time were extracted from IMU data placed on the foot (Hannink et al., 2016) to be used in numerous applications such as monitoring a patient's gait with Parkinson's disease. It was also implemented to classify body movements for gait assessment of patients with Multiple Sclerosis. In wearable devices such as exoskeletons, CNN was able to classify EEG signals for the BMI. Classification rates were up to 99.28% and 94.03% for static and

ambulatory tasks respectively (Kwak, Müller, & Lee, 2017). Other work such as in (Alotaibi & Mahmood, 2017), implemented deep convolutional ANN, for gait recognition using imaging technique that converts the human body features automatically into silhouette image for identity detection.

The RNN and its subclass LSTM are known to be able to model sequential information in problems such as gait analysis and speech recognition. Using data from a foot switch, LSTM was able to binary classify patients with a Neurodegenerative Disease (ND) (i.e. PD) and healthy participants up to 97.43% (A. Zhao, Qi, Dong, & Yu, 2018). In the same study, it achieved a classification accuracy up to 95.67% in further classifying 3 NDs. Foot events (Heel Strike – HS and Toe Off – TO) were also classified using LSTM based on data from accelerometers placed on the wrist and the ankle (Tan, Aung, Tian, Chua, & Yang, 2019). Recorded F1 scores were 0.98 for HS and TO in steady walking at an indoor environment. It has also achieved 0.94 for HS and 0.68 for TO in steady walking at an outdoor environment (Tan et al., 2019).

Hybrid models that combine CNN and RNN architectures were also applied in gait analysis, referred to as ConvLSTM model (Yuqian Zhang & Gu, 2019). ConvLSTM model was able to classify fallers from non-fallers (AUC = 0.75) using accelerometer data from 296 participants (Nait Aicha et al., 2018).

## **2.5 Applications of ML in assistive devices**

Robots were designed to assist humans to complete repetitive or monotonous tasks, such as part assembly in factories. However, currently robots are moving toward richer interaction with human operators. Instead of solely exchanging commands to/from the user, they are now becoming an extension of the human body, interacting both physically as well as cognitively. This has given rise to the term “wearable robotics” or robots worn by human operators. According to Carpino et al. (Carpino, Accoto, Tagliamonte, Ghilardi, & Guglielmelli, 2013), wearable robotics are a type of a mechatronic system that is designed to assist the human body for either performance augmentation or for rehabilitation and assistance of physically challenged persons. Wearable technologies are becoming prolific in today’s society and thus their purpose has moved away from the purely functional into a form of self-expression. This induces a heightened social awareness of wearables and their purpose (Shinohara & Wobbrock, 2016). Poor form design can have an adverse effect on social inclusion, perception of ability and a user’s self-confidence. Wearables design needs to balance

form and function equally as assistive devices used outside of rehabilitation design show decreasing frequency of use due to physical and psychological discomfort of the users (Radder et al., 2015).

Wearable robotics can be grouped into three main categories; orthoses, prostheses and exoskeletons (Pons, 2008). Orthoses, as well as exoskeletons, are defined as mechanical devices that are outfitted by a user, mimics the joint's/limb's motion and is anthropomorphic in nature (Dollar & Herr, 2008). On the other hand, exoskeletons are used to describe devices used by an able-bodied wearer (Herr, 2009), and occasionally when they span multiple joints, for rehabilitation purposes (Dollar & Herr, 2008). Orthoses are devices designed for individuals with limb pathology (Dollar & Herr, 2008; Herr, 2009). Finally, prostheses are artificial limbs predominantly designed for amputees and the device replaces the lost limb/joint function.

There is an emerging need to synchronize wearable function with user intention. In order to achieve good synchronization, a closed loop feedback is required. This will necessitate an architecture composed of networked sensors and actuators, i.e. wireless sensor networks (Akyildiz et al., 2002). In addition, smart control algorithms will be required to fuse sensor data and create smooth actuation (D. T. H. Lai, Palaniswami, & Begg, 2011). ML helps in categorising large datasets by observing their regularities and recognising their patterns. This class of algorithms would be integral to future wearable robotic designs. Within the last decade several review papers in the literature have addressed exoskeleton research (Carpino et al., 2013; Dollar & Herr, 2008; Herr, 2009; Yan, Cempini, Oddo, & Vitiello, 2015) and established the need for this technology. The application areas include rehabilitation and for human performance augmentation. The literature in lower limb devices research tends to be more abundant, as they review walking assistance for most of the works, which is the most rudimentary physical task performed on a daily basis. Besides, lower limb devices are easier to design compared to its upper limb counterpart (Yan et al., 2015).

With these impressive developments in performance augmentation as well as rehabilitation devices, humans are able to go beyond their limits and expend less physical effort in the defence industry. Patients can reduce rehabilitation periods and because the devices are portable, patients can receive assistance when needed. However, in all of these devices, humans have to initiate the movement, or activate a certain muscle in the body for the device to follow and support. This leads to inaccurate movement intention detection and create a delayed response for the exoskeleton control system to address the user's needs. For example, HAL implemented dual controls for monitoring user intentions (Nilsson et al., 2014). Which are the

Cybernic Voluntary Control relying on EMG signals, and the Cybernic Autonomous Control relying on body weight shifts to initiate gait cycles. However, EMGs are very sensitive to electrode placement, noise from neighbouring muscles and the influence of human sweat. Hence, they are deemed unreliable for prolonged use, as they require calibration for inter-subject variability in rehabilitative devices (G. Chen et al., 2013).

In addition, the devices mentioned earlier do not rely on historical gait events, trajectories and patterns. Historical gait data is important to improve how the exoskeleton judges different user movements and the change of user gait intentions so that it adapts to user's physical changes over time and function smoothly without interrupting the user. For example, calculating the probability that both the user's hips and knees moments should change (i.e. milliseconds scale), in order to predict squatting or change in walking speed based on user's past walking gait kinematic and kinetic data. The case of user interruption was reported in Elliot *et al* running exoskeleton, where there was undesirable clutch locking during stair descending and walking (Elliott et al., 2014). Also, in Shamaei *et al* stance control orthoses where an engagement delay was reported, and the device tends to suppress the knee flexion of healthy participants (Shamaei et al., 2013).

## **2.6 Applications of ML in falls prevention**

Falling is the 18<sup>th</sup> most common cause of death in Australia and it accounts for 9.7% of hospital emergency attendance in the state of Victoria (Cox et al., 2018; Rowbotham & Blau, 2017). More than 50% of falling incidents are due to tripping while walking in healthy older adults (Santhiranayagam et al., 2015). A leading cause of falls is tripping and the Minimum Toe Clearance (MTC) has been found to be a critical tripping risk feature (Gillain et al., 2019; D. T. Lai, Shilton, et al., 2009; Santhiranayagam et al., 2015). The MTC describes the minimum toe height during the mid-swing phase (Caldas et al., 2017). The measurement of MTC has been made possible with the aid of motion capture systems as well as IMU devices in real-time (Benoussaad, Sijobert, Mombaur, & Azevedo Coste, 2016; Dadashi et al., 2014; Shi, Zou, Jin, Cui, & Li, 2009; Zhou & Hu, 2008). Tirosh *et al.* suggested that the risk of tripping could be reduced by training young and older participants to target a safer MTC band above the baseline (Tirosh, Cambell, Begg, & Sparrow, 2013). The participants were trained with a real-time feedback display of toe-trajectory and MTC measured with a 3D motion capture system. Based on a shoe-mounted IMU, Santhiranayagam *et al.* implemented a Generalised Regression Neural Networks (GRNN) for MTC height estimation in young and older adults and achieved a root mean square of 7 mm within 1 standard deviation of the group mean (Santhiranayagam

et al., 2015). The combination of SVM and an autoregressive process (i.e. based on LR) was able to reliably predict during the pre-fall phase whether a subject is at the risk of tripping in the next gait cycle using the MTC features (D. T. Lai, Begg, Taylor, & Palaniswami, 2008). Lai *et al.* have also been able to predict critical gait variables related to the MTC before their occurrence as a precursor to mitigate the risk of tripping or falling (D. T. Lai et al., 2012). Given the remarkable outcome of the previous studies, there is still a lack of research to forecast the foot kinematic trajectories which are the means by which the MTC is monitored and detected (Alcock, Galna, Lord, & Rochester, 2016; Santhiranayagam et al., 2015). When a hazardous foot kinematic trajectory is predicted and anticipated, it would alarm the subject of an imminent tripping incident within a time window in the range of fast and slow muscle twitches (Winter, 1991, 2009).

## **2.7 Summary and thesis scope**

It should be emphasised that each ML algorithm excels at a specific problem. For example, HMM has shown better performance in motions classification compared to SVM, GMM, and LDA in (Mannini & Sabatini, 2010). It offers a good advantage when intent transitions are prerequisite actions to each other, such as in the upper extremity, where “approach” is a prerequisite to “grasp” (Dugad & Desai, 1996). Unlike other classifiers which classify each input feature at each time independently, HMM considers the entire motion sequence over time. Hence, it is suitable to work with stochastic signals, such as EMGs (A. D. Chan & Englehart, 2005; Siu et al., 2016). Comparing HMM to ANN, they outweigh each other from different perspectives. The HMM has a robust capacity in modelling the time series actions, while ANN is better in categorising the actions using spatial data (D.-X. Liu et al., 2016). In addition, HMM offers much better performance in classification of stochastic signals compared to ANN (A. D. Chan & Englehart, 2005).

The swathe of ML applications and its performance quality in the modelling of human movements have motivated many biomechanics researchers to further draw gait insights using ML models (Caldas et al., 2017; Halilaj et al., 2018; Phinyomark et al., 2018). The classification of human movements (e.g. Pathological vs. Non-Pathological gait pattern) was the most studied area (80.6%) in the literature (Halilaj et al., 2018). While regression (11.6%) and clustering (7.8%) were the least investigated in human movement biomechanics (Halilaj et al., 2018). Regression was predominantly applied as a method to model gait patterns and infer specific measures based on given patterns, such as predicting walking gait kinematics of

a person from the speed of walking, gender, age and their BMI (Moissenet et al., 2019; Santhiranayagam, Lai, Shilton, Begg, & Palaniswami, 2011). Although the application of ML models in human movement biomechanics have brought several promising findings and was extensively reported, there is a lack of standardised reported methods overall (Caldas et al., 2017). That included; (i) the justification absence of why a specific ML model has been the choice (Yuwono, Su, Guo, Moulton, & Nguyen, 2014), (ii) the unclear performance metrics evaluation (Guenterberg et al., 2009; Mijailovic, Gavrilovic, Rafajlovic, Đuric-Jovicic, & Popovic, 2009) and (iii) the lack of comparison to previous results (Caldas et al., 2017). The potential of standardised development and reporting of ML models for human movement, facilitates reproducibility and the reasonable comparison between applied ML models (Caldas et al., 2017).

The ascending growth of human movement data necessitate the investigation of suitable algorithms that are able to reliably predict the human movement sequential motion. There is no previous work was found that investigated and utilised ML regression techniques to predict the future lower limb trajectories using simulated inertial measurement data which could have a profound impact on human movement science. The aim of this thesis was to determine the best ML model that is able to extrapolate the kinematics of the lower limb trajectory at different walking speeds based on simulated IMU data. Simulated measurement data such as the kinematics output from IMUs (i.e. LA and AV) offer the opportunity to transcend an intelligent model outside the laboratory settings. Besides, changes on walking speed are known to have substantial effects on the pattern and the trajectories of lower limb kinematics (**Section 1.2**). As such, the aim of this thesis was carried out in 3 studies. Study 1 (Chapter 3) focused on exploring, developing and determining the optimum model and the essential techniques to forecast the lower limb trajectories at an imposed walking speed. Study 2 (Chapter 4) further investigated the optimum model to forecast the lower limb trajectories at the preferred walking speed. Study 3 (Chapter 5) examined the developed ML models from Chapter 4 to forecast the lower limb trajectories at fast and slow walking speeds. Study 3 also reported the optimum model in forecasting the lower limb trajectories at the imposed, preferred, fast and slow walking speeds.

### **3 CHAPTER THREE: PREDICTION OF LOWER LIMB KINEMATICS AT IMPOSED WALKING SPEED– Study 1**

#### **3.1 Overview**

This study determined whether the kinematics of lower limb trajectories during walking could be extrapolated using a non-linear ML model such as the Long Short Term Memory (LSTM) neural networks and a linear model such as the Linear Regression (LR). It was hypothesised that LSTM autoencoders could forecast multiple timestep trajectories of the lower limb kinematics, specifically the LA and the AV. Using 3D motion capture, lower limb position-time coordinates were sampled (100 Hz) from 6 male participants (age  $22 \pm 2$  years, height  $1.77 \pm 0.02$  m, body mass  $82 \pm 4$  kg) who walked for 10 minutes at  $5\text{km}\cdot\text{h}^{-1}$  on a 0% gradient motor driven treadmill. This data was fed into a LSTM model with a sliding window of 4 kinematic variables with 25 timesteps; LA and AV for thigh and shank. The LSTM was tested to forecast 5 timesteps of the 4 kinematic input variables. To attain generalisation, the ED-LSTM and the LR were trained on a dataset of 2,665 strides from 5 participants and evaluated on a test-set of 1 stride from a sixth participant. Both the ED-LSTM and the LR models have learned the lower limb kinematic trajectories using the training datasets and tested for generalisation across participants. The forecasting horizon of the ED-LSTM suggested higher model accuracy in predicting earlier future trajectories. For the ED-LSTM, the Mean Absolute Error (MAE) was evaluated on each variable across the single tested stride and for the 5 sample forecast it obtained satisfactory results  $0.047\text{ m}\cdot\text{s}^{-2}$  thigh LA,  $0.047\text{ m}\cdot\text{s}^{-2}$  shank LA,  $0.028\text{ deg}\cdot\text{s}^{-1}$  thigh AV and  $0.024\text{ deg}\cdot\text{s}^{-1}$  shank AV. For the LR, the MAE was evaluated on each variable across the single tested stride and for the 5 sample forecast it obtained better prediction accuracy  $0.030\text{ m}\cdot\text{s}^{-2}$  thigh LA,  $0.029\text{ m}\cdot\text{s}^{-1}$  shank LA,  $0.006\text{ deg}\cdot\text{s}^{-1}$  thigh AV and  $0.006\text{ deg}\cdot\text{s}^{-1}$  shank AV. All predicted trajectories were highly correlated with the measured trajectories, with correlation coefficients greater than 0.98. The motion prediction model may have a wide range of applications, such as mitigating the risk of falls or balance loss and improving the human-machine interface for wearable assistive devices. This chapter was published at the *Frontiers in Bioengineering and Biotechnology* journal under the research topic Machine Learning Approaches to human Movement Analysis (Zaroug et al., 2020).

## 3.2 Introduction

An increasingly useful application of ML is in predicting features of human actions. If it can be shown that algorithm inputs related to actual movement mechanics can predict a limb or limb segment's future trajectory, a range of apparently intractable problems in movement science could be solved. One such problem is how to anticipate movement characteristics that can predict the risk of tripping, slipping or balance loss. Previous work has investigated balance control using wearable sensors to estimate the body's Centre of Mass (CoM) trajectory (Fuschillo et al., 2012). The Internet of Things has also created a new paradigm of algorithms and systems to predict and subsequently, apply interventions to prevent falls (Nait Aicha et al., 2018; Rubenstein, 2006; X. Tao & Yun, 2017). Perhaps the most valuable motion-prediction application is in the design and control of wearable assistive devices, such as prostheses, bionics and exoskeletons. In which smart algorithms can ensure safer, more efficient integration of the assistive device with the user's natural limb and body motion (G. Lee et al., 2017; Rupal et al., 2017).

Previous computational methods have investigated motion trajectory prediction, using position-time inputs and their derivatives (velocity and acceleration). Lower limb trajectory prediction has been implemented in rehabilitation robotics (Duschau-Wicke, von Zitzewitz, Caprez, Lunenburger, & Riener, 2009). Using inverse dynamics, Wang and Low designed a model for foot trajectory generation using a predefined pelvic trajectory and line fitting ten data points from a single gait cycle (P. Wang, Low, & McGregor, 2011). Also using inverse dynamics, Ren et al. predicted all segment motions and ground reaction forces from the average forward velocity gait, double stance duration and gait cycle period (Ren, Jones, & Howard, 2007). Another technique was implemented in the Lower Extremity Powered Exoskeleton (i.e. LOPES) device to emulate the trajectories from a healthy limb to the impaired limb (Vallery, Van Asseldonk, Buss, & Van Der Kooij, 2008). Prediction of the lower limb joint angles future trajectory that effectively lead to foot events timing was also investigated in (Aertbeliën & De Schutter, 2014; Tanghe et al., 2019), using Probabilistic Principal Component Analysis (PPCA).

Recent methods implemented ML algorithms such as the ANN to identify subject gait trajectories to recognize neurological as well as pathological gait patterns (Alaqtash et al., 2011; Fabian Horst, Lapuschkin, Samek, Müller, & Schöllhorn, 2019). ANN was also used to improve user intention detection in wearable assistive devices (Islam & Hsiao-Wecksler, 2016;

Jung et al., 2015; Moon, Kim, & Hong, 2019; Trigili et al., 2019). A variation to the ANN called Generalised Regression Neural Networks (GRNN) was found to be capable of predicting lower limb joint angles (hip, knee and ankle) from the Linear Acceleration (LA) and Angular Velocity (AV) of foot and shank segments (Findlow et al., 2008), or from subject gait and anthropomorphic parameters (Luu et al., 2014). The RNN and the CNN which are classes of ANN, were able to classify human motions and activities (B.-K. Han, Ryu, & Kim, 2019; Murad & Pyun, 2017).

The Long Short Term Memory (LSTM) neural networks is a subclass of RNN and it has proven success in modelling a wide range of sequence problems, including; human activity recognition (Ordóñez & Roggen, 2016), gait diagnosis (A. Zhao et al., 2018), falls prediction (Nait Aicha et al., 2018) and gait event detection (Kidziński, Delp, & Schwartz, 2019). The LSTM autoencoder (ED-LSTM) is an architecture of LSTM that has been implemented in an array of applications such as language translation (Cho et al., 2014) and in forecasting of video frames (Srivastava, Mansimov, & Salakhudinov, 2015), weather (Gangopadhyay, Tan, Huang, & Sarkar, 2018; Poornima & Pushpalatha, 2019; Reddy, Yedavalli, Mohanty, & Nakhat, 2018), traffic flow (S. H. Park, Kim, Kang, Chung, & Choi, 2018; Wei, Wu, & Ma, 2019) and stock prices (H. Li, Shen, & Zhu, 2018).

Given the potential of lower limb trajectory prediction, no previous work was found that utilised ML regression techniques to predict future lower limb trajectories using simulated inertial measurement data which could have a profound impact on human movement science. Simulated measurement data such as the kinematics output from IMUs (i.e. LA and AV) offer the opportunity to transcend a predictive model outside the laboratory settings. The LR have been widely adopted by biomechanist researchers for gait inference or the kinematics prediction (Buchner, Larson, Wagner, Koepsell, & De Lateur, 1996; Moissenet et al., 2019; Olney, Griffin, & McBride, 1994). It has been reported that statistical models (i.e. parametric ML) may not be able to learn complex relationships and highly dimensional biomechanical data (Halilaj et al., 2018; Phinyomark et al., 2018). This however, was not investigated in the context of predicting future trajectories of independent variables and it was not clear whether linear assumptions might be enough to surpass the performance of sequential ML models such as the LSTM. The aim of this study was to determine whether the kinematics of lower limb trajectories during imposed walking speed could be accurately extrapolated using ED-LSTM. The study also aims to investigate whether linear statistical methods such as the simple LR is

enough to predict the trajectories of lower limb kinematics. It was hypothesised that ML regression methods could forecast multiple timestep trajectories of the lower limb kinematics.

### **3.3 Materials and Methods**

#### **3.3.1 Collection protocol**

Ethics approval was granted by the Department of Defence and Veterans' Affairs Human Research Ethics Committee and Victoria University Human Research Ethics Committee (Protocol 852-17). All participants signed a consent form and volunteered freely to participate. Walking data were obtained from 6 male participants ( $22 \pm 2$  years old,  $1.77 \pm 0.02$  m in height,  $82 \pm 4$  kg in mass) who walked for 10 minutes at  $5\text{km}\cdot\text{h}^{-1}$  on a 0% gradient treadmill. A set of 25 retroreflective markers were attached to each participant in the form of clusters (Findlow et al., 2008). Each cluster comprises a group of individual markers that represent a single body segment (e.g. shank). This include left and right foot (3 markers), left shank (4 markers), right shank (5 markers), left thigh (3 markers), right thigh (4 markers) and pelvis (3 markers). The 3D position of each cluster was tracked using a 14 camera motion analysis system (Vicon Bonita, Version 2.8.2) at 150Hz. Virtual markers were also established to calibrate the position and orientation of the lower body skeletal system (Garofolini, 2019). Three-dimensional ground reaction force and moment data were collected from a force-plate instrumented treadmill (Advanced Mechanical Technology, Inc., Watertown, MA) at 1500Hz.

#### **3.3.2 Dataset Processing**

Recorded 3D positional and force data were processed using Visual 3D (C-motion, Inc, Version 6) to obtain LA and AV. In Visual 3D (**Figure 3-1**), the data was firstly filtered using a lowpass digital filter with a 15Hz cut-off frequency and normalised using z-scores. Secondly, raw AV was obtained as the derivative of Euler/Cardan angles (C-motion, 2015) and the raw LA was generated by the double derivative of segment linear displacement using built-in pipelines commands (Hibbeler, 2007). This data (LA and AV) simulated the kinematic outputs from body-mounted IMUs widely used in wearable assistive devices, monitoring lower limb kinematics (D. T. Lai et al., 2012; Santhiranayagam et al., 2011), controlling powered actuators (G. Lee et al., 2017) and recognising human actions (Jimenez-Fabian & Verlinden, 2012; Koller, Gates, Ferris, & Remy, 2016; Van Laerhoven & Cakmakci, 2000).

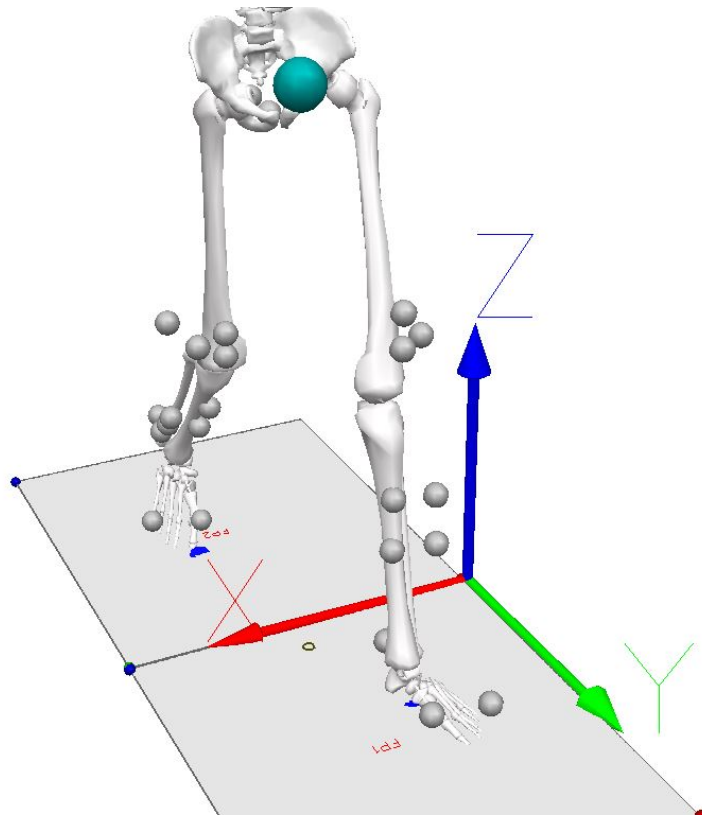


**Figure 3-1:** The skeletal model along with the components (X,Y,Z) definition and the markers setup. Grey balls are the retroreflective markers. The Turquoise ball is a virtual marker refers to the participant's centre of mass.

As shown in **Figure 3-1**, main direction of movements included the translation along the Y-axis (i.e. LA) and the rotation along the X-axis (i.e. AV) were used for LSTM prediction, resulting in four predictor variables, (i)  $Y_1$  thigh LA (ii)  $Y_2$  shank LA (iii)  $X_3$  thigh AV and (iv)  $X_4$  shank AV. The thigh segment was defined as the reference frame to the shank and the shank segment was defined as the reference frame to the thigh (**Figure 3-2**).

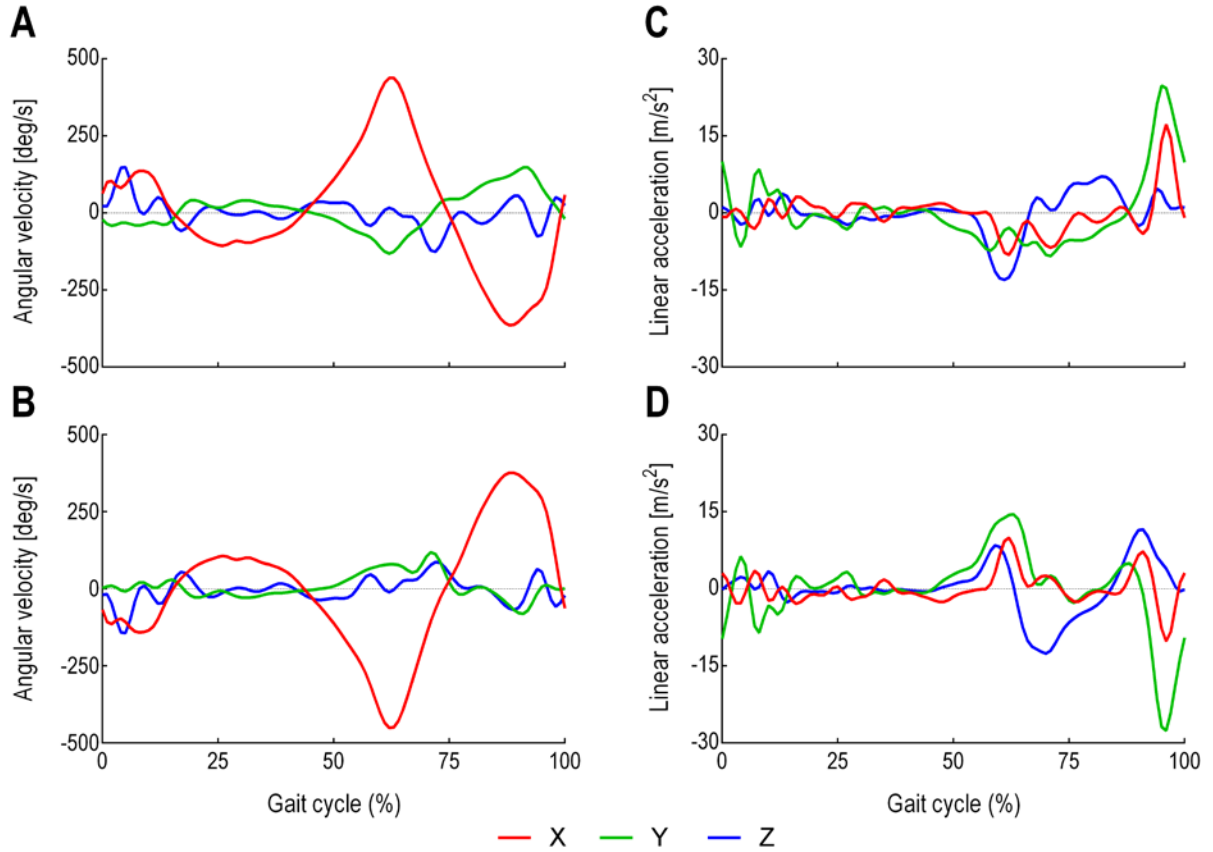


**Figure 3-2:** Average thigh and shank LA and AV within a stride. A stride was defined as the interval between two successive heel strikes of the same foot (Soutas-Little, 1998). A) Thigh three dimensional AV (Direction of rotation around the X-axis). B) Shank three dimensional AV (Direction of rotation around the X-axis). C) Thigh three dimensional LA (direction of progression along the Y-axis). D) Shank three dimensional LA (direction of progression along the Y-axis). Red is the X-axis. Green is the Y-axis. Blue is the Z-axis.

### 3.3.3 Dataset Description

The data were divided into training and testing sets. The training set comprised 2,665 strides from 5 participants that included 4 kinematic feature variables ( $Y_1$ ,  $Y_2$ ,  $X_3$ ,  $X_4$ ) (N-columns) and 453,060 timesteps (M-rows) for each variable. A single timestep is equivalent to 0.006s (i.e. 1/150Hz). To attain generalisation, a testing set was used that comprised of a single stride from the sixth participant with the 4 feature variables and 170 timesteps (i.e. 1.1s) for each variable.

### 3.3.4 Time Series Transformation to a Supervised Learning Problem

The input to the LSTM was 4 parallel feature variables and the output was the successive 4 parallel feature variables. Prior to feeding into the LSTM model, the  $M \times N$  training

and testing datasets were transformed to 3D dataset using a sliding window technique (Banos, Galvez, Damas, Pomares, & Rojas, 2014). The sliding window comprised of an input window, an output window and a sliding size. The input window consists of  $M$  timesteps and  $N$  features, so as the output window. The timesteps are the camera frames and it is equivalent to 6ms (i.e. 1/150Hz). The input window is the input data to the LSTM model and the output window is the future prediction output from the LSTM model. The sliding size is how much of  $M$  timesteps that both the input and the output windows are sliding forward with (see **Figure 3-3**). The sliding size ( $M$  timesteps) was always equal to the output size.

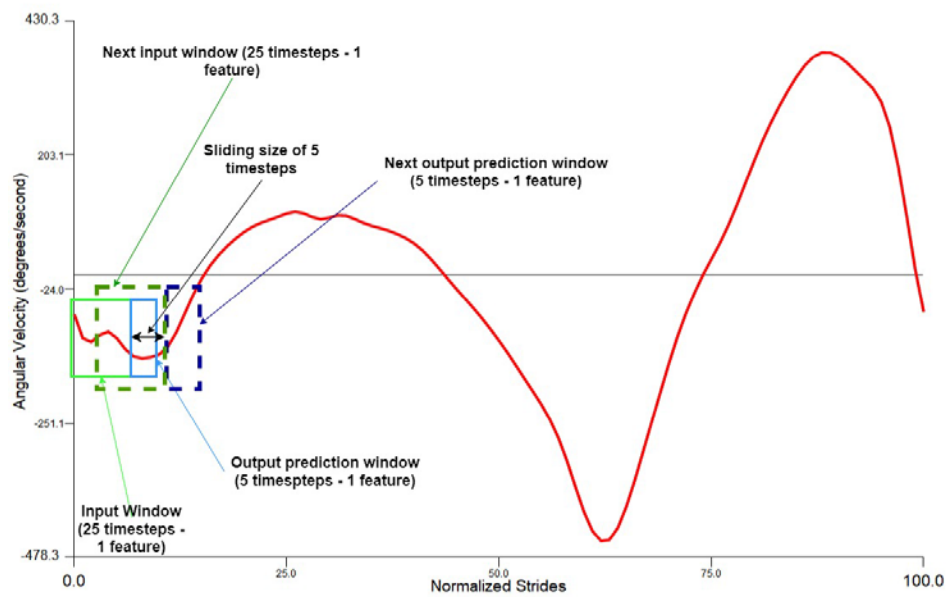


**Figure 3-3:** Sliding window illustration example using the normalised shank angular velocity X-axis component (1 feature). The window in this model is 25 timesteps and 4 features and the prediction output is 5 timesteps of 4 features.

### 3.3.5 Linear Regression (LR)

The LR is a statistical method used to estimate future variables from the past variables. As demonstrated in Chapter 2 (**Section 2.4.2**), the LR is the most implemented approach for time series prediction (Bishop, 2006; Ristanoski, Liu, & Bailey, 2013). It aims to minimise the least linear squares loss function based on the assumption that the input and output variables are linearly correlated. The implemented LR can be expressed as:  $y(x, w) = w_0 + w_1x_1 + \dots + w_Dx_D$ . Where,  $y$  is the forecast variable,  $x = (x_1, \dots, x_D)^T$  are the predictor variables and  $w_0, \dots, w_D$  are unknown coefficients estimated using the ordinary least squares (Bishop, 2006; Draper & Smith, 1998). In this work, the forecast and predictor variables refer to the same independent variable (e.g. Foot AV) such that  $x$  refer to the past values and  $y$  refers to the future values. The coefficients  $w_0, \dots, w_D$  were fitted (i.e. trained) to each feature vector at the

imposed speed (5km.h<sup>-1</sup>) walking trials. The LR equation was independently applied to each of the feature variables; (a) Thigh LA Y<sub>1</sub>. (b) Shank LA Y<sub>2</sub>. (c) Thigh AV X<sub>3</sub>. (d) Shank AV X<sub>4</sub>

### 3.3.6 Recurrent Neural Networks (RNN)

While the Multiple Layer Perceptrons (MLP) consider all inputs as independent, the RNN are designed to work with time series data (Ordóñez & Roggen, 2016). Recurrent neural networks (RNN) are a class of ANN architecture designed specifically to model sequence problems and exploit the temporal correlations between input data samples (Elman, 1990; Murad & Pyun, 2017). It contains feedback connections between each of its units which enables the network to relate all the previous inputs to its outputs (**Figure 3-4**).

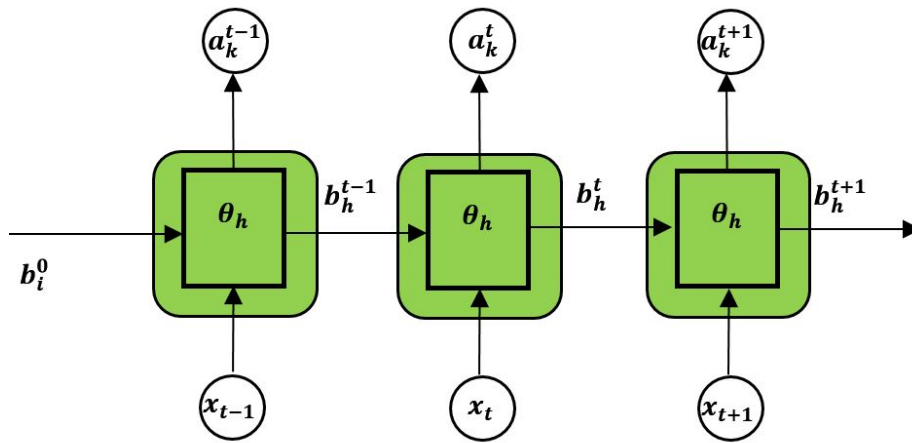


**Figure 3-4:** Unfolded structure of the Recurrent Neural Network.

The forward pass equations from the inputs to the outputs of the RNN are given as:

For the hidden units:

$$a_h^t = \sum_{i=1}^I w_{ih} x_i^t + \sum_{h'=1}^H w_{h'h} b_{h'}^{t-1} \quad (3-1)$$

and differentiable activation functions are then applied:

$$b_h^t = \theta_h(a_h^t) \quad (3-2)$$

The network input to output units:

$$a_k^t = \sum_{h=1}^H w_{hk} b_h^t \quad (3-3)$$

Where:

$a_h^t$  is the sum of inputs to unit  $h$  at time  $t$ ,  $b_h^t$  is the activation of unit  $h$  at time  $t$ ,  $\theta_h$  is the nonlinear and differentiable activation function of unit  $h$ ,  $a_k^t$  is the sum of all inputs to output unit  $k$  at time  $t$ ,  $x_i^t$  is the input  $i$  at time  $t$ ,  $w_{ih}$  is the connection weights between input unit  $i$  and hidden unit  $h$ ,  $w_{h'h}$  is the connection weights between the previous hidden state  $h'$  and it self  $h$  and  $w_{hk}$  is the connection weights between hidden state  $h$  and output unit  $k$ . Bias was neglected for simplicity.

### 3.3.7 Long Short Term Memory (LSTM) Networks

As the input data propagates through the standard RNN's hidden connections to the output units, it either slowly attenuates or amplifies exponentially, referred to respectively, as vanishing or exploding gradients (Bengio, Simard, & Frasconi, 1994; Hochreiter, Bengio, Frasconi, & Schmidhuber, 2001). The problems with this approach are that the vanishing gradient prevents the network from learning long term dependencies and the exploding gradient leads to weights oscillation. These difficulties have been addressed using gradient norm clipping to tackle the exploding gradient and a soft constraint to deal with the vanishing gradient (Pascanu, Mikolov, & Bengio, 2013). The LSTM design addresses these problems by maintaining a memory cell  $C$  (Figure 3-5) that enables the network to retain information over a longer period by using an explicit gating mechanism (Graves, 2012b; Hochreiter & Schmidhuber, 1997; Karpathy, Johnson, & Fei-Fei, 2015).

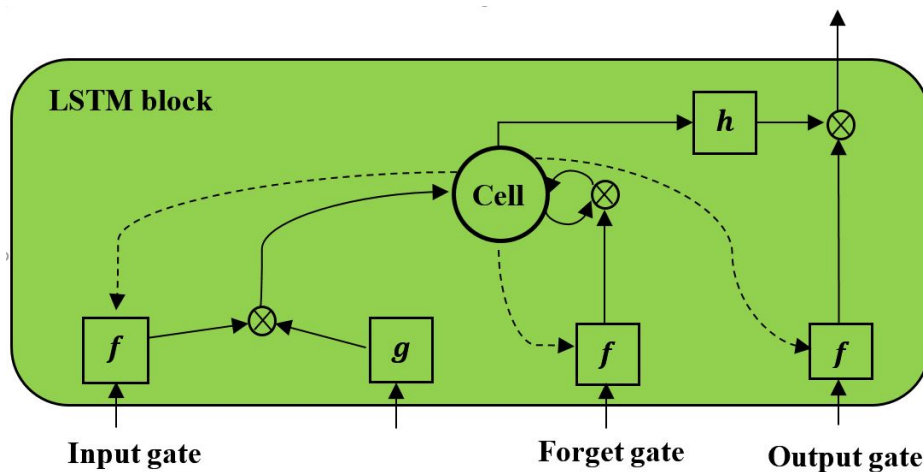


Figure 3-5: Standard LSTM memory cell with peephole connections.

Each LSTM cell has an input gate, forget gate and output gate. The input gate dictates the information used to update the memory state and the forget gate decides which information

to discard or remove from the cell. The final gate specifies the information to output based on the cell input and memory. All gates are designed such that information is exchanged from inside and outside the block (**Figure 3-5**). Furthermore, each memory block contains three peephole-weighted connections (dotted lines in **Figure 3-5**) which are the input weight  $w_{ci}$ , the output weight  $w_{c\omega}$  and the memory state  $w_{c\phi}$ . The functions  $f$ ,  $g$  and  $h$  are usually tanh or logistic sigmoid activation functions (Graves, 2012b). Below are the network equations (Graves, 2012b) that govern the LSTM architecture used:

Input gates:

$$a_i^t = \sum_{i=1}^I w_{ii} x_i^t + \sum_{h=1}^H w_{hi} b_h^{t-1} + \sum_{c=1}^C w_{ci} s_c^{t-1} \quad (3-4)$$

$$b_i^t = f(a_i^t) \quad (3-5)$$

Forget gates:

$$a_\phi^t = \sum_{i=1}^I w_{i\phi} x_i^t + \sum_{h=1}^H w_{h\phi} b_h^{t-1} + \sum_{c=1}^C w_{c\phi} s_c^{t-1} \quad (3-6)$$

$$b_\phi^t = f(a_\phi^t) \quad (3-7)$$

Cells:

$$a_c^t = \sum_{i=1}^I w_{ic} x_i^t + \sum_{h=1}^H w_{hc} b_h^{t-1} \quad (3-8)$$

$$s_c^t = b_\phi^t s_c^{t-1} + b_i^t g(a_c^t) \quad (3-9)$$

Output gates:

$$a_w^t = \sum_{i=1}^I w_{iw} x_i^t + \sum_{h=1}^H w_{hw} b_h^{t-1} + \sum_{c=1}^C w_{cw} s_c^t \quad (3-10)$$

$$b_w^t = f(a_w^t) \quad (3-11)$$

Cell outputs:

$$b_c^t = b_w^t h(s_c^t) \quad (3-12)$$

Where,  $w_{ij}$  is the weight of the connection from unit  $i$  to unit  $j$ ,  $a_j^t$  is the network input to unit  $j$  at time  $t$ ,  $b_j^t$  is the activation of unit  $j$  at time  $t$ ,  $i, \phi, \omega$  are respectively stands for the input gate, forget gate, and output gate,  $C$  is the memory cell,  $w_{ci}, w_{c\phi}, w_{c\omega}$  are peephole weights,  $s_c^t$  is the state of cell  $C$  at time  $t$ ,  $f$  is the input, output and forget gates activation function,  $g$  and  $h$  are the cell input and output activations,  $I$  is the number of inputs,  $H$  is the

number of cells in the hidden layer and index  $h$  is the cell outputs from other blocks in the hidden layer. Bias was neglected for simplicity.

### 3.3.8 Design of the LSTM model

The implemented model was based on the LSTM autoencoder, a neural network architecture composed of an Encoder and a Decoder (i.e. ED-LSTM) (Cho et al., 2014). The encoder encodes the input variable length vector into a fixed length feature vector that captures the attributes of the variable length vector. The LSTM decoder decodes the encoded fixed length feature vector back into a variable length vector (**Figure 3-6**). The final layer is a fully connected dense (feedforward) mechanism for outputting predictions. The network weights and biases were updated at the end of each batch using an Adaptive Moment Estimation (Adam) optimisation algorithm (Kingma & Ba, 2014) with Mean Absolute Error (MAE) as an optimisation criterion. A single batch consists of 100 input/output windows. The activation for all LSTM layers was set to a Rectified Rectilinear Unit (ReLU) activation function (Nair & Hinton, 2010). The LSTM autoencoder model was implemented in Google Colab as well as the Amazon Web Services (AWS) using Python 3 (Libraries: Keras, Numpy, Pandas and Scikit learn).

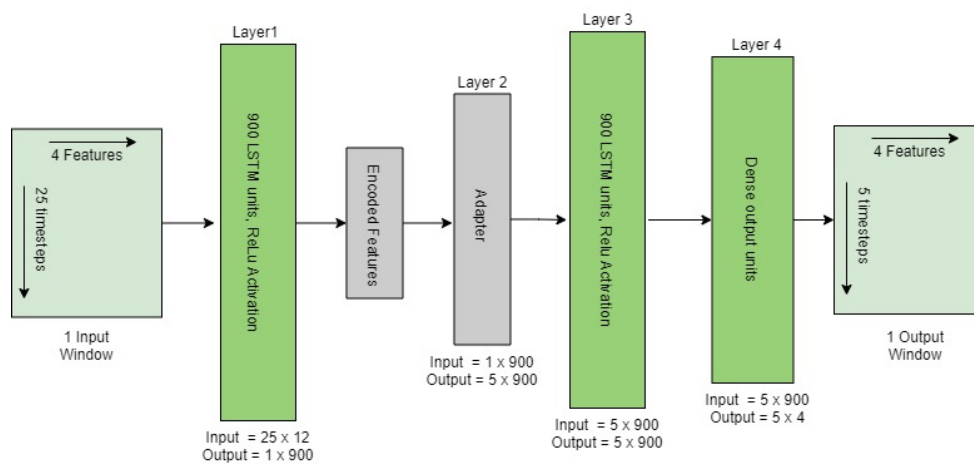


**Figure 3-6:** Structure of the implemented Encoder-Decoder LSTM architecture given 1 input window. The adapter converts the 2D encoded features into 3D output to be adopted by LSTM. The last layer is a fully connected dense layer for outputting 1 window predictions.

### 3.3.9 Evaluation metrics

To evaluate the network quality, three parameters were considered to calculate how closely the network predicted variable trajectories  $\hat{y}_j (Y_1, Y_2, X_3, X_4)$  was to the actual variable trajectories  $y_j (Y_1, Y_2, X_3, X_4)$  across the  $n$  timesteps:

1. Mean Absolute Error (MAE) given as:

$$MAE = \frac{1}{n} \sum_{j=1}^n |y_j - \hat{y}_j| \quad (3-13)$$

2. Mean Squared Error (MSE) given as:

$$MSE = \frac{1}{n} \sum_{j=1}^n (y_j - \hat{y}_j)^2 \quad (3-14)$$

3. Correlation coefficient (CC) given as:

$$P = \frac{cov(y, \hat{y})}{std(y) * std(\hat{y})} \quad (3-15)$$

Where,  $std()$  is the standard deviation and  $cov(y, \hat{y})$  is the covariance between variables  $y$  and  $\hat{y}$ .

### 3.4 Results

Using sparse grid search approach, model's hyperparameters were tuned to determine the optimum model design (least MAE), including number of epochs, batch size, layers, and cells. The optimum model was then trained for 50 epochs (repetitions) and performance evaluated on the test set using MAE, MSE and the CC. The test set was a single stride consists of 170 timesteps (i.e. 1.1s). An initial 25 timesteps was used from the preceding cycle in order to start predicting the trajectories of the single stride.

#### 3.4.1 ED-LSTM performance with different input window sizes

The size of the input window was varied 8 times at 5 timestep intervals (5-40 timesteps) to demonstrate the optimum input window size (least error). The output sliding window was fixed to 5 timesteps prediction. Model performance is shown in **Figure 3-7** where the impact of each input window size on the prediction of each variable is computed.

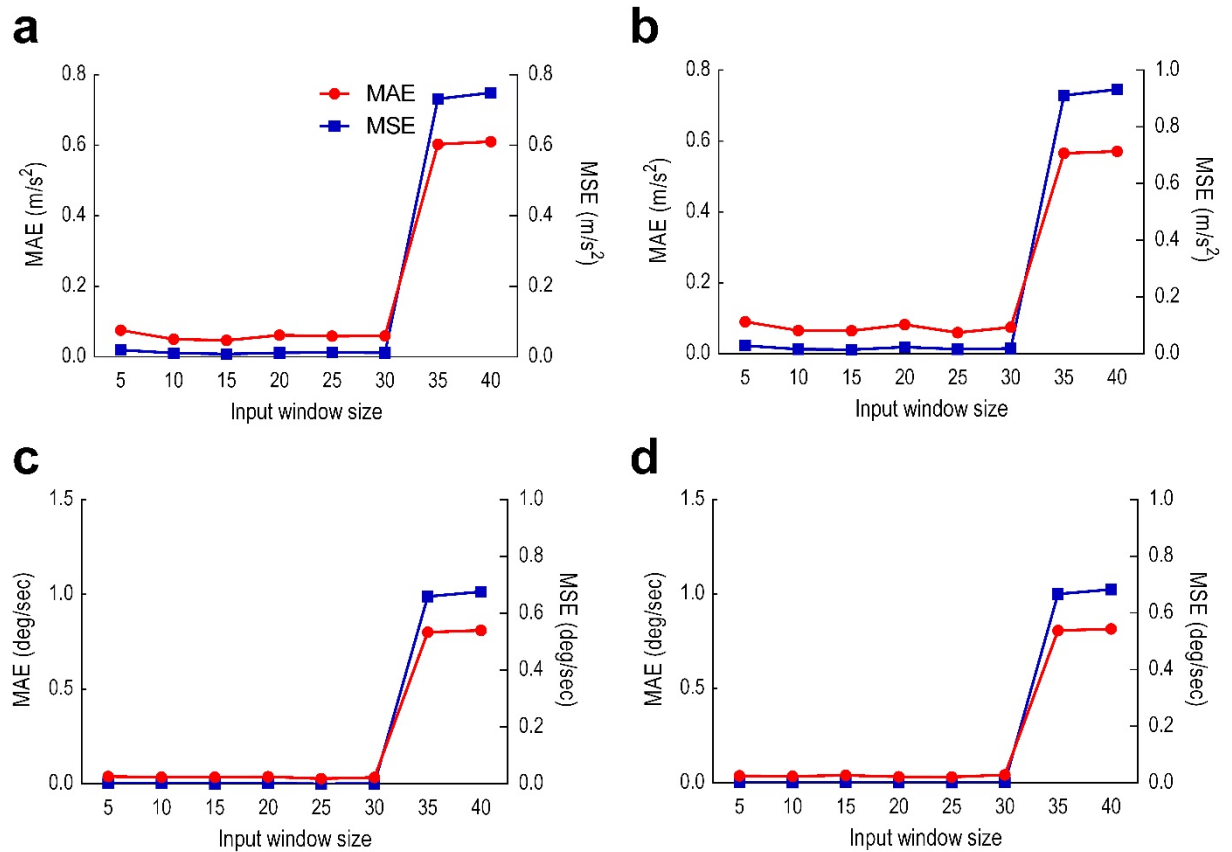


**Figure 3-7:** Model performance with different input window sizes. Red is MAE. Blue is MSE. A) Thigh LA ( $Y_1$ ). B) Shank LA ( $Y_2$ ). C) Thigh AV ( $X_3$ ). D) Shank AV ( $X_4$ ).

### 3.4.2 ED-LSTM performance with 5 timesteps prediction window

This sliding window comprised of 25 timesteps input and timesteps prediction output and 5 timesteps sliding size. Results were given in two analyses; (i) predicted versus actual trajectories including the absolute error for each timestep in the first output window (**Figure 3-8**) and for the whole gait cycle (**Figure 3-9**) (ii) Performance metrics (MAE, MSE and CC) for the first window of 5 timesteps (**Table 3-1**) and for all windows combined (

**Table 3-2).**

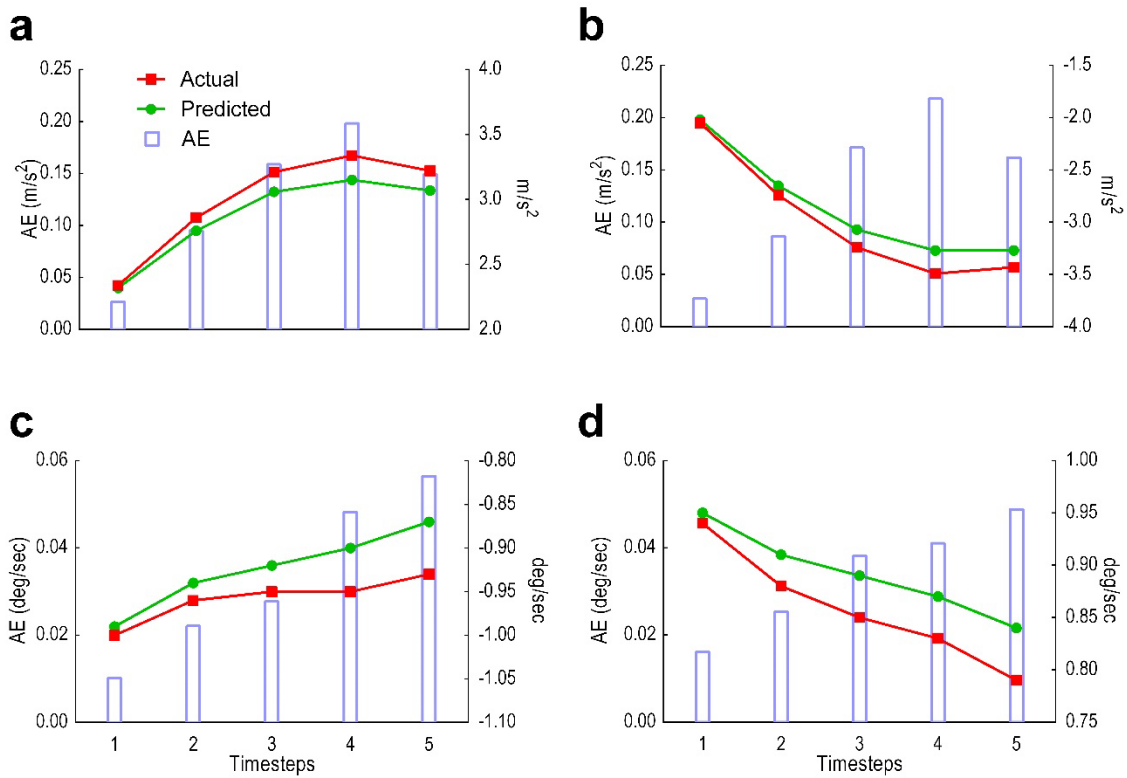


**Figure 3-8:** The ED-LSTM performance for the first window, showing predicted trajectories (green) and actual trajectories (red). Columns represent the Absolute Error (AE) for the 5 predicted timesteps. (a) Thigh LA  $Y_1$ . (b) Shank LA  $Y_2$ . (c) Thigh AV  $X_3$ . (d) Shank AV  $X_4$

**Table 3-1:** ED-LSTM performance for predicting the first 5 predicted timesteps.

| Feature | MAE                       | MSE                       | CC   |
|---------|---------------------------|---------------------------|------|
| $Y_1$   | 0.125 m.s <sup>-2</sup>   | 0.019 m.s <sup>-2</sup>   | 0.99 |
| $Y_2$   | 0.133 m.s <sup>-2</sup>   | 0.022 m.s <sup>-2</sup>   | 0.99 |
| $X_3$   | 0.032 deg.s <sup>-1</sup> | 0.001 deg.s <sup>-1</sup> | 0.98 |
| $X_4$   | 0.033 deg.s <sup>-1</sup> | 0.001 deg.s <sup>-1</sup> | 0.99 |

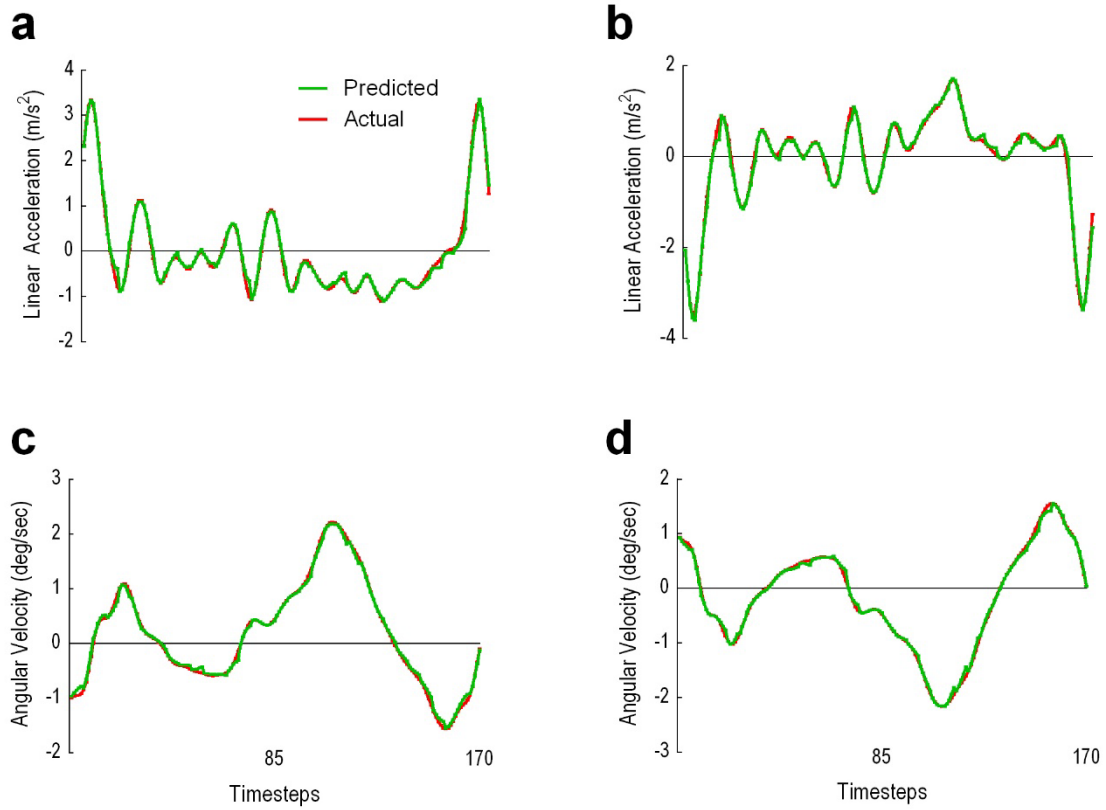


**Figure 3-9:** The ED-LSTM performance over the entire gait cycle when 5 timesteps prediction window is used. The figure shows predicted trajectories (orange) and actual trajectories (blue). (A) Thigh LA  $Y_1$ . (B) Shank LA  $Y_2$ . (C) Thigh AV  $X_3$ . (D) Shank AV  $X_4$ .

**Table 3-2:** The ED-LSTM performance for predicting the complete stride using an input window size of 25 timesteps and an output window size of 5 timesteps.

| Feature | MAE                       | MSE                       | CC   |
|---------|---------------------------|---------------------------|------|
| $Y_1$   | 0.047 m.s <sup>-2</sup>   | 0.006 m.s <sup>-2</sup>   | 0.99 |
| $Y_2$   | 0.047 m.s <sup>-2</sup>   | 0.006 m.s <sup>-2</sup>   | 0.99 |
| $X_3$   | 0.028 deg.s <sup>-1</sup> | 0.001 deg.s <sup>-1</sup> | 0.99 |
| $X_4$   | 0.024 deg.s <sup>-1</sup> | 0.001 deg.s <sup>-1</sup> | 0.99 |

### 3.4.3 ED-LSTM performance with 10 timesteps prediction window

This sliding window comprised of 25 timesteps input, 10 timesteps prediction output and 10 timesteps sliding size. **Figure 3-10** illustrates results as predicted versus actual trajectories including the Absolute Error (AE) for each timestep in the first output window whereas **Figure 3-11** displays for the whole gait cycle. Performance metrics (MAE, MSE and CC) for the first window of 10 timesteps are presented in **Table 3-3** and for all windows combined in **Table 3-4**.

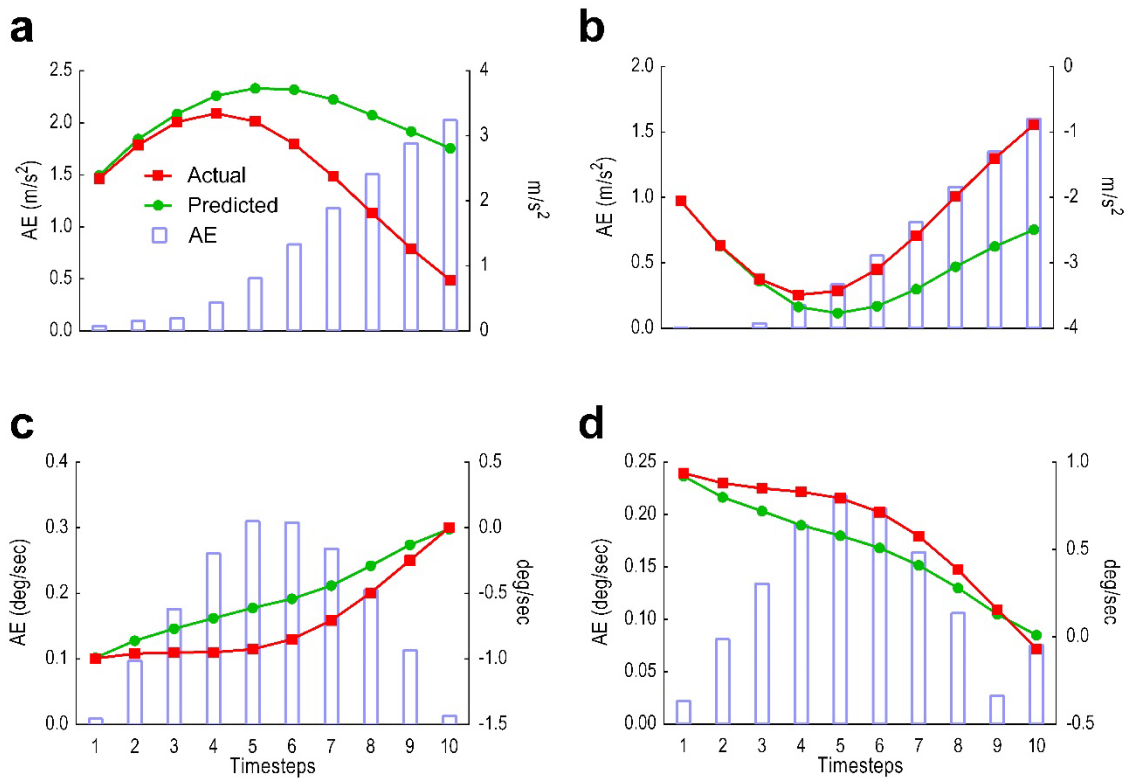


**Figure 3-10:** The ED-LSTM performance for the first window, showing predicted trajectories (green) and actual trajectories (red). Columns represent the Absolute Error (AE) for the 10 predicted timesteps. (a) Thigh LA  $Y_1$ . (b) Shank LA  $Y_2$ . (c) Thigh AV  $X_3$ . (d) Shank AV  $X_4$ .

**Table 3-3:** The ED-LSTM performance for predicting the first 10 predicted timesteps.

| Feature | MAE                       | MSE                       | CC   |
|---------|---------------------------|---------------------------|------|
| $Y_1$   | 0.839 m.s <sup>-2</sup>   | 1.206 m.s <sup>-2</sup>   | 0.52 |
| $Y_2$   | 0.596 m.s <sup>-2</sup>   | 0.667 m.s <sup>-2</sup>   | 0.75 |
| $X_3$   | 0.176 deg.s <sup>-1</sup> | 0.042 deg.s <sup>-1</sup> | 0.94 |
| $X_4$   | 0.122 deg.s <sup>-1</sup> | 0.019 deg.s <sup>-1</sup> | 0.96 |

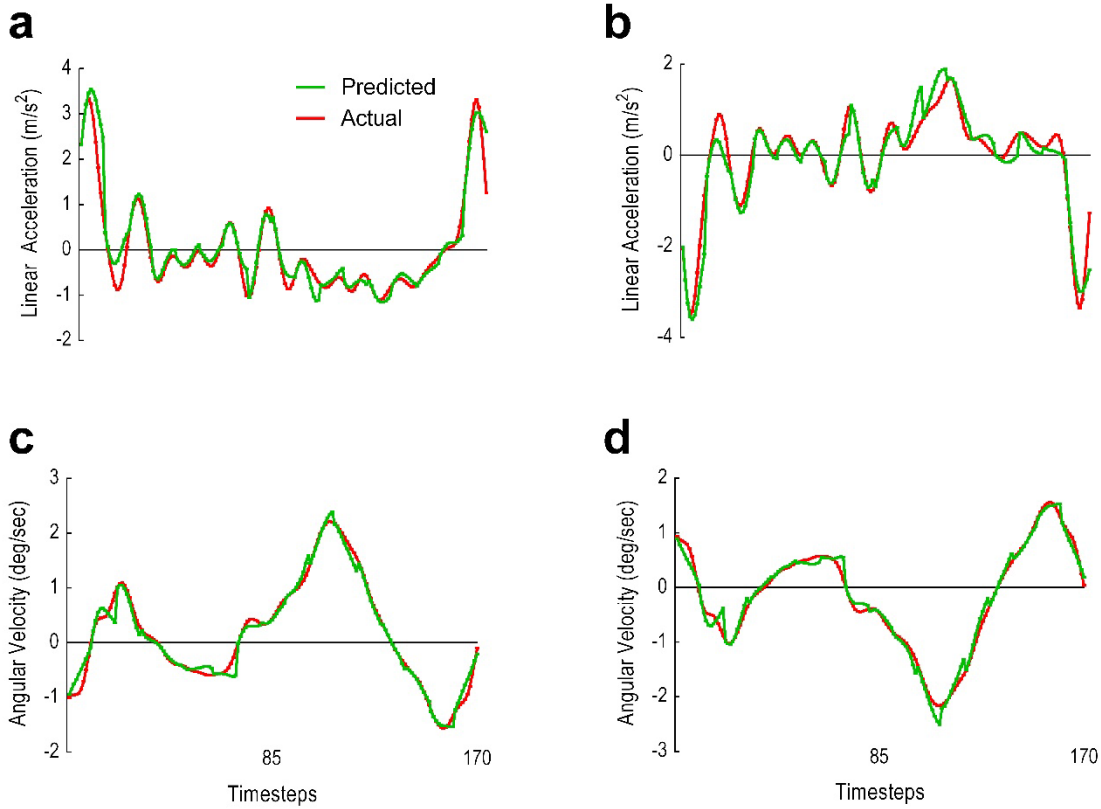


**Figure 3-11:** The ED-LSTM performance over the entire gait cycle when 10 timesteps prediction window is used. The figure shows predicted trajectories (orange) and actual trajectories (blue). (A) Thigh LA  $Y_1$ . (B) Shank LA  $Y_2$ . (C) Thigh AV  $X_3$ . (D) Shank AV  $X_4$ .

**Table 3-4:** The ED-LSTM performance for predicting the complete stride using an input window size of 25 timesteps and an output window size of 10 timesteps.

| Feature | MAE                       | MSE                       | CC   |
|---------|---------------------------|---------------------------|------|
| $Y_1$   | 0.170 m.s <sup>-2</sup>   | 0.096 m.s <sup>-2</sup>   | 0.96 |
| $Y_2$   | 0.202 m.s <sup>-2</sup>   | 0.096 m.s <sup>-2</sup>   | 0.96 |
| $X_3$   | 0.079 deg.s <sup>-1</sup> | 0.015 deg.s <sup>-1</sup> | 0.98 |
| $X_4$   | 0.086 deg.s <sup>-1</sup> | 0.014 deg.s <sup>-1</sup> | 0.98 |

### 3.4.4 The LR prediction performance

The LR model was tested on 170 timesteps (i.e. 1.1s) from an unseen participant with the 5 timesteps output window (see **Figure 3-12**) and the 10 timesteps output window (see **Figure 3-13**). The LR accurately estimated the predicted trajectories with the 5 timesteps output window (**Table 3-5**) than the 10 timesteps output window (**Table 3-6**).

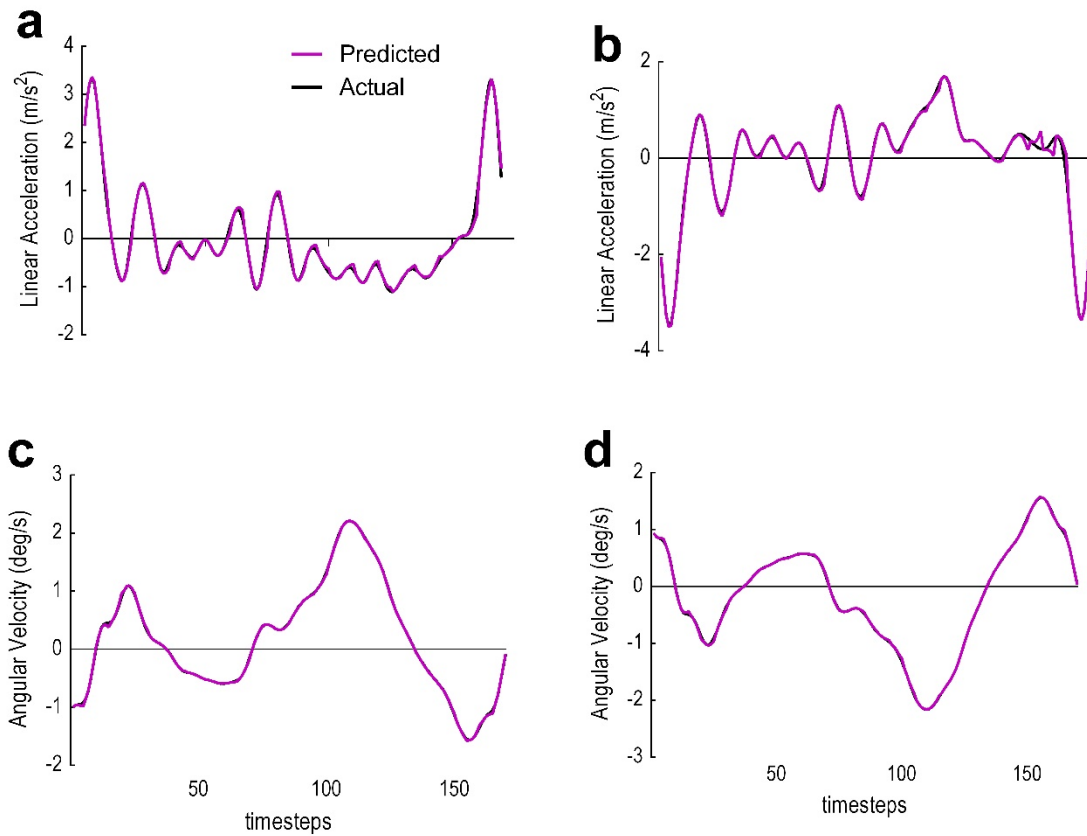


**Figure 3-12:** The LR prediction performance over the gait cycle when 5 timesteps output prediction window is used. The figure shows predicted trajectories (Magenta) and actual trajectories (black). (a) Thigh LA  $Y_1$ . (b) Shank LA  $Y_2$ . (c) Thigh AV  $X_3$ . (d) Shank AV  $X_4$ .

**Table 3-5:** The LR average model performance for all output prediction windows using an input window size of 25 timesteps and an output window size of 5 timesteps.

| Feature | MAE                       | MSE                     | CC   |
|---------|---------------------------|-------------------------|------|
| $Y_1$   | 0.030 m.s <sup>-2</sup>   | 0.003 m.s <sup>-2</sup> | 0.99 |
| $Y_2$   | 0.029 m.s <sup>-2</sup>   | 0.004 m.s <sup>-2</sup> | 0.99 |
| $X_3$   | 0.006 deg.s <sup>-1</sup> | 0 deg.s <sup>-1</sup>   | 0.99 |
| $X_4$   | 0.006 deg.s <sup>-1</sup> | 0 deg.s <sup>-1</sup>   | 0.99 |

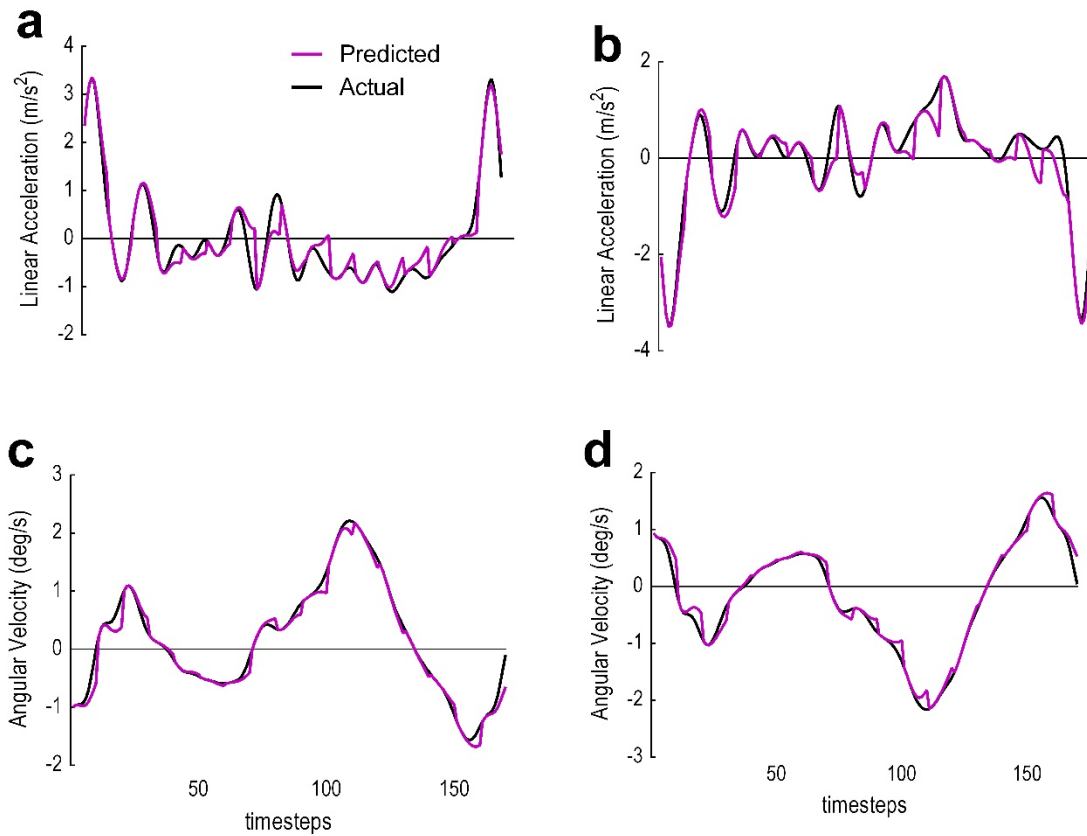


**Figure 3-13:** The LR prediction performance over the gait cycle when 10 timesteps output prediction window is used. The figure shows predicted trajectories (Magenta) and actual trajectories (black). (a) Thigh LA  $Y_1$ . (b) Shank LA  $Y_2$ . (c) Thigh AV  $X_3$ . (d) Shank AV  $X_4$ .

**Table 3-6:** The LR average model performance for all output prediction windows using an input window size of 25 timesteps and an output window size of 10 timesteps.

| Feature | MAE                       | MSE                       | CC   |
|---------|---------------------------|---------------------------|------|
| $Y_1$   | 0.155 m.s <sup>-2</sup>   | 0.072 m.s <sup>-2</sup>   | 0.96 |
| $Y_2$   | 0.180 m.s <sup>-2</sup>   | 0.094 m.s <sup>-2</sup>   | 0.96 |
| $X_3$   | 0.070 deg.s <sup>-1</sup> | 0.017 deg.s <sup>-1</sup> | 0.99 |
| $X_4$   | 0.070 deg.s <sup>-1</sup> | 0.016 deg.s <sup>-1</sup> | 0.99 |

### 3.5 Discussion

The aim of this study was to develop and evaluate ED-LSTM and the simple LR to predict the trajectories of 4 kinematic variables ( $Y_1, Y_2, X_3, X_4$ ), simulating the output from wearable IMU sensors. The study found that the simple LR obtained better prediction performance than the ED-LSTM for all the 4 kinematic variables. The predicted kinematic feature variables, LA and AV, for the shank and thigh were well predicted based on the LR and the ED-LSTM up to 10 timesteps, i.e., up to 0.06s in the future. A 0.06s prediction of future trajectories adds a feedforward term to an assistive device controller rather than being re-active and predominantly rely on feedback terms (i.e. sensory information) (Tanghe et al., 2019). This enables the assistive device to adapt to changes in human gait, allowing smoother synchronization with user intentions and minimize interruptions when the user changes their movement pattern (Ding et al., 2018; Elliott et al., 2014; Zaroug et al., 2019; J. Zhang et al., 2017). A known future trajectory might also monitor the risk of balance loss, tripping and falling, in which impending incidents can be remotely reported for early intervention (R. Begg, Best, et al., 2007; R. Begg & Kamruzzaman, 2006; Hemmatpour et al., 2019; Naghavi et al., 2019; Nait Aicha et al., 2018). Since 0.06s falls in the range of a slow (0.06-0.12s) and fast (0.01-0.05s) twitch motor units (Winter, 2009), this would enable wearable devices such as IMUs to alert (e.g. by audio/visual signal) an elderly user about an imminent risk of tripping and potentially gives them a chance to adjust their gait accordingly.

In contrast to the proposed 1-2 s window for human activity recognition proposed by Banos *et al.* (2014), no window has previously been suggested for forecasting human movement trajectories (Banos et al., 2014). In addressing this limitation, the present project input and output sliding windows were tested to discover the optimum prediction model. The input window was varied from 5 timesteps to 40 timesteps, while the output window was fixed at 5 timesteps during each test. Results showed that both MAE and MSE increased after 25 timesteps for all variables except for the thigh LA  $Y_1$  in which 15 timesteps scored lowest. Due to the majority score, 25 timesteps was fixed and the output window size was manipulated between 5 and 10 timesteps. Prediction error MAE and MSE gradually increased across the first 5 and 10 timestep prediction windows, indicating better prediction early in the stride cycle. This prediction horizon suggests that an output window exceeding 5 timestep may not be sufficiently reliable for forecasting gait trajectories. The ED-LSTM predicted trajectories for the LA began to deviate earlier than the AV, possibly due to the double derivative in LA that generated a noisier signal. The gradual decrease in the difference between the actual and

predicted trajectories in **Figure 3-10** (c) and (d) is an intersection between the two trajectories that continued to undertake different directions.

The ED-LSTM model obtained lower MAE trends for the first 5 timesteps output window (**Table 3-3**) than the first 10 timesteps output window (**Table 3-1**). Similarly, across the stride cycle, an output window of 5 timesteps (**Figure 3-8**) showed better model performance (lower MAE scores) than the 10 timesteps output window (**Figure 3-10**), particularly when there are less noise in the predicted signal for all variables. Predictions of 5 timesteps for all variables achieved high CC (0.99) and maintained below MAE  $0.048 \text{ deg.s}^{-1}$  and  $0.029 \text{ m.s}^{-2}$ . The LR attained similar behaviour with better performance results for the 5 timesteps output window (**Table 3-5**) than the 10 timesteps output window (**Table 3-6**). Across the gait cycle, the LR obtained smoother predictions (less MAE) and better predicted pattern (high CC) with the 5 timesteps output window (**Figure 3-12**) than the 10 timesteps output window (**Figure 3-13**). The LR showed better prediction performance overall (**Table 3-5** and **Table 3-6**) than the ED LSTM (**Table 3-2** and **Table 3-4**). Such performance results indicate that prediction of future lower limb trajectories at an imposed walking speed ( $5\text{km.h}^{-1}$ ) is possible using only the simple LR. However, the simple LR is a linear parametric model which means that the coefficient size is fixed and may not automatically adapt to different walking speed (Montgomery, Peck, & Vining, 2021). The LR performance is unknown when the given human movement task is realistic or random such as the preferred walking speed which is a special walking speed to every individual (Samson et al., 2001). The ED-LSTM model is complex and computationally expensive, but it is a non-parametric and a stochastic method which may perform different from the simple LR when the given task is random and requires a probabilistic estimation (Bush & Mosteller, 1955; Kröse, Krose, van der Smagt, & Smagt, 1993).

These result parameters are different from earlier work (Findlow et al., 2008; Luu et al., 2014). The difference is in the type of predicted data (lower limb joint angles of the hips, knees and ankles) and in the type of output, which was not a forecast, but rather a prediction of joint angles from the LA and AV of the lower limb segments. Nonetheless, the work presented in this work showed higher CC values than the earlier works (Findlow et al., 2008; Luu et al., 2014) at the inter-subject test. Overall, the ED-LSTM model was able to learn the trajectories and generalise across participants. This generalisation is invaluable to adapt algorithm performance to a wider population in assistive devices, particularly when each user responds differently to the same device (J. Zhang et al., 2017).

This study was limited to the walking movement with a 0.06s prediction horizon and healthy participants walking at 5km.h<sup>-1</sup>. The imposed speed 5km.h<sup>-1</sup> was found to be the general average preferred walking speed in previous studies (Browning, Baker, Herron, & Kram, 2006; Mohamed & Appling, 2020; Mohler, Thompson, Creem-Regehr, Pick, & Warren, 2007; Waters, Lunsford, Perry, & Byrd, 1988). Besides, the 5km.h<sup>-1</sup> speed was imposed to report the feasibility of whether lower limb future trajectories are predictable. Future work may proceed with the model developed to accommodate a higher gait variance from more participants and other populations, such as female, older adults and individuals with gait disorders walking at their preferred as well as slower and faster speeds (Winter, 1991). More participants (i.e. stride examples) would potentially improve the model performance to predict trajectories above 60ms and also provide a more comprehensive validation set, a strategy to find the optimum number of epochs and avoid model overfitting (Graves, 2013). The ED-LSTM can be made flexible by automating the input/output window size depending on the detected human activity which revamp the LSTM capacity to recognise a wider range of human action transitions, such as slow to fast walking.

Although the ED-LSTM and the simple LR described here were able to learn and predict future trajectories, further research is needed to investigate the models' performance at preferred walking speed. The performance of other standard LSTM architectures such as the Bi-directional LSTM may need to be explored as well (Graves & Schmidhuber, 2005). Bi-directional LSTM can be useful in forward and backward modelling of sequential data, giving further insights into sequential pattern modelling (G. Liu & Guo, 2019; Yuezhou Zhang et al., 2019).

### **3.6 Conclusion**

This study confirmed the possibility of predicting the future trajectories of human lower limb kinematics at imposed walking speed 5km.h<sup>-1</sup>, i.e., thigh AV, shank AV, thigh LA and shank LA. The study found that the simple LR performs better than the ED-LSTM in predicting the future lower limb kinematics at impose walking speed. An input window of 25 timesteps and an output window of 5 timesteps were found to be the optimum sliding window sizes for future trajectories prediction. The ED-LSTM model prediction horizon was better able to forecast the earlier timestep trajectories and was also able to learn trajectories across different participants. Future work could focus on automating input/output window size and using predicted

kinematics to identify discrete gait cycle events such as heel strike and toe-off (Kidziński et al., 2019). LSTM methods for human movement prediction have applications to balance loss, falls prevention and controlling assistive devices. The next chapter analyses the performance of the simple LR as well as other standard LSTM architectures (i.e. bidirectional LSTM neural networks) at the preferred walking speed (Graves, 2012a).

## **4 CHAPTER FOUR: PREDICTION OF LOWER LIMB KINEMATICS AT PREFERRED WALKING SPEED – Study 2.**

### **4.1 Overview**

The forecasting of lower limb trajectories can improve the operation of assistive devices and predict the toe clearance to minimise the risk of tripping and balance loss. In the previous chapter, the future lower limb kinematics were found to be predictable at imposed walking speed ( $5\text{km}\cdot\text{h}^{-1}$ ) using LSTM autoencoders and the LR. The aim of this chapter was to examine whether standard LSTM neural networks (Vanilla, Stacked, Bidirectional and Autoencoders) are able to predict the future trajectories of lower limb kinematics (i.e. AV and LA) at the Preferred Walking Speed (PWS). This chapter also investigates whether basic learning methods such as the simple LR is sufficient to predict the future kinematics of lower limb trajectories at the PWS. Kinematics data of foot, shank and thigh (LA and AV) were collected from 13 male and 3 female participants ( $28 \pm 4$  years old,  $1.72 \pm 0.07$  m in height,  $66 \pm 10$  kg in mass) who walked for 10 minutes at preferred walking speed ( $4.34 \pm 0.43$   $\text{km}\cdot\text{h}^{-1}$ ) and at an imposed speed ( $5\text{km}\cdot\text{h}^{-1}$ ,  $15.4\% \pm 7.6\%$  faster) on a 0% gradient treadmill. The 5 timesteps prediction output sliding window technique was adopted from the previous chapter for training and testing the LSTM models with total kinematics time-series data of 10,500 strides. Results based on leave-one-out cross validation, suggested that stacked LSTM and LSTM autoencoders are better predictors of the lower limb kinematics trajectories (i.e. up to 0.1s). The normalised mean squared error was evaluated on trajectory predictions at each timestep and it obtained 4.70-7.58% for the stacked LSTM and 4.55-7.91% for the LSTM autoencoders. The LR obtained worse predictions than all of the LSTM models and was deemed unreliable in predicting the lower limb kinematics at PWS. The ability to predict future lower limb motions may have a wide range of applications including the design and control of bionics allowing improved human-machine interface and mitigating the risk of falls and balance loss.

### **4.2 Introduction**

Prediction of gait kinematics is a useful approach to improve the operation of assistive devices (i.e. bionics) and minimise the risk of falling or balance loss (Ahn, Kim, Koo, & Kim, 2019; Anam & Al-Jumaily, 2012; Hori et al., 2019; D. T. Lai, Begg, & Palaniswami, 2009; Sawicki, Beck, Kang, & Young, 2020). Prediction of the human gait however has been a

challenging process due to the locomotor system's high degrees of freedom that continuously change and the asymmetrical foot contact with the ground (Srinivasan, Raptis, & Westervelt, 2008). One of the most common straightforward approach for gait prediction is to combine forward dynamics with optimisation methods in which human muscle forces and limb movements are determined by minimising a cost function (Yamaguchi, 1990; Zajac & Winters, 1990). The method, however, requires a long computational time, and it is highly dependent on the measured data (Marshall, Wood, & Jennings, 1989; Pandy, 2001). In order to achieve efficient computational time and to set the optimisation parameters without relying on the measured data, inverse dynamics along with optimisation methods are implemented to predict the human walking trajectories (Chevallereau & Aoustin, 2001). Ren *et al.* (Ren et al., 2007) predicted all segments motion and ground reaction forces from the average gait forward velocity, double stance duration and the period of the gait cycle. Other basic approaches were typically low-dimensional and were approximating the walking gait cycle as a simple mechanical system (i.e. inverted pendulum) (Kuo, 2007). This was reflected on the work by Doke et al (Doke, Donelan, & Kuo, 2005) in which the swing leg was modelled as a pendulum and by Donelan et al (Donelan, Kram, & Kuo, 2002) in which a step to step transition was modelled as a two link point-foot biped. Although those methods are able to capture the gait features, they idealise the human motions and were unable to generalise the gait trajectories (Kuo, 2001; Kuo, Donelan, & Ruina, 2005).

Hybrid zero dynamics (HZD) is an example that was found to be complex enough to capture several gait features simultaneously along with rapid optimisation process and doesn't idealise the human motions (Westervelt, Grizzle, Chevallereau, Choi, & Morris, 2018). The HZD represents the joint trajectories as a function of a phase variable based on step progression (Westervelt et al., 2018) and was found to be accurately modelling the hip and knee kinematics at a fixed walking speed (Srinivasan et al., 2008). The method was soon replicated to the bipedal robots (Sinnott & Ames, 2012) and assistive devices (Martin & Schmedeler, 2014). In assistive devices however, the defined gait trajectories has long been studied for rehabilitation purposes (Duschau-Wicke et al., 2009; Glackin et al., 2014; Hesse, Uhlenbrock, & Sarkodie-Gyan, 1999). Some of the robotic rehabilitation devices such as the Lokomat (Colombo, Joerg, Schreier, & Dietz, 2000) rely on a cooperative strategy in which a pre-defined trajectories were influenced by the patient movements (Veneman et al., 2007). Complementary Limb Motion Estimation (CLME) was applied to the LOPES exoskeleton in which the device would

simultaneously emulate the trajectories from the healthy limb to the impaired limb (Vallery et al., 2008).

The emergence of inexpensive wearable sensors such as the IMUs (Sabatini, 2011; Vargas-Valencia et al., 2016) have posed new challenges (i.e. increase in dimensionality) and opportunities (i.e. new insights) to the analysis of the human movement (Halilaj et al., 2018) outside laboratory settings (Hori et al., 2019). In response to these challenges, a new set of ML algorithmic models have been widely adopted by biomechanists (Halilaj et al., 2018; Phinyomark et al., 2018). The ML algorithms are a subfield of AI concerned with the establishment of computer programmes that learn patterns from data (Mitchell, 1997). Computational techniques related to ML have been successful in solving several aspects of biomechanics gait research problems (R. Begg & Palaniswami, 2006; D. T. Lai, Levinger, Begg, Gilleard, & Palaniswami, 2009), such as the gait classification (R. Begg & Kamruzzaman, 2005; R. K. Begg et al., 2005; Kamruzzaman & Begg, 2006), joint angle prediction (Chong & Park, 2017) and energy expenditure minimisation in lower limb exoskeletons (Ding et al., 2018). Tanghe *et al.* have applied the Probabilistic Principal Component Analysis (PPCA) to predict the future lower limb joint kinematics and achieved an error rate between 4.5-12.5% (Tanghe et al., 2019). The data however were collected at an imposed speeds (2 and 5 km.h<sup>-1</sup>) and the error was calculated at 3 points only in the gait cycle (10, 50 and 100 %) (Tanghe et al., 2019).

One of the most utilised algorithms for the human movement prediction are the ANN (R. Begg, Lai, & Palaniswami, 2007; Halilaj et al., 2018; Zaroug et al., 2019). A class of ANN known as deep learning (inspired by the structure and function of the brain) (LeCun et al., 2015), were found to be insightful in human activity classification (Fernandez-Lopez, Liu-Jimenez, Kiyokawa, Wu, & Sanchez-Reillo, 2019; B.-K. Han et al., 2019; Murad & Pyun, 2017), gait pattern recognition (Fabian Horst et al., 2019) and the improvement of user intention detection in wearable assistive devices (i.e. bionics) (Islam & Hsiao-Wecksler, 2016; Jung et al., 2015; Moon et al., 2019; Trigili et al., 2019). It was also applied in regression tasks such as the prediction of lower limb joint angles from the AV and LA of foot and shank segments (Findlow et al., 2008). Gholami *et al.* implemented CNN to predict the lower limb joint angles from the foot LA data and achieved between 6.5-11.1% error rate (Gholami et al., 2020). Nonetheless, the developed ANNs in the literature were predicting the gait trajectories (i.e. knee angles) from an independent variable (i.e. foot LA) and it was not implemented to predict the future gait trajectories. Su and Gutierrez-Farewik applied LSTM neural networks

to predict lower limb kinematic trajectories at imposed walking speed and achieved a mean absolute error between 0.187-0.308 (B. Su & M Gutierrez-Farewik, 2020).

The kinematics of the lower limbs are the means by which powered exoskeletons are controlled, falls are prevented and abnormal gaits are identified (Ahn et al., 2019; Anam & Al-Jumaily, 2012; Hori et al., 2019; Sawicki et al., 2020). There was no previous work that was found to investigate sequential ML models such as LSTM neural networks to predict future gait trajectories at preferred walking speed (PWS) and imposed speed based on simulated IMU kinematics. The LSTM neural networks are an ANN architecture known for modelling time-series information (Graves, 2012a, 2013). The LSTM neural networks have proven wide success in modelling human movement data such as the lower limb kinematics prediction (B. Su & M Gutierrez-Farewik, 2020) neurodegenerative disease diagnosis (A. Zhao et al., 2018), gait event detection (Kidziński et al., 2019; Tan et al., 2019) and falls recognition (Nait Aicha et al., 2018). On the other hand, commonly implemented statistical models such as the LR was not examined for predicting future lower limb trajectories at PWS. The LR was investigated in the previous chapter at imposed walking speed and found to be performing better than LSTM autoencoders (ED-LSTM).

The aim of this work was to develop and compare four standard LSTM architectures (Vanilla, Stacked, Bidirectional and Auto-encoders) for the prediction of future lower limb trajectories, i.e. foot AV, shank AV, thigh AV, foot LA, shank LA and thigh LA. In the previous chapter (Zaroug et al., 2020), the ED-LSTM and the LR were found to be able to predict the future gait trajectories at an imposed speed. This chapter further investigates different standard LSTM architectures and the LR in predicting future gait kinematics when individuals walk at PWS.

## **4.3 Methods**

### **4.3.1 Study participants**

Walking data were collected from 13 male and 3 female participants ( $28 \pm 4$  years old, height  $1.72 \pm 0.07$  m, mass  $66 \pm 10$  kg) who walked for 10 minutes at their PWS ( $4.34 \pm 0.43$  km·h<sup>-1</sup>) and at an imposed speed ( $5$  km·h<sup>-1</sup>,  $15.4\% \pm 7.6\%$  faster) on a 0% gradient treadmill. Trials were randomised and one participant's data (male) was omitted due to incomplete data. The PWS was calculated by starting the treadmill at  $3$  km·h<sup>-1</sup>, then it was gradually increased until the participant says "this is comfortable". It was again increased until an uncomfortable speed (i.e fast walking) was reached. After that, speed was gradually decreased until the

participant says “this is comfortable”. An average value was then calculated from the two comfortable recorded speeds to represent the PWS (Ichinosawa et al., 2018). Each trial was started with a 2 minutes familiarisation session for treadmill walking. Ethics approval was granted by the Victoria University Human Research Ethics Committee (ID HRE18-230) and the Department of Defence and Veterans’ Affairs Human Research Ethics Committee (Protocol 852-17). All participants signed a consent form and volunteered freely to participate.

#### 4.3.2 Gait analysis

A set of 30 retroreflective markers (**Figure 4-1**) were attached to each participant in the form of clusters (Findlow et al., 2008). Each cluster comprised of a group of individual markers that represent a single body segment (e.g. shank). This include left and right foot clusters (3 markers), left shank cluster (5 markers), right shank cluster (5 markers), left thigh cluster (5 markers), right thigh cluster (5 markers) and pelvis cluster (4 markers). The 3D position of each cluster was tracked using a 14 camera motion analysis system (Vicon Bonita, Version 2.8.2) recording at 250Hz. Before capturing the dynamic trials, a static pose (1 second) was recorded where an additional 8 retroreflective markers were placed on anatomical landmarks (e.g. lateral femur medial epicondyle) identified by palpation (Alexander & Andriacchi, 2001; Cappozzo, Catani, Della Croce, & Leardini, 1995; Dyrby & Andriacchi, 2004). The static pose was used to calibrate the position and orientation of the lower body skeletal system (Garofolini, 2019).

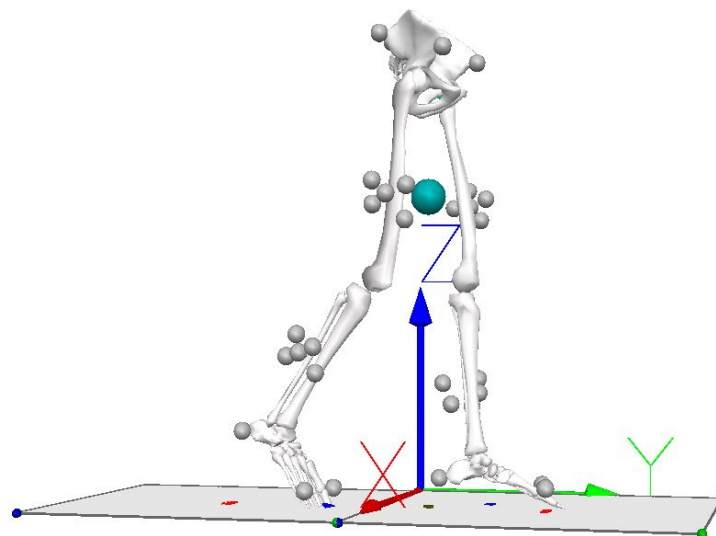


**Figure 4-1:** The skeletal model along with the components (X,Y,Z) definition and the markers setup. Grey balls are the retroreflective markers. The turquoise ball is a virtual marker refers to the centre of mass.

### 4.3.3 Kinematic walking profiles

Recorded 3D positional data were processed using Visual 3D (C-motion, Inc, Version 6) to compute LA and AV for the thigh, shank, and foot segments of the right limb (Zaroug et al., 2020). LA and AV were then interpolated with a least-squares fit on a 3<sup>rd</sup> order polynomial and filtered using a lowpass digital filter with a 15Hz cut-off frequency (Butterworth, 1930; Davis, 1975). A stride was defined as the interval between two successive heel strikes of the right foot (Soutas-Little, 1998). Outlier strides (i.e. bad strides) were labelled as bad and excluded from the final time series data. The final time series data were downsampled to 50 Hz (to accelerate LSTM computational time) (B. Su & M Gutierrez-Farewik, 2020) and normalised with z-scores using Matlab (Mathworks, Inc, R2020a). The sagittal plane kinematics (**Figure 4-2**) included the translation along the Y-axis (i.e. LA) and the rotation along the X-axis (i.e. AV), and were used for LSTM prediction, resulting in six predictor variables, (i)  $X_1$  foot AV (ii)  $X_2$  shank AV (iii)  $X_3$  thigh AV (iv)  $Y_4$  foot LA (v)  $Y_5$  foot LA and (vi)  $Y_6$  foot LA (**Figure 4-3**).

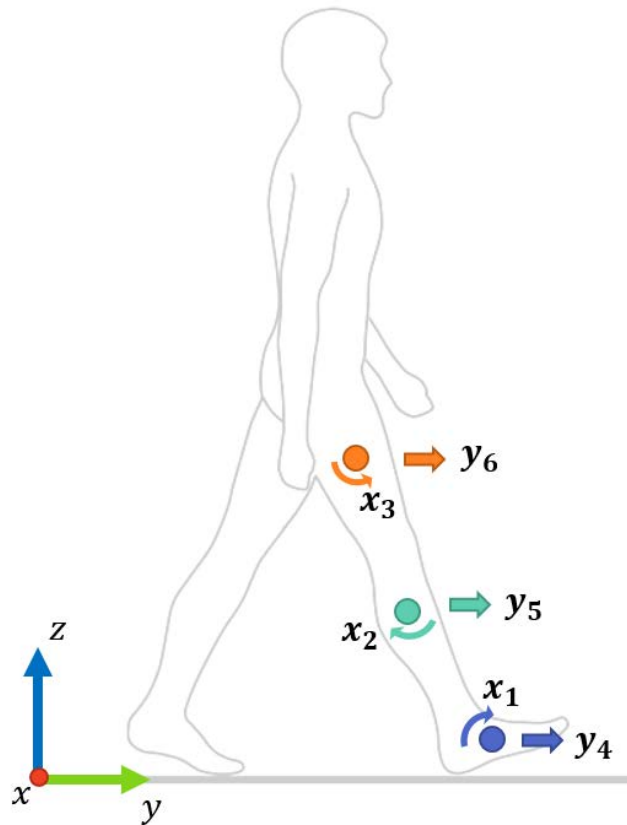


**Figure 4-2:** Definition of sagittal plane movements as well as the (X,Y) coordinates. Sagittal plane movements included the rotation around the X-axis (i.e., AV) and the translation along the Y-axis (i.e., LA).

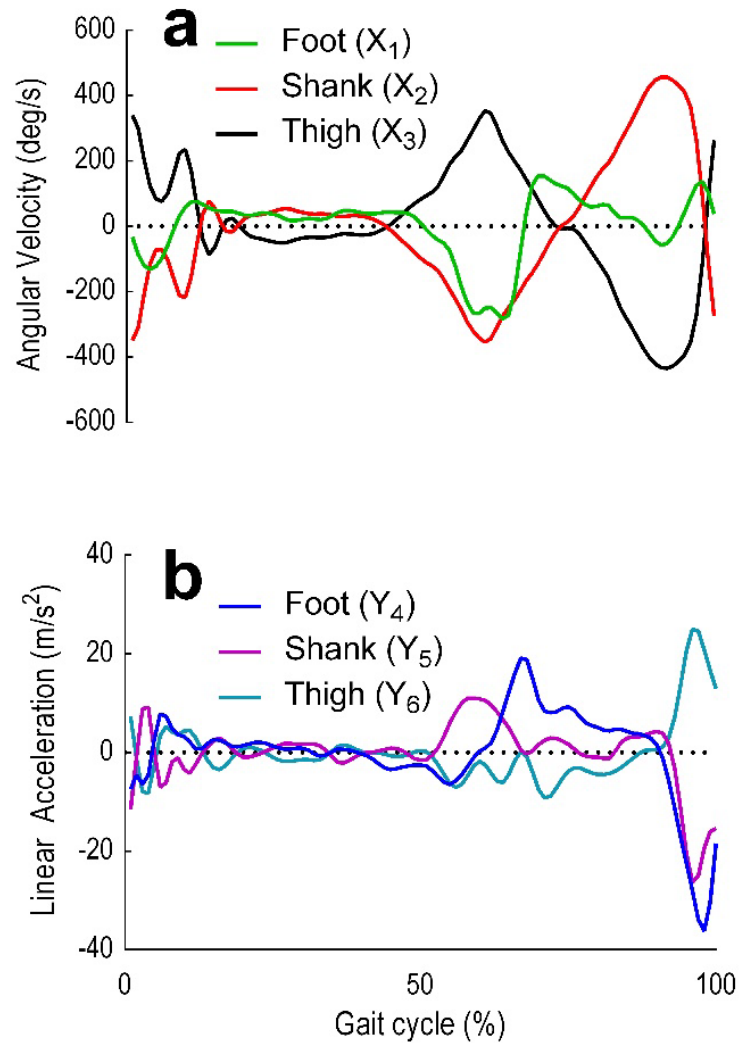


**Figure 4-3:** Foot, shank and thigh Sagittal plane AV and LA. Those were selected as the model's independent variables predominantly because primary motions of the human movement are flexion and extension in the sagittal plane (Srinivasan et al., 2008). (a) Foot ( $X_1$ ), shank ( $X_2$ ) and thigh ( $X_3$ ) AV. (b) Foot ( $Y_1$ ), shank ( $Y_2$ ) and thigh ( $Y_3$ ) LA.

#### 4.3.4 Datasets

Processed time series data (10,500 strides) were combined to include the two walking speeds. The data were then divided into training and testing sets. The training set comprised of 10,500 strides from 15 participants that included 6 kinematic feature variables ( $X_1$ ,  $X_2$ ,  $X_3$ ,  $Y_4$ ,  $Y_5$ ,  $Y_6$ ). To evaluate generalisation capability, a testing set was created for each participant that comprised of 75 timesteps (i.e. 1.5s of the gait cycle) and the 6 kinematic feature variables (**Table 4-1**). A single timestep is equivalent to 0.02s (i.e. 1/50Hz).

**Table 4-1:** Train-test split datasets. The model was trained and tested using leave-one-out cross validation. At each epoch, the training set doesn't contain all trials of the tested participant.

| Validation protocol | Number of participants |                      |
|---------------------|------------------------|----------------------|
|                     | Training               | Testing              |
| leave-one-out       | 14                     | 1, 75 timesteps only |

#### 4.3.5 Time Series transformation to a supervised Learning problem

The  $T \times F$  (i.e. Timesteps\*Features) data structure was transformed into  $S \times T \times F$  (i.e. Samples\*Timesteps\*Features) structure (**Figure 4-4**) (Zaroug et al., 2020). One sample is a one window that consists of multiple timesteps and the 6 features. A single timestep is equivalent to 0.02s (i.e. 1/50Hz). The training input data was transformed from 614,083 timesteps and 6 features into 122,811 samples and inside of each sample are 25 timesteps and 6 features. While the corresponding output training data was 112,811 samples and inside of each sample are 5 timesteps and 6 features. The testing input data was converted from 75 timesteps and 6 features to 15 samples, 25 timesteps and 6 features. While the corresponding output testing data was converted to 15 samples, 5 timesteps and 6 features.

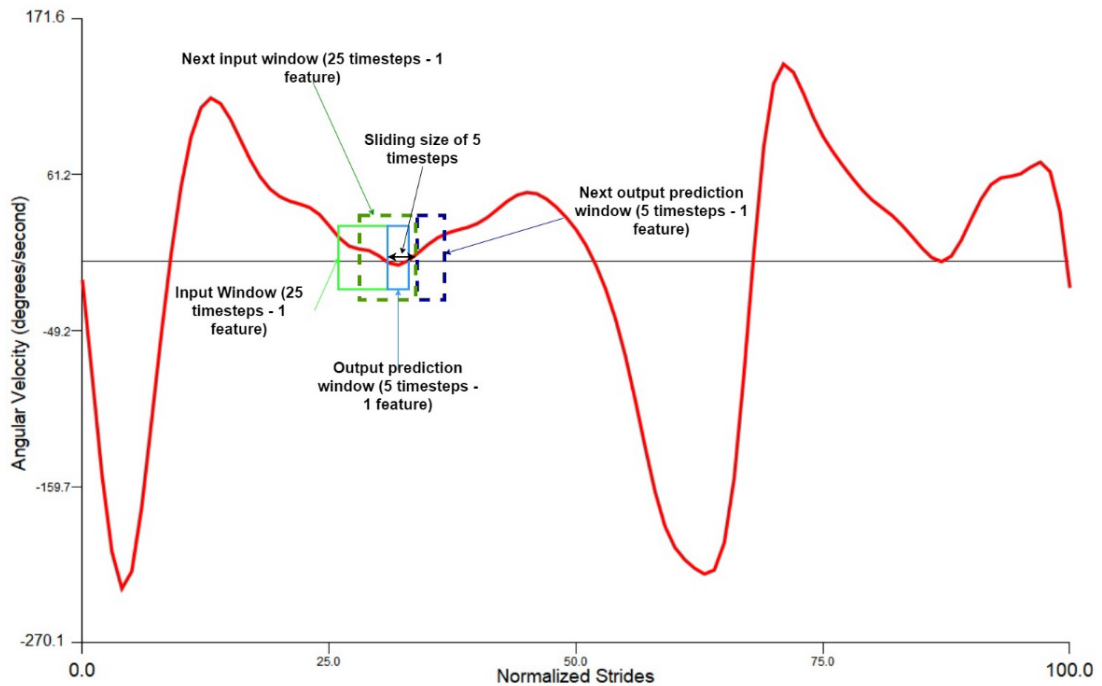


**Figure 4-4:** Sliding window demonstration on 1 feature. The graph shows the sliding window operation on the foot angular velocity ( $X_1$ ). In this work, the input/output window comprises of 6 features.

#### 4.3.6 Implemented LSTM model architectures

Regression problems are amongst the challenging tasks to ANN (Sagheer & Kotb, 2019b). Due to the parameters' initialisation (i.e. neuron weights), the bias-variance trade-off and the function approximation that may trap at a local minima (Sagheer & Kotb, 2019b). As such, it is necessary to experiment with different network architectures to find the optimum solution. After determining the possibility of future trajectories in the last chapter (Zaroug et al., 2020), this work was to determine which LSTM architecture performs the best. There was no report that was found looking into the optimum LSTM neural networks model for gait forecasting prediction. There were 4 LSTM neural network (with similar cells described in Chapter 3) variants that have been tested in this work. This include; (1) Vanilla LSTM neural networks, (2) Stacked LSTM neural networks, (3) Bidirectional LSTM neural networks and (4) LSTM autoencoders neural networks.

The sliding windows and the LSTM models were developed using Python 3 (Libraries: Keras, Numpy, Pandas and Scikit learn) and executed in AWS elastic computing (i.e. EC2) (Francois, 2017; Géron, 2019). The networks were optimised using the SGD optimisation

algorithm (Bottou, 2010, 2012; Sra, Nowozin, & Wright, 2012). Proposed by Rumelhart *et al.*, 1986 (Rumelhart, Hinton, & Williams, 1986), the SGD algorithm aims to obtain the minimum error (MAE in this work) at each batch using the network weights and biases. Using a sparse grid-search, for all models the SGD’s learning rate was tuned to 0.07, the the gradient norm was clipped to 1.0 and the momentum (for accelerating the gradient descent) was set to 0.9 (Sutskever, Martens, Dahl, & Hinton, 2013).

#### 4.3.7 Vanilla LSTM neural network

The vanilla LSTM neural network is the simplest and most commonly used LSTM architecture in the literature (Greff, Srivastava, Koutník, Steunebrink, & Schmidhuber, 2016; Y. Wu, Yuan, Dong, Lin, & Liu, 2018). It is the architecture defined in the original LSTM paper (Hochreiter & Schmidhuber, 1997). It consists of single interconnected LSTM hidden layer and a final dense layer for outputting predictions (see **Figure 4-5**). In this work, there were 1024 LSTM units.

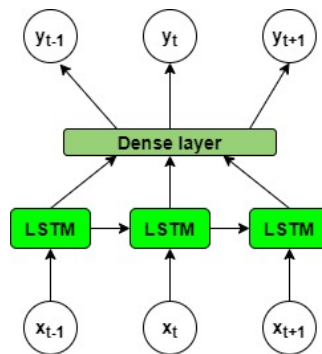


**Figure 4-5:** Vanilla LSTM neural networks (Y. Wu et al., 2018).

#### 4.3.8 Stacked LSTM neural network

It is widely understood that the generalisation of the LSTM model is a function of how deep the network is (Greff et al., 2016; Hermans & Schrauwen, 2013; Sagheer & Kotb, 2019a). A deeper neural network that consists of multiple LSTM hidden layers is known to have higher learning capacity (Hermans & Schrauwen, 2013). The stacked LSTM architecture as shown in **Figure 4-6** consists of multiple LSTM hidden layers and a final dense layer for outputting predictions (Graves, 2013). In this work, there were 5 LSTM hidden layers each with 256 units.

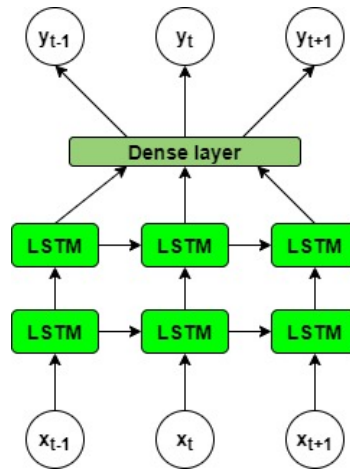


**Figure 4-6:** Stacked LSTM neural networks (Graves, 2013).

#### 4.3.9 Bidirectional LSTM (Bi-LSTM) neural network

Bi-LSTM neural network was introduced as an extension to RNN (Schuster & Paliwal, 1997). Given the entire input data is available, the focus of the bidirectional LSTM neural networks is to maximise modelling of the input sequence by processing the data in forward and backward directions. The architecture works by duplicating the hidden layer side-by-side (see **Figure 4-7**) and process the input sequence as-is to the original hidden layer (forward layer) and as a reversed copy to the duplicate layer (backward layer). The states from the forward layer are not connected to the backward layer, however, both layers are connected to the output layer (Graves & Schmidhuber, 2005; Schuster & Paliwal, 1997). The means by which Bi-LSTM models the input sequence in this manner is the fact that there is a scientific evidence that humans may use sounds, or words that only make sense at a future context (Graves & Schmidhuber, 2005). In this work, there was a single Bi-LSTM with 1024 LSTM units and a Batch Normalisation (BN) applied to the inputs. The aim of the BN is to expedite the neural network training by stabilising the distributions (mean and variance) of the input layer (Ioffe & Szegedy, 2015). The technique was initially deemed to be successful because it reduces the internal covariate shift, however, Santurkar *et al.* suggested that BN reparametrises the optimisation problem by smoothening the loss function landscape (Santurkar, Tsipras, Ilyas, & Madry, 2018). Therefore the optimisation problem become easier to solve (especially in the case of sharp minima or flat regions (H. Li, Xu, Taylor, Studer, & Goldstein, 2018)) and the gradients become reliable and predictive. BN was added to Bi-LSTM because the convergence to local minima was found slower compared to other LSTM models (Siemi-Namini, Tavakoli, & Namin, 2019).

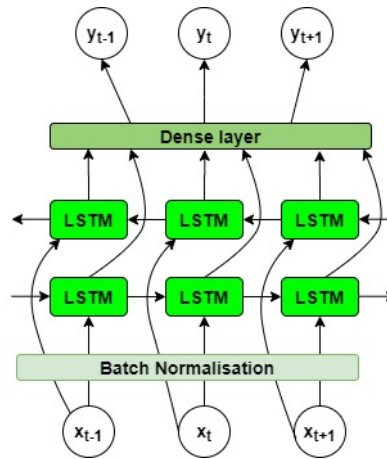


**Figure 4-7:** Bi-LSTM neural networks with a BN input layer (Schuster & Paliwal, 1997).

#### 4.3.10 LSTM autoencoder (ED-LSTM) neural network

Proposed by Srivastava *et al.*, 2015, the ED-LSTM (see **Figure 4-8**) is an unsupervised learning method that seeks to learn from a fixed length input sequence representation (Srivastava *et al.*, 2015). Although it is normally trained with supervised learning, the ED-LSTM recreates the input sequence into a fixed length feature vector. It is composed of two main layers, the encoder layer and the decoder layer. At first, the encoder encodes the variable length input sequence into a fixed length feature vector that represents the input attributes. Then the decoder layer decodes the fixed length feature vector into a variable length output sequence. The general LSTM autoencoder model implemented in Chapter 3 (Zaroug *et al.*, 2020) was kept unchanged, except that the number of units was increased to 1024 per-side (encoder and decoder).

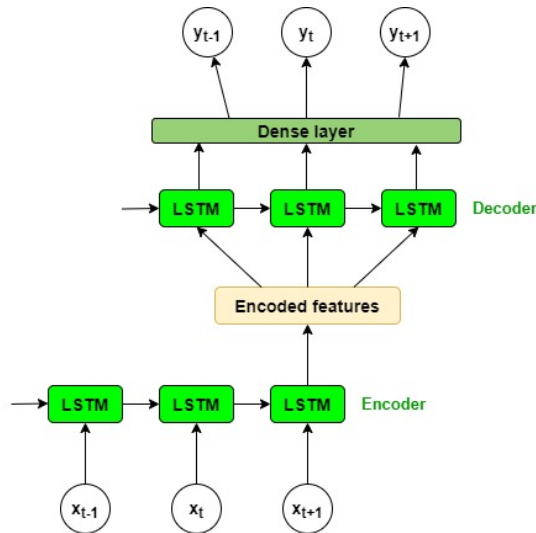


**Figure 4-8:** ED-LSTM neural networks architecture (Sagheer & Kotb, 2019b; Zaroug et al., 2020).

#### 4.3.11 Evaluation and performance metrics

The input/output sliding window size was kept fixed throughout models (Banos et al., 2014; Graves & Schmidhuber, 2005). The input window was 25 timesteps (0.5s) and the output window (future prediction – 0.1s) was 5 timesteps (0.1s) for the 6 feature variables; foot ( $X_1$ ), shank ( $X_2$ ), thigh ( $X_3$ ) AV and foot ( $Y_4$ ), shank ( $Y_5$ ) and thigh ( $Y_6$ ) LA (Zaroug et al., 2020).

In order to allow model comparison, all models were firstly tested with the same participant when the initial number of epochs was reached (**Table 4-2**). The initial number of epochs is when the model was found to attain generalisation by obtaining the least MAE on an unseen participant. Subsequent 14 participants were tested after 10 epochs each using the leave-one-out cross validation technique. When a participant is tested all of their associated trials were removed from the training set ( $5\text{km}\cdot\text{h}^{-1}$  and PWS). Due to the complexity of LSTM neural networks, Transfer Learning (TL) was adopted to reduce the training time for leave-one-out cross validation test. The TL, also known as knowledge transfer, is a method by which training doesn't start from the original point at each time new data is available (Pan & Yang, 2009; Torrey & Shavlik, 2010). The technique was found to lower the cost of training and improve based-line performance. Due to the uniqueness of individual walking patterns and the different PWS across participants (F Horst, Mildner, & Schöllhorn, 2017; Schöllhorn, Nigg, Stefanyshyn, & Liu, 2002), the testing set for all participants was kept fixed at 75 timesteps (starting from the foot strike).

**Table 4-2:** Models' configuration for inter-subject leave-one-out cross validation test. The number of epochs is the starting point for testing the first participant. Using TL, subsequent participants were tested after 10 epochs each.

| Models       | Hidden layers | Units per layer | Epochs (Initial) | Epochs (Final) |
|--------------|---------------|-----------------|------------------|----------------|
| Vanilla LSTM | 1             | 1024            | 100              | 240            |
| Stacked LSTM | 5             | 256             | 260              | 400            |
| BI-LSTM      | 2             | 1024            | 200              | 340            |
| ED-LSTM      | 2             | 1024            | 200              | 340            |

In addition to the performance metrics implemented in Chapter 3 – Section 3.3.9, 2 more metrics were considered to calculate how closely the predicted variable trajectories  $\hat{y}_j$  ( $X_1, X_2, X_3, Y_4, Y_5, Y_6$ ) was to the actual variable trajectories  $y_j$  ( $X_1, X_2, X_3, Y_4, Y_5, Y_6$ ) across the  $n$  timesteps:

1. Root Mean Square Error (RMSE) given as:

$$RMSE = \sqrt{\frac{1}{n} \sum_{j=1}^n (y_j - \hat{y}_j)^2} \quad (4 - 1)$$

2. Normalised RMSE (NRMSE) (Gholami et al., 2020; Tanghe et al., 2019) given as:

$$NRMSE(\%) = \frac{RMSE}{\max(y) - \min(y)} \quad (4 - 2)$$

Where  $\max(y)$  and  $\min(y)$  are the maximum and minimum values of the trial's ground truth.

## 4.4 Results

### 4.4.1 LSTM models

All models were firstly evaluated at PWS after the initial number of epochs and on the same participant across 75 timesteps. Trials related to the tested participant were removed from the training set. Models performance (combined output windows) for each of the independent variables that belong to the tested participant are shown in **Figure 4-9** for all LSTM models. A single output window (prediction horizon) is a 5 timesteps window (0.1s). All models have shown good tracking of the actual trajectories for the shank and thigh AV (**Figure 4-9– c and e**). Poorer predictions were attained for all segment predictions based on LA.

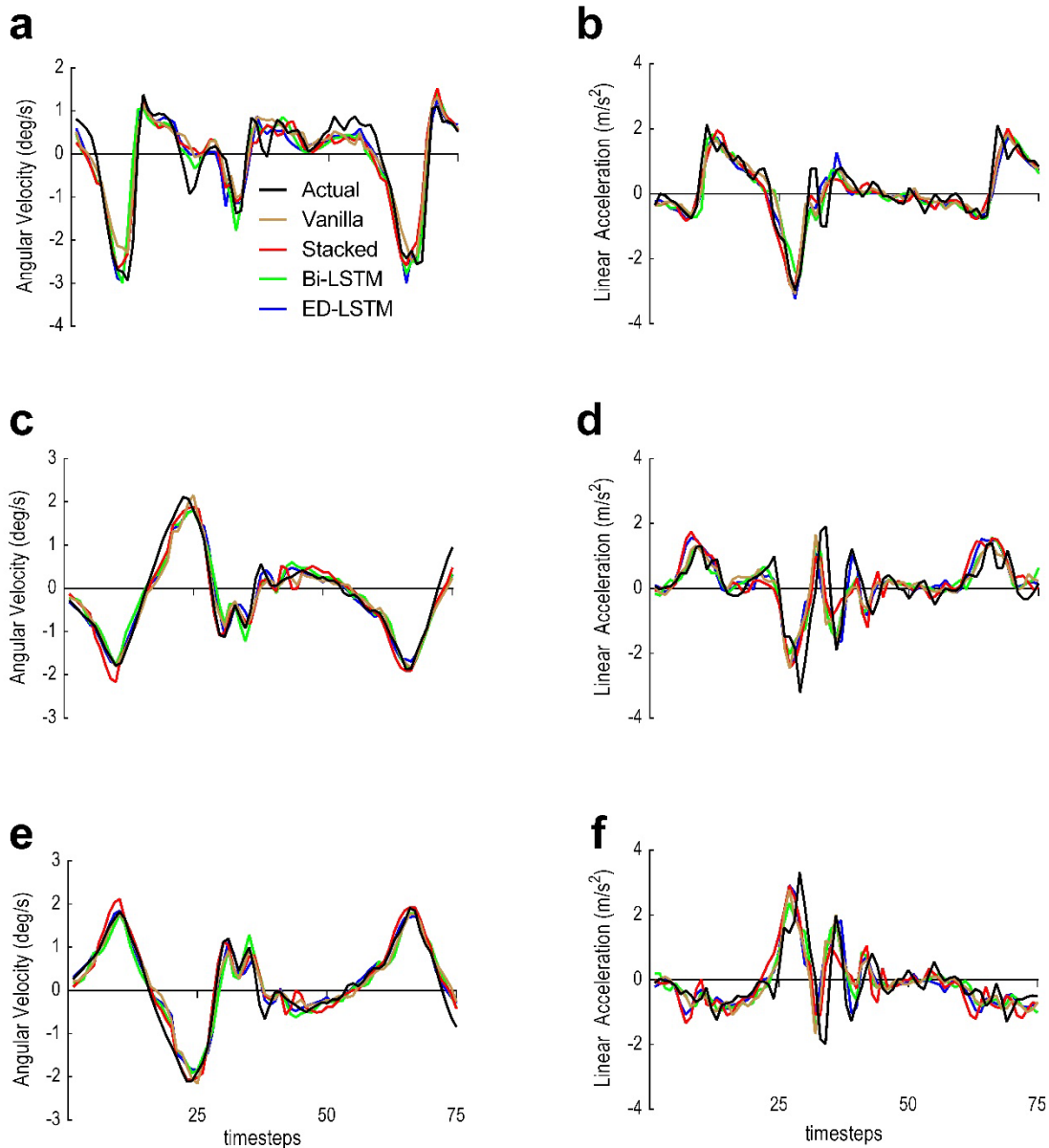


**Figure 4-9:** LSTM models prediction performance based on the inter-subject test for each feature vector at PWS only. Models were tested with 75 timesteps (i.e. 1.5s) and the same participant was tested across LSTM models. Black is the actual trajectory. Brown is the Vanilla LSTM predicted trajectory. Red is the Stacked LSTM predicted trajectory. Green is the Bi-LSTM predicted trajectory. Blue is the ED-LSTM predicted trajectory. (a) Foot AV ( $X_1$ ). (b) Foot LA ( $Y_4$ ). (c) Shank AV ( $X_2$ ). (d) Shank LA ( $Y_5$ ). (e) Thigh AV ( $X_3$ ). (f) Thigh LA ( $Y_6$ ).

Models were then evaluated at PWS and 5km.h<sup>-1</sup> combined based on leave-one-out cross validation technique after every 10 epochs for each participant (see **Table 4-3**, **Table 4-4** and **Table 4-5**). All models achieved good predicted trajectories for AV related to the shank ( $X_2$ ) and thigh ( $X_3$ ) (low RMSE in **Figure 4-10** c and e) and good vector patterns for all feature vectors (High CC in **Table 4-5** and **Figure 4-10**). Predicted trajectories based on the AV (MAE

0.101-0.260 deg.s<sup>-1</sup>) were generally less erroneous than the predicted trajectories based on the LA (MAE 0.164-0.300 m.s<sup>-2</sup>) across all the LSTM models (see **Table 4-3**). The Stacked and ED LSTM are found the best predictive models for future predictions of the lower limb kinematic trajectories at PWS and 5km.h<sup>-1</sup>. The wider the gap between the two points (CC and RMSE) in **Figure 4-10** indicates a good performance achieved by the LSTM model. The Stacked and ED LSTM were the only models that maintained a good predicted LA and AV patterns (Higher CC in **Figure 4-10**) and a more accurate predicted LA and AV trajectories (lower RMSE in **Table 4-3** and **Figure 4-10**). The Vanilla LSTM obtained the worse prediction results (6.34-9.46%) compared to the Stacked LSTM (4.70-7.58%) and the ED-LSTM (4.55-7.91%) (**Table 4-4** and **Figure 4-11**). The Bi-LSTM have shown the highest error rate in this research (5.92-9.98%) (**Table 4-4** and **Figure 4-11**).

**Table 4-3:** Leave-one-out cross validation test error based on the MAE, MSE and the RMSE at the PWS and 5km.h<sup>-1</sup> combined. Each of the predicted variables (i.e.  $X_1, X_2, \dots, Y_6$ ) was evaluated for the 4 trained LSTM architectures.

| Error metric | Architecture | $X_1$<br>(deg.s <sup>-1</sup> ) | $X_2$<br>(deg.s <sup>-1</sup> ) | $X_3$<br>(deg.s <sup>-1</sup> ) | $Y_4$<br>(m.s <sup>-2</sup> ) | $Y_5$<br>(m.s <sup>-2</sup> ) | $Y_6$<br>(m.s <sup>-2</sup> ) |
|--------------|--------------|---------------------------------|---------------------------------|---------------------------------|-------------------------------|-------------------------------|-------------------------------|
| <b>MAE</b>   | Vanilla LSTM | 0.276                           | 0.196                           | 0.198                           | 0.246                         | 0.319                         | 0.316                         |
|              | Stacked LSTM | 0.226                           | 0.137                           | 0.144                           | 0.209                         | 0.241                         | 0.262                         |
|              | Bi-LSTM      | 0.292                           | 0.181                           | 0.186                           | 0.263                         | 0.319                         | 0.332                         |
|              | ED-LSTM      | 0.225                           | 0.127                           | 0.133                           | 0.2                           | 0.235                         | 0.255                         |
| <b>MSE</b>   | Vanilla LSTM | 0.227                           | 0.09                            | 0.083                           | 0.193                         | 0.232                         | 0.248                         |
|              | Stacked LSTM | 0.187                           | 0.059                           | 0.058                           | 0.176                         | 0.161                         | 0.19                          |
|              | Bi-LSTM      | 0.236                           | 0.082                           | 0.075                           | 0.204                         | 0.239                         | 0.266                         |
|              | ED-LSTM      | 0.201                           | 0.059                           | 0.047                           | 0.154                         | 0.164                         | 0.191                         |
| <b>RMSE</b>  | Vanilla LSTM | 0.422                           | 0.273                           | 0.273                           | 0.381                         | 0.459                         | 0.467                         |
|              | Stacked LSTM | 0.355                           | 0.204                           | 0.209                           | 0.331                         | 0.364                         | 0.388                         |
|              | Bi-LSTM      | 0.436                           | 0.257                           | 0.255                           | 0.401                         | 0.467                         | 0.487                         |
|              | ED-LSTM      | 0.37                            | 0.199                           | 0.197                           | 0.317                         | 0.364                         | 0.386                         |

**Table 4-4:** Leave-one-out cross validation test error based on the NRMSE (%) at the PWS and 5km.h<sup>-1</sup> combined. Each of the predicted variables (i.e.  $X_1, X_2, \dots, Y_6$ ) was evaluated for the 4 trained LSTM architectures.

| Architecture        | $X_1$ % | $X_2$ % | $X_3$ % | $Y_4$ % | $Y_5$ % | $Y_6$ % |
|---------------------|---------|---------|---------|---------|---------|---------|
| <b>Vanilla LSTM</b> | 9.46    | 6.34    | 6.44    | 6.68    | 8.63    | 9.28    |
| <b>Stacked LSTM</b> | 7.58    | 4.70    | 4.94    | 5.63    | 6.83    | 7.58    |
| <b>Bi-LSTM</b>      | 9.87    | 5.92    | 6.02    | 7.17    | 8.90    | 9.98    |
| <b>ED-LSTM</b>      | 7.91    | 4.55    | 4.69    | 5.49    | 6.76    | 7.50    |

**Table 4-5:** Leave-one-out cross validation test evaluation based on the CC at the PWS and 5km.h<sup>-1</sup> combined. Each of the predicted variables (i.e.  $X_1, X_2, \dots, Y_6$ ) was evaluated for the 4 trained LSTM architectures.

| Architecture        | $X_1$ | $X_2$ | $X_3$ | $Y_4$ | $Y_5$ | $Y_6$ |
|---------------------|-------|-------|-------|-------|-------|-------|
| <b>Vanilla LSTM</b> | 0.89  | 0.95  | 0.96  | 0.90  | 0.84  | 0.84  |
| <b>Stacked LSTM</b> | 0.91  | 0.97  | 0.97  | 0.91  | 0.88  | 0.88  |
| <b>Bi-LSTM</b>      | 0.89  | 0.95  | 0.96  | 0.90  | 0.83  | 0.82  |
| <b>ED-LSTM</b>      | 0.91  | 0.97  | 0.97  | 0.92  | 0.88  | 0.88  |

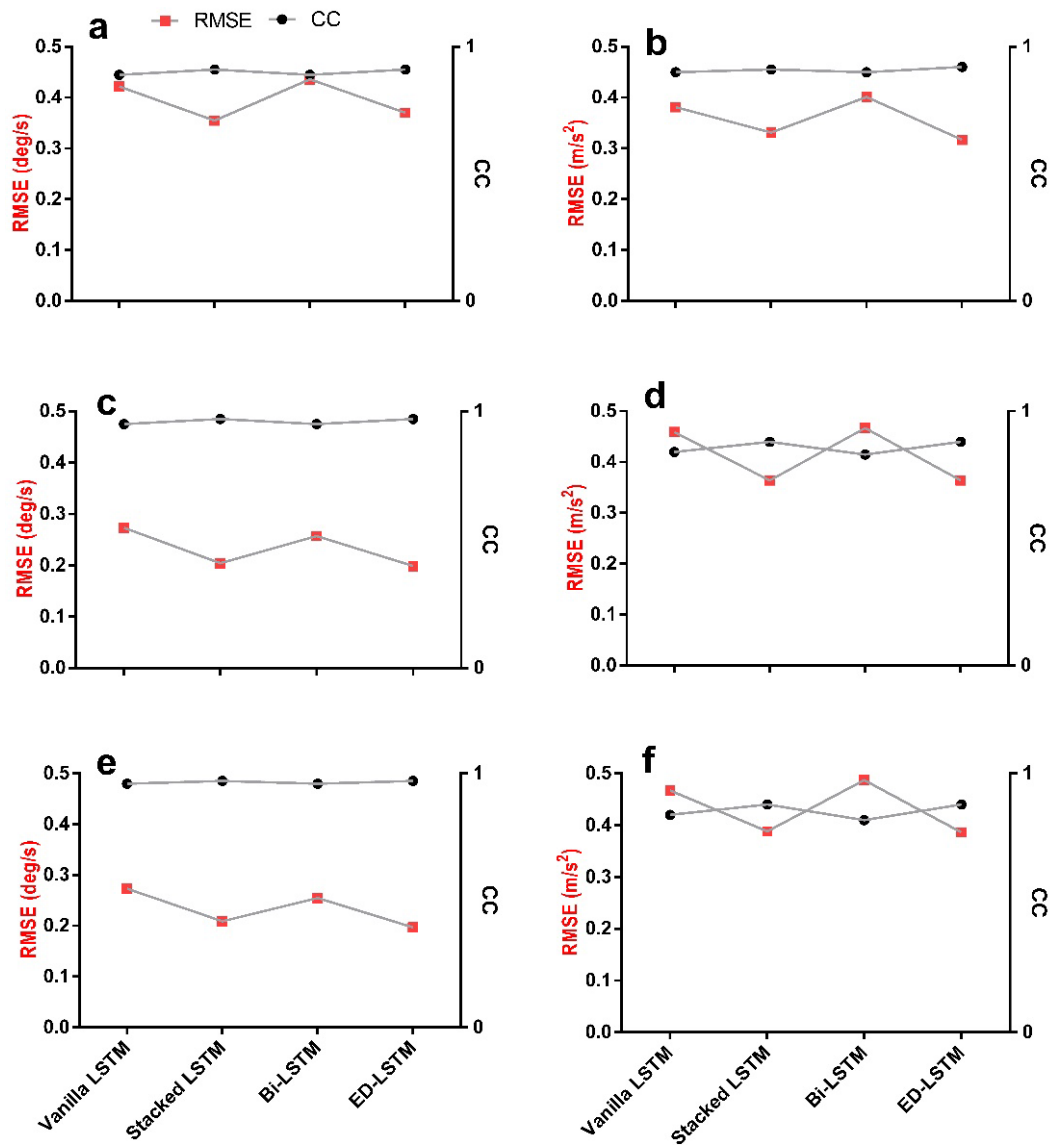


**Figure 4-10:** Performance comparison between LSTM models based on leave-one-out cross validation at PWS and  $5\text{km}\cdot\text{h}^{-1}$  for each feature vector. Red is the RMSE (Left Y-axis). Black is the CC (Right Y-axis). Wider gaps between the two error lines (CC and RMSE) means better prediction quality for the related feature vector. The Stacked and ED LSTM maintained the gap for all feature vectors. (a) Foot AV ( $X_1$ ). (b) Foot LA ( $Y_4$ ). (c) Shank AV ( $X_2$ ). (d) Shank LA ( $Y_5$ ). (e) Thigh AV ( $X_3$ ). (f) Thigh LA ( $Y_6$ ).

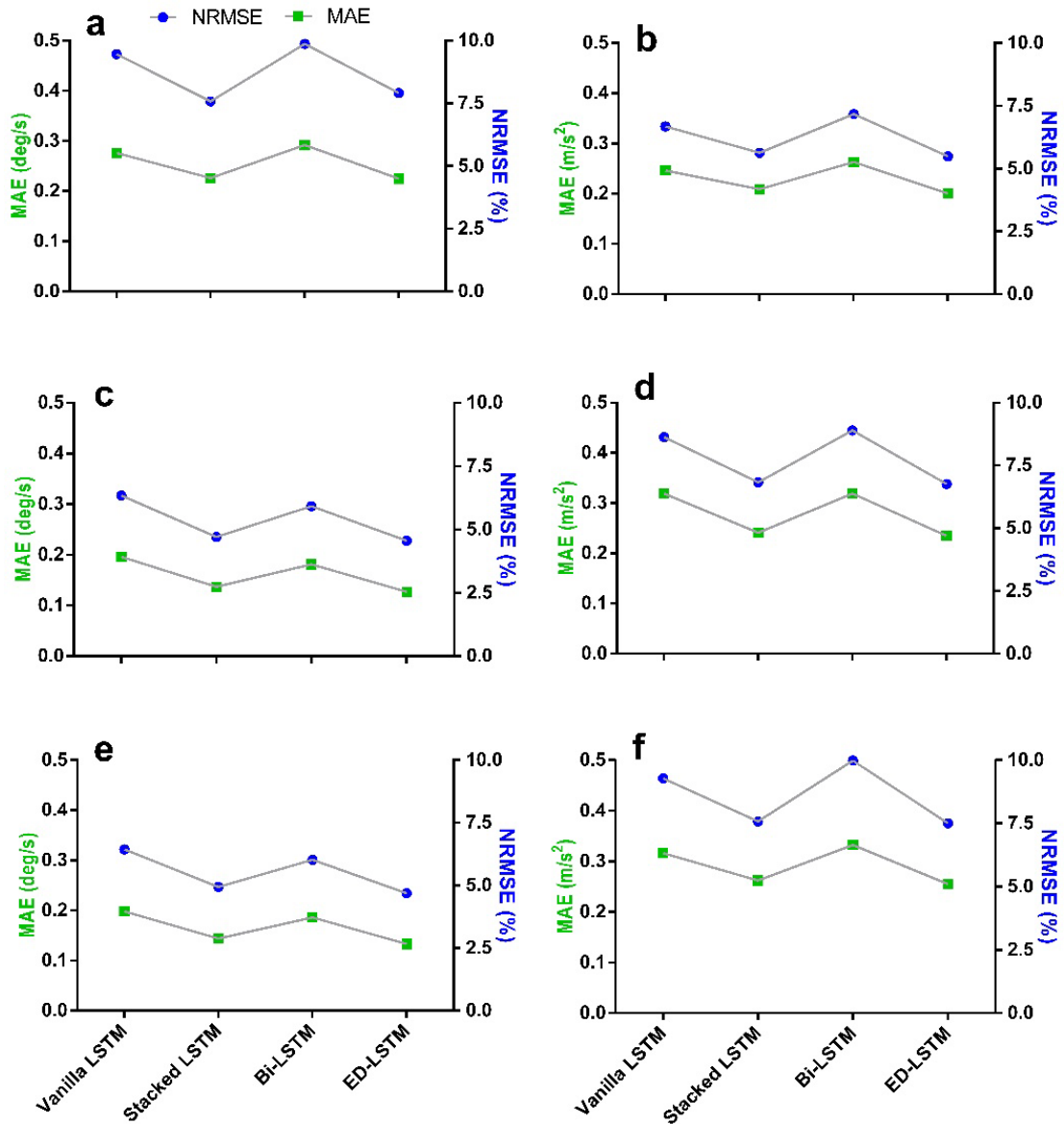


**Figure 4-11:** Performance comparison between LSTM models based on leave-one-out cross validation at PWS and  $5\text{km}\cdot\text{h}^{-1}$  for each feature vector. Green is the RMSE (Left Y-axis). Blue is the NRMSE (Right Y-axis). Lower error points for the MAE and NRMSE means a better predictive model for the related feature vector. (a) Foot AV ( $X_1$ ). (b) Foot LA ( $Y_4$ ). (c) Shank AV ( $X_2$ ). (d) Shank LA ( $Y_5$ ). (e) Thigh AV ( $X_3$ ). (f) Thigh LA ( $Y_6$ ).

#### 4.4.2 The LR prediction performance

The LR model was tested on 75 timesteps (i.e. 1.5s) from an unseen participant (see **Figure 4-12**) walking at PWS. The LR weakly estimated the actual LA trajectory patterns and demonstrated the worst overall prediction performance compared to the LSTM models across all predicted variables as shown in **Table 4-6**. The model was cross validated for all participants and attained similar performance as shown in **Table 4-7**.

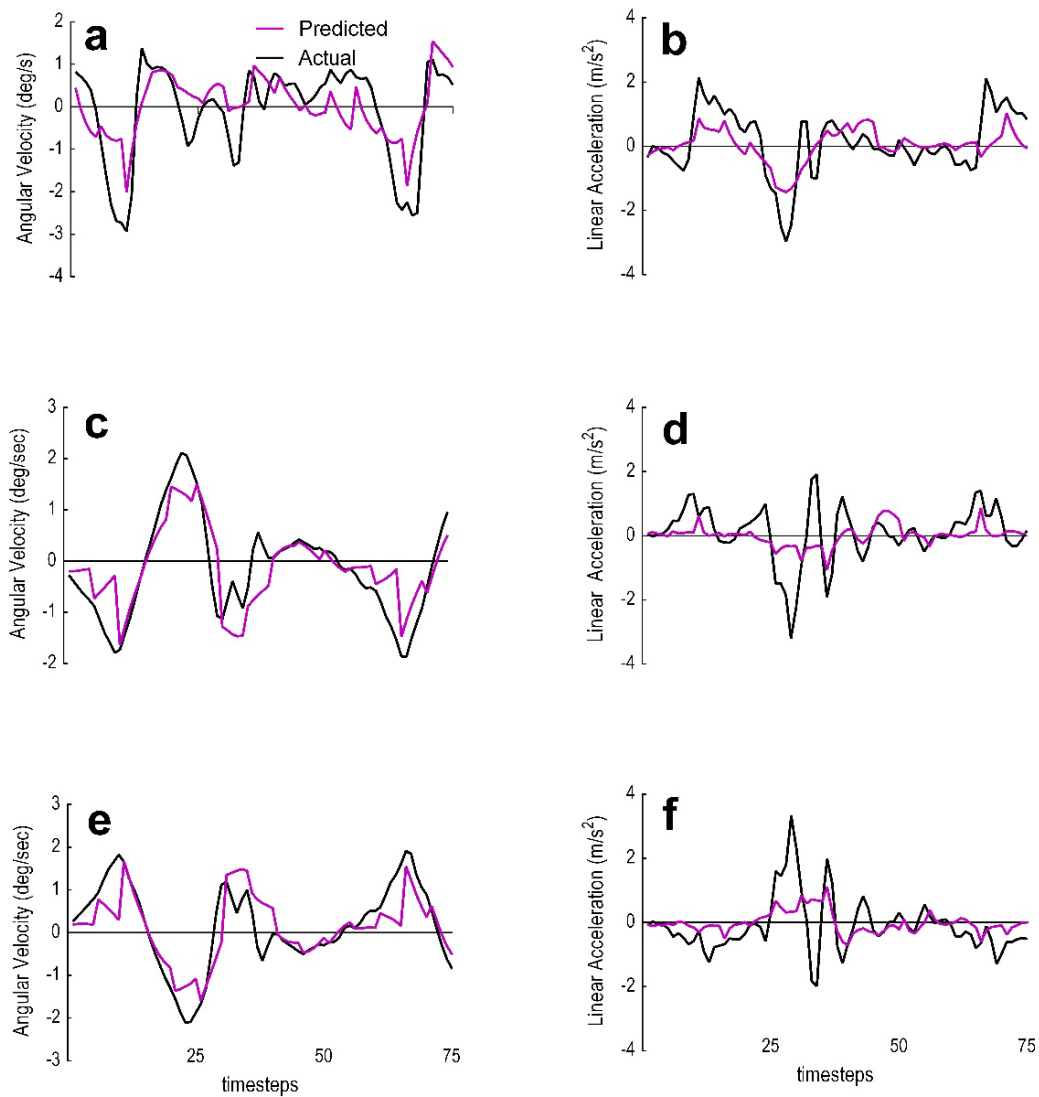


**Figure 4-12:** The LR prediction performance with 75 timesteps (i.e. 1.5s) based on the inter-subject test for each feature vector at PWS only. Black is the actual trajectory. Magenta is the LR predicted trajectory. (a) Foot AV ( $X_1$ ). (b) Foot LA ( $Y_4$ ). (c) Shank AV ( $X_2$ ). (d) Shank LA ( $Y_5$ ). (e) Thigh AV ( $X_3$ ). (f) Thigh LA ( $Y_6$ ).

**Table 4-6:** The LR performance results across 75 timesteps of walking on an unseen participant prior to TL. All participant's associated trials (e.g. 5k) were removed from the training set.

| Feature | MAE                       | MSE                       | RMSE                      | NRMSE% | CC   |
|---------|---------------------------|---------------------------|---------------------------|--------|------|
| $X_1$   | 0.663 deg.s <sup>-1</sup> | 0.676 deg.s <sup>-1</sup> | 0.822 deg.s <sup>-1</sup> | 19.05  | 0.69 |
| $X_2$   | 0.415 deg.s <sup>-1</sup> | 0.315 deg.s <sup>-1</sup> | 0.561 deg.s <sup>-1</sup> | 14.12  | 0.80 |
| $X_3$   | 0.412 deg.s <sup>-1</sup> | 0.328 deg.s <sup>-1</sup> | 0.572 deg.s <sup>-1</sup> | 14.26  | 0.80 |
| $Y_4$   | 0.606 m.s <sup>-2</sup>   | 0.555 m.s <sup>-2</sup>   | 0.745 m.s <sup>-2</sup>   | 14.60  | 0.67 |
| $Y_5$   | 0.547 m.s <sup>-2</sup>   | 0.606 m.s <sup>-2</sup>   | 0.778 m.s <sup>-2</sup>   | 15.21  | 0.44 |
| $Y_6$   | 0.512 m.s <sup>-2</sup>   | 0.607 m.s <sup>-2</sup>   | 0.779 m.s <sup>-2</sup>   | 14.67  | 0.42 |

**Table 4-7:** The LR leave-one-out cross validation test among 15 participants across 75 timesteps. When a participant's data are used for testing, all their associated trials are removed from the training set.

| Feature | MAE                       | MSE                       | RMSE                      | NRMSE% | CC   |
|---------|---------------------------|---------------------------|---------------------------|--------|------|
| $X_1$   | 0.583 deg.s <sup>-1</sup> | 0.721 deg.s <sup>-1</sup> | 0.821 deg.s <sup>-1</sup> | 17.47  | 0.66 |
| $X_2$   | 0.429 deg.s <sup>-1</sup> | 0.375 deg.s <sup>-1</sup> | 0.599 deg.s <sup>-1</sup> | 14.42  | 0.79 |
| $X_3$   | 0.440 deg.s <sup>-1</sup> | 0.374 deg.s <sup>-1</sup> | 0.606 deg.s <sup>-1</sup> | 14.67  | 0.80 |
| $Y_4$   | 0.579 m.s <sup>-2</sup>   | 0.673 m.s <sup>-2</sup>   | 0.787 m.s <sup>-2</sup>   | 14.09  | 0.62 |
| $Y_5$   | 0.571 m.s <sup>-2</sup>   | 0.664 m.s <sup>-2</sup>   | 0.806 m.s <sup>-2</sup>   | 15.81  | 0.43 |
| $Y_6$   | 0.588 m.s <sup>-2</sup>   | 0.681 m.s <sup>-2</sup>   | 0.813 m.s <sup>-2</sup>   | 16.39  | 0.44 |

## 4.5 Discussion

The aim of this study was to investigate the capability of 4 standard LSTM architectures and the LR in predicting future lower limb trajectories of sagittal plane kinematic variables (simulated IMU output) at the PWS. The predicted kinematic variables are the foot AV ( $X_1$ ), shank AV ( $X_2$ ), thigh AV ( $X_3$ ), foot LA ( $Y_4$ ), shank LA ( $Y_5$ ) and thigh LA ( $Y_6$ ). Prediction was performed using the LR as well as the (i) Vanilla LSTM, (ii) Stacked LSTM, (iii) Bi-LSTM and (iv) ED-LSTM. Results suggested that the LR is unreliable in predicting the lower limb kinematics at PWS. The performance of LSTM architectures indicated that the Stacked and ED LSTM models are more accurate in predicting the future trajectory of the lower limb kinematics up to 0.1s (5 timesteps) (**Figure 4-11**). The ED-LSTM achieved the most accurate predicted kinematic trajectories among the other LSTM architectures (see **Table 4-3**). The prediction of future gait trajectory has the potential to expand the horizon of solving several problems in human movement science. A known future gait trajectory adds a feedforward term to powered exoskeleton devices instead of predominantly relying on feedback sensors (Anam & Al-Jumaily, 2012; Proud et al., 2020; Tanghe et al., 2019; Zaroug et al., 2019). This would improve device performance by narrowing down the nonlinear kinematic differences between the user and the device and therefore avoid altering the user's natural gait trajectories (Rupal et al., 2017; Torricelli et al., 2018). Prediction of future gait trajectory could substantially improve the design of prosthetics by adapting the device controlling parameters according to the user's movement (Shafiul Hasan et al., 2020). Additionally, a known 0.1s future gait trajectory facilitates the prediction of low foot clearance and falls in the range of slow and fast twitch (0.01-0.12s) motor units (Winter, 2009). That may allow the user (i.e. person with fall history) to develop countermeasures and adjust their gait to avoid an imminent risk of tripping or

balance loss (Barrett, Mills, & Begg, 2010; R. K. Begg & Rahman, 2000; Khandoker, Lai, Begg, & Palaniswami, 2006; D. T. Lai et al., 2012; Winter, 2009).

The input (25 timesteps) and output (5 timesteps) sliding window sizes were designed as per the work by Zaroug *et al.* (Zaroug et al., 2020). The combination of PWS and imposed speed  $5\text{km.h}^{-1}$  timeseries data, widens the variability in the training data and further challenges the ML model to maintain a good prediction quality across different walking speeds. A ML model trained on PWS allows a generalised predictive model that could be fine tuned across different participants. The number of participants was increased for both genders (Male and female) to our previous work (Zaroug et al., 2020). The foot segment was also added as the foot is the basis of human balance, support and locomotion. Its movement directly affects the lower extremities (i.e. ankle) dynamics and control (Garofolini, Taylor, Mclaughlin, Mickle, & Frigo, 2019) as well as the body's Centre of Mass (COM) movement (C. W. Chan & Rudins, 1994; Mun, Song, Chun, & Kim, 2018).

Five metrics were implemented to evaluate the LSTM prediction quality (**Table 4-3** and to **Table 4-5**). Results have shown that LSTM predictions based on the LA were worse than predictions based on the AV in all models, possibly due to the double derivative generating a noisier signal (**Figure 4-9**). The foot AV ( $X_1$ ) predictions showed greater error (MAE 0.225-0.292  $\text{deg.s}^{-1}$ ) throughout models compared to the shank (MAE 0.127-0.196  $\text{deg.s}^{-1}$ ) and thigh (MAE 0.133-0.198  $\text{deg.s}^{-1}$ ) AV, likely due to the greater variation of the foot trajectory throughout the gait cycle (Gholami et al., 2020). The NRMSE was used to facilitate the comparison between the LSTM models performance and to simplify the understanding of error rates for cross-disciplinary research. The Vanilla LSTM attained generalisation earlier (100 epochs) compared to all other models due to its simplicity and the fewer required parameters to train (Sagheer & Kotb, 2019b). Albeit, it obtained higher error rates compared to the Stacked LSTM and the ED-LSTM (**Figure 4-11** and **Table 4-3**). Although the Bi-LSTM have shown good performance in financial time series forecasting (Siami-Namini et al., 2019) and in coordination with CNN for Electrocardiogram (ECG) signal generation (Zhu, Ye, Fu, Liu, & Shen, 2019), it has shown the poorest prediction quality in this research (**Table 4-4**). Despite being the only network with inputs BN layer, it was not clear whether learning from the past and the future on human movement data have added any value to the prediction quality.

All models were good at predicting the signal patterns but were erroneous at obtaining the actual trajectories (see **Figure 4-10** and **Table 4-5**). This indicates that prediction at PWS further

challenges the prediction quality and it can be improved by training and testing the model on the same participant. The walking speed was found to be the most influential variable amongst sex, age and body mass index on the ambulatory kinematic and kinetic profiles (Chehab et al., 2017). The changes of speed are known to have substantial impacts on the spatiotemporal as well as the kinematic and kinetic patterns of the gait cycle among different age groups (Claudiane Arakaki Fukuchi et al., 2019; Grant & Chester, 2015). Normal (comfortable or preferred) walking speed reported in the literature had averages ranging from  $1.05\text{m}\cdot\text{s}^{-1}$  to  $1.43\text{m}\cdot\text{s}^{-1}$  (cadence of 101 to 122 steps/min,) (Kwon et al., 2015; Winter, 1991). The imposed speed  $5\text{km}\cdot\text{h}^{-1}$  was found to be the general average PWS in previous studies (Browning et al., 2006; Mohamed & Appling, 2020; Mohler et al., 2007; Waters et al., 1988) and it was adopted in this work to generalise the LSTM models to populations outside the recruited participants cohort. Prediction at the imposed walking speed of  $5\text{km}\cdot\text{h}^{-1}$  was found to be good in our previous work using the ED-LSTM (Zaroug et al., 2020) and in the literature using the PPCA (Tanghe et al., 2019). The prediction at PWS however, allows the development of ML models that are better suited to individuals who might have different PWS which in return naturalise the human-machine (i.e. bionics) interface.

In Chapter 3, the prediction of future kinematics trajectory (up to 0.06 s) was possible at an imposed speed ( $5\text{km}\cdot\text{h}^{-1}$ ) using the ED-LSTM and LR. In this work the prediction horizon was expanded up to 0.1s and investigated the other LSTM architectures to predict the kinematics trajectory at PWS and imposed speed ( $5\text{km}\cdot\text{h}^{-1}$ ). The input (25 timesteps – 0.5s) and output (5 timesteps – 0.1s) sliding window sizes were designed as per the work by Zaroug *et al.* (Zaroug et al., 2020). The combination of PWS and imposed speed  $5\text{km}\cdot\text{h}^{-1}$  timeseries data, widens the variability in the training data and further challenges the ML model to maintain a good prediction quality across different walking speeds. A ML model trained on PWS allows a generalised predictive model that could be fine tuned across different participants. The number of participants was increased for both genders (Male and female) to our previous work (Zaroug et al., 2020). The foot segment was also added as the foot is the most distal segment of the human locomotor multisegment chain and plays an important part in maintaining balance, support and locomotion. Foot's movement directly affects the lower extremities (i.e. ankle) dynamics and control (Garofolini, Taylor, McLaughlin, et al., 2019) as well as the body's Centre of Mass (COM) movement (C. W. Chan & Rudins, 1994; Mun et al., 2018).

In contrast to the predicted trajectories evaluation technique by Tanghe et al. (Tanghe et al., 2019) (i.e. 3 selected timesteps), the performance evaluations of this work were calculated

relative to the mean based on each of the predicted 75 timesteps (i.e. 1.5s). The ED-LSTM in this work (**Table 4-8**) attained lower MAE range (0.127-0.255) than Su and Gutierrez-Farewik results (0.187-0.308) (B. Su & M Gutierrez-Farewik, 2020) and lower NRMSE range (4.55-7.91%) than the CNN implemented by Gholami et al. (6.5-11.1%) (Gholami et al., 2020). These results suggest that ED LSTM neural networks are a more suitable model to capture features related to sequential time-series lower limb kinematic data (Graves, 2012a; A. Zhao et al., 2018). The ED LSTM achieved the most accurate predictions in this work (see **Table 4-3**). As demonstrated in (see **Figure 4-8**) and in the last chapter (Zaroug et al., 2020), the internal learning process for the ED LSTM is unsupervised (Srivastava et al., 2015).

**Table 4-8:** ML-based methods for lower limb kinematics estimation (inter-subject test).

| Study   | Regression problem  | Model   | Participants     | Conditions  | Error (%)  | CC                                       |
|---|---|---|------------------|---|--|--|
| <b>Gholami <i>et al.</i></b><br>(Gholami et al., 2020)      | Prediction of lower limb joint angles from shoe mounted accelerometer.  | Convolutional Neural Networks (CNN)               | 10               | Running at 8, 9, 10, 11 and 12 km.h <sup>-1</sup>         | <ul style="list-style-type: none"> <li>• Hip: 9.9%.</li> <li>• Knee: 6.5%.</li> <li>• Ankle: 11.1%.</li> </ul>   | -  |
| <b>Su <i>et al.</i></b> (B. Su & M Gutierrez-Farewik, 2020) | Prediction of future AV only of foot, thigh and shank segments.         | Vanilla LSTM                                      | 12               | Walking at 5 different speeds according to the literature | -  | Thigh: 0.91<br>Shank: 0.97<br>Foot: 0.93 |
| <b>Tanghe <i>et al.</i></b><br>(Tanghe et al., 2019)        | Prediction of future lower limb joint kinematics.                       | Probabilistic principal component analysis (PPCA) | 28 (1,098 steps) | Walking at 2 and 5km.h <sup>-1</sup>                      | <ul style="list-style-type: none"> <li>• Hip:<br/>Velocity = 7-9%.<br/>Acceleration = 9.8-12.1%.</li> <li>• Knee:<br/>Velocity = 4.5-8.5%.<br/>Acceleration = 6.3-10.5%.</li> <li>• Ankle:<br/>Velocity = 7.8% - 10.7%.<br/>Acceleration = 8.8-12.5%.</li> </ul> | -  |
| <b>Findlow <i>et al.</i></b><br>(Findlow et al., 2008)      | Prediction of lower limb joint angles from AV and LA of shank and foot. | Generalised Regression Neural Networks (GRNN)     | 8                | 30 gait cycles of walking at PWS                          | -  | Overall = 0.80                           |

---

|                   |  |  |                   |   |  |  |
|-------------------|--|--|-------------------|---|--|--|
| <b>This study</b> | Prediction of future lower limb AV and LA of thigh, shank and foot segments. | <ul style="list-style-type: none"> <li>• Vanilla LSTM.</li> <li>• Stacked LSTM.</li> <li>• Bi-LSTM.</li> <li>• ED-LSTM.</li> </ul> | 15 (10,500 steps) | Walking st PWS and imposed speed at 5km.h <sup>-1</sup> . | <ul style="list-style-type: none"> <li>• Vanilla LSTM:<br/>AV = 6.34-9.46%.<br/>LA = 6.68-9.28%.</li> <li>• Stacked LSTM:<br/>AV = 4.70-7.58%.<br/>LA = 5.63-7.58%.</li> <li>• Bi-LSTM:<br/>AV = 5.92-9.87%.<br/>LA = 7.17-9.98%.</li> <li>• ED-LSTM:<br/>AV = 4.55-7.91%.<br/>LA = 5.49-7.50%.</li> </ul> | <ul style="list-style-type: none"> <li>• Vanilla LSTM:<br/>AV = 0.89-0.96.<br/>LA = 0.84-0.90.</li> <li>• Stacked LSTM:<br/>AV = 0.91-0.97.<br/>LA = 0.88-0.91.</li> <li>• Bi-LSTM:<br/>AV = 0.89-0.96.<br/>LA = 0.82-0.90.</li> <li>• ED-LSTM:<br/>AV = 0.91-0.97.<br/>LA = 0.88-0.92.</li> </ul> |
|-------------------|--|--|-------------------|---|--|--|

---

Although the LR is simple and easy to apply, it assumes a linear relationship between dependent (i.e. output trajectories) and independent variables (i.e. input trajectories). The LR is a parametric model that significantly simplifies the learning process into a set of fixed size coefficients (Russell & Norvig, 2002). As such, the LR obtained worse prediction performance than all of the LSTM models in this study (**Figure 4-12, Table 4-6 and Table 4-7**). Particularly because it can easily overfit to the training data without adjusting the function form (i.e. straight line). Hanlon and Anderson have suggested that the LR can best performs when it is trained and tested on the same speed (Hanlon & Anderson, 2006). In this study, the training and testing data resembled the PWS and the imposed speed ( $5\text{km}\cdot\text{h}^{-1}$ ) which means a high variance in the walking speed range for the LR to capture. Regularisation techniques such as the Lasso regression (i.e. L1), Ridge regression (i.e. L2) and the Elastic Net (i.e. L1+L2) may help addressing the problems of LR by penalising the regressor coefficients (Bishop, 2006; Hans, 2011; Hoerl & Kennard, 1970; Ogutu, Schulz-Streeck, & Piepho, 2012; Robert Tibshirani, 1996). The performance results suggest that while the linear regression may be a great tool to analyse the relationship between gait variables, it is not recommended for predicting the future gait kinematics.

This work was limited to young healthy participants. There exists a proportional relationship between the human age and their walking speeds. The walking speed was found to be slightly decreasing each year among healthy male and female populations (Schimpl et al., 2011). Future work is needed to test the models' performance on predicting slower speeds than that tested and accommodate predictions related to elderly population who may walk slower. Patients with balance issues or fall history should be recruited to further understand the potential application of this work for estimating the minimum toe clearance (Barrett et al., 2010; D. T. Lai et al., 2012; Levinger et al., 2016; Nagano, Said, James, & Begg, 2020). Finally, a more complex model such as the hybrid models (i.e. ConvLSTM) or a different learning technique such as the greedy-layer wise pre-training (Bengio, Lamblin, Popovici, & Larochelle, 2006) may help expand the prediction horizon while maintaining the prediction quality.

## **4.6 Conclusion**

In this study, 4 LSTM architectures and a linear statistical model have been developed and examined for the prediction of future lower limb kinematics (i.e. foot AV, shank AV, thigh AV, foot LA, shank LA and thigh LA). Results suggested that future lower limb kinematics

while walking at PWS and at  $5\text{km}\cdot\text{h}^{-1}$  can be well predicted up to 0.1s with ED-LSTM and Stacked LSTM. The study does not recommend the application of linear models such as the LR to predict future gait kinematics. These findings highlight the potential of LSTM neural networks to predict the future trajectories of the human movements. This could have application in exoskeleton control systems or falls prevention. Future work could focus on understanding the model's robustness under different walking conditions and in participants with a pathological gait. The next chapter further investigates the performance of the 4 LSTM architectures at faster (+20%) and slower (-20%) walking speeds relative to PWS and reports the best performing LSTM architecture.

## 5 CHAPTER FIVE: PREDICTION OF LOWER LIMB KINEMATICS AT SLOWER AND FASTER WALKING SPEEDS – Study 3.

### 5.1 Overview

There exists a strong relationship between the walking speed and the lower limb kinematic trajectories. Since the performance of the developed LSTM models is known at PWS and  $5\text{km}\cdot\text{h}^{-1}$ , the aim of this chapter is to understand the models' performance at faster (+20 %PWS) and slower walking speeds (-20% PWS). All models obtained the poorest predictions at 20% slower speeds and achieved best predictions at 20% faster speeds compared to the PWS and  $5\text{km}\cdot\text{h}^{-1}$  walking speeds predictions combined. The ED LSTM maintained and achieved the best predictive model throughout walking speed conditions. Developing ML Models that have been trained and validated to predict across different walking speeds, is precisely essential in order to acclimate to the human's walking speed changes. The potential of predicting kinematics at slower and faster walking speeds relative to PWS, expands the utility of the LSTM models to different walking conditions.

### 5.2 Introduction

During healthy human ambulation, the walking speed may be adjusted voluntarily throughout the day in response to environmental changes (Hanlon & Anderson, 2006; A. R. Wu, Simpson, van Asseldonk, van der Kooij, & Ijspeert, 2019). Walking speed changes are known to have substantial impacts on the ambulatory kinematics (**Section 1.2**). Spatiotemporal parameters such as the stride/step length and the sagittal plane kinematics (i.e. joint angles) are highly correlated with the walking speed (Claudiane Arakaki Fukuchi et al., 2019; Røislien et al., 2009). The strong association between the gait speed and the walking patterns allowed the use of gait speed as one of the major features to predict the lower limb kinematics (Lelas, Merriman, Riley, & Kerrigan, 2003). Among other gait features (i.e. age, gender and BMI), the walking speed accounted for 85% of regression coefficients to reconstruct waveforms related to sagittal plane kinematics (i.e. hip, knee and ankle angles) (Moissenet et al., 2019).

This work is the first of its kind to examine the effects of walking speed changes on the LSTM models' performance. Since the performance of the LSTM models at PWS and the  $5\text{km}\cdot\text{h}^{-1}$  imposed speed are known (**Chapter 4**), the aim of this chapter was to train and test the

LSTM models at faster and slower walking speeds (i.e.  $\pm 20\%$  of PWS). Trained models in the previous chapter were further trained and cross validated with TL on faster and slower walking trials before testing.

### 5.3 Methods

The walking data were recorded for 10 minutes on a 0% gradient treadmill from 7 male and 3 female participants ( $28 \pm 4$  years old,  $1.72 \pm 0.07$ m in height,  $66 \pm 10$  kg in mass) at 20% faster walking speed ( $5.26 \pm 0.53$  km.h<sup>-1</sup>) and 20% slower walking speed ( $3.59 \pm 0.47$  km.h<sup>-1</sup>). The fast and slow walking data were collected in a randomised order at the same session when the PWS and the 5km.h<sup>-1</sup> were recorded in the previous chapter (Chapter 4). The faster and slower walking speeds were calculated relative to the PWS and randomised for each participant. A 2 minutes familiarisation session was added to the start of each walking trial. Ethics approval was granted by the Victoria University (ID HRE18-230) and all participants have signed a consent form and volunteered freely to participate.

#### 5.3.1 Datasets

Collected faster and slower walking data were processed as per Chapter 4 (**Section 4.3.2** and **4.3.3**). The sagittal plane kinematics included the translation along the Y-axis (i.e. LA) and the rotation along the X-axis (i.e. AV) were used for LSTM prediction, resulting in six predictor variables, (i)  $X_1$  foot AV (ii)  $X_2$  shank AV (iii)  $X_3$  thigh AV (iv)  $Y_4$  foot LA (v)  $Y_5$  foot LA and (vi)  $Y_6$  foot LA. The phase shift difference between the faster, slower walking speeds, the PWS and the 5km.h<sup>-1</sup> is presented in **Figure 5-1** for all the predictor variables. The 6 predictor variables were transformed into 3D data to be prepared for the LSTM models using the sliding window technique in Chapter 4 (**Section 4.3.5**). The T\*F (i.e. Timesteps\*Features) 2D data structure of Dataset 1 and Dataset 2 was transformed into S\*T\*F (i.e. Samples\*Timesteps\*Features) 3D data structure of input and corresponding output examples to train the LSTM models with supervised learning (Graves, 2012a; Zaroug et al., 2020). A one sample is a one window that consists of multiple timesteps and the 6 features (i.e.  $X_1, X_2, X_3, Y_4, Y_5, Y_6$ ).

The Dataset 1 was transformed from 836,020 timesteps and 6 features into input and corresponding output examples. The input training data comprised of 167,199 samples and inside of each sample are 25 timesteps (0.5s) and 6 features. While the corresponding output training data was 167,199 samples and inside of each sample are 5 timesteps (0.1s) and 6

features. The testing input data was converted from 75 timesteps and 6 features to 15 samples, 25 timesteps (0.5s) and 6 features. While the corresponding output testing data was converted to 15 samples, 5 timesteps (0.1s) and 6 features.

The Dataset 2 was transformed from 1, 045, 521 timesteps and 6 features into input and coresponding output examples. The input training data comprised of 209,099 samples and inside of each sample are 25 timesteps (0.5s) and 6 features. While the corresponding output training data was 209,099 samples and inside of each sample are 5 timesteps (0.1s) and 6 features. The testing input data was converted from 75 timesteps (1.5s) and 6 features to 15 samples, 25 timesteps (0.5s) and 6 features. While the corresponding output testing data was converted to 15 samples, 5 timesteps (0.1s) and 6 features.

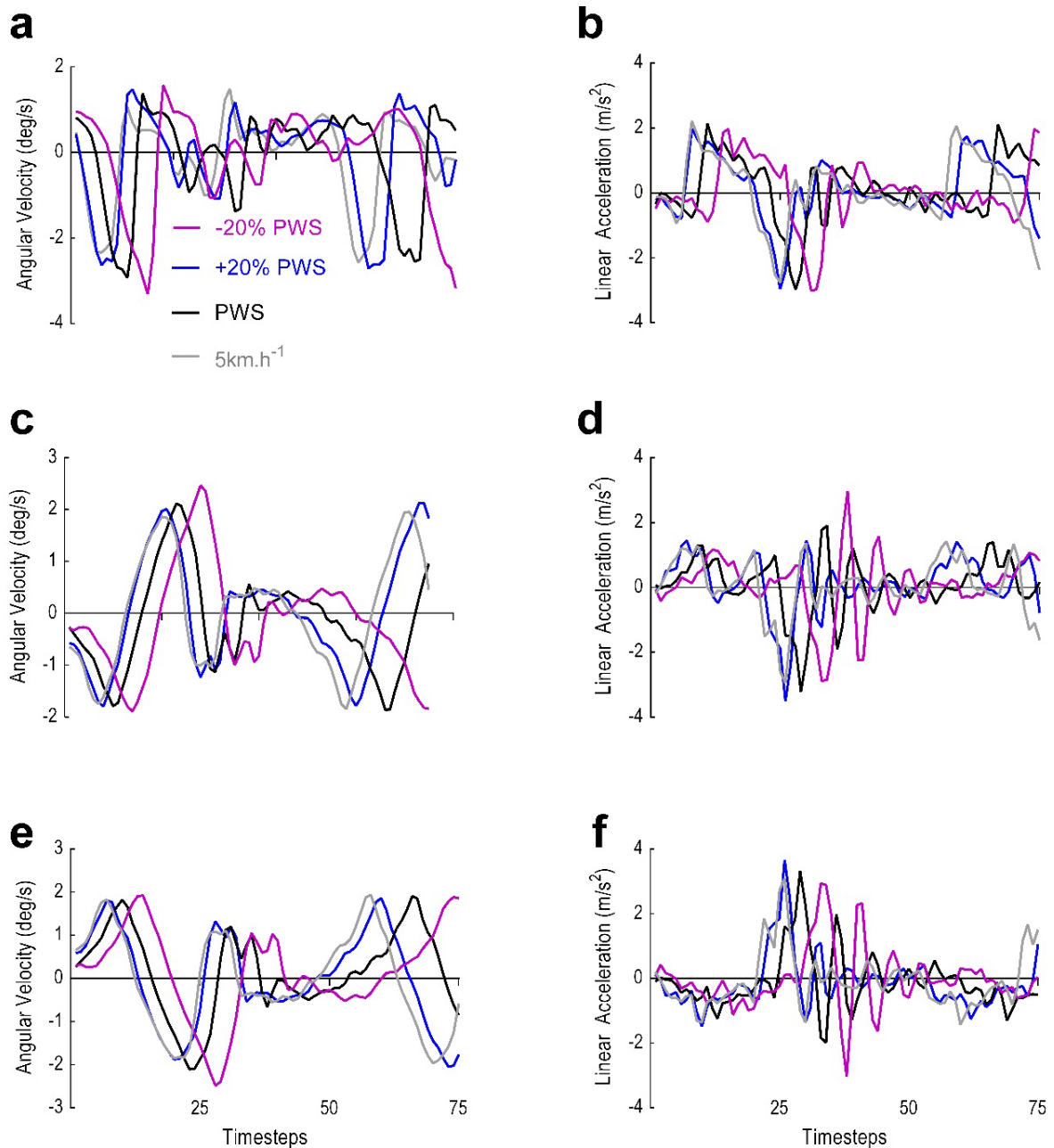


**Figure 5-1:** The phase shift difference between the slower (-20% PWS) and faster (+20% PWS) walking speeds, and the normal (PWS) and 5km.h<sup>-1</sup> walking conditions at 75 timesteps (1.5s) of the gait cycle starting from the right foot strike. In this chapter, the LSTM models are tested to predict the kinematics of slower and faster walking speeds only. Magenta is the slower walking speed. Blue is the faster walking speed. Black is the PWS. Grey is the 5km.h<sup>-1</sup>. (a) Foot AV ( $X_1$ ). (b) Foot LA ( $Y_4$ ). (c) Shank AV ( $X_2$ ). (d) Shank LA ( $Y_5$ ). (e) Thigh AV ( $X_3$ ). (f) Thigh LA ( $Y_6$ ). This dataset is a superimposed signals of all test sets related to the same participant evaluated before the cross validations in Chapter 4 and 5.

As per **Table 5-1**, the Dataset 1 comprised of faster speed trials (4,187 strides) and the previous trials (Chapter 4 – 10,500 strides) to carry out training (Total 14,687 strides) and testing (75 timesteps of faster speed) with leave-one-out cross validation protocol. When faster speed cross

validation was completed, the slower speed trials (2,951 strides) were added to Dataset 1 (**Table 5-1**). The new Dataset 2 comprised of 17,638 strides and due to the uniqueness of each participant’s walking speed, the testing set was kept fixed at 75 timesteps.

**Table 5-1:** Description of training and testing datasets.

| Datasets  | Training                                | Testing Dataset              |
|-----------|---|------------------------------|
| Dataset 1 | 5k + PWS + 20% faster = 14,687 strides  | 75 timesteps of faster speed |
| Dataset 2 | Dataset 1 + 20% slower = 17,638 strides | 75 timesteps of slower speed |

### 5.3.2 Evaluation and performance metrics

Models trained in Chapter 4 were further trained using TL on faster speeds (Dataset 1) and slower speeds (Dataset 2). As shown in **Table 5-2**, models training started from the last number of epochs left off at Chapter 4. Input/Output sliding windows as well as the performance metrics were kept the same as per Chapter 4. Performance evaluations were carried out for each of the predicted 5 timesteps (0.1s) output prediction window. Output sliding windows were then combined and the predicted versus actual trajectories are shown for the first tested participant. Then leave-one-out cross validation is carried out after Dataset 1/Dataset 2 training epochs have been performed.

**Table 5-2:** Models training process. The number of epochs is the starting point for testing the first participant. Using TL, subsequent participants were tested after 10 epochs each.

| Trained models | Original epochs | Dataset 1 training epochs | Final validation epochs | Dataset 2 training epochs | Final validation epochs |
|----------------|-----------------|---------------------------|-------------------------|---------------------------|-------------------------|
| Vanilla LSTM   | 240             | 50                        | 370                     | 50                        | 500                     |
| Stacked LSTM   | 400             | 50                        | 530                     | 50                        | 660                     |
| Bi-LSTM        | 340             | 50                        | 470                     | 50                        | 600                     |
| ED-LSTM        | 340             | 50                        | 470                     | 50                        | 600                     |

## 5.4 Results for faster walking speed (+20% PWS)

Results in this section describes the performance of all LSTM architectures at +20% PWS only. The LSTM models were trained on Dataset 1 (14,687 strides) for 50 epochs as per **Table 5-2** and tested with 75 timesteps (1.5s) on the same participant. To attain generalisation,

all trials related to the tested participant were removed from the training set. All of the predicted trajectories (output windows – 5 timesteps – 0.1s) were combined and shown in Figure 5-2. In contrast to trajectories prediction at PWS (Chapter 4 – **Figure 4-9**), the predicted trajectories in this study (at +20% PWS) are closer to the actual trajectories (**Figure 5-2**). Particularly predictions based on the LA at +20% PWS are showing less noise compared to the PWS predictions.

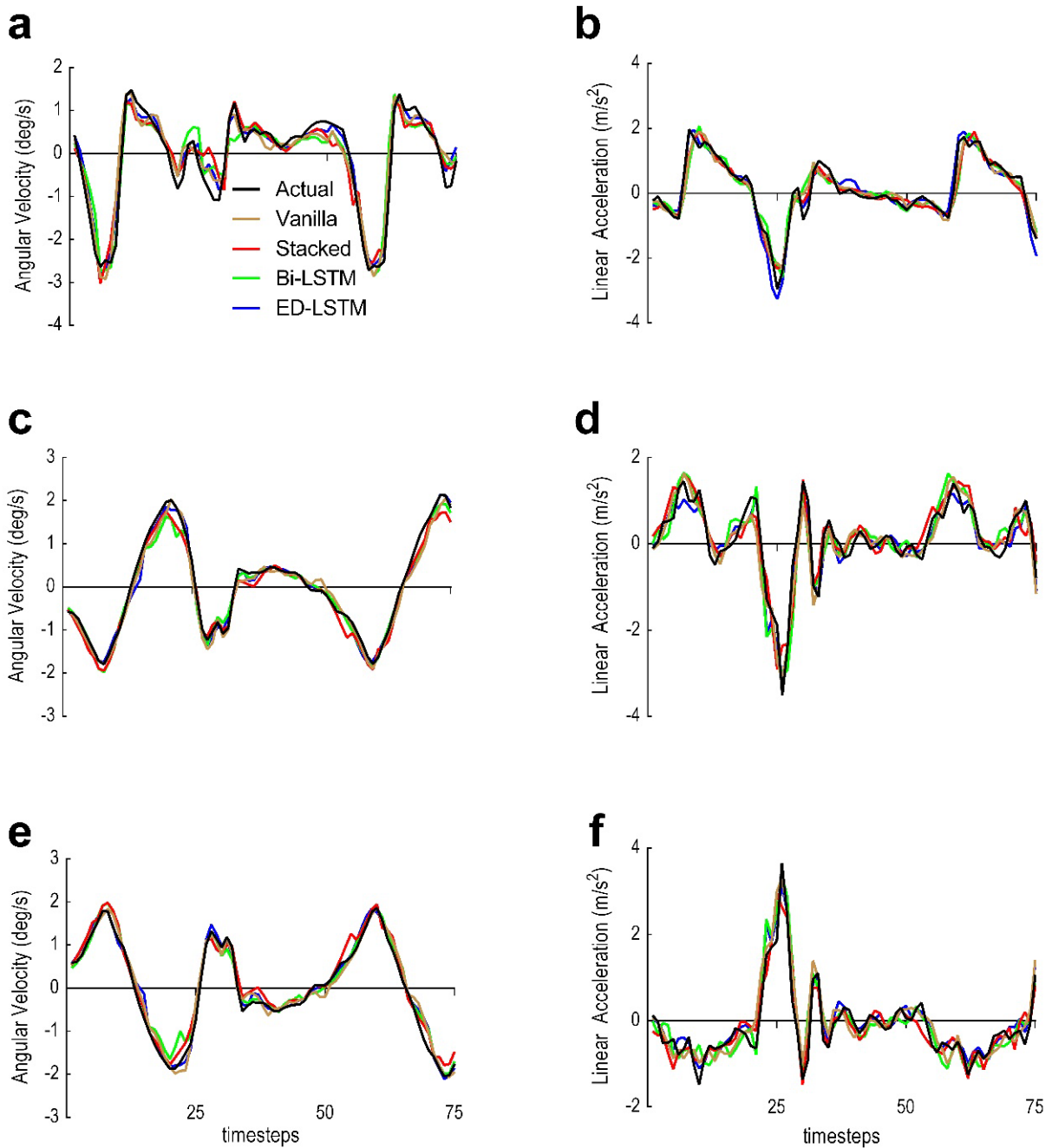


**Figure 5-2:** LSTM models prediction performance based on the inter-subject test for each feature vector at +20% PWS only. Models were tested with 75 timesteps and the same participant was tested across LSTM models. Black is the actual trajectory. Brown is the Vanilla LSTM predicted trajectory. Red is the Stacked LSTM predicted trajectory. Green is the Bi-LSTM predicted trajectory. Blue is the ED-LSTM predicted trajectory. (a) Foot AV ( $X_1$ ). (b) Foot LA ( $Y_4$ ). (c) Shank AV ( $X_2$ ). (d) Shank LA ( $Y_5$ ). (e) Thigh AV ( $X_3$ ). (f) Thigh LA ( $Y_6$ ).

Predicted dependent variables ( $X_1$ ,  $X_2$ ,  $X_3$ ,  $Y_4$ ,  $Y_5$ ,  $Y_6$ ) were evaluated based on the performance metrics; MAE, MSE, and RMSE in **Table 5-3** and the NRMSE and CC in **Table**

5-4 and Table 5-5 respectively. The ED-LSTM demonstrated the best performance (least error – MAE, MSE and RMSE) between the rest of the LSTM models with NRMSE range between 4.07 – 6.09%. The ED-LSTM achieved predicted pattern was also the highest with CC range between 0.95-0.99.

**Table 5-3:** All LSTM models performance evaluation results based on the MAE, MSE and the RMSE. Each of the predicted independent variables (i.e.  $X_1, X_2, \dots, Y_6$ ) was tested at +20% PWS. The tested dataset comprised of 75 timesteps and is related to the first participant. Results were obtained after training the model with TL at 50 epochs.

| Error Type  | Architecture | $X_1$<br>(deg.s <sup>-1</sup> ) | $X_2$<br>(deg.s <sup>-1</sup> ) | $X_3$<br>(deg.s <sup>-1</sup> ) | $Y_4$<br>(m.s <sup>-2</sup> ) | $Y_5$<br>(m.s <sup>-2</sup> ) | $Y_6$<br>(m.s <sup>-2</sup> ) |
|-------------|--------------|---------------------------------|---------------------------------|---------------------------------|-------------------------------|-------------------------------|-------------------------------|
| <b>MAE</b>  | Vanilla LSTM | 0.249                           | 0.144                           | 0.143                           | 0.188                         | 0.250                         | 0.248                         |
|             | Stacked LSTM | 0.283                           | 0.163                           | 0.166                           | 0.177                         | 0.279                         | 0.226                         |
|             | Bi-LSTM      | 0.293                           | 0.143                           | 0.148                           | 0.217                         | 0.289                         | 0.253                         |
|             | ED-LSTM      | 0.199                           | 0.113                           | 0.109                           | 0.187                         | 0.214                         | 0.183                         |
| <b>MSE</b>  | Vanilla LSTM | 0.105                           | 0.033                           | 0.034                           | 0.076                         | 0.103                         | 0.107                         |
|             | Stacked LSTM | 0.129                           | 0.041                           | 0.041                           | 0.065                         | 0.138                         | 0.105                         |
|             | Bi-LSTM      | 0.142                           | 0.037                           | 0.040                           | 0.113                         | 0.140                         | 0.111                         |
|             | ED-LSTM      | 0.065                           | 0.024                           | 0.025                           | 0.060                         | 0.069                         | 0.055                         |
| <b>RMSE</b> | Vanilla LSTM | 0.325                           | 0.182                           | 0.186                           | 0.275                         | 0.321                         | 0.326                         |
|             | Stacked LSTM | 0.359                           | 0.202                           | 0.202                           | 0.255                         | 0.371                         | 0.324                         |
|             | Bi-LSTM      | 0.376                           | 0.193                           | 0.199                           | 0.336                         | 0.375                         | 0.334                         |
|             | ED-LSTM      | 0.255                           | 0.155                           | 0.159                           | 0.244                         | 0.263                         | 0.235                         |

**Table 5-4:** All LSTM models performance evaluation results based on the NRMSE (%). Each of the predicted independent variables (i.e.  $X_1, X_2, \dots, Y_6$ ) was tested at +20% PWS. The tested dataset comprised of 75 timesteps and is related to the first participant. Results were obtained after training the model with TL at 50 epochs.

| Architecture        | $X_1$ (%) | $X_2$ (%) | $X_3$ (%) | $Y_4$ (%) | $Y_5$ (%) | $Y_6$ (%) |
|---------------------|-----------|-----------|-----------|-----------|-----------|-----------|
| <b>Vanilla LSTM</b> | 7.74      | 4.64      | 4.74      | 5.56      | 6.47      | 6.34      |
| <b>Stacked LSTM</b> | 8.56      | 5.14      | 5.17      | 5.15      | 7.49      | 6.30      |
| <b>Bi-LSTM</b>      | 8.98      | 4.92      | 5.08      | 6.80      | 7.56      | 6.48      |
| <b>ED-LSTM</b>      | 6.09      | 3.94      | 4.07      | 4.94      | 5.31      | 4.56      |

**Table 5-5:** All LSTM models performance evaluation results based on the CC. Each of the predicted independent variables (i.e.  $X_1, X_2, \dots, Y_6$ ) was tested at +20% PWS. The tested dataset comprised of 75 timesteps and is related to the first participant. Results were obtained after training the model with TL at 50 epochs.

| Architecture        | $X_1$ | $X_2$ | $X_3$ | $Y_4$ | $Y_5$ | $Y_6$ |
|---------------------|-------|-------|-------|-------|-------|-------|
| <b>Vanilla LSTM</b> | 0.96  | 0.98  | 0.98  | 0.95  | 0.93  | 0.93  |
| <b>Stacked LSTM</b> | 0.95  | 0.99  | 0.98  | 0.96  | 0.90  | 0.92  |
| <b>Bi-LSTM</b>      | 0.94  | 0.98  | 0.98  | 0.93  | 0.91  | 0.92  |
| <b>ED-LSTM</b>      | 0.97  | 0.99  | 0.99  | 0.97  | 0.95  | 0.96  |

#### 5.4.1 Leave-one-out cross validation test results for +20% PWS

Models were cross validated for each 9 participants at +20% PWS. Between each participant testing, the models were trained for 10 epochs excluding all trials related to the tested participant until the final validation epochs was reached as per **Table 5-2**. Predicted dependent variables ( $X_1, X_2, X_3, Y_4, Y_5, Y_6$ ) were evaluated for each participant based on the performance metrics (MAE, MSE, RMSE, NRMSE and the CC) and averaged in **Table 5-6** to **Table 5-8**. Predicted trajectories based on the AV (MAE 0.101-0.260 deg.s<sup>-1</sup>) were generally less erroneous than the predicted trajectories based on the LA (MAE 0.164-0.300 m.s<sup>-2</sup>) across all the LSTM models (**Table 5-6**). The ED-LSTM demonstrated the best performance amongst the rest of the LSTM models with NRMSE between 4.43-5.76% for both AV and LA predicted trajectories (**Table 5-7**). To facilitate models performance comparison, predicted variables were graphically presented in **Figure 5-3** and **Figure 5-4**. The Vanilla and the Stacked LSTM attained similar performance results for predicted LA and AV trajectories in **Figure 5-3**. While the Bi-LSTM performance have shown a pronounced highest error for all predicted trajectories. Wider gaps between the RMSE and the CC in **Figure 5-4** indicates a good predicted pattern and a more accurate prediction for the relevant LSTM model. The ED-LSTM attained the widest gap for all predicted feature vectors.

**Table 5-6:** Leave-one-out cross validation (9 participants) test for the faster walking speed (+20% PWS) based on the MAE, MSE and the RMSE for all the LSTM architectures

| Error matrix | Architecture | X <sub>1</sub><br>(deg.s <sup>-1</sup> ) | X <sub>2</sub><br>(deg.s <sup>-1</sup> ) | X <sub>3</sub><br>(deg.s <sup>-1</sup> ) | Y <sub>4</sub><br>(m.s <sup>-2</sup> ) | Y <sub>5</sub><br>(m.s <sup>-2</sup> ) | Y <sub>6</sub><br>(m.s <sup>-2</sup> ) |
|--------------|--------------|--|--|--|--|--|--|
| <b>MAE</b>   | Vanilla LSTM | 0.223                                    | 0.132                                    | 0.141                                    | 0.186                                  | 0.245                                  | 0.257                                  |
|              | Stacked LSTM | 0.200                                    | 0.119                                    | 0.125                                    | 0.169                                  | 0.218                                  | 0.220                                  |
|              | Bi-LSTM      | 0.260                                    | 0.142                                    | 0.154                                    | 0.217                                  | 0.281                                  | 0.300                                  |
|              | ED-LSTM      | 0.178                                    | 0.101                                    | 0.106                                    | 0.164                                  | 0.196                                  | 0.206                                  |
| <b>MSE</b>   | Vanilla LSTM | 0.221                                    | 0.037                                    | 0.038                                    | 0.179                                  | 0.124                                  | 0.141                                  |
|              | Stacked LSTM | 0.089                                    | 0.030                                    | 0.030                                    | 0.068                                  | 0.100                                  | 0.102                                  |
|              | Bi-LSTM      | 0.155                                    | 0.041                                    | 0.045                                    | 0.101                                  | 0.167                                  | 0.184                                  |
|              | ED-LSTM      | 0.074                                    | 0.023                                    | 0.024                                    | 0.063                                  | 0.089                                  | 0.101                                  |
| <b>RMSE</b>  | Vanilla LSTM | 0.387                                    | 0.183                                    | 0.190                                    | 0.337                                  | 0.337                                  | 0.360                                  |
|              | Stacked LSTM | 0.278                                    | 0.164                                    | 0.167                                    | 0.244                                  | 0.301                                  | 0.305                                  |
|              | Bi-LSTM      | 0.371                                    | 0.196                                    | 0.206                                    | 0.305                                  | 0.394                                  | 0.415                                  |
|              | ED-LSTM      | 0.249                                    | 0.144                                    | 0.149                                    | 0.234                                  | 0.278                                  | 0.298                                  |

**Table 5-7:** Leave-one-out cross validation (9 participants) test for the faster walking speed (+20% PWS) based on the NRMSE (%) for all LSTM architectures.

| Architecture        | X <sub>1</sub> % | X <sub>2</sub> % | X <sub>3</sub> % | Y <sub>4</sub> % | Y <sub>5</sub> % | Y <sub>6</sub> % |
|---------------------|------------------|------------------|------------------|------------------|------------------|------------------|
| <b>Vanilla LSTM</b> | 7.03             | 4.36             | 4.52             | 5.07             | 6.56             | 7.05             |
| <b>Stacked LSTM</b> | 6.29             | 4.01             | 4.06             | 4.62             | 5.85             | 5.95             |
| <b>Bi-LSTM</b>      | 8.41             | 4.79             | 4.98             | 5.93             | 7.68             | 8.25             |
| <b>ED-LSTM</b>      | 5.55             | 3.50             | 3.59             | 4.43             | 5.36             | 5.76             |

**Table 5-8:** Leave-one-out cross validation (9 participants) test for the faster walking speed (+20% PWS) based on the CC for all LSTM architectures.

| Architecture        | X <sub>1</sub> | X <sub>2</sub> | X <sub>3</sub> | Y <sub>4</sub> | Y <sub>5</sub> | Y <sub>6</sub> |
|---------------------|----------------|----------------|----------------|----------------|----------------|----------------|
| <b>Vanilla LSTM</b> | 0.94           | 0.98           | 0.98           | 0.96           | 0.92           | 0.91           |
| <b>Stacked LSTM</b> | 0.95           | 0.98           | 0.98           | 0.96           | 0.94           | 0.94           |
| <b>Bi-LSTM</b>      | 0.92           | 0.98           | 0.98           | 0.95           | 0.90           | 0.88           |
| <b>ED-LSTM</b>      | 0.96           | 0.99           | 0.99           | 0.96           | 0.95           | 0.94           |

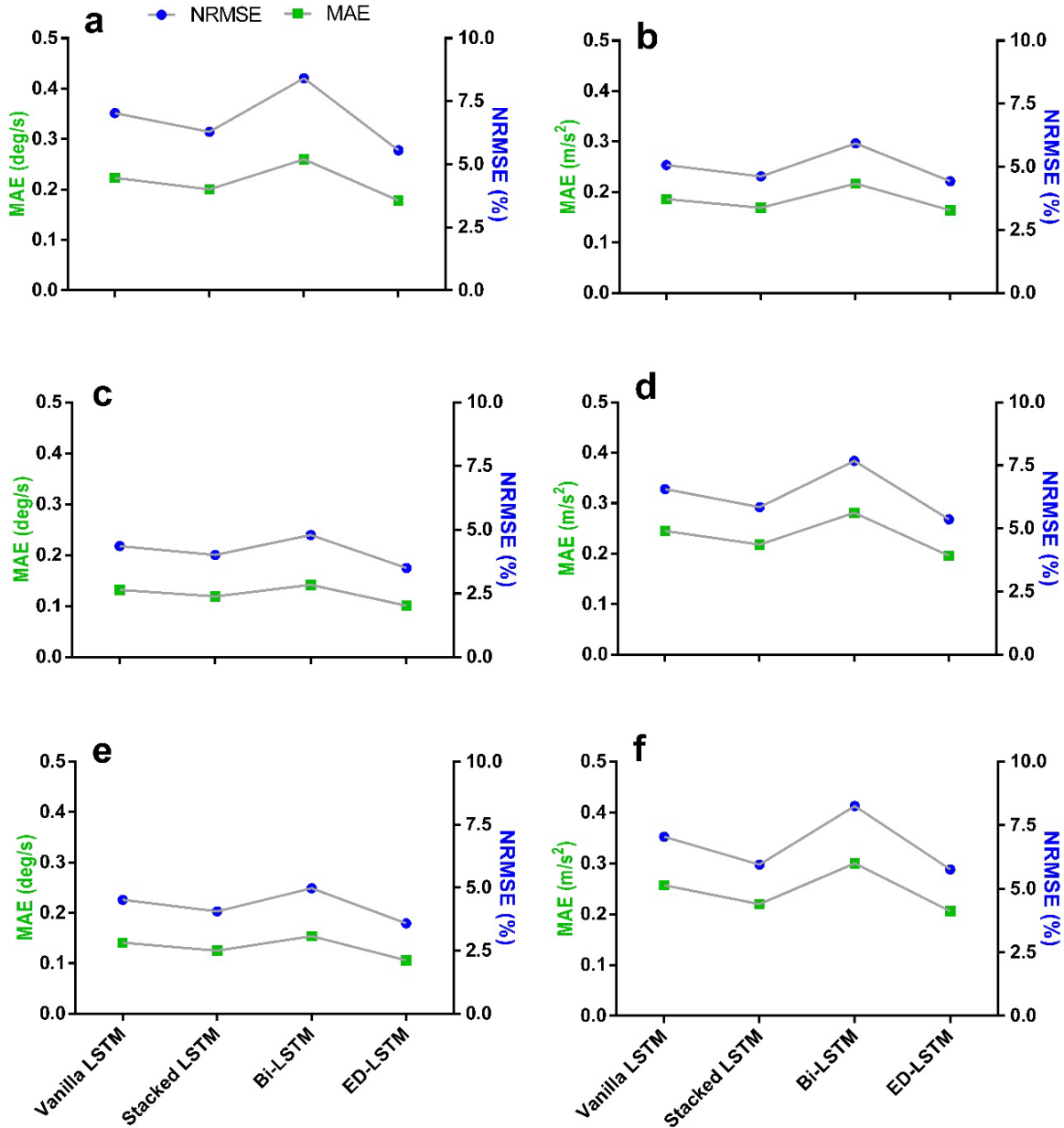


**Figure 5-3:** Performance comparison between LSTM models based on leave-one-out cross validation at +20% PWS for each feature vector. Green is the RMSE (Left Y-axis). Blue is the NRMSE (Right Y-axis). Lower error points for the MAE and NRMSE means a better predictive model for the related feature vector. (a) Foot AV ( $X_1$ ). (b) Foot LA ( $Y_4$ ). (c) Shank AV ( $X_2$ ). (d) Shank LA ( $Y_5$ ). (e) Thigh AV ( $X_3$ ). (f) Thigh LA ( $Y_6$ ).

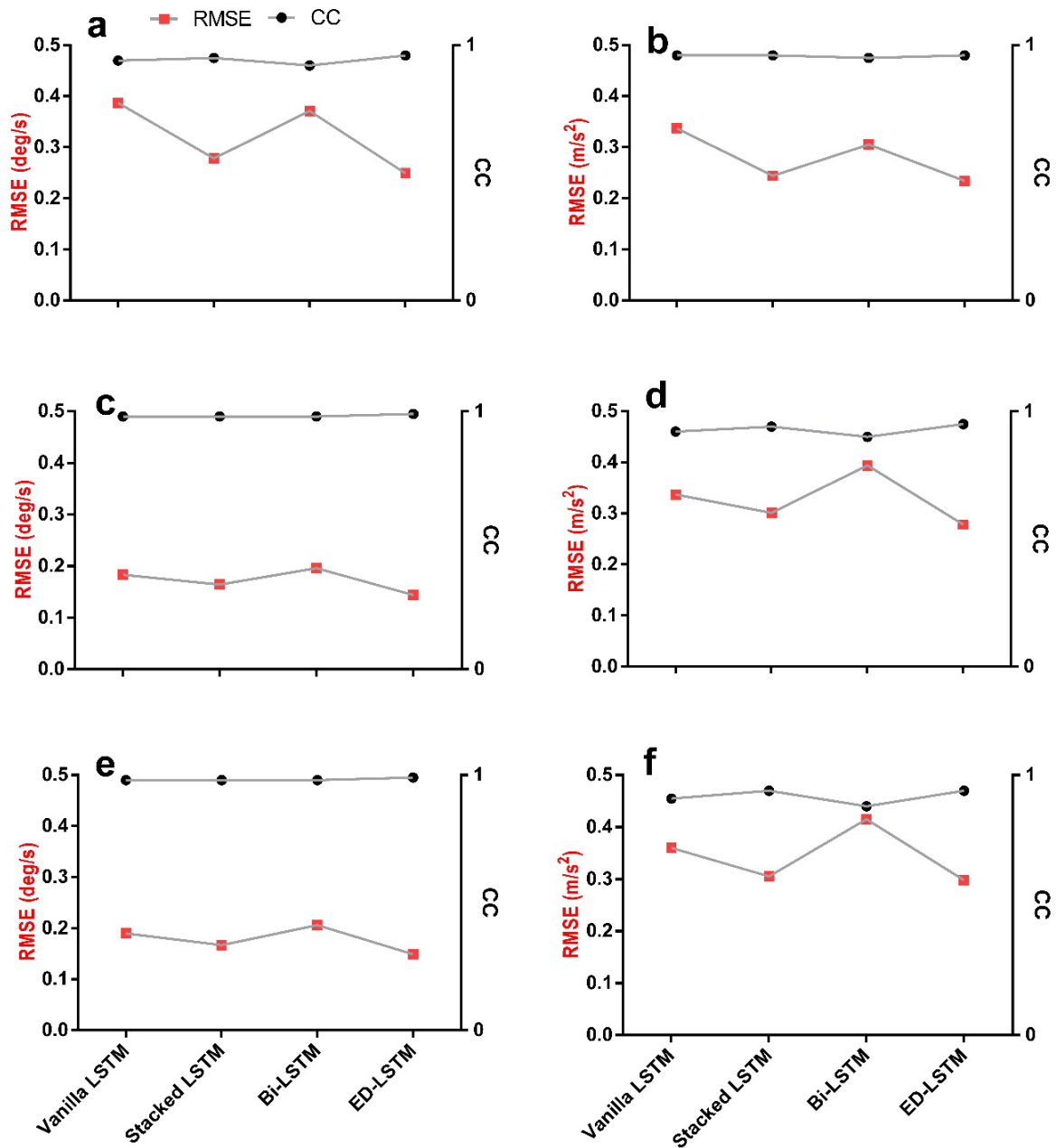


**Figure 5-4:** Performance comparison between LSTM models based on the leave-one-out cross validation at +20% PWS for each feature vector. Red is the RMSE (Left Y-axis). Black is the CC (Right Y-axis). Wider gaps between the two error lines (CC and RMSE) means better prediction quality for the related feature vector. (a) Foot AV ( $X_1$ ). (b) Foot LA ( $Y_4$ ). (c) Shank AV ( $X_2$ ). (d) Shank LA ( $Y_5$ ). (e) Thigh AV ( $X_3$ ). (f) Thigh LA ( $Y_6$ ).

## 5.5 Results for slower walking speeds (-20% PWS)

Results in this section describes the performance of the developed LSTM architectures at -20% PWS only. The LSTM models were trained on Dataset 2 (17,638 strides) for 50 epochs as per **Table 5-2** and tested with 75 timesteps and on the same participant. The same participant was tested across LSTM models and trials related to the tested participant were removed from the training set. The actual versus predicted trajectories (0.1s – 5 timesteps per output window) for all models were combined and shown in **Figure 5-5**. Predicted trajectories based on the AV and LA are found not maintaining a consistent track to the actual trajectories across LSTM models, particularly at the foot AV in **Figure 5-5-a**.

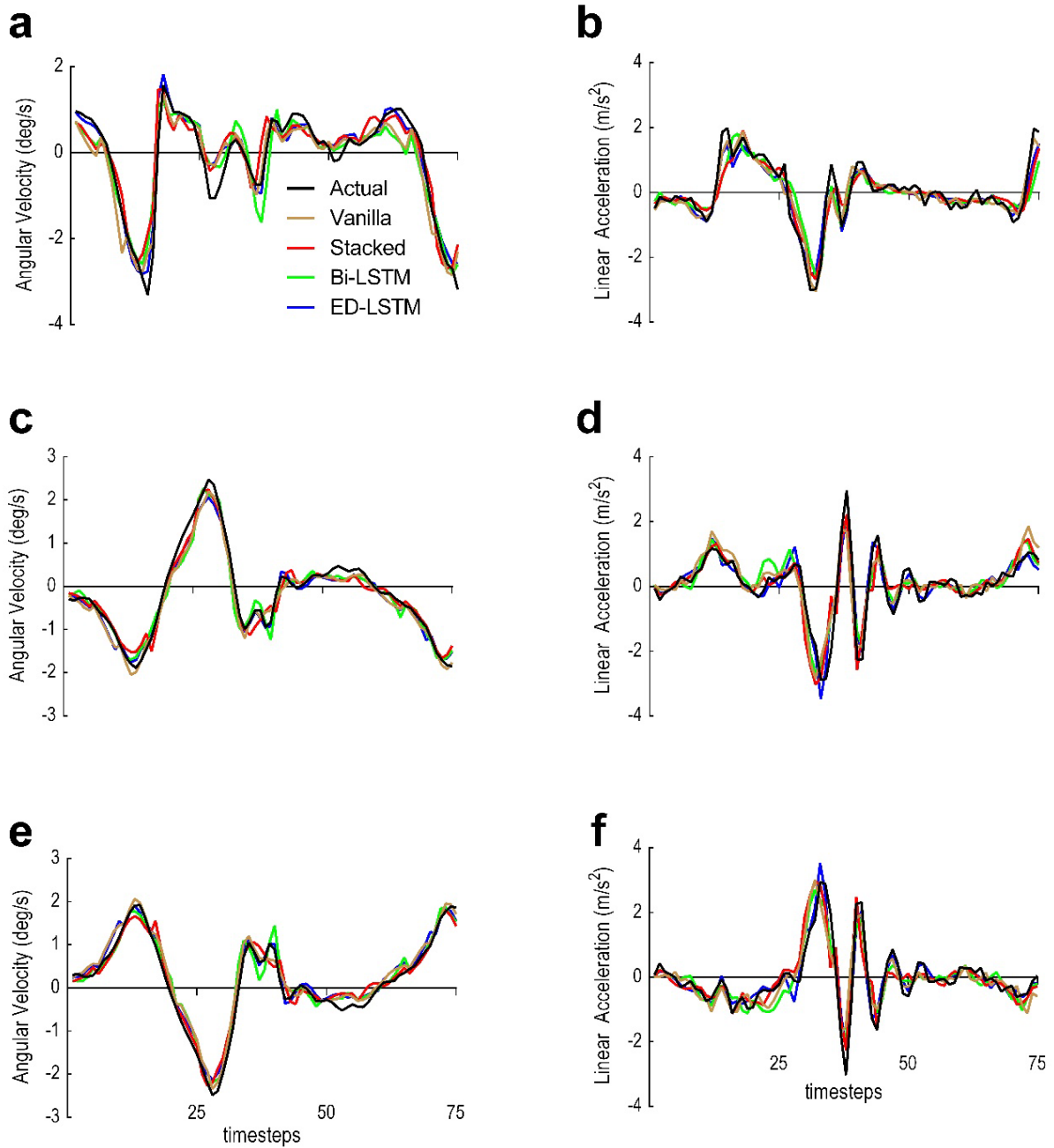


**Figure 5-5:** Predicted versus actual trajectories for the Vanilla (brown), Stacked (red), Bi (green) and ED (blue) LSTM at -20% PWS. All models were tested on the same participant at the same speed. Each single predicted output window was 5 timesteps (0.1s). (a) Foot AV ( $X_1$ ). (b) Foot LA ( $Y_4$ ). (c) Shank AV ( $X_2$ ). (d) Shank LA ( $Y_5$ ). (e) Thigh AV ( $X_3$ ). (f) Thigh LA ( $Y_6$ ).

Predicted dependent variables ( $X_1, X_2, X_3, Y_4, Y_5, Y_6$ ) were individually evaluated for all models and shown in **Table 5-9** to **Table 5-11**. Across LSTM models, higher error rates are attained at the LA than AV trajectories. The ED-LSTM however demonstrated the best prediction performance across error metrics (4.15-5.94%) for all feature vectors.

**Table 5-9:** All LSTM models performance evaluation results based on the MAE, MSE and the RMSE. Each of the predicted independent variables (i.e.  $X_1, X_2, \dots, Y_6$ ) was tested at -20% PWS. The tested dataset comprised of 75 timesteps and is related to the first participant. Results were obtained after training the model with TL at 50 epochs.

| Error metric | Architecture | $X_1$<br>(deg.s <sup>-1</sup> ) | $X_2$<br>(deg.s <sup>-1</sup> ) | $X_3$<br>(deg.s <sup>-1</sup> ) | $Y_4$<br>(m.s <sup>-2</sup> ) | $Y_5$<br>(m.s <sup>-2</sup> ) | $Y_6$<br>(m.s <sup>-2</sup> ) |
|--------------|--------------|---------------------------------|---------------------------------|---------------------------------|-------------------------------|-------------------------------|-------------------------------|
| <b>MAE</b>   | Vanilla LSTM | 0.306                           | 0.163                           | 0.174                           | 0.233                         | 0.331                         | 0.329                         |
|              | Stacked LSTM | 0.323                           | 0.172                           | 0.178                           | 0.261                         | 0.302                         | 0.321                         |
|              | Bi-LSTM      | 0.309                           | 0.160                           | 0.164                           | 0.322                         | 0.304                         | 0.333                         |
|              | ED-LSTM      | 0.197                           | 0.146                           | 0.150                           | 0.216                         | 0.225                         | 0.225                         |
| <b>MSE</b>   | Vanilla LSTM | 0.156                           | 0.041                           | 0.044                           | 0.097                         | 0.198                         | 0.220                         |
|              | Stacked LSTM | 0.186                           | 0.045                           | 0.051                           | 0.146                         | 0.215                         | 0.227                         |
|              | Bi-LSTM      | 0.177                           | 0.046                           | 0.046                           | 0.221                         | 0.169                         | 0.183                         |
|              | ED-LSTM      | 0.085                           | 0.034                           | 0.033                           | 0.086                         | 0.104                         | 0.112                         |
| <b>RMSE</b>  | Vanilla LSTM | 0.395                           | 0.203                           | 0.209                           | 0.312                         | 0.445                         | 0.469                         |
|              | Stacked LSTM | 0.431                           | 0.212                           | 0.226                           | 0.382                         | 0.463                         | 0.476                         |
|              | Bi-LSTM      | 0.420                           | 0.215                           | 0.215                           | 0.470                         | 0.411                         | 0.428                         |
|              | ED-LSTM      | 0.291                           | 0.185                           | 0.183                           | 0.293                         | 0.323                         | 0.335                         |

**Table 5-10:** All LSTM models performance evaluation results based on the NRMSE (%). Each of the predicted independent variables (i.e.  $X_1, X_2, \dots, Y_6$ ) was tested at -20% PWS. The tested dataset comprised of 75 timesteps and is related to the first participant. Results were obtained after training the model with TL at 50 epochs.

| Architecture        | $X_1$ (%) | $X_2$ (%) | $X_3$ (%) | $Y_4$ (%) | $Y_5$ (%) | $Y_6$ (%) |
|---------------------|-----------|-----------|-----------|-----------|-----------|-----------|
| <b>Vanilla LSTM</b> | 8.09      | 4.65      | 4.74      | 6.25      | 7.61      | 7.86      |
| <b>Stacked LSTM</b> | 8.82      | 4.87      | 5.13      | 7.64      | 7.91      | 7.97      |
| <b>Bi-LSTM</b>      | 8.59      | 4.93      | 4.88      | 9.42      | 7.01      | 7.16      |
| <b>ED-LSTM</b>      | 5.94      | 4.24      | 4.15      | 5.87      | 5.52      | 5.61      |

**Table 5-11:** All LSTM models performance evaluation results based on the CC. Each of the predicted independent variables (i.e.  $X_1, X_2, \dots, Y_6$ ) was tested at -20% PWS. The tested dataset comprised of 75 timesteps and is related to the first participant. Results were obtained after training the model with TL at 50 epochs.

| Architecture        | $X_1$ | $X_2$ | $X_3$ | $Y_4$ | $Y_5$ | $Y_6$ |
|---------------------|-------|-------|-------|-------|-------|-------|
| <b>Vanilla LSTM</b> | 0.94  | 0.98  | 0.98  | 0.95  | 0.88  | 0.86  |
| <b>Stacked LSTM</b> | 0.93  | 0.98  | 0.97  | 0.93  | 0.87  | 0.86  |
| <b>Bi-LSTM</b>      | 0.94  | 0.98  | 0.98  | 0.88  | 0.90  | 0.89  |
| <b>ED-LSTM</b>      | 0.97  | 0.99  | 0.99  | 0.96  | 0.94  | 0.93  |

### 5.5.1 Leave-one-out cross validation test results for -20% PWS

Models were cross validated for each of the 9 participants at -20% PWS. Models were trained for 10 epochs before testing each of the 9 participants until the final validation epochs was reached (**Table 5-2**). To maintain generalisation of LSTM models, all trials related to the tested participant were excluded from the training set. Predicted dependent variables ( $X_1, X_2, X_3, Y_4, Y_5, Y_6$ ) were evaluated and averaged for each participant based on the performance metrics (MAE, MSE, RMSE, NRMSE and the CC) in **Table 5-12** to **Table 5-14**.

The inaccuracy of predicted LA trajectories (MAE 0.216-0.329 m.s<sup>-2</sup>) are higher than the AV predicted trajectories (MAE 0.146-0.323 deg.s<sup>-1</sup>) throughout LSTM models (**Table 5-12**). Amongst all evaluated LSTM models, the ED-LSTM demonstrated the best performance in predicting trajectories at slower walking speed (-20% PWS) with NRMSE between 5.91-9.86% for both AV and LA predicted trajectories (see **Table 5-13** and **Figure 5-6**). The Bi-LSTM is found not suitable for trajectories prediction at -20% PWS. The Vanilla and the Stacked LSTM attained similar performance results for predicted LA and AV trajectories (**Figure 5-6** and **Figure 5-7**). The wider the gaps between the RMSE (red) and the CC (black) in **Figure 5-7** indicates a good predicted pattern and a better achieved accuracy for the relevant LSTM model. The ED-LSTM maintained the gap for all predicted feature vectors except for the Thigh LA ( $Y_6$ ).

**Table 5-12:** Leave-one-out cross validation (9 participants) test for the faster walking speed (-20% PWS) based on the MAE, MSE and th RMSE for all the LSTM architectures

| Error metric | Architecture | $X_1$<br>(deg.s <sup>-1</sup> ) | $X_2$<br>(deg.s <sup>-1</sup> ) | $X_3$<br>(deg.s <sup>-1</sup> ) | $Y_4$<br>(m.s <sup>-2</sup> ) | $Y_5$<br>(m.s <sup>-2</sup> ) | $Y_6$<br>(m.s <sup>-2</sup> ) |
|--------------|--------------|---------------------------------|---------------------------------|---------------------------------|-------------------------------|-------------------------------|-------------------------------|
| <b>MAE</b>   | Vanilla LSTM | 0.306                           | 0.163                           | 0.174                           | 0.233                         | 0.331                         | 0.329                         |
|              | Stacked LSTM | 0.323                           | 0.172                           | 0.178                           | 0.261                         | 0.302                         | 0.321                         |
|              | Bi-LSTM      | 0.309                           | 0.160                           | 0.164                           | 0.322                         | 0.304                         | 0.333                         |
|              | ED-LSTM      | 0.197                           | 0.146                           | 0.150                           | 0.216                         | 0.225                         | 0.225                         |
| <b>MSE</b>   | Vanilla LSTM | 0.156                           | 0.041                           | 0.044                           | 0.097                         | 0.198                         | 0.220                         |
|              | Stacked LSTM | 0.186                           | 0.045                           | 0.051                           | 0.146                         | 0.215                         | 0.227                         |
|              | Bi-LSTM      | 0.177                           | 0.046                           | 0.046                           | 0.221                         | 0.169                         | 0.183                         |
|              | ED-LSTM      | 0.085                           | 0.034                           | 0.033                           | 0.086                         | 0.104                         | 0.112                         |
| <b>RMSE</b>  | Vanilla LSTM | 0.395                           | 0.203                           | 0.209                           | 0.312                         | 0.445                         | 0.469                         |
|              | Stacked LSTM | 0.431                           | 0.212                           | 0.226                           | 0.382                         | 0.463                         | 0.476                         |
|              | Bi-LSTM      | 0.420                           | 0.215                           | 0.215                           | 0.470                         | 0.411                         | 0.428                         |
|              | ED-LSTM      | 0.291                           | 0.185                           | 0.183                           | 0.293                         | 0.323                         | 0.335                         |

**Table 5-13:** Leave-one-out cross validation (9 participants) test for the faster walking speed (-20% PWS) based on the NRMSE (%) for all LSTM architectures.

| Architecture        | $X_1$ % | $X_2$ % | $X_3$ % | $Y_4$ % | $Y_5$ % | $Y_6$ % |
|---------------------|---------|---------|---------|---------|---------|---------|
| <b>Vanilla LSTM</b> | 10.34   | 6.98    | 6.90    | 8.96    | 11.48   | 10.50   |
| <b>Stacked LSTM</b> | 10.36   | 6.61    | 6.52    | 8.76    | 10.86   | 9.57    |
| <b>Bi-LSTM</b>      | 12      | 7.94    | 7.82    | 9.87    | 12.37   | 11.07   |
| <b>ED-LSTM</b>      | 9.46    | 5.91    | 5.91    | 8.27    | 9.86    | 9       |

**Table 5-14:** Leave-one-out cross validation (9 participants) test for the faster walking speed (-20% PWS) based on the CC for all LSTM architectures.

| Architecture        | $X_1$ | $X_2$ | $X_3$ | $Y_4$ | $Y_5$ | $Y_6$ |
|---------------------|-------|-------|-------|-------|-------|-------|
| <b>Vanilla LSTM</b> | 0.81  | 0.95  | 0.94  | 0.84  | 0.77  | 0.75  |
| <b>Stacked LSTM</b> | 0.85  | 0.95  | 0.95  | 0.85  | 0.81  | 0.80  |
| <b>Bi-LSTM</b>      | 0.81  | 0.93  | 0.93  | 0.82  | 0.73  | 0.71  |
| <b>ED-LSTM</b>      | 0.85  | 0.96  | 0.96  | 0.86  | 0.84  | 0.82  |

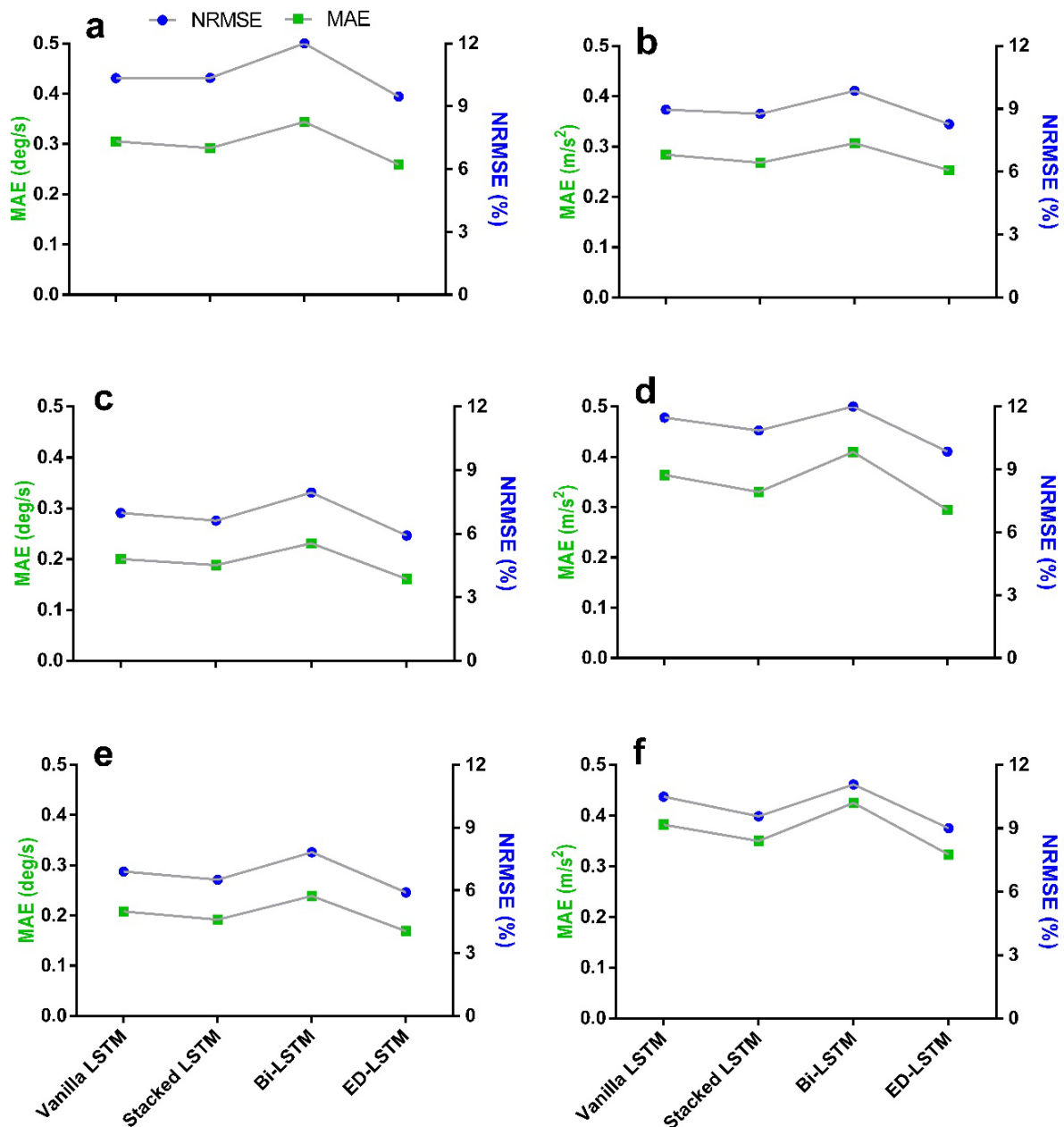


**Figure 5-6:** Performance comparison between LSTM models based on leave-one-out cross validation at +20% PWS for each feature vector. Green is the RMSE (Left Y-axis). Blue is the NRMSE (Right Y-axis). Lower error points for the MAE and NRMSE means a better predictive model for the related feature vector. (a) Foot AV ( $X_1$ ). (b) Foot LA ( $Y_4$ ). (c) Shank AV ( $X_2$ ). (d) Shank LA ( $Y_5$ ). (e) Thigh AV ( $X_3$ ). (f) Thigh LA ( $Y_6$ ).

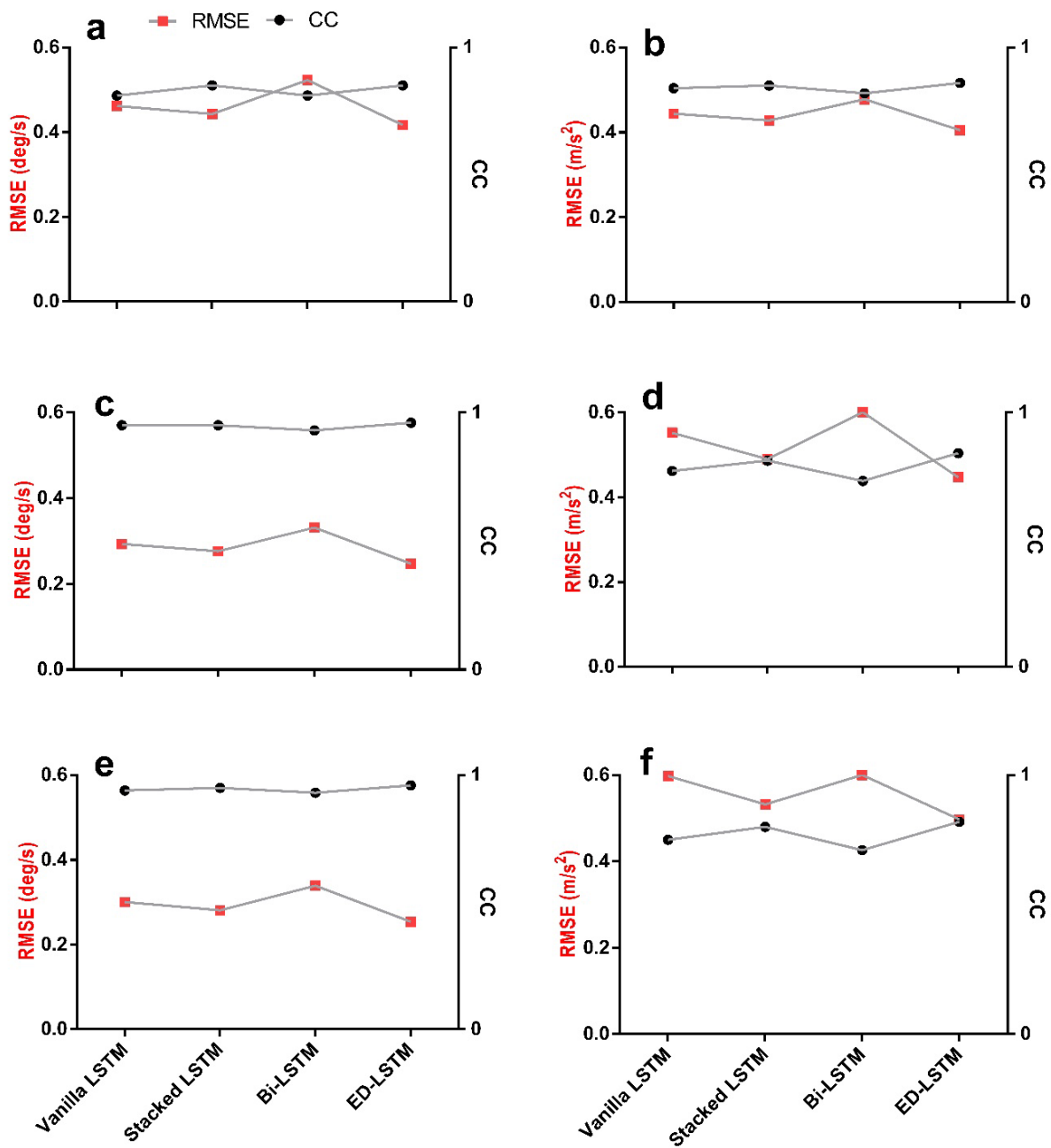


**Figure 5-7:** Performance comparison between LSTM models based on leave-one-out cross validation at +20% PWS for each feature vector. Red is the RMSE (Left Y-axis). Black is the CC (Right Y-axis). Wider gaps between the two error lines (CC and RMSE) means better prediction quality for the related feature vector. (a) Foot AV ( $X_1$ ). (b) Foot LA ( $Y_4$ ). (c) Shank AV ( $X_2$ ). (d) Shank LA ( $Y_5$ ). (e) Thigh AV ( $X_3$ ). (f) Thigh LA ( $Y_6$ ).

## **5.6 Performance comparison between the developed LSTM models in Study 2 and Study 3**

The performance of all cross validated LSTM models (Vanilla, Stacked, Bi and ED) is summarised and shown in **Figure 5-8** below for each tested walking speed condition; PWS and  $5\text{km}\cdot\text{h}^{-1}$ , +20% PWS and the -20% PWS. The best model that maintained a low percentage error for all conditions is the ED-LSTM. While the Bi-LSTM demonstrated the most erroneous predicted trajectories for all feature vectors. The Vanilla and the Stacked LSTM performance error range fall in between the two other models. The Stacked LSTM sometimes perform almost the same as good as the ED-LSTM, particularly at the PWS and  $5\text{km}\cdot\text{h}^{-1}$  conditions.

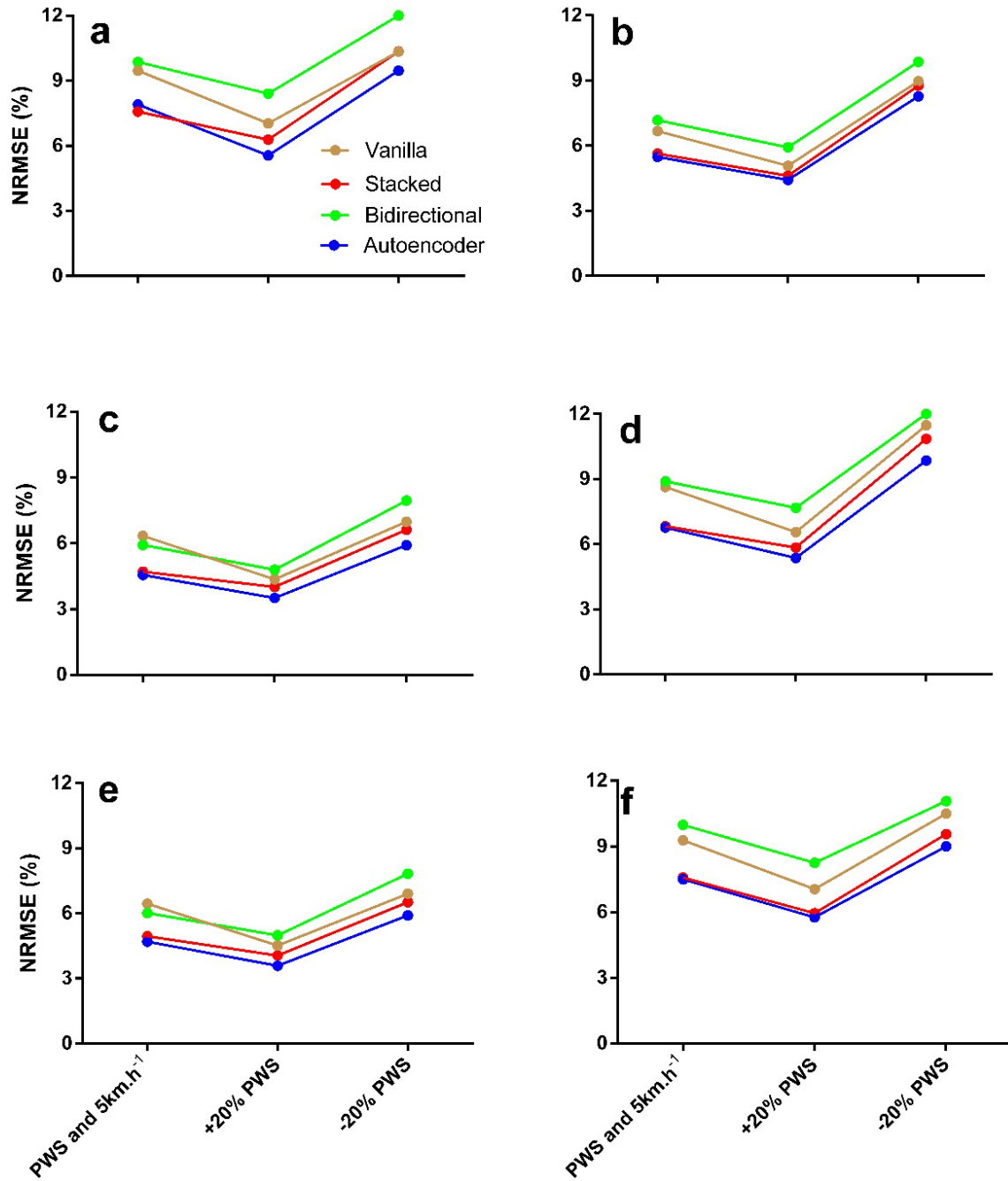


**Figure 5-8:** Leave-one-out cross validation error (%) summary for the cross validated LSTM models in study 1 (PWS and 5km.h<sup>-1</sup>) and study 2 ( $\pm 20\%$  PWS). Brown is the Vanilla LSTM. Lower error point indicates better performing model for the relevant speed. Red is the Stacked LSTM. Green is the Bi-LSTM. Blue is the ED-LSTM. (a) Foot AV ( $X_1$ ). (b) Foot LA ( $Y_4$ ). (c) Shank AV ( $X_2$ ). (d) Shank LA ( $Y_5$ ). (e) Thigh AV ( $X_3$ ). (f) Thigh LA ( $Y_6$ ).

## 5.7 Discussion

Due to the significant changes found at the kinematic walking profiles when ambulation speed changes (see **Section 1.2**), the aim of this study was to further challenge and evaluate the

developed LSTM models (i.e. Vanilla, Stacked, Bi-LSTM and ED-LSTM) at  $\pm 20\%$  PWS. All models obtained poorer predictions at 20% slower speeds and achieved best predictions at 20% faster speeds compared to the PWS and  $5\text{km}\cdot\text{h}^{-1}$  walking speeds. The ED LSTM maintained and achieved the best predictive model throughout walking speed conditions (see **Figure 5-8**).

Developing ML Models that have been trained and validated to predict across different walking speeds (i.e.  $5\text{ km}\cdot\text{h}^{-1}$ , PWS, fast and slow), is precisely essential in-order to acclimate to the human's walking speed changes (A. R. Wu et al., 2019). Particularly in the design of bionics to better synchronise assistive devices to the varying human motion dynamics (Hanlon & Anderson, 2006; Sawicki et al., 2020; Tanghe et al., 2019; A. R. Wu et al., 2019). Studies have shown that older adults sporadically walk at a faster pace in outdoor activities which may increase the risk of falling (W. Li et al., 2006; Oliveira et al., 2017). The potential of predicting kinematics at slower walking speed than PWS, expands the utility of the LSTM models to the older populations whom are known to walk slower than younger adults. There exists a proportional relationship between the human age and their walking speeds. The walking speed was found to be slightly decreasing each year among healthy male and female populations (Schimpl et al., 2011). Starting from  $4.89\text{ km}\cdot\text{h}^{-1}$  (male) and  $4.82\text{ km}\cdot\text{h}^{-1}$  (female) at 20-29 years old up to  $3.49\text{ km}\cdot\text{h}^{-1}$  (male) and  $3.38\text{ km}\cdot\text{h}^{-1}$  (female) at 80-89 years old. Slow walking speeds are especially relevant to the design of powered exoskeletons and orthotics for users with neurological disorders (Louie, Eng, & Lam, 2015).

Pilot trials were firstly conducted in-order-to observe walking speed changes that does not alter the human walking nature (Winter, 1991). The preliminary results suggested that  $\pm 20\%$  walking speed changes are enough to induce differences into the walking kinematic patterns without altering the nature of walking. These findings were also consistent with the literature for the 20% faster walking speed ( $5.26 \pm 0.53\text{ km}\cdot\text{h}^{-1}$ ) (Khan, Khan, & Usman, 2016; Weinhandl, Irmischer, & Sievert, 2017; Yang, Yoshida, Hortobágyi, & Suzuki, 2013) and the 20% slower walking speed ( $3.59 \pm 0.47\text{ km}\cdot\text{h}^{-1}$ ) (Hsiao, Knarr, Higginson, & Binder-Macleod, 2015; Kwon et al., 2015; X. Wang, Ma, Hou, & Lam, 2017). Drastic changes in walking speed (i.e.  $\pm 30\%$ ) were found to develop into postural control at very slow walking (Smith & Lemaire, 2018) or it may increase the risk of tripping at very fast or uncomfortable walking speed (Oliveira et al., 2017; W.-F. Wang, Lien, Liu, & Yang, 2018). Falling in particular is highly associated with fast walking in older adults (Fan, Li, Han, Lv, & Zhang, 2016; Kang & Dingwell, 2008; Nagano, James, Sparrow, & Begg, 2014; Oliveira et al., 2017).

The Faster speed predictions (+20% PWS) were the most accurate in this research (**Figure 5-8**). The least erroneous and most accurate trajectory signals were achieved at this speed (**Figure 5-3** and **Figure 5-4**). The dissimilarities between the RMSE error of LA and AV predicted trajectories were found lower for all LSTM models (**Figure 5-3**). The results suggest that all of the LSTM models may not perform as good at faster walking speed as at the PWS or slower walking speeds (M. Murray, Mollinger, Gardner, & Sepic, 1984; Oliveira et al., 2017).

In general however, all of the LSTM models exhibited the worse predictions at -20% PWS (**Figure 5-8**). The weak performance at slower speed is demonstrated in **Figure 5-7** where models obtained higher error rates for all LA trajectories and the foot AV. The thigh and shank AV obtained lower rates possibly due to the less variability movements in these segments in contrast with the foot (**Figure 5-1**) (Gholami et al., 2020). The predicted pattern (CC) was below 0.9 for most of the trajectories (**Table 5-14**) compared to faster speed and the PWS. Locomotion predictions at slower speeds were commonly found to be challenging (Moissenet et al., 2019) due to the utilisation of different muscle and locomotor coordination strategies (Den Otter, Geurts, Mulder, & Duysens, 2004; Nymark, Balmer, Melis, Lemaire, & Millar, 2005). Such differences in locomotor strategies may be translated into a succession of postures rather than an ambulatory task during slow walking (Moissenet et al., 2019; Smith & Lemaire, 2018) which may lead to longer double support phase (Martin & Schmiedeler, 2014) and discontinuity on temporal parameters (i.e. stride and stance length) (Smith & Lemaire, 2018). Besides, the coordination of left-right limbs was found to be weakening at slower walking speeds due to increased control attention demands (Plotnik, Bartsch, Zeev, Giladi, & Hausdorff, 2013). Poorer predictions at slower speeds may also be attributed to the training data. The distribution of the training data was largely centred on PWS, 15.4% faster (i.e. 5km.h<sup>-1</sup>) and 20% faster speed which resulted on models that were trained on fewer examples of slow walking speeds (i.e. only at -20% slower).

The most accurate kinematic trajectory predictions at all of the tested walking speeds were achieved by the ED LSTM model (**Figure 5-8**) in which the internal learning process is unsupervised (Srivastava et al., 2015). As shown in Chapter 3 – **Section 3.3.8**, the ED LSTM obtains predictions based on a two learning phases. The encoder maps the input data (i.e. the input window) into a hidden layer and learns a compressed feature representation of the independent variables. While the decoder reconstructs the input data from the hidden layer to obtain the target dependent variables from the compressed feature representation. The

optimiser (i.e. SGD) then minimises the reconstruction error which is the difference between the input and the reconstructed output (Sagheer & Kotb, 2019b). This type of learning approach allowed the ED LSTM to obtain quality features from a given input of kinematic trajectories (Zabalza et al., 2016). The unsupervised feature learning paradigm (i.e. encoder) and the reconstruction of time series information (i.e. decoder) has made the ED LSTM a good architecture for high level deep features formation and for generative models (Bao, Yue, & Rao, 2017; Blaschke, Olivecrona, Engkvist, Bajorath, & Chen, 2018; Srivastava et al., 2015). The complexity and the power of the ED LSTM could be extended to other learning techniques such as the unsupervised greedy layer-wise pre-training referred to as pretraining (Sagheer & Kotb, 2019b). The pretraining involves the training of a shallow layer and sequentially adding up and refitting a new hidden layer to learn inputs from the existing previous layer (i.e. shallow layer) while keeping fixed the learned weights and biases of the previous layer (Goodfellow, Bengio, Courville, & Bengio, 2016). The pretraining structure opened up the opportunity to train very deep stacked ED LSTM with less possibility of overfitting (because the training is performed in layer-wise) and a lower generalisation error (Bengio et al., 2006).

The second best LSTM model for kinematics trajectory prediction at all of the tested walking speeds was the Stacked LSTM (**Figure 5-8**) in which the model consists of multiple hidden layers with each layer comprised of multiple memory cells (Chapter 4 – **Figure 4-6**). The concept of multiple hidden layers or sometimes referred to as deep learning is commonly attributed to the success of solving several challenging prediction problems (LeCun et al., 2015). The hierarchy of the several layers resembles a processing pipeline where each layer processes part of the given problem and convey it is output to the next layer until the last layer generates the sequence prediction output (Hermans & Schrauwen, 2013). Therefore, the Stacked LSTM is a hierarchical model that was able to achieve good predictions (the closest to ED LSTM) by dissecting the given prediction problem into several sub-problems that are solved by each of the hidden LSTM layers (Pascanu, Gulcehre, Cho, & Bengio, 2013). The Stacked LSTM may be improved to achieve better performance with supervised greedy layer-wise pretraining (Bengio et al., 2006) and regularisation techniques (Goodfellow et al., 2016).

The Vanilla LSTM (Chapter 4 – **Figure 4-5**) is a simple LSTM architecture adopted from the original 1997 LSTM paper (Hochreiter & Schmidhuber, 1997). The Vanilla LSTM (**Figure 5-8**) achieved a moderate performance at all of the tested walking speeds. The LA and AV predicted trajectories were not as good as the ED and the Stacked LSTM and were not as poor as the Bi-LSTM. This type of performance indicates that the Vanilla LSTM model was capable

of predicting future kinematic trajectories but was not able to learn enough features from the independent variables. Unlike the Stacked LSTM, the Vanilla LSTM model consists of a single layer of LSTM memory cells that may not be able to capture all features and characteristics related to the AV and the LA kinematic variables. The Vanilla LSTM model is found not suitable for the future kinematics trajectory prediction.

The Bi-LSTM achieved the poorest predictions throughout walking speeds (**Figure 5-8**). The Bi-LSTM architecture (Chapter 4 – **Section 4.3.9**) maximises modelling of the input sequence by processing the input signals in forward and backward directions (Schuster & Paliwal, 1997). The bases of the Bi-LSTM architecture is on the scientific evidence that humans may use sounds, or words that only make sense at a future context (Graves & Schmidhuber, 2005). Without the BN layer the Bi-LSTM model was found slower in converging to the local minima compared to the other developed LSTM models (Siarni-Namini et al., 2019). In this theses, a BN input layer has been added to the Bi-LSTM model in order to expedite the neural network training by stabilising the distributions (mean and variance) of the input layer (Ioffe & Szegedy, 2015). The model achieved good performance in challenging prediction problems such as the financial timeseries forecasting and in coordination with CNN for EEG signal generation (Zhu et al., 2019). However, it was not clear whether learning the human lower limb trajectories from the past and the future have added any value to the prediction quality. The Bi-LSTM model is found not suitable for the future kinematics trajectory prediction.

This study was limited to young and healthy participants. The application of future known trajectories at slower and faster walking speeds is largely relevant to the elder populations and patients with pathological gait pattern. Expanding the recruitment cohort to those populations allow the developed LSTM models to learn trajectories that are sophisticated enough to assist in falls prevention for the elderly (Barrett et al., 2010; D. T. Lai et al., 2012; Levinger et al., 2016; Nagano et al., 2020) and in the design of bionics for individuals with gait disorders (Dollar & Herr, 2007; Esquenazi, Talaty, Packel, & Saulino, 2012; Tanghe et al., 2019). The second limitation of this work is the constrained walking nature over the treadmill. There exist a statistically significant differences in the kinematic variables between the treadmill and the overground walking nature (Alton, Baldey, Caplan, & Morrissey, 1998; S. J. Lee & Hidler, 2008; Riley, Paolini, Della Croce, Paylo, & Kerrigan, 2007). The bases of collecting walking data over a treadmill was to understand the possibility of predicting kinematics trajectory at faster and slower speeds relative to the PWS. Collecting overground walking data however

exposes the LSTM models to trajectories that are realistic and natural so that the predicted kinematic trajectories are better suited to the human movement dynamics.

## **5.8 Conclusion**

In this study, 4 LSTM architectures were trained and tested to predict the future lower limb kinematics (i.e. foot AV, shank AV, thigh AV, foot LA, shank LA and thigh LA) at faster (+20% PWS) and slower (-20% PWS) walking speeds. Results indicated that at the faster and slower walking speeds, the ED and the Stacked LSTM are the most accurate models to predict kinematic trajectories up to 0.1s in the future. The 0.1s known future lower limb trajectories is in the range between fast and slow muscle twitches (0.01-0.12s) and therefore highlight the possibility for the LSTM models to prevent falls and improve in the bionics human-machine interface. Further work is needed to understand the ED and the Stacked LSTM models robustness under different walking conditions (i.e. overground) and in the elder population as well as in participants with a pathological gait. The next chapter concludes the findings for all the 3 studies (Chapters 3 to 5) and outlines the limitations and future directions. It also highlights the practical applications for a known human movement biomechanics.

## 6 CHAPTER SIX: CONCLUSION AND FUTURE DIRECTIONS

### 6.1 Summary

This thesis investigated the potential of LSTM neural networks to predict the future lower limb trajectories of the foot AV ( $X_1$ ), foot LA ( $Y_4$ ), shank AV ( $X_2$ ), shank LA ( $Y_5$ ), thigh AV ( $X_3$ ) and the thigh LA ( $Y_6$ ). Four LSTM architectures have been developed and generalised to predict the lower limb kinematics at imposed walking speed, PWS, faster walking speed and slower walking speed. The LSTM autoencoder (ED-LSTM) have been found to be the most accurate and robust ML model for kinematic trajectories forecasting up to 0.1s. Prevalent statistical models such as the LR is found not suitable for the prediction of future lower limb kinematics. The aim and findings of this work were carried out in 3 studies as follows (see **Figure 1-4**):

1. Study 1 (Chapter 3) – To investigate the possibility of ML and statistical techniques to predict the human movement biomechanics:

In Chapter 2, the potential applications of ML in human movement biomechanics have been investigated and reviewed. Studies have shown that ML models were better able to capture the relationships between heterogeneous and highly dimensional biomechanical variables than conventional statistical techniques. Fewer studies have been found to address the human movement future trajectories prediction using ML and statistical methods with no sliding window technique specified for ML regression tasks. In Chapter 3, the study confirmed the possibility of predicting the future trajectories of human lower limb kinematics (i.e., thigh AV, shank AV, thigh LA and shank LA) using ED-LSTM and the LR during an imposed walking speed ( $5\text{km}\cdot\text{h}^{-1}$ ). A new sliding window technique have been proposed and validated for the optimum size to convert the time series data into 3D data to be modelled with ED-LSTM and LR models for the human movement regression tasks. Both models achieved satisfactory predicted trajectories up to 0.06s. A prediction horizon of 0.06s can be used to compensate for delays in an exoskeleton's feed-forward controller to better estimate the human motions and synchronise with intended movement trajectories (B. Su & M Gutierrez-Farewik, 2020; Tanghe et al., 2019). The ED-LSTM prediction horizon was better able to forecast earlier future trajectories and was able to learn and predict the future kinematics. The LR obtained better prediction performance than the

ED-LSTM at the imposed speed. However, the findings along with the linear prediction principle of the LR necessitate further investigation of the LR performance at the PWS.

2. Study 2 (Chapter 4) – To develop and generalise ML models and a statistical model to predict the future lower limb kinematics at preferred walking speed.

In the previous study, the possibility to predict the future lower limb kinematics at imposed speed ( $5\text{km}\cdot\text{h}^{-1}$ ) is confirmed and the optimum sliding window sizes have been recognized. In this study, there were 4 standard LSTM architectures that have been developed and generalised to predict the future lower limb kinematics, i.e. foot AV, shank AV, thigh AV, foot LA, shank LA and thigh LA. The LR is a popular prediction method among biomechanists that have also been investigated for the same task to comprehend the performance of parametric statistical models. The sliding window design to convert the 2D data into 3D was kept the same as per study 1. The performance of the LR model at PWS indicated that it is not suitable for the prediction of future lower limb kinematics. The LSTM performance results suggested that the ED-LSTM and the Stacked LSTM are more accurate to predict the future lower limb kinematics up to 0.1s at PWS and imposed walking speed ( $5\text{km}\cdot\text{h}^{-1}$ ). The average duration for a gait cycle ranges between 0.98-1.07s, and a prediction horizon of 0.1s accounts for about 10% of the gait cycle (M. P. Murray, Drought, & Kory, 1964). Such a forecast may assist in anticipating a low foot clearance to develop early countermeasures such as slowing down or stopping (D. T. Lai et al., 2012).

3. Study 3 (Chapter 5) – To finalise and test the developed models' architecture on the effects of walking speed variations:

In this study, the developed 4 LSTM architectures were further trained with TL and cross evaluated to predict the future lower limb kinematics at faster (+20% PWS) and slower (-20% PWS) walking speeds. The design of the LSTM architectures was kept the same to forecast the same variables (i.e. foot AV, shank AV, thigh AV, foot LA, shank LA and thigh LA) up to 0.1s. At +20% PWS, results have shown that the LSTM models' performance obtained better predictions compared to all tested walking speeds (i.e. PWS, -20% PWS and  $5\text{km}\cdot\text{h}^{-1}$ ). While at -20% PWS, results indicated that at slower walking speeds all of the LSTM architectures obtained weaker predictions compared to all tested walking speeds (i.e. PWS, +20% PWS and  $5\text{km}\cdot\text{h}^{-1}$ ). In addition to the applications of a known future trajectories at the PWS mentioned in study 1 and 2, the prediction at fast and slow walking speeds familiarised the developed ML models with changes in human

walking speed which are known to have large effects on lower limb kinematics (A. R. Wu et al., 2019). When intelligent ML methods are familiarised with the degree of kinematic changes due to speed variations, it could be used to improve human-machine interface in bionics design for various walking speeds.

#### 4. The key findings of Studies 1, 2 and 3:

The complexity of the human movements might not be estimated with linear statistical models such as the LR. ML methods such as the LSTM were found to be better able to learn the trajectories of human movement kinematics. The ED LSTM was found to be the most accurate and robust model to predict and adapt to the human motion kinematics at PWS,  $\pm 20\%$  PWS and  $5\text{km}\cdot\text{h}^{-1}$  (see **Figure 5-8**). All models attained the best performance at  $+20\%$  PWS and obtained the weakest predictions at the  $-20\%$  PWS (**Figure 5-8**) due to imbalances in the training data (**Section 5.7**).

## 6.2 Limitations and future directions

In order to apply the findings of this thesis to real-life scenarios of human movement biomechanics, there exist some technical challenges to practical implementation of ML. The LSTM model was validated for steady state walking. More walking movement conditions may need to be studied such as walking at home or in office to understand how the LSTM model performs in human daily life tasks. Kinematic motions based on human daily life tasks are rich of non-periodic trajectories (Simonsick, Guralnik, Volpato, Balfour, & Fried, 2005). Such kinematics are useful to widen the application of the LSTM model to the human motion dynamics.

Future directions could also be carried out to tackle the limitations of this work as follows:

- Limitation 1 (Treadmill walking) – This work was to investigate the possibility and the accuracy of LSTM to predict the future kinematics of the lower limb trajectories. The LSTM models were trained and cross-validated on lower limb kinematics data collected during a treadmill walking to obtain a high quality training data and in return simplify the model's development and tuning (Batista, Prati, & Monard, 2004; Goodfellow et al., 2016). There exist a statistical differences between the lower limb kinematics in treadmill and overground walking (Alton et al., 1998; S. J. Lee & Hidler, 2008). This work is the first of its kind, and there was no specific data collection protocol in order to understand the performance of ML in forecasting the human movement trajectories.

Due to the higher kinematics variance in overground walking, the treadmill walking facilitates a baseline to develop, tune and compare the performance of different ML models to empirically choose the optimum model (i.e. ED-LSTM) for human movement trajectories prediction. Future training data should be based on overground walking in order to expose the ED-LSTM and the Stacked LSTM to a more realistic and natural human movement kinematics. This would have a direct impact to naturalise the operation of bionics and to facilitate the compensation of control system delays.

- Limitation 2 (Healthy and young participants) – One of the major application of this work is to prevent falls and tripping incidents. Future participant recruitment should be expanded to include elders and individuals with pathological gait that are known to walk slower than the general population and in high risk to fall at faster than preferred walking speeds. This would convey the potential application of future lower limb kinematics prediction to users that may mostly benefit from this work.
- Limitation 3 (Prediction horizon of 0.1s) – The ED LSTM has been found to be the most accurate and robust LSTM model to predict the trajectories of human movement biomechanics up to 0.1s. Further work is need to expand the ED LSTM prediction horizon while maintaining or improving the prediction quality. This could be tackled by firstly introducing different learning techniques to the LSTM model such as the greedy layer-wise pretraining (Sagheer & Kotb, 2019b). Secondly the LSTM model should be exposed to more training (i.e. more participants) data to overcome the weak performance at slow speed (Batista et al., 2004). While the addition of a more training means there is a possibility of overfitting, it might be necessary to include regularisation techniques such as the weight regularisation or the dropout.

### **6.3 Practical ML-based applications of a known human movement biomechanics**

While ML has proven wide success in modelling the complexity of human movement biomechanics, it allowed biomechanists, clinicians and engineers to deliver new technologies that improve our safety and lifestyle. The hardware implementation of ML models have been a challenging process across many research studies (Sze, Chen, Emer, Suleiman, & Zhang, 2017). Particularly due to the required strong computational power. Deep learning platforms such as NVIDIA Jetson Nano is a promising platform that provides a low-cost embedded ML applications (Mittal, 2019). The LSTM model in this thesis was developed and validated using Amazon Web Services (AWS – EC2) platform which is a cloud-computing service that offers

super computational power (Mishra, 2019). The developed LSTM model is expected to require higher computational power than the Jetson Nano. In the future, the LSTM model is expected to be transformed into a user-friendly hardware when the suitable technology is available in the market.

In a bigger picture, if this path of research is expanded further to include the full human body motion estimation, the findings of this thesis can be transferred into a diverse range of applications. Nowadays, robots are becoming a major component to assist in repetitive tasks (i.e. factory operations and defence purposes) and powerful robots (i.e. automated guided vehicles) are posing manifold difficulties for human-robot interaction (Heyer, 2010; Kratzer, Toussaint, & Mainprice, 2020; Lasota, Fong, & Shah, 2017; Sheridan, 2016). One such difficulty is when humans have to strategise their movements in order to work in a close proximity with mobile robots (Ge & Cui, 2000; Patle, Pandey, Parhi, & Jagadeesh, 2019). Although robots are possibly equipped with path planning technologies, the additional knowledge of future human motions minimises the hazardous human-robot interaction (i.e. unexpected human motion trajectory) and improves the safety of a work environment (Fu et al., 2018; Kratzer et al., 2020; Lasota et al., 2017). The smart human-robot interaction can also be integrated with the internet of things (IoT) for a safer collaborative work environment (Ray, 2018). The IoT facilitates the autonomous robot communication with the environment which eventually leads to autonomous learning and self-awareness (Vermesan et al., 2020).

In robotic rehabilitation training, the patient-robotic cooperative strategies have been actively researched and are considered an important attribute towards safe and comfortable assistive technology (Duschau-Wicke et al., 2009; Glackin et al., 2014; Hesse et al., 1999). Some of the robotic rehabilitation devices such as the Lokomat (Colombo et al., 2000) rely on a cooperative strategy in which a pre-defined trajectories were influenced by the patient movements (Veneman et al., 2007). A foreseen motion trajectories based on historical gait pattern (i.e. sliding window), improves the cooperative strategy and better assist the user to achieve natural and genuinely assisted movements. Particularly the non-parametric ML based (i.e. LSTM) cooperative strategy are capable of automatically adapting its predictive parameters to better align with the continuously varying human movement trajectories (Fong, Ocampo, Gross, & Tavakoli, 2020; M. Zhang et al., 2017; K. Zhao, Teng, Gong, Chen, & Zhao, 2019).

The known human movement biomechanics could be a game changer in sports such that it could improve skill acquisition (Hodges & Williams, 2012; Xiao-wei, 2020). The prediction

of swimming movements have been found to enhance the swimmer performance (Stanula et al., 2012; Webb et al., 2011; J. Xie, Xu, Nie, & Nie, 2015, 2017). The known swimming motions could also be applied to assist an amputee to achieve their potential and perhaps expedite the re-gaining of their swimming skills (Lecrivain, Payton, Slaouti, & Kennedy, 2010; Osborough, Payton, & Daly, 2010). When a movement trajectory is known, it can be classified and that enables the classification of an incorrect foot movement for instance which may lead to a bad stroke. Such information could be transferred to a wearable device and alert the user to rectify their movement pattern and suggest synchronisation techniques for optimum swimming performance.

Overall, the possibility to forecast the human motion dynamics expands the capacity of bionics, wearable sensors and robotics to enrich the human-machine interaction.

## 7 REFERENCES

- Abaid, N., Cappa, P., Palermo, E., Petrarca, M., & Porfiri, M. (2013). Gait detection in children with and without hemiplegia using single-axis wearable gyroscopes. *PloS one*, 8(9), e73152.
- Aertbeliën, E., & De Schutter, J. (2014). *Learning a predictive model of human gait for the control of a lower-limb exoskeleton*. Paper presented at the 5th IEEE RAS/EMBS International Conference on Biomedical Robotics and Biomechatronics.
- Ahn, S., Kim, J., Koo, B., & Kim, Y. (2019). Evaluation of inertial sensor-based pre-impact fall detection algorithms using public dataset. *Sensors*, 19(4), 774.
- Akyildiz, I. F., Su, W., Sankarasubramaniam, Y., & Cayirci, E. (2002). Wireless sensor networks: a survey. *Computer networks*, 38(4), 393-422.
- Alaqtash, M., Sarkodie-Gyan, T., Yu, H., Fuentes, O., Brower, R., & Abdelgawad, A. (2011). *Automatic classification of pathological gait patterns using ground reaction forces and machine learning algorithms*. Paper presented at the 2011 Annual International Conference of the IEEE Engineering in Medicine and Biology Society.
- Albert, J. A., Owolabi, V., Gebel, A., Brahms, C. M., Granacher, U., & Arnrich, B. (2020). Evaluation of the pose tracking performance of the azure kinect and kinect v2 for gait analysis in comparison with a gold standard: A pilot study. *Sensors*, 20(18), 5104.
- Alcock, L., Galna, B., Lord, S., & Rochester, L. (2016). Characterisation of foot clearance during gait in people with early Parkinson's disease: Deficits associated with a dual task. *Journal of biomechanics*, 49(13), 2763-2769.
- Alexander, E. J., & Andriacchi, T. P. (2001). Correcting for deformation in skin-based marker systems. *Journal of biomechanics*, 34(3), 355-361.
- Allen, F. R., Ambikairajah, E., Lovell, N. H., & Celler, B. G. (2006). *An adapted gaussian mixture model approach to accelerometry-based movement classification using time-domain features*. Paper presented at the Engineering in Medicine and Biology Society, 2006. EMBS'06. 28th Annual International Conference of the IEEE.
- Alotaibi, M., & Mahmood, A. (2017). Improved Gait Recognition Based on Specialized Deep Convolutional Neural Network. *Computer Vision and Image Understanding*.
- Alton, F., Baldey, L., Caplan, S., & Morrissey, M. (1998). A kinematic comparison of overground and treadmill walking. *Clinical biomechanics*, 13(6), 434-440.
- Anam, K., & Al-Jumaily, A. A. (2012). Active exoskeleton control systems: State of the art. *Procedia Engineering*, 41, 988-994.
- Astephen, J., & Deluzio, K. (2005). Changes in frontal plane dynamics and the loading response phase of the gait cycle are characteristic of severe knee osteoarthritis application of a multidimensional analysis technique. *Clinical biomechanics*, 20(2), 209-217.
- Bai, O., Rathi, V., Lin, P., Huang, D., Battapady, H., Fei, D.-Y., . . . Hallett, M. (2011). Prediction of human voluntary movement before it occurs. *Clinical Neurophysiology*, 122(2), 364-372.
- Baker, R. (2007). The history of gait analysis before the advent of modern computers. *Gait & posture*, 26(3), 331-342.
- Banos, O., Damas, M., Pomares, H., Rojas, F., Delgado-Marquez, B., & Valenzuela, O. (2013). Human activity recognition based on a sensor weighting hierarchical classifier. *Soft Computing*, 17(2), 333-343.
- Banos, O., Galvez, J.-M., Damas, M., Pomares, H., & Rojas, I. (2014). Window size impact in human activity recognition. *Sensors*, 14(4), 6474-6499.

- Bao, W., Yue, J., & Rao, Y. (2017). A deep learning framework for financial time series using stacked autoencoders and long-short term memory. *PloS one*, *12*(7), e0180944.
- Barrett, R., Mills, P., & Begg, R. (2010). A systematic review of the effect of ageing and falls history on minimum foot clearance characteristics during level walking. *Gait & posture*, *32*(4), 429-435.
- Barton, G., Lees, A., Lisboa, P., & Attfield, S. (2006). Visualisation of gait data with Kohonen self-organising neural maps. *Gait & posture*, *24*(1), 46-53.
- Baskwill, A. J., Belli, P., & Kelleher, L. (2017). Evaluation of a gait assessment module using 3D motion capture technology. *International journal of therapeutic massage & bodywork*, *10*(1), 3.
- Batista, G. E., Prati, R. C., & Monard, M. C. (2004). A study of the behavior of several methods for balancing machine learning training data. *ACM SIGKDD explorations newsletter*, *6*(1), 20-29.
- Begg, R., Best, R., Dell'Oro, L., & Taylor, S. (2007). Minimum foot clearance during walking: strategies for the minimisation of trip-related falls. *Gait & posture*, *25*(2), 191-198.
- Begg, R., & Kamruzzaman, J. (2005). A machine learning approach for automated recognition of movement patterns using basic, kinetic and kinematic gait data. *Journal of biomechanics*, *38*(3), 401-408.
- Begg, R., & Kamruzzaman, J. (2006). Neural networks for detection and classification of walking pattern changes due to ageing. *Australasian Physical & Engineering Science in Medicine*, *29*(2), 188-195.
- Begg, R., Lai, D. T., & Palaniswami, M. (2007). *Computational intelligence in biomedical engineering*: CRC Press.
- Begg, R., & Palaniswami, M. (2006). *Computational intelligence for movement sciences: neural networks and other emerging techniques*: IGI Global.
- Begg, R. K., Palaniswami, M., & Owen, B. (2005). Support vector machines for automated gait classification. *IEEE transactions on biomedical engineering*, *52*(5), 828-838.
- Begg, R. K., & Rahman, S. M. (2000). A method for the reconstruction of ground reaction force-time characteristics during gait from force platform recordings of simultaneous foot falls. *IEEE transactions on biomedical engineering*, *47*(4), 547-551.
- Begg, R. K., Tirosh, O., Said, C. M., Sparrow, W. A., Steinberg, N., Lvinger, P., & Galea, M. P. (2014). Gait training with real-time augmented toe-ground clearance information decreases tripping risk in older adults and a person with chronic stroke. *Frontiers in human neuroscience*, *8*, 243.
- Bengio, Y., Lamblin, P., Popovici, D., & Larochelle, H. (2006). Greedy layer-wise training of deep networks. *Advances in neural information processing systems*, *19*, 153-160.
- Bengio, Y., Simard, P., & Frasconi, P. (1994). Learning long-term dependencies with gradient descent is difficult. *IEEE transactions on neural networks*, *5*(2), 157-166.
- Benoussaad, M., Sijobert, B., Mombaur, K., & Azevedo Coste, C. (2016). Robust foot clearance estimation based on the integration of foot-mounted IMU acceleration data. *Sensors*, *16*(1), 12.
- Beravs, T., Reberšek, P., Novak, D., Podobnik, J., & Munih, M. (2011). *Development and validation of a wearable inertial measurement system for use with lower limb exoskeletons*. Paper presented at the Humanoid Robots (Humanoids), 2011 11th IEEE-RAS International Conference on.
- Bergamini, E., Ligorio, G., Summa, A., Vannozzi, G., Cappozzo, A., & Sabatini, A. (2014). Estimating orientation using magnetic and inertial sensors and different sensor fusion approaches: Accuracy assessment in manual and locomotion tasks. *Sensors*, *14*(10), 18625-18649.

- Best, R., & Begg, R. (2008). A method for calculating the probability of tripping while walking. *Journal of biomechanics*, 41(5), 1147-1151.
- Bi, L., & Guan, C. (2019). A review on EMG-based motor intention prediction of continuous human upper limb motion for human-robot collaboration. *Biomedical Signal Processing and Control*, 51, 113-127.
- Biasiucci, A., Franceschiello, B., & Murray, M. M. (2019). Electroencephalography. *Current Biology*, 29(3), R80-R85.
- Biggar, S., & Yao, W. (2016). Design and Evaluation of a Soft and Wearable Robotic Glove for Hand Rehabilitation. *IEEE Transactions on Neural Systems and Rehabilitation Engineering*, 24(10), 1071-1080. doi:10.1109/tnsre.2016.2521544
- Binnie, C., & Prior, P. (1994). Electroencephalography. *Journal of Neurology, Neurosurgery & Psychiatry*, 57(11), 1308-1319.
- Bishop, C. M. (2006). *Pattern recognition and machine learning*: springer.
- Blaschke, T., Olivecrona, M., Engkvist, O., Bajorath, J., & Chen, H. (2018). Application of generative autoencoder in de novo molecular design. *Molecular informatics*, 37(1-2), 1700123.
- Bohannon, R. W. (1997). Comfortable and maximum walking speed of adults aged 20—79 years: reference values and determinants. *Age and ageing*, 26(1), 15-19.
- Botchkarev, A. (2018). Performance metrics (error measures) in machine learning regression, forecasting and prognostics: Properties and typology. *arXiv preprint arXiv:1809.03006*.
- Bottou, L. (2010). Large-scale machine learning with stochastic gradient descent. In *Proceedings of COMPSTAT'2010* (pp. 177-186): Springer.
- Bottou, L. (2012). Stochastic gradient descent tricks. In *Neural networks: Tricks of the trade* (pp. 421-436): Springer.
- Boulgouris, N. V., & Chi, Z. X. (2007). Gait recognition using radon transform and linear discriminant analysis. *IEEE transactions on image processing*, 16(3), 731-740.
- Breiman, L. (2001). Statistical modeling: The two cultures (with comments and a rejoinder by the author). *Statistical science*, 16(3), 199-231.
- Brenière, Y. (1996). Why we walk the way we do. *Journal of motor behavior*, 28(4), 291-298.
- Browning, R. C., Baker, E. A., Herron, J. A., & Kram, R. (2006). Effects of obesity and sex on the energetic cost and preferred speed of walking. *Journal of Applied Physiology*, 100(2), 390-398.
- Brownlee, J. (2014). Machine learning mastery. URL: <http://machinelearningmastery.com/discover-feature-engineering-howtoengineer-features-and-how-to-getgood-at-it>.
- Brownlee, J. (2019). *Master machine learning algorithms: Discover How They Work and Implement Them From Scratch* (2019 ed.): Machine Learning Mastery.
- Buchner, D. M., Larson, E. B., Wagner, E. H., Koepsell, T. D., & De Lateur, B. J. (1996). Evidence for a non-linear relationship between leg strength and gait speed. *Age and ageing*, 25(5), 386-391.
- Bush, R. R., & Mosteller, F. (1955). Stochastic models for learning.
- Butterworth, S. (1930). On the theory of filter amplifiers. *Wireless Engineer*, 7(6), 536-541.
- C-motion. (2015). Joint Velocity. *wiki documentation* Retrieved from [https://c-motion.com/v3dwiki/index.php/Joint\\_Velocity](https://c-motion.com/v3dwiki/index.php/Joint_Velocity)
- Cai, C., Han, L., Ji, Z. L., Chen, X., & Chen, Y. Z. (2003). SVM-Prot: web-based support vector machine software for functional classification of a protein from its primary sequence. *Nucleic acids research*, 31(13), 3692-3697.

- Caldas, R., Mundt, M., Potthast, W., de Lima Neto, F. B., & Markert, B. (2017). A systematic review of gait analysis methods based on inertial sensors and adaptive algorithms. *Gait & posture*, *57*, 204-210.
- Cappozzo, A., Catani, F., Della Croce, U., & Leardini, A. (1995). Position and orientation in space of bones during movement: anatomical frame definition and determination. *Clinical biomechanics*, *10*(4), 171-178.
- Carpino, G., Accoto, D., Tagliamonte, N. L., Ghilardi, G., & Guglielmelli, E. (2013). Lower limb wearable robots for physiological gait restoration: state of the art and motivations. *Medic*, *21*(2), 72-80.
- Carvalho, R., Dias, N., & Cerqueira, J. J. (2019). Brain-machine interface of upper limb recovery in stroke patients rehabilitation: a systematic review. *Physiotherapy Research International*, *24*(2), e1764.
- Chan, A. D., & Englehart, K. B. (2005). Continuous myoelectric control for powered prostheses using hidden Markov models. *IEEE transactions on biomedical engineering*, *52*(1), 121-124.
- Chan, C. W., & Rudins, A. (1994). *Foot biomechanics during walking and running*. Paper presented at the Mayo Clinic Proceedings.
- Chapman, A. D. (2005). principles and methods of data cleaning  $\exists$  primary species and species-occurrence data.
- Chau, T. (2001). A review of analytical techniques for gait data. Part 1: fuzzy, statistical and fractal methods. *Gait & posture*, *13*(1), 49-66.
- Chavarriaga, R., Sagha, H., Calatroni, A., Digumarti, S. T., Tröster, G., Millán, J. d. R., & Roggen, D. (2013). The Opportunity challenge: A benchmark database for on-body sensor-based activity recognition. *Pattern Recognition Letters*, *34*(15), 2033-2042.
- Chehab, E., Andriacchi, T., & Favre, J. (2017). Speed, age, sex, and body mass index provide a rigorous basis for comparing the kinematic and kinetic profiles of the lower extremity during walking. *Journal of biomechanics*, *58*, 11-20.
- Chen, G., Chan, C. K., Guo, Z., & Yu, H. (2013). A review of lower extremity assistive robotic exoskeletons in rehabilitation therapy. *Critical Reviews™ in Biomedical Engineering*, *41*(4-5).
- Chen, X., Yin, Y., & Fan, Y. (2014). EMG oscillator model-based energy kernel method for characterizing muscle intrinsic property under isometric contraction. *Chinese science bulletin*, *59*(14), 1556-1567.
- Chen, X., Zeng, Y., & Yin, Y. (2017). Improving the transparency of an exoskeleton knee joint based on the understanding of motor intent using energy kernel method of EMG. *IEEE Transactions on Neural Systems and Rehabilitation Engineering*, *25*(6), 577-588.
- Chéron, G., Duvinage, M., De Saedeleer, C., Castermans, T., Bengoetxea, A., Petieau, M., . . . Dutoit, T. (2012). From spinal central pattern generators to cortical network: integrated BCI for walking rehabilitation. *Neural plasticity*, *2012*.
- Chevallereau, C., & Aoustin, Y. (2001). Optimal reference trajectories for walking and running of a biped robot. *Robotica*, *19*(5), 557-569.
- Ching, W.-K., Huang, X., Ng, M. K., & Siu, T.-K. (2013). *Markov Chains Models, Algorithms and Applications* (Second Edition ed.). New York: Springer.
- Cho, K., Van Merriënboer, B., Gulcehre, C., Bahdanau, D., Bougares, F., Schwenk, H., & Bengio, Y. (2014). Learning phrase representations using RNN encoder-decoder for statistical machine translation. *arXiv preprint arXiv:1406.1078*.
- Chong, E., & Park, F. C. (2017). Movement prediction for a lower limb exoskeleton using a conditional restricted Boltzmann machine. *Robotica*, *35*(11), 2177-2200.

- Clouthier, A. L., Ross, G. B., & Graham, R. B. (2020). Sensor data required for automatic recognition of athletic tasks using deep neural networks. *Frontiers in bioengineering and biotechnology*, 7, 473.
- Colombo, G., Joerg, M., Schreier, R., & Dietz, V. (2000). Treadmill training of paraplegic patients using a robotic orthosis. *Journal of rehabilitation research and development*, 37(6), 693.
- Cortes, C., & Vapnik, V. (1995). Support-vector networks. *Machine learning*, 20(3), 273-297.
- Cox, S., Roggenkamp, R., Bernard, S., & Smith, K. (2018). The epidemiology of elderly falls attended by emergency medical services in Victoria, Australia. *Injury*, 49(9), 1712-1719.
- Crea, S., De Rossi, S. M., Donati, M., Reberšek, P., Novak, D., Vitiello, N., . . . Carrozza, M. C. (2012). *Development of gait segmentation methods for wearable foot pressure sensors*. Paper presented at the Engineering in Medicine and Biology Society (EMBC), 2012 Annual International Conference of the IEEE.
- Cuesta-Vargas, A. I., Galán-Mercant, A., & Williams, J. M. (2010). The use of inertial sensors system for human motion analysis. *Physical Therapy Reviews*, 15(6), 462-473.
- Da Silva, I. N., Spatti, D. H., Flauzino, R. A., Liboni, L. H. B., & dos Reis Alves, S. F. (2017). *Artificial Neural Networks: A Practical Course*: Springer.
- Dadashi, F., Mariani, B., Rochat, S., Büla, C. J., Santos-Eggimann, B., & Aminian, K. (2014). Gait and foot clearance parameters obtained using shoe-worn inertial sensors in a large-population sample of older adults. *Sensors*, 14(1), 443-457.
- Davidson, R. J., Jackson, D. C., & Larson, C. L. (2000). Human electroencephalography.
- Davis, P. J. (1975). *Interpolation and approximation*: Courier Corporation.
- De Brabandere, A., Emmerzaal, J., Timmermans, A., Jonkers, I., Vanwanseele, B., & Davis, J. (2020). A machine learning approach to estimate hip and knee joint loading using a mobile phone-embedded IMU. *Frontiers in bioengineering and biotechnology*, 8, 320.
- De Cock, A.-M., Fransen, E., Perkisas, S., Verhoeven, V., Beauchet, O., Remmen, R., & Vandewoude, M. (2017). Gait characteristics under different walking conditions: association with the presence of cognitive impairment in community-dwelling older people. *PloS one*, 12(6).
- Dehzangi, O., Taherisadr, M., & ChangalVala, R. (2017). IMU-based gait recognition using convolutional neural networks and multi-sensor fusion. *Sensors*, 17(12), 2735.
- DeLisa, J. A. (1998). *Gait analysis in the science of rehabilitation* (Vol. 2): Diane Publishing.
- Deluzio, K. J., Wyss, U. P., Zee, B., Costigan, P. A., & Serbie, C. (1997). Principal component models of knee kinematics and kinetics: normal vs. pathological gait patterns. *Human movement science*, 16(2-3), 201-217.
- Den Otter, A., Geurts, A., Mulder, T., & Duysens, J. (2004). Speed related changes in muscle activity from normal to very slow walking speeds. *Gait & posture*, 19(3), 270-278.
- Di Nardo, F., Morbidoni, C., Cucchiarelli, A., & Fioretti, S. (2021). Influence of EMG-signal processing and experimental set-up on prediction of gait events by neural network. *Biomedical Signal Processing and Control*, 63, 102232.
- Ding, Y., Kim, M., Kuindersma, S., & Walsh, C. J. (2018). Human-in-the-loop optimization of hip assistance with a soft exosuit during walking. *Sci. Robot.*, 3(15), eaar5438.
- do Carmo Vilas-Boas, M., Choupina, H. M. P., Rocha, A. P., Fernandes, J. M., & Cunha, J. P. S. (2019). Full-body motion assessment: Concurrent validation of two body tracking depth sensors versus a gold standard system during gait. *Journal of biomechanics*, 87, 189-196.

- Doke, J., Donelan, J. M., & Kuo, A. D. (2005). Mechanics and energetics of swinging the human leg. *Journal of Experimental Biology*, 208(3), 439-445.
- Dollar, A. M., & Herr, H. (2007). *Active orthoses for the lower-limbs: challenges and state of the art*. Paper presented at the Rehabilitation Robotics, 2007. ICORR 2007. IEEE 10th International Conference on.
- Dollar, A. M., & Herr, H. (2008). Lower extremity exoskeletons and active orthoses: challenges and state-of-the-art. *IEEE Transactions on robotics*, 24(1), 144-158.
- Donelan, J. M., Kram, R., & Kuo, A. D. (2002). Simultaneous positive and negative external mechanical work in human walking. *Journal of biomechanics*, 35(1), 117-124.
- Dorschky, E., Nitschke, M., Martindale, C. F., van den Bogert, A. J., Koelewijn, A. D., & Eskofier, B. M. (2020). CNN-Based Estimation of Sagittal Plane Walking and Running Biomechanics From Measured and Simulated Inertial Sensor Data. *Frontiers in bioengineering and biotechnology*, 8, 604.
- Draper, N. R., & Smith, H. (1998). *Applied regression analysis* (Vol. 326): John Wiley & Sons.
- Dubbeldam, R., Buurke, J., Simons, C., Groothuis-Oudshoorn, C., Baan, H., Nene, A., & Hermens, H. (2010). The effects of walking speed on forefoot, hindfoot and ankle joint motion. *Clinical biomechanics*, 25(8), 796-801.
- Dugad, R., & Desai, U. B. (1996). A tutorial on hidden Markov models. *Signal Processing and Artificial Neural Networks Laboratory, Dept of Electrical Engineering, Indian Institute of Technology, Bombay Technical Report No.: SPANN-96.1*.
- Duschau-Wicke, A., von Zitzewitz, J., Caprez, A., Lunenburger, L., & Riener, R. (2009). Path control: a method for patient-cooperative robot-aided gait rehabilitation. *IEEE Transactions on Neural Systems and Rehabilitation Engineering*, 18(1), 38-48.
- Dyrby, C. O., & Andriacchi, T. P. (2004). Secondary motions of the knee during weight bearing and non-weight bearing activities. *Journal of Orthopaedic Research*, 22(4), 794-800.
- Elliott, G., Marecki, A., & Herr, H. (2014). Design of a clutch–spring knee exoskeleton for running. *Journal of Medical Devices*, 8(3), 031002.
- Elman, J. L. (1990). Finding structure in time. *Cognitive science*, 14(2), 179-211.
- Esquenazi, A., Talaty, M., Packel, A., & Saulino, M. (2012). The ReWalk powered exoskeleton to restore ambulatory function to individuals with thoracic-level motor-complete spinal cord injury. *American journal of physical medicine & rehabilitation*, 91(11), 911-921.
- Ewing, K. A., Fernandez, J. W., Begg, R. K., Galea, M. P., & Lee, P. V. (2016). Prophylactic knee bracing alters lower-limb muscle forces during a double-leg drop landing. *Journal of biomechanics*, 49(14), 3347-3354.
- Fan, Y., Li, Z., Han, S., Lv, C., & Zhang, B. (2016). The influence of gait speed on the stability of walking among the elderly. *Gait & posture*, 47, 31-36.
- Fawcett, T. (2006). An introduction to ROC analysis. *Pattern Recognition Letters*, 27(8), 861-874.
- Fernandez-Lopez, P., Liu-Jimenez, J., Kiyokawa, K., Wu, Y., & Sanchez-Reillo, R. (2019). Recurrent neural network for inertial gait user recognition in smartphones. *Sensors*, 19(18), 4054.
- Findlow, A., Goulermas, J., Nester, C., Howard, D., & Kenney, L. (2008). Predicting lower limb joint kinematics using wearable motion sensors. *Gait & posture*, 28(1), 120-126.
- Fink, G. A. (2014). *Markov models for pattern recognition: from theory to applications*: Springer Science & Business Media.
- Finley, F. (1969). Locomotion patterns in elderly women. *Arch. Phys. Med. Rehabil.*, 50, 140-146.

- Finley, F., & Cody, K. (1970). Locomotive characteristics of urban pedestrians. *Archives of physical medicine and rehabilitation*, 51(7), 423.
- Fisher, R. A. (1936). The use of multiple measurements in taxonomic problems. *Annals of human genetics*, 7(2), 179-188.
- Fleischer, C., Reinicke, C., & Hommel, G. (2005). *Predicting the intended motion with EMG signals for an exoskeleton orthosis controller*. Paper presented at the Intelligent robots and systems, 2005.(IROS 2005). 2005 IEEE/RSJ international conference on.
- Fong, J., Ocampo, R., Gross, D. P., & Tavakoli, M. (2020). Intelligent robotics incorporating machine learning algorithms for improving functional capacity evaluation and occupational rehabilitation. *Journal of occupational rehabilitation*, 1-9.
- Francois, C. (2017). Deep learning with Python. In: Manning Publications Company.
- Fu, B., Chen, L., Zhou, Y., Zheng, D., Wei, Z., Dai, J., & Pan, H. (2018). An improved A\* algorithm for the industrial robot path planning with high success rate and short length. *Robotics and Autonomous Systems*, 106, 26-37.
- Fukuchi, C. A., & Duarte, M. (2019). A prediction method of speed-dependent walking patterns for healthy individuals. *Gait & posture*, 68, 280-284.
- Fukuchi, C. A., Fukuchi, R. K., & Duarte, M. (2019). Effects of walking speed on gait biomechanics in healthy participants: a systematic review and meta-analysis. *Systematic reviews*, 8(1), 153.
- Fukuchi, R. K., Eskofier, B. M., Duarte, M., & Ferber, R. (2011). Support vector machines for detecting age-related changes in running kinematics. *Journal of biomechanics*, 44(3), 540-542.
- Fukunaga, K. (2013). *Introduction to statistical pattern recognition*: Elsevier.
- Fuschillo, V. L., Bagalà, F., Chiari, L., & Cappello, A. (2012). Accelerometry-based prediction of movement dynamics for balance monitoring. *Medical & biological engineering & computing*, 50(9), 925-936.
- Gangopadhyay, T., Tan, S. Y., Huang, G., & Sarkar, S. (2018). Temporal Attention and Stacked LSTMs for Multivariate Time Series Prediction.
- Gareth, J., Daniela, W., Trevor, H., & Robert, T. (2013). *An introduction to statistical learning: with applications in R*: Springer.
- Garofolini, A. (2019). *Exploring adaptability in long-distance runners: effect of foot strike pattern on lower limb neuro-muscular-skeletal capacity*. Victoria University,
- Garofolini, A., Taylor, S., & Lepine, J. (2019). Evaluating dynamic error of a treadmill and the effect on measured kinetic gait parameters: implications and possible solutions. *Journal of biomechanics*, 82, 156-163.
- Garofolini, A., Taylor, S., Mclaughlin, P., Mickle, K. J., & Frigo, C. A. (2019). Ankle Joint Dynamic Stiffness in Long-Distance Runners: Effect of Foot Strike and Shoes Features. *Applied Sciences*, 9(19), 4100.
- Ge, S. S., & Cui, Y. J. (2000). New potential functions for mobile robot path planning. *IEEE Transactions on robotics and automation*, 16(5), 615-620.
- Géron, A. (2019). *Hands-on machine learning with Scikit-Learn, Keras, and TensorFlow: Concepts, tools, and techniques to build intelligent systems*: O'Reilly Media.
- Gholami, M., Napier, C., & Menon, C. (2020). Estimating Lower Extremity Running Gait Kinematics with a Single Accelerometer: A Deep Learning Approach. *Sensors*, 20(10), 2939.
- Gillain, S., Boutaayamou, M., Schwartz, C., Brùls, O., Bruyère, O., Croisier, J.-L., . . . Petermans, J. (2019). Using supervised learning machine algorithm to identify future fallers based on gait patterns: A two-year longitudinal study. *Experimental gerontology*, 127, 110730.

- Glackin, C., Salge, C., Greaves, M., Polani, D., Slavnić, S., Ristić-Durrant, D., . . . Matjačić, Z. (2014). *Gait trajectory prediction using Gaussian process ensembles*. Paper presented at the 2014 IEEE-RAS International Conference on Humanoid Robots.
- Gloor, P. (1969). Hans Berger on electroencephalography. *American Journal of EEG Technology*, 9(1), 1-8.
- Goldstein, H., Poole, C., & Safko, J. (2002). Classical mechanics. In: American Association of Physics Teachers.
- González, R. C., López, A. M., Rodríguez-Uría, J., Álvarez, D., & Alvarez, J. C. (2010). Real-time gait event detection for normal subjects from lower trunk accelerations. *Gait & posture*, 31(3), 322-325.
- Good, P. I. (2006). *Resampling methods*: Springer.
- Goodfellow, I., Bengio, Y., Courville, A., & Bengio, Y. (2016). *Deep learning* (Vol. 1): MIT press Cambridge.
- Goršič, M., Kamnik, R., Ambrožič, L., Vitiello, N., Lefeber, D., Pasquini, G., & Munih, M. (2014). Online phase detection using wearable sensors for walking with a robotic prosthesis. *Sensors*, 14(2), 2776-2794.
- Grant, J., & Chester, V. (2015). The effects of walking speed on adult multi-segment foot kinematics. *Journal of Bioengineering & Biomedical Science*, 5(2), 181-183.
- Graves, A. (2012a). Supervised sequence labelling. In *Supervised sequence labelling with recurrent neural networks* (pp. 5-13): Springer.
- Graves, A. (2012b). Supervised sequence labelling with recurrent neural networks. 2012. URL <http://books.google.com/books>.
- Graves, A. (2013). Generating sequences with recurrent neural networks. *arXiv preprint arXiv:1308.0850*.
- Graves, A., & Schmidhuber, J. (2005). Framewise phoneme classification with bidirectional LSTM and other neural network architectures. *Neural networks*, 18(5-6), 602-610.
- Greff, K., Srivastava, R. K., Koutník, J., Steunebrink, B. R., & Schmidhuber, J. (2016). LSTM: A search space odyssey. *IEEE transactions on neural networks and learning systems*, 28(10), 2222-2232.
- Guentherberg, E., Yang, A. Y., Ghasemzadeh, H., Jafari, R., Bajcsy, R., & Sastry, S. S. (2009). A method for extracting temporal parameters based on hidden Markov models in body sensor networks with inertial sensors. *IEEE transactions on information technology in biomedicine*, 13(6), 1019-1030.
- Guyon, I., & Elisseeff, A. (2003). An introduction to variable and feature selection. *Journal of Machine Learning Research*, 3(Mar), 1157-1182.
- Guyon, I., Saffari, A., Dror, G., & Cawley, G. (2010). Model selection: Beyond the bayesian/frequentist divide. *Journal of Machine Learning Research*, 11(Jan), 61-87.
- Hageman, P. A., & Blanke, D. J. (1986). Comparison of gait of young women and elderly women. *Physical therapy*, 66(9), 1382-1387.
- Hakonen, M., Piitulainen, H., & Visala, A. (2015). Current state of digital signal processing in myoelectric interfaces and related applications. *Biomedical Signal Processing and Control*, 18, 334-359.
- Halilaj, E., Rajagopal, A., Fiterau, M., Hicks, J. L., Hastie, T. J., & Delp, S. L. (2018). Machine learning in human movement biomechanics: best practices, common pitfalls, and new opportunities. *Journal of biomechanics*, 81, 1-11.
- Hallett, M. (2007). Volitional control of movement: the physiology of free will. *Clinical Neurophysiology*, 118(6), 1179-1192.
- Han, B.-K., Ryu, J.-K., & Kim, S.-C. (2019). Context-Aware Winter Sports Based on Multivariate Sequence Learning. *Sensors*, 19(15), 3296.

- Han, J., & Bhanu, B. (2005). Individual recognition using gait energy image. *IEEE transactions on pattern analysis and machine intelligence*, 28(2), 316-322.
- Hanley, B., Tucker, C. B., & Bissas, A. (2018). Differences between motion capture and video analysis systems in calculating knee angles in elite-standard race walking. *Journal of sports sciences*, 36(11), 1250-1255.
- Hanlon, M., & Anderson, R. (2006). Prediction methods to account for the effect of gait speed on lower limb angular kinematics. *Gait & posture*, 24(3), 280-287.
- Hanlon, M., & Anderson, R. (2009). Real-time gait event detection using wearable sensors. *Gait & posture*, 30(4), 523-527.
- Hannink, J., Kautz, T., Pasluosta, C. F., Gaßmann, K.-G., Klucken, J., & Eskofier, B. M. (2016). Sensor-based gait parameter extraction with deep convolutional neural networks. *IEEE journal of biomedical and health informatics*, 21(1), 85-93.
- Hans, C. (2011). Elastic net regression modeling with the orthant normal prior. *Journal of the American Statistical Association*, 106(496), 1383-1393.
- Hasan, S. S., Siddiquee, M. R., & Bai, O. (2020). Asynchronous Prediction of Human Gait Intention in a Pseudo Online Paradigm Using Wavelet Transform. *IEEE Transactions on Neural Systems and Rehabilitation Engineering*, 28(7), 1623-1635.
- Hemmatpour, M., Ferrero, R., Montrucchio, B., & Rebaudengo, M. (2019). A Review on Fall Prediction and Prevention System for Personal Devices: Evaluation and Experimental Results. *Advances in Human-Computer Interaction*, 2019.
- Hermans, M., & Schrauwen, B. (2013). *Training and analysing deep recurrent neural networks*. Paper presented at the Advances in neural information processing systems.
- Herr, H. (2009). Exoskeletons and orthoses: classification, design challenges and future directions. *Journal of NeuroEngineering and Rehabilitation*, 6(1), 21.
- Hesse, S., Uhlenbrock, D., & Sarkodie-Gyan, T. (1999). Gait pattern of severely disabled hemiparetic subjects on a new controlled gait trainer as compared to assisted treadmill walking with partial body weight support. *Clinical Rehabilitation*, 13(5), 401-410.
- Heyer, C. (2010). *Human-robot interaction and future industrial robotics applications*. Paper presented at the 2010 IEEE/RSJ International Conference on Intelligent Robots and Systems.
- Hibbeler, R. C. (2007). *Engineering Mechanics Dynamics SI Units*. In: Pearson Education South Asia, Singapore.
- Hochreiter, S., Bengio, Y., Frasconi, P., & Schmidhuber, J. (2001). Gradient flow in recurrent nets: the difficulty of learning long-term dependencies. In: *A field guide to dynamical recurrent neural networks*. IEEE Press.
- Hochreiter, S., & Schmidhuber, J. (1997). Long short-term memory. *Neural computation*, 9(8), 1735-1780.
- Hodges, N. J., & Williams, A. M. (2012). *Skill acquisition in sport: Research, theory and practice*.
- Hoerl, A. E., & Kennard, R. W. (1970). Ridge regression: Biased estimation for nonorthogonal problems. *Technometrics*, 12(1), 55-67.
- Hori, K., Mao, Y., Ono, Y., Ora, H., Hirobe, Y., Sawada, H., . . . Miyake, Y. (2019). Inertial measurement unit-based estimation of foot trajectory for clinical gait analysis. *Frontiers in Physiology*, 10.
- Horst, F., Lopuschkin, S., Samek, W., Müller, K.-R., & Schöllhorn, W. I. (2019). Explaining the unique nature of individual gait patterns with deep learning. *Scientific reports*, 9(1), 2391.
- Horst, F., Mildner, M., & Schöllhorn, W. (2017). One-year persistence of individual gait patterns identified in a follow-up study—A call for individualised diagnose and therapy. *Gait & posture*, 58, 476-480.

- Hotelling, H. (1933). Analysis of a complex of statistical variables into principal components. *Journal of educational psychology*, 24(6), 417.
- Hsiao, H., Knarr, B. A., Higginson, J. S., & Binder-Macleod, S. A. (2015). The relative contribution of ankle moment and trailing limb angle to propulsive force during gait. *Human movement science*, 39, 212-221.
- Hubley-Kozey, C., & Vezina, M. (2002). Differentiating temporal electromyographic waveforms between those with chronic low back pain and healthy controls. *Clinical biomechanics*, 17(9-10), 621-629.
- Ichinosawa, Y., Shimizu, S., Takemura, N., Taira, K., Hamakawa, M., Nakachi, Y., . . . Miura, H. (2018). Gait speed and balance function strongly determine the ability to walk independently without using a wheelchair in a facility setting for stroke patients. *The Kitasato medical journal*, 48(1), 16-25.
- Ingram, J. N., Sadeghi, M., Flanagan, J. R., & Wolpert, D. M. (2017). An error-tuned model for sensorimotor learning. *PLoS computational biology*, 13(12), e1005883.
- Inman, V. T., & Eberhart, H. D. (1953). The major determinants in normal and pathological gait. *JBJS*, 35(3), 543-558.
- Ioffe, S., & Szegedy, C. (2015). Batch normalization: Accelerating deep network training by reducing internal covariate shift. *arXiv preprint arXiv:1502.03167*.
- Isabelle, G. (2006). Feature Extraction Foundations and Applications. Pattern Recognition.
- Islam, M., & Hsiao-Wecksler, E. T. (2016). Detection of gait modes using an artificial neural network during walking with a powered ankle-foot orthosis. *Journal of Biophysics*, 2016.
- Japkowicz, N., & Shah, M. (2011). *Evaluating Learning Algorithms: A Classification Perspective*: Cambridge University Press.
- Jee, H., Lee, K., & Pan, S. (2004). *Eye and face detection using SVM*. Paper presented at the Intelligent Sensors, Sensor Networks and Information Processing Conference, 2004. Proceedings of the 2004.
- Jimenez-Fabian, R., & Verlinden, O. (2012). Review of control algorithms for robotic ankle systems in lower-limb orthoses, prostheses, and exoskeletons. *Medical engineering & physics*, 34(4), 397-408.
- Joshi, C. D., Lahiri, U., & Thakor, N. V. (2013). *Classification of gait phases from lower limb EMG: Application to exoskeleton orthosis*. Paper presented at the Point-of-Care Healthcare Technologies (PHT), 2013 IEEE.
- Jung, J.-Y., Heo, W., Yang, H., & Park, H. (2015). A Neural Network-Based Gait Phase Classification Method Using Sensors Equipped on Lower Limb Exoskeleton Robots. *Sensors*, 15(11), 27738.
- Jurafsky, D., & Martin, J. H. (2014). *Speech and language processing (Vol. 3)*: Pearson London.
- Kaczmarczyk, K., Wit, A., Krawczyk, M., Zaborski, J., & Piłsudski, J. (2011). Artificial neural networks (ANN) applied for gait classification and physiotherapy monitoring in post stroke patients. *Artificial neural networks—methodological advances and biomedical applications*.
- Kamruzzaman, J., & Begg, R. K. (2006). Support vector machines and other pattern recognition approaches to the diagnosis of cerebral palsy gait. *IEEE transactions on biomedical engineering*, 53(12), 2479-2490.
- Kang, H. G., & Dingwell, J. B. (2008). Effects of walking speed, strength and range of motion on gait stability in healthy older adults. *Journal of biomechanics*, 41(14), 2899-2905.
- Karpathy, A., Johnson, J., & Fei-Fei, L. (2015). Visualizing and understanding recurrent networks. *arXiv preprint arXiv:1506.02078*.

- Karvanen, J. (2003). The statistical basis of laboratory data normalization. *Drug information journal*, 37(1), 101-107.
- Kawamoto, H., & Sankai, Y. (2002). *Comfortable power assist control method for walking aid by HAL-3*. Paper presented at the Systems, Man and Cybernetics, 2002 IEEE International Conference on.
- Khan, S., Khan, S., & Usman, J. (2016). *Effects of toe-out and toe-in gait with varying walking speeds on knee adduction moment and mechanical work done—a pilot study*. Paper presented at the International Conference on Movement, Health and Exercise.
- Khandoker, A. H., Lai, D., Begg, R. K., & Palaniswami, M. (2006). *A wavelet-based approach for screening falls risk in the elderly using support vector machines*. Paper presented at the 2006 Fourth International Conference on Intelligent Sensing and Information Processing.
- Kidziński, Ł., Delp, S., & Schwartz, M. (2019). Automatic real-time gait event detection in children using deep neural networks. *PloS one*, 14(1), e0211466.
- Kim, P. (2017). *MATLAB Deep Learning With Machine Learning, Neural Networks and Artificial Intelligence*: Springer.
- Kingma, D. P., & Ba, J. (2014). Adam: A method for stochastic optimization. *arXiv preprint arXiv:1412.6980*.
- Kleinbaum, D. G., Dietz, K., Gail, M., Klein, M., & Klein, M. (2002). *Logistic regression*: Springer.
- Knudson, D. (2007). *Fundamentals of biomechanics*: Springer Science & Business Media.
- Kok, M., Hol, J. D., & Schön, T. B. (2017). Using inertial sensors for position and orientation estimation. *arXiv preprint arXiv:1704.06053*.
- Koller, J. R., Gates, D. H., Ferris, D. P., & Remy, C. D. (2016). *'Body-in-the-Loop' Optimization of Assistive Robotic Devices: A Validation Study*. Paper presented at the Robotics: Science and Systems.
- Komnik, I., Weiss, S., Pagani, C. F., & Potthast, W. (2015). Motion analysis of patients after knee arthroplasty during activities of daily living—a systematic review. *Gait & posture*, 41(2), 370-377.
- Kornhuber, H.-H. (1965). Changes in the brain potential in voluntary movements and passive movements in man: readiness potential and reafferent potentials. *Pflugers Arch Gesamte Physiol Menschen Tiere*, 10, 1-17.
- Kornhuber, H. H., & Deecke, L. (1965). Hirnpotentialänderungen bei Willkürbewegungen und passiven Bewegungen des Menschen: Bereitschaftspotential und reafferente Potentiale. *Pflüger's Archiv für die gesamte Physiologie des Menschen und der Tiere*, 284(1), 1-17.
- Kratzer, P., Toussaint, M., & Mainprice, J. (2020). *Prediction of human full-body movements with motion optimization and recurrent neural networks*. Paper presented at the 2020 IEEE International Conference on Robotics and Automation (ICRA).
- Kröse, B., Krose, B., van der Smagt, P., & Smagt, P. (1993). An introduction to neural networks.
- Kubat, M. (2015). *An Introduction to Machine Learning*: Springer.
- Kuhn, M., & Johnson, K. (2013). *Applied predictive modeling* (Vol. 26): Springer.
- Kuo, A. D. (2001). A simple model of bipedal walking predicts the preferred speed–step length relationship. *J. Biomech. Eng.*, 123(3), 264-269.
- Kuo, A. D. (2007). The six determinants of gait and the inverted pendulum analogy: A dynamic walking perspective. *Human movement science*, 26(4), 617-656.
- Kuo, A. D., & Donelan, J. M. (2010). Dynamic principles of gait and their clinical implications. *Physical therapy*, 90(2), 157-174.

- Kuo, A. D., Donelan, J. M., & Ruina, A. (2005). Energetic consequences of walking like an inverted pendulum: step-to-step transitions. *Exercise and sport sciences reviews*, 33(2), 88-97.
- Kwak, N.-S., Müller, K.-R., & Lee, S.-W. (2017). A convolutional neural network for steady state visual evoked potential classification under ambulatory environment. *PloS one*, 12(2), e0172578.
- Kwon, J. W., Son, S. M., & Lee, N. K. (2015). Changes of kinematic parameters of lower extremities with gait speed: a 3D motion analysis study. *Journal of Physical Therapy Science*, 27(2), 477-479.
- Lage, K. J., White, S. C., & Yack, H. J. (1995). The effects of unilateral knee immobilization on lower extremity gait mechanics. *Medicine and science in sports and exercise*, 27(1), 8-14.
- Lai, D. T., Begg, R. K., & Palaniswami, M. (2009). Computational intelligence in gait research: a perspective on current applications and future challenges. *IEEE transactions on information technology in biomedicine*, 13(5), 687-702.
- Lai, D. T., Begg, R. K., Taylor, S., & Palaniswami, M. (2008). Detection of tripping gait patterns in the elderly using autoregressive features and support vector machines. *Journal of biomechanics*, 41(8), 1762-1772.
- Lai, D. T., Levinger, P., Begg, R. K., Gilleard, W. L., & Palaniswami, M. (2009). Automatic recognition of gait patterns exhibiting patellofemoral pain syndrome using a support vector machine approach. *IEEE transactions on information technology in biomedicine*, 13(5), 810-817.
- Lai, D. T., Shilton, A., Charry, E., Begg, R., & Palaniswami, M. (2009). *A machine learning approach to k-step look-ahead prediction of gait variables from acceleration data*. Paper presented at the 2009 Annual International Conference of the IEEE Engineering in Medicine and Biology Society.
- Lai, D. T., Taylor, S. B., & Begg, R. K. (2012). Prediction of foot clearance parameters as a precursor to forecasting the risk of tripping and falling. *Human movement science*, 31(2), 271-283.
- Lai, D. T. H., Palaniswami, M., & Begg, R. (2011). *Healthcare sensor networks: challenges toward practical implementation*: CRC Press.
- Lakshmanan, V., & Kain, J. S. (2010). A Gaussian mixture model approach to forecast verification. *Weather and Forecasting*, 25(3), 908-920.
- Lasota, P. A., Fong, T., & Shah, J. A. (2017). *A survey of methods for safe human-robot interaction*: Now Publishers.
- Lauer, R. T., Smith, B. T., & Betz, R. R. (2005). Application of a neuro-fuzzy network for gait event detection using electromyography in the child with cerebral palsy. *IEEE transactions on biomedical engineering*, 52(9), 1532-1540.
- Le Borgne, H., & O'Connor, N. (2005). *Natural scene classification and retrieval using ridgelet-based image signatures*. Paper presented at the International Conference on Advanced Concepts for Intelligent Vision Systems.
- Lecrivain, G., Payton, C., Slaouti, A., & Kennedy, I. (2010). Effect of body roll amplitude and arm rotation speed on propulsion of arm amputee swimmers. *Journal of biomechanics*, 43(6), 1111-1117.
- LeCun, Y., Bengio, Y., & Hinton, G. (2015). Deep learning. *Nature*, 521(7553), 436.
- Lee, G., Kim, J., Panizzolo, F., Zhou, Y., Baker, L., Galiana, I., . . . Walsh, C. (2017). Reducing the metabolic cost of running with a tethered soft exosuit. *Science Robotics*, 2(6), eaan6708.

- Lee, M., Roan, M., Smith, B., & Lockhart, T. E. (2009). Gait analysis to classify external load conditions using linear discriminant analysis. *Human movement science*, 28(2), 226-235.
- Lee, S. J., & Hidler, J. (2008). Biomechanics of overground vs. treadmill walking in healthy individuals. *Journal of Applied Physiology*, 104(3), 747-755.
- Lee, T. H., Tsuchida, T., Kitahara, H., & Moriya, H. (1999). Gait analysis before and after unilateral total knee arthroplasty. Study using a linear regression model of normal controls—women without arthropathy. *Journal of orthopaedic science*, 4(1), 13-21.
- Lasell, J. L., Merriman, G. J., Riley, P. O., & Kerrigan, D. C. (2003). Predicting peak kinematic and kinetic parameters from gait speed. *Gait & posture*, 17(2), 106-112.
- Lenzi, T., De Rossi, S. M. M., Vitiello, N., & Carrozza, M. C. (2012). Intention-based EMG control for powered exoskeletons. *IEEE transactions on biomedical engineering*, 59(8), 2180-2190.
- Levinger, P., Nagano, H., Downie, C., Hayes, A., Sanders, K. M., Cicuttini, F., & Begg, R. (2016). Biomechanical balance response during induced falls under dual task conditions in people with knee osteoarthritis. *Gait & posture*, 48, 106-112.
- Li, H., Shen, Y., & Zhu, Y. (2018). *Stock Price Prediction Using Attention-based Multi-Input LSTM*. Paper presented at the Asian Conference on Machine Learning.
- Li, H., Xu, Z., Taylor, G., Studer, C., & Goldstein, T. (2018). *Visualizing the loss landscape of neural nets*. Paper presented at the Advances in neural information processing systems.
- Li, J., Chen, G., Thangavel, P., Yu, H., Thakor, N., Bezerianos, A., & Sun, Y. (2016). *A robotic knee exoskeleton for walking assistance and connectivity topology exploration in EEG signal*. Paper presented at the Biomedical Robotics and Biomechatronics (BioRob), 2016 6th IEEE International Conference on.
- Li, W., Keegan, T. H., Sternfeld, B., Sidney, S., Quesenberry Jr, C. P., & Kelsey, J. L. (2006). Outdoor falls among middle-aged and older adults: a neglected public health problem. *American journal of public health*, 96(7), 1192-1200.
- Lim, H., Kim, B., & Park, S. (2020). Prediction of lower limb kinetics and kinematics during walking by a single IMU on the lower back using machine learning. *Sensors*, 20(1), 130.
- Liu, D.-X., Wu, X., Du, W., Wang, C., & Xu, T. (2016). Gait Phase Recognition for Lower-Limb Exoskeleton with Only Joint Angular Sensors. *Sensors*, 16(10), 1579.
- Liu, G., & Guo, J. (2019). Bidirectional LSTM with attention mechanism and convolutional layer for text classification. *Neurocomputing*, 337, 325-338.
- Liu, X., Zhou, Z., Mai, J., & Wang, Q. (2017). *Multi-class SVM Based Real-Time Recognition of Sit-to-Stand and Stand-to-Sit Transitions for a Bionic Knee Exoskeleton in Transparent Mode*. Paper presented at the International Conference on Intelligent Robotics and Applications.
- Long, Y., Du, Z.-j., Dong, W., & Wang, W.-d. (2017). Human Gait Trajectory Learning Using Online Gaussian Process for Assistive Lower Limb Exoskeleton. In *Wearable Sensors and Robots* (pp. 165-179): Springer.
- Louie, D. R., Eng, J. J., & Lam, T. (2015). Gait speed using powered robotic exoskeletons after spinal cord injury: a systematic review and correlational study. *Journal of NeuroEngineering and Rehabilitation*, 12(1), 82.
- Luu, T. P., Low, K., Qu, X., Lim, H., & Hoon, K. (2014). An individual-specific gait pattern prediction model based on generalized regression neural networks. *Gait & posture*, 39(1), 443-448.
- Madinei, S., Alemi, M. M., Kim, S., Srinivasan, D., & Nussbaum, M. A. (2020). Biomechanical Evaluation of Passive Back-Support Exoskeletons in a Precision

- Manual Assembly Task: “Expected” Effects on Trunk Muscle Activity, Perceived Exertion, and Task Performance. *Human Factors*, 0018720819890966.
- Mai, J., Zhang, Z., & Wang, Q. (2017). *A Real-Time Intent Recognition System Based on SoC-FPGA for Robotic Transtibial Prosthesis*. Paper presented at the International Conference on Intelligent Robotics and Applications.
- Mangasarian, O. (1998). *Generalized support vector machines*. Retrieved from
- Manning, C. D., Raghavan, P., & Schütze, H. (2008). *Introduction to information retrieval*: Cambridge university press.
- Mannini, A., & Sabatini, A. M. (2010). Machine learning methods for classifying human physical activity from on-body accelerometers. *Sensors*, *10*(2), 1154-1175.
- Mannini, A., & Sabatini, A. M. (2012). Gait phase detection and discrimination between walking–jogging activities using hidden Markov models applied to foot motion data from a gyroscope. *Gait & posture*, *36*(4), 657-661.
- Mannini, A., Trojaniello, D., Cereatti, A., & Sabatini, A. M. (2016). A machine learning framework for gait classification using inertial sensors: application to elderly, post-stroke and huntington’s disease patients. *Sensors*, *16*(1), 134.
- Marshall, R., Wood, G., & Jennings, L. (1989). Performance objectives in human movement: A review and application to the stance phase of normal walking. *Human movement science*, *8*(6), 571-594.
- Martin, A. E., & Schmiedeler, J. P. (2014). Predicting human walking gaits with a simple planar model. *Journal of biomechanics*, *47*(6), 1416-1421.
- Martínez, A. M., & Kak, A. C. (2001). Pca versus lda. *IEEE transactions on pattern analysis and machine intelligence*, *23*(2), 228-233.
- Mason, J. E., Traoré, I., & Woungang, I. (2016). *Machine Learning Techniques for Gait Biometric Recognition: Using the Ground Reaction Force*: Springer.
- McLachlan, G., & Peel, D. (2004). *Finite mixture models*: John Wiley & Sons.
- Mijailovic, N., Gavrilovic, M., Rafajlovic, S., Đuric-Jovicic, M., & Popovic, D. (2009). Gait phases recognition from accelerations and ground reaction forces: Application of neural networks. *Telfor Journal*, *1*(1), 34-36.
- Mikos, V., Yen, S.-C., Tay, A., Heng, C.-H., Chung, C. L. H., Liew, S. H. X., . . . Au, W. L. (2018). Regression analysis of gait parameters and mobility measures in a healthy cohort for subject-specific normative values. *PloS one*, *13*(6), e0199215.
- Miller, J. D., Beazer, M. S., & Hahn, M. E. (2013). Myoelectric walking mode classification for transtibial amputees. *IEEE transactions on biomedical engineering*, *60*(10), 2745-2750.
- Mishra, A. (2019). *Machine Learning in the Aws Cloud: Add Intelligence to Applications with Amazon Sagemaker and Amazon Rekognition*: Sybex.
- Mitchell, T. M. (1997). Machine learning. In: McGraw-hill New York.
- Mittal, S. (2019). A Survey on optimized implementation of deep learning models on the NVIDIA Jetson platform. *Journal of Systems Architecture*, *97*, 428-442.
- Mohamed, O., & Appling, H. (2020). Clinical Assessment of Gait. In K. K. Chui, M. M. Jorge, S.-C. Yen, & M. M. Lusardi (Eds.), *Orthotics and Prosthetics in Rehabilitation (Fourth Edition)* (4 ed., pp. 102-143): Elsevier. Retrieved from (<http://www.sciencedirect.com/science/article/pii/B9780323609135000052>). doi:<https://doi.org/10.1016/B978-0-323-60913-5.00005-2>
- Mohler, B. J., Thompson, W. B., Creem-Regehr, S. H., Pick, H. L., & Warren, W. H. (2007). Visual flow influences gait transition speed and preferred walking speed. *Experimental brain research*, *181*(2), 221-228.
- Moissenet, F., Leboeuf, F., & Armand, S. (2019). Lower limb sagittal gait kinematics can be predicted based on walking speed, gender, age and BMI. *Scientific reports*, *9*(1), 1-12.

- Montgomery, D. C., Peck, E. A., & Vining, G. G. (2021). *Introduction to linear regression analysis*: John Wiley & Sons.
- Moon, D.-H., Kim, D., & Hong, Y.-D. (2019). Development of a Single Leg Knee Exoskeleton and Sensing Knee Center of Rotation Change for Intention Detection. *Sensors*, *19*(18), 3960.
- Morbidoni, C., Cucchiarelli, A., Fioretti, S., & Di Nardo, F. (2019). A deep learning approach to EMG-based classification of gait phases during level ground walking. *Electronics*, *8*(8), 894.
- Moyer, B., Chambers, A., Redfern, M. S., & Cham, R. (2006). Gait parameters as predictors of slip severity in younger and older adults. *Ergonomics*, *49*(4), 329-343.
- Mudie, K. L., Boynton, A. C., Karakolis, T., O'Donovan, M. P., Kanagaki, G. B., Crowell, H. P., . . . Billing, D. C. (2018). Consensus paper on testing and evaluation of military exoskeletons for the dismounted combatant. *Journal of science and medicine in sport*, *21*(11), 1154-1161.
- Mullineaux, D. R., Bartlett, R. M., & Bennett, S. (2001). Research design and statistics in biomechanics and motor control. *Journal of sports sciences*, *19*(10), 739-760.
- Mun, K.-R., Song, G., Chun, S., & Kim, J. (2018). Gait estimation from anatomical foot parameters measured by a foot feature measurement system using a deep neural network model. *Scientific reports*, *8*(1), 1-10.
- Mundt, M., Koeppel, A., David, S., Witter, T., Bamer, F., Potthast, W., & Markert, B. (2020). Estimation of gait mechanics based on simulated and measured IMU data using an artificial neural network. *Frontiers in bioengineering and biotechnology*, *8*.
- Murad, A., & Pyun, J.-Y. (2017). Deep recurrent neural networks for human activity recognition. *Sensors*, *17*(11), 2556.
- Murray, M., Mollinger, L., Gardner, G., & Sepic, S. (1984). Kinematic and EMG patterns during slow, free, and fast walking. *Journal of Orthopaedic Research*, *2*(3), 272-280.
- Murray, M. P., Drought, A. B., & Kory, R. C. (1964). Walking patterns of normal men. *JBJS*, *46*(2), 335-360.
- Nagano, H., James, L., Sparrow, W. A., & Begg, R. K. (2014). Effects of walking-induced fatigue on gait function and tripping risks in older adults. *Journal of NeuroEngineering and Rehabilitation*, *11*(1), 1-7.
- Nagano, H., Said, C. M., James, L., & Begg, R. K. (2020). Feasibility of Using Foot–Ground Clearance Biofeedback Training in Treadmill Walking for Post-Stroke Gait Rehabilitation. *Brain Sciences*, *10*(12), 978.
- Naghavi, N., Miller, A., & Wade, E. (2019). Towards Real-Time Prediction of Freezing of Gait in Patients With Parkinson's Disease: Addressing the Class Imbalance Problem. *Sensors*, *19*(18), 3898.
- Nair, V., & Hinton, G. E. (2010). *Rectified linear units improve restricted boltzmann machines*. Paper presented at the Proceedings of the 27th international conference on machine learning (ICML-10).
- Nait Aicha, A., Englebienne, G., van Schooten, K., Pijnappels, M., & Kröse, B. (2018). Deep learning to predict falls in older adults based on daily-life trunk accelerometry. *Sensors*, *18*(5), 1654.
- Nakano, T., Nukala, B. T., Zupancic, S., Rodriguez, A., Lie, D. Y., Lopez, J., & Nguyen, T. Q. (2016). *Gaits classification of normal vs. patients by wireless gait sensor and Support Vector Machine (SVM) classifier*. Paper presented at the Computer and Information Science (ICIS), 2016 IEEE/ACIS 15th International Conference on.
- Nilsson, A., Vreede, K. S., Häglund, V., Kawamoto, H., Sankai, Y., & Borg, J. (2014). Gait training early after stroke with a new exoskeleton—the hybrid assistive limb: a study of safety and feasibility. *Journal of NeuroEngineering and Rehabilitation*, *11*(1), 92.

- Noble, W. S. (2006). What is a support vector machine? *Nature biotechnology*, 24(12), 1565-1567.
- Nogueira, S. L., Lambrecht, S., Inoue, R. S., Bortole, M., Montagnoli, A. N., Moreno, J. C., . . . Pons, J. L. (2017). Global Kalman Filter approaches to estimate absolute angles of lower limb segments. *Biomedical engineering online*, 16(1), 58.
- Nogueira, S. L., Siqueira, A. A., Inoue, R. S., & Terra, M. H. (2014). Markov jump linear systems-based position estimation for lower limb exoskeletons. *Sensors*, 14(1), 1835-1849.
- Nukala, B. T., Shibuya, N., Rodriguez, A., Tsay, J., Lopez, J., Nguyen, T., . . . Lie, D. Y.-C. (2014). An efficient and robust fall detection system using wireless gait analysis sensor with artificial neural network (ANN) and support vector machine (SVM) algorithms. *Open J. Appl. Biosens*, 3, 29-39.
- Nymark, J. R., Balmer, S. J., Melis, E. H., Lemaire, E. D., & Millar, S. (2005). Electromyographic and kinematic nondisabled gait differences at extremely slow overground and treadmill walking speeds. *Journal of Rehabilitation Research & Development*, 42(4).
- O'Reilly, M. A., Whelan, D. F., Ward, T. E., Delahunt, E., & Caulfield, B. M. (2017). Classification of deadlift biomechanics with wearable inertial measurement units. *Journal of biomechanics*, 58, 155-161.
- O'Connor, C. M., Thorpe, S. K., O'Malley, M. J., & Vaughan, C. L. (2007). Automatic detection of gait events using kinematic data. *Gait & posture*, 25(3), 469-474.
- Ogutu, J. O., Schulz-Streeck, T., & Piepho, H.-P. (2012). *Genomic selection using regularized linear regression models: ridge regression, lasso, elastic net and their extensions*. Paper presented at the BMC proceedings.
- Oliveira, C. F., Vieira, E. R., Machado Sousa, F. M., & Vilas-Boas, J. P. (2017). Kinematic changes during prolonged fast-walking in old and young adults. *Frontiers in Medicine*, 4, 207.
- Olney, S. J., Griffin, M. P., & McBride, I. D. (1994). Temporal, kinematic, and kinetic variables related to gait speed in subjects with hemiplegia: a regression approach. *Physical therapy*, 74(9), 872-885.
- Ordóñez, F., & Roggen, D. (2016). Deep convolutional and lstm recurrent neural networks for multimodal wearable activity recognition. *Sensors*, 16(1), 115.
- Osborough, C. D., Payton, C. J., & Daly, D. J. (2010). Influence of swimming speed on inter-arm coordination in competitive unilateral arm amputee front crawl swimmers. *Human movement science*, 29(6), 921-931.
- Paluszek, M., & Thomas, S. (2017). *MATLAB machine learning*. USA: Apress.
- Pan, S. J., & Yang, Q. (2009). A survey on transfer learning. *IEEE Transactions on knowledge and data engineering*, 22(10), 1345-1359.
- Pandy, M. G. (2001). Computer modeling and simulation of human movement. *Annual review of biomedical engineering*, 3(1), 245-273.
- Papavasileiou, I., Zhang, W., & Han, S. (2016). *Real-time data-driven gait phase detection using infinite gaussian mixture model and parallel particle filter*. Paper presented at the Connected Health: Applications, Systems and Engineering Technologies (CHASE), 2016 IEEE First International Conference on.
- Papavasileiou, I., Zhang, W., & Han, S. (2017). Real-time data-driven gait phase detection using ground contact force measurements: Algorithms, platform design and performance. *Smart Health*, 1, 34-49.
- Park, S., Mustafa, S. K., & Shimada, K. (2013). *Learning based robot control with sequential Gaussian process*. Paper presented at the Robotic Intelligence In Informationally Structured Space (RiiSS), 2013 IEEE Workshop on.

- Park, S. H., Kim, B., Kang, C. M., Chung, C. C., & Choi, J. W. (2018). *Sequence-to-sequence prediction of vehicle trajectory via LSTM encoder-decoder architecture*. Paper presented at the 2018 IEEE Intelligent Vehicles Symposium (IV).
- Pascanu, R., Gulcehre, C., Cho, K., & Bengio, Y. (2013). How to construct deep recurrent neural networks. *arXiv preprint arXiv:1312.6026*.
- Pascanu, R., Mikolov, T., & Bengio, Y. (2013). *On the difficulty of training recurrent neural networks*. Paper presented at the International conference on machine learning.
- Patle, B., Pandey, A., Parhi, D., & Jagadeesh, A. (2019). A review: On path planning strategies for navigation of mobile robot. *Defence Technology, 15*(4), 582-606.
- Pavol, M. J., Owings, T. M., Foley, K. T., & Grabiner, M. D. (1999). Gait characteristics as risk factors for falling from trips induced in older adults. *Journals of Gerontology Series A: Biomedical Sciences and Medical Sciences, 54*(11), M583-M590.
- Peng, C.-Y. J., Lee, K. L., & Ingersoll, G. M. (2002). An introduction to logistic regression analysis and reporting. *The journal of educational research, 96*(1), 3-14.
- Petersen, T. H., Willerslev-Olsen, M., Conway, B. A., & Nielsen, J. B. (2012). The motor cortex drives the muscles during walking in human subjects. *The Journal of physiology, 590*(10), 2443-2452.
- Pfurtscheller, G. (1981). Central beta rhythm during sensorimotor activities in man. *Electroencephalography and clinical neurophysiology, 51*(3), 253-264.
- Pfurtscheller, G., & Aranibar, A. (1979). Evaluation of event-related desynchronization (ERD) preceding and following voluntary self-paced movement. *Electroencephalography and clinical neurophysiology, 46*(2), 138-146.
- Pfurtscheller, G., & Da Silva, F. L. (1999). Event-related EEG/MEG synchronization and desynchronization: basic principles. *Clinical Neurophysiology, 110*(11), 1842-1857.
- Pfurtscheller, G., & Neuper, C. (1994). Event-related synchronization of mu rhythm in the EEG over the cortical hand area in man. *Neuroscience letters, 174*(1), 93-96.
- Phinyomark, A., Hettinga, B. A., Osis, S., & Ferber, R. (2015). Do intermediate-and higher-order principal components contain useful information to detect subtle changes in lower extremity biomechanics during running? *Human movement science, 44*, 91-101.
- Phinyomark, A., Hettinga, B. A., Osis, S. T., & Ferber, R. (2014). Gender and age-related differences in bilateral lower extremity mechanics during treadmill running. *PloS one, 9*(8).
- Phinyomark, A., Petri, G., Ibáñez-Marcelo, E., Osis, S. T., & Ferber, R. (2018). Analysis of big data in gait biomechanics: Current trends and future directions. *Journal of medical and biological engineering, 38*(2), 244-260.
- Platt, J. (1998). Sequential minimal optimization: A fast algorithm for training support vector machines.
- Plotnik, M., Bartsch, R. P., Zeev, A., Giladi, N., & Hausdorff, J. M. (2013). Effects of walking speed on asymmetry and bilateral coordination of gait. *Gait & posture, 38*(4), 864-869.
- Pogorelc, B., Bosnić, Z., & Gams, M. (2012). Automatic recognition of gait-related health problems in the elderly using machine learning. *Multimedia Tools and Applications, 58*(2), 333-354.
- Pons, J. L. (2008). *Wearable robots: biomechatronic exoskeletons*: John Wiley & Sons.
- Poornima, S., & Pushpalatha, M. (2019). Prediction of Rainfall Using Intensified LSTM Based Recurrent Neural Network with Weighted Linear Units. *Atmosphere, 10*(11), 668.
- Potdevin, F. J., Femery, V. G., Decatoire, A., & Bosquet, L. (2007). Using effect size to quantify plantar pressure asymmetry of gait of nondisabled adults and patients with hemiparesis. *Journal of rehabilitation research and development, 44*(3), 347.

- Preatoni, E., Nodari, S., & Lopomo, N. F. (2020). Supervised Machine Learning Applied to Wearable Sensor Data Can Accurately Classify Functional Fitness Exercises Within a Continuous Workout. *Frontiers in bioengineering and biotechnology*, 8, 664.
- Preece, S. J., Kenney, L. P., Major, M. J., Dias, T., Lay, E., & Fernandes, B. T. (2011). Automatic identification of gait events using an instrumented sock. *Journal of NeuroEngineering and Rehabilitation*, 8(1), 32.
- Proud, J. K., Lai, D. T., Mudie, K. L., Carstairs, G. L., Billing, D. C., Garofolini, A., & Begg, R. K. (2020). Exoskeleton Application to Military Manual Handling Tasks. *Human Factors*, 0018720820957467.
- Punt, M., Bruijn, S. M., van Schooten, K. S., Pijnappels, M., van de Port, I. G., Wittink, H., & van Dieën, J. H. (2016). Characteristics of daily life gait in fall and non fall-prone stroke survivors and controls. *Journal of NeuroEngineering and Rehabilitation*, 13(1), 67.
- Radder, B., Kottink, A., Vaart, N. v. d., Oosting, D., Buurke, J., Nijenhuis, S., . . . Rietman, J. (2015, 11-14 Aug. 2015). *User-centred input for a wearable soft-robotic glove supporting hand function in daily life*. Paper presented at the 2015 IEEE International Conference on Rehabilitation Robotics (ICORR).
- Rajnoha, M., Burget, R., & Dutta, M. K. (2017). *Offline handwritten text recognition using support vector machines*. Paper presented at the Signal Processing and Integrated Networks (SPIN), 2017 4th International Conference on.
- Ray, P. P. (2018). A survey on Internet of Things architectures. *Journal of King Saud University-Computer and Information Sciences*, 30(3), 291-319.
- Reddy, V., Yedavalli, P., Mohanty, S., & Nakhat, U. (2018). Deep Air: Forecasting Air Pollution in Beijing, China. In.
- Rehman, R. Z. U., Del Din, S., Guan, Y., Yarnall, A. J., Shi, J. Q., & Rochester, L. (2019). Selecting clinically relevant gait characteristics for classification of early parkinson's disease: A comprehensive machine learning approach. *Scientific reports*, 9(1), 1-12.
- Ren, L., Jones, R. K., & Howard, D. (2007). Predictive modelling of human walking over a complete gait cycle. *Journal of biomechanics*, 40(7), 1567-1574.
- Reynolds, D. A. (2009). Gaussian Mixture Models. *Encyclopedia of biometrics*, 741, 659-663.
- Ricciardi, C., Amboni, M., De Santis, C., Improta, G., Volpe, G., Iuppariello, L., . . . Barone, P. (2019). Using gait analysis' parameters to classify Parkinsonism: A data mining approach. *Computer methods and programs in biomedicine*, 180, 105033.
- Riley, P. O., Paolini, G., Della Croce, U., Paylo, K. W., & Kerrigan, D. C. (2007). A kinematic and kinetic comparison of overground and treadmill walking in healthy subjects. *Gait & posture*, 26(1), 17-24.
- Ristanoski, G., Liu, W., & Bailey, J. (2013). *Time series forecasting using distribution enhanced linear regression*. Paper presented at the Pacific-Asia Conference on Knowledge Discovery and Data Mining.
- Røislien, J., Skare, Ø., Gustavsen, M., Broch, N. L., Rennie, L., & Opheim, A. (2009). Simultaneous estimation of effects of gender, age and walking speed on kinematic gait data. *Gait & posture*, 30(4), 441-445.
- Rosencher, E., & Vinter, B. (2002). *Optoelectronics*: Cambridge University Press.
- Ross, G. B., Dowling, B., Troje, N. F., Fischer, S. L., & Graham, R. B. (2020). Classifying elite from novice athletes using simulated wearable sensor data. *Frontiers in bioengineering and biotechnology*, 8.
- Rothwell, J. C. (2012). *Control of human voluntary movement*: Springer Science & Business Media.

- Rowbotham, S. K., & Blau, S. (2017). The circumstances and characteristics of fatal falls in Victoria, Australia: a descriptive study. *Australian journal of forensic sciences*, 49(4), 403-420.
- Rubenstein, L. Z. (2006). Falls in older people: epidemiology, risk factors and strategies for prevention. *Age and ageing*, 35(suppl\_2), ii37-ii41.
- Rudenko, A., Palmieri, L., Lilienthal, A. J., & Arras, K. O. (2018). *Human Motion Prediction Under Social Grouping Constraints*. Paper presented at the 2018 IEEE/RSJ International Conference on Intelligent Robots and Systems (IROS).
- Rueterbories, J., Spaich, E. G., & Andersen, O. K. (2014). Gait event detection for use in FES rehabilitation by radial and tangential foot accelerations. *Medical engineering & physics*, 36(4), 502-508.
- Rueterbories, J., Spaich, E. G., Larsen, B., & Andersen, O. K. (2010). Methods for gait event detection and analysis in ambulatory systems. *Medical engineering & physics*, 32(6), 545-552.
- Rumelhart, D. E., Hinton, G. E., & Williams, R. J. (1986). Learning representations by back-propagating errors. *Nature*, 323(6088), 533-536.
- Rupal, B. S., Rafique, S., Singla, A., Singla, E., Isaksson, M., & Virk, G. S. (2017). Lower-limb exoskeletons: Research trends and regulatory guidelines in medical and non-medical applications. *International Journal of Advanced Robotic Systems*, 14(6), 1729881417743554.
- Russell, S., & Norvig, P. (2002). Artificial intelligence: a modern approach.
- Sabatini, A. M. (2011). Estimating three-dimensional orientation of human body parts by inertial/magnetic sensing. *Sensors*, 11(2), 1489-1525.
- Sagheer, A., & Kotb, M. (2019a). Time series forecasting of petroleum production using deep LSTM recurrent networks. *Neurocomputing*, 323, 203-213.
- Sagheer, A., & Kotb, M. (2019b). Unsupervised pre-training of a Deep LStM-based Stacked Autoencoder for Multivariate time Series forecasting problems. *Scientific reports*, 9(1), 1-16.
- Salvador, R., Radua, J., Canales-Rodríguez, E. J., Solanes, A., Sarró, S., Goikolea, J. M., . . . Guerrero-Pedraza, A. (2017). Evaluation of machine learning algorithms and structural features for optimal MRI-based diagnostic prediction in psychosis. *PloS one*, 12(4), e0175683.
- Samson, M. M., Crowe, A., De Vreede, P., Dessens, J. A., Duursma, S. A., & Verhaar, H. J. (2001). Differences in gait parameters at a preferred walking speed in healthy subjects due to age, height and body weight. *Aging clinical and experimental research*, 13(1), 16-21.
- Santhiranayagam, B. K., Lai, D., Shilton, A., Begg, R., & Palaniswami, M. (2011). *Regression models for estimating gait parameters using inertial sensors*. Paper presented at the 2011 Seventh International Conference on Intelligent Sensors, Sensor Networks and Information Processing.
- Santhiranayagam, B. K., Lai, D. T., Sparrow, W. A., & Begg, R. K. (2015). A machine learning approach to estimate minimum toe clearance using inertial measurement units. *Journal of biomechanics*, 48(16), 4309-4316.
- Santurkar, S., Tsipras, D., Ilyas, A., & Madry, A. (2018). *How does batch normalization help optimization?* Paper presented at the Advances in neural information processing systems.
- Savić, A., Lontis, R., Jiang, N., Popović, M., Farina, D., Dremstrup, K., & Mrachacz-Kersting, N. (2014). Movement related cortical potentials and sensory motor rhythms during self initiated and cued movements. In *Replace, Repair, Restore, Relieve-*

- Bridging Clinical and Engineering Solutions in Neurorehabilitation* (pp. 701-707): Springer.
- Sawicki, G. S., Beck, O. N., Kang, I., & Young, A. J. (2020). The exoskeleton expansion: improving walking and running economy. *Journal of NeuroEngineering and Rehabilitation*, *17*(1), 1-9.
- Sburlea, A. I., Montesano, L., de la Cuerda, R. C., Diego, I. M. A., Miangolarra-Page, J. C., & Minguez, J. (2015). Detecting intention to walk in stroke patients from pre-movement EEG correlates. *Journal of NeuroEngineering and Rehabilitation*, *12*(1), 1-12.
- Sburlea, A. I., Montesano, L., & Minguez, J. (2015). Continuous detection of the self-initiated walking pre-movement state from EEG correlates without session-to-session recalibration. *Journal of neural engineering*, *12*(3), 036007.
- Schimpl, M., Moore, C., Lederer, C., Neuhaus, A., Sambrook, J., Danesh, J., . . . Daumer, M. (2011). Association between walking speed and age in healthy, free-living individuals using mobile accelerometry—a cross-sectional study. *PloS one*, *6*(8), e23299.
- Schmidhuber, J. (2015). Deep learning in neural networks: An overview. *Neural networks*, *61*, 85-117.
- Schmidt, R. A., Lee, T. D., Winstein, C., Wulf, G., & Zelaznik, H. N. (2018). *Motor control and learning: A behavioral emphasis: Human kinetics*.
- Schöllhorn, W., Nigg, B., Stefanyshyn, D., & Liu, W. (2002). Identification of individual walking patterns using time discrete and time continuous data sets. *Gait & posture*, *15*(2), 180-186.
- Schraudolph, N. N., Yu, J., & Günter, S. (2007). *A stochastic quasi-Newton method for online convex optimization*. Paper presented at the Artificial intelligence and statistics.
- Schuster, M., & Paliwal, K. K. (1997). Bidirectional recurrent neural networks. *IEEE transactions on Signal Processing*, *45*(11), 2673-2681.
- Severens, M., Nienhuis, B., Desain, P., & Duysens, J. (2012). *Feasibility of measuring event related desynchronization with electroencephalography during walking*. Paper presented at the 2012 Annual International Conference of the IEEE Engineering in Medicine and Biology Society.
- Shafiul Hasan, S., Siddiquee, M. R., Atri, R., Ramon, R., Marquez, J. S., & Bai, O. (2020). Prediction of gait intention from pre-movement EEG signals: a feasibility study. *Journal of NeuroEngineering and Rehabilitation*, *17*, 1-16.
- Shakeel, A., Navid, M. S., Anwar, M. N., Mazhar, S., Jochumsen, M., & Niazi, I. K. (2015). A review of techniques for detection of movement intention using movement-related cortical potentials. *Computational and mathematical methods in medicine*, 2015.
- Shamaei, K., Napolitano, P. C., & Dollar, A. M. (2013). *A quasi-passive compliant stance control knee-ankle-foot orthosis*. Paper presented at the Rehabilitation Robotics (ICORR), 2013 IEEE International Conference on.
- Sheridan, T. B. (2016). Human–robot interaction: status and challenges. *Human Factors*, *58*(4), 525-532.
- Shi, G., Zou, Y., Jin, Y., Cui, X., & Li, W. J. (2009). *Towards HMM based human motion recognition using MEMS inertial sensors*. Paper presented at the 2008 IEEE International Conference on Robotics and Biomimetics.
- Shibasaki, H., & Hallett, M. (2006). What is the Bereitschaftspotential? *Clinical Neurophysiology*, *117*(11), 2341-2356.
- Shinohara, K., & Wobbrock, J. O. (2016). Self-conscious or self-confident? A diary study conceptualizing the social accessibility of assistive technology. *ACM Transactions on Accessible Computing*, *8*(2). doi:10.1145/2827857

- Siarni-Namini, S., Tavakoli, N., & Namin, A. S. (2019). A comparative analysis of forecasting financial time series using arima, lstm, and bilstm. *arXiv preprint arXiv:1911.09512*.
- Simonsick, E. M., Guralnik, J. M., Volpato, S., Balfour, J., & Fried, L. P. (2005). Just get out the door! Importance of walking outside the home for maintaining mobility: findings from the women's health and aging study. *Journal of the American Geriatrics Society*, 53(2), 198-203.
- Sinnet, R. W., & Ames, A. D. (2012). Bio-inspired feedback control of three-dimensional humanlike bipedal robots. *Journal of Robotics and Mechatronics*, 24(4), 595.
- Siu, H. C., Shah, J. A., & Stirling, L. A. (2016). Classification of Anticipatory Signals for Grasp and Release from Surface Electromyography. *Sensors*, 16(11), 1782.
- Smith, A. J., & Lemaire, E. D. (2018). Temporal-spatial gait parameter models of very slow walking. *Gait & posture*, 61, 125-129.
- Sokolova, M., & Lapalme, G. (2009). A systematic analysis of performance measures for classification tasks. *Information processing & management*, 45(4), 427-437.
- Soutas-Little, R. W. (1998). Motion analysis and biomechanics. *J Rehabil Res Dev*, 49-68.
- Sra, S., Nowozin, S., & Wright, S. J. (2012). *Optimization for machine learning*: Mit Press.
- Srinivasan, S., Raptis, I., & Westervelt, E. R. (2008). Low-dimensional sagittal plane model of normal human walking. *Journal of biomechanical engineering*, 130(5).
- Srivastava, N., Mansimov, E., & Salakhudinov, R. (2015). *Unsupervised learning of video representations using lstms*. Paper presented at the International conference on machine learning.
- Stanula, A., Maszczyk, A., Rocznik, R., Pietraszewski, P., Ostrowski, A., Zajac, A., & Strzala, M. (2012). The development and prediction of athletic performance in freestyle swimming. *Journal of human kinetics*, 32, 97-107.
- Stepanek, M., Kus, V., & Franc, J. (2015). *Modification of Gaussian mixture models for data classification in high energy physics*. Paper presented at the J. Phys. Conf. Ser.
- Stone, T., Sarangi, V., & Pelah, A. (2019). *Application of Skeletal Pose Estimation from Video to Clinical Gait Analysis in Lower Limb Prosthetics in Comparison to Gold Standard Vicon Motion Capture*. Paper presented at the London: IET Conference on Human Motion Analysis for Healthcare Applications (accessed June 26, 219).
- Su, B., & M Gutierrez-Farewik, E. (2020). Gait Trajectory and Gait Phase Prediction Based on an LSTM Network. *Sensors*, 20(24), 7127.
- Su, M.-C., Chen, Y.-Y., Wang, K.-H., Tew, C.-Y., & Huang, H. (2000). 3D arm movement recognition using syntactic pattern recognition. *Artificial Intelligence in Engineering*, 14(2), 113-118.
- Sun, D., Fekete, G., Mei, Q., & Gu, Y. (2018). The effect of walking speed on the foot inter-segment kinematics, ground reaction forces and lower limb joint moments. *PeerJ*, 6, e5517.
- Sundaram, V. H., Hemler, S. L., Chanda, A., Haight, J. M., Redfern, M. S., & Beschoner, K. E. (2020). Worn Region Size of Shoe Outsole Impacts Human Slips: Testing a Mechanistic Model. *Journal of biomechanics*, 109797.
- Sutskever, I., Martens, J., Dahl, G., & Hinton, G. (2013). *On the importance of initialization and momentum in deep learning*. Paper presented at the International conference on machine learning.
- Sze, V., Chen, Y.-H., Emer, J., Suleiman, A., & Zhang, Z. (2017). *Hardware for machine learning: Challenges and opportunities*. Paper presented at the 2017 IEEE Custom Integrated Circuits Conference (CICC).

- Taborri, J., Rossi, S., Palermo, E., Patanè, F., & Cappa, P. (2014). A novel HMM distributed classifier for the detection of gait phases by means of a wearable inertial sensor network. *Sensors*, *14*(9), 16212-16234.
- Tahernezhad-Javazm, F., Azimirad, V., & Shoaran, M. (2018). A review and experimental study on the application of classifiers and evolutionary algorithms in EEG-based brain-machine interface systems. *Journal of neural engineering*, *15*(2), 021007.
- Tan, H. X., Aung, N. N., Tian, J., Chua, M. C. H., & Yang, Y. O. (2019). Time series classification using a modified LSTM approach from accelerometer-based data: A comparative study for gait cycle detection. *Gait & posture*, *74*, 128-134.
- Tanghe, K., De Groote, F., Lefeber, D., De Schutter, J., & Aertbeliën, E. (2019). Gait Trajectory and Event Prediction from State Estimation for Exoskeletons during Gait. *IEEE Transactions on Neural Systems and Rehabilitation Engineering*.
- Tao, W., Liu, T., Zheng, R., & Feng, H. (2012). Gait analysis using wearable sensors. *Sensors*, *12*(2), 2255-2283.
- Tao, X., & Yun, Z. (2017). Fall prediction based on biomechanics equilibrium using Kinect. *International Journal of Distributed Sensor Networks*, *13*(4), 1550147717703257.
- Taylor, S. (2012). *The effect of ageing on the control of toe clearance during walking*. Victoria University.
- Tesio, L., & Rota, V. (2019). The motion of body center of mass during walking: a review oriented to clinical applications. *Frontiers in neurology*, *10*, 999.
- Tibshirani, R. (1996). Regression shrinkage and selection via the lasso. *Journal of the Royal Statistical Society: Series B (Methodological)*, *58*(1), 267-288.
- Tibshirani, R. (2018). Statistics 315a. *Modern Applied Statistics: Elements of Statistical Learning (Winter 2018)*. Retrieved from <https://statweb.stanford.edu/~tibs/stat315a.html>
- Tinder, R. F. (2006). Relativistic flight mechanics and space travel. *Synthesis lectures on engineering*, *1*(1), 1-140.
- Tinetti, M. E., Speechley, M., & Ginter, S. F. (1988). Risk factors for falls among elderly persons living in the community. *New England journal of medicine*, *319*(26), 1701-1707.
- Tirosh, O., Cambell, A., Begg, R. K., & Sparrow, W. A. (2013). Biofeedback training effects on minimum toe clearance variability during treadmill walking. *Annals of Biomedical Engineering*, *41*(8), 1661-1669.
- Titterton, D., Weston, J. L., & Weston, J. (2004). *Strapdown inertial navigation technology* (Vol. 17): IET.
- Tobias, R. D. (1995). *An introduction to partial least squares regression*. Paper presented at the Proceedings of the twentieth annual SAS users group international conference.
- Tong, K., & Granat, M. H. (1999). A practical gait analysis system using gyroscopes. *Medical engineering & physics*, *21*(2), 87-94.
- Torrey, L., & Shavlik, J. (2010). Transfer learning. In *Handbook of research on machine learning applications and trends: algorithms, methods, and techniques* (pp. 242-264): IGI global.
- Torricelli, D., Cortés, C., Lete, N., Bertelsen Simonetti, Á., Gonzalez-Vargas, J., del-Ama, A. J., . . . Pons, J. L. (2018). A subject-specific kinematic model to predict human motion in exoskeleton-assisted gait. *Frontiers in neurorobotics*, *12*, 18.
- Trigili, E., Grazi, L., Crea, S., Accogli, A., Carpaneto, J., Micera, S., . . . Panarese, A. (2019). Detection of movement onset using EMG signals for upper-limb exoskeletons in reaching tasks. *Journal of NeuroEngineering and Rehabilitation*, *16*(1), 45.

- Tulchin, K., Orendurff, M., Adolfsen, S., & Karol, L. (2009). The effects of walking speed on multisegment foot kinematics in adults. *Journal of Applied Biomechanics*, 25(4), 377-386.
- Vallery, H., Van Asseldonk, E. H., Buss, M., & Van Der Kooij, H. (2008). Reference trajectory generation for rehabilitation robots: complementary limb motion estimation. *IEEE Transactions on Neural Systems and Rehabilitation Engineering*, 17(1), 23-30.
- Van Laerhoven, K., & Cakmakci, O. (2000). *What shall we teach our pants?* Paper presented at the Digest of Papers. Fourth International Symposium on Wearable Computers.
- Vapnik, V. (2013). *The nature of statistical learning theory*: Springer science & business media.
- Vargas-Valencia, L. S., Elias, A., Rocon, E., Bastos-Filho, T., & Frizera, A. (2016). An IMU-to-body alignment method applied to human gait analysis. *Sensors*, 16(12), 2090.
- Veneman, J. F., Kruidhof, R., Hekman, E. E., Ekkelenkamp, R., Van Asseldonk, E. H., & Van Der Kooij, H. (2007). Design and evaluation of the LOPES exoskeleton robot for interactive gait rehabilitation. *IEEE Transactions on Neural Systems and Rehabilitation Engineering*, 15(3), 379-386.
- Vermesan, O., Bahr, R., Ottella, M., Serrano, M., Karlsen, T., Wahlstrøm, T., . . . Gamba, M. T. (2020). Internet of robotic things intelligent connectivity and platforms. *Frontiers in Robotics and AI*, 7, 104.
- Vögele, A. M., Zsoldos, R. R., Krüger, B., & Licka, T. (2016). Novel Methods for Surface EMG Analysis and Exploration Based on Multi-Modal Gaussian Mixture Models. *PloS one*, 11(6), e0157239.
- Vu, H. T. T., Gomez, F., Cherelle, P., Lefeber, D., Nowé, A., & Vanderborght, B. (2018). ED-FNN: A new deep learning algorithm to detect percentage of the gait cycle for powered prostheses. *Sensors*, 18(7), 2389.
- Wahid, F., Begg, R., Lythgo, N., Hass, C. J., Halgamuge, S., & Ackland, D. C. (2016). A multiple regression approach to normalization of spatiotemporal gait features. *Journal of Applied Biomechanics*, 32(2), 128-139.
- Wang, L., & Buchanan, T. S. (2002). Prediction of joint moments using a neural network model of muscle activations from EMG signals. *IEEE Transactions on Neural Systems and Rehabilitation Engineering*, 10(1), 30-37.
- Wang, P., Low, K., & McGregor, A. (2011). *A subject-based motion generation model with adjustable walking pattern for a gait robotic trainer: NaTUre-gaits*. Paper presented at the 2011 IEEE/RSJ International Conference on Intelligent Robots and Systems.
- Wang, S., Wang, L., Meijneke, C., Van Asseldonk, E., Hoellinger, T., Cheron, G., . . . Molinari, M. (2015). Design and control of the MINDWALKER exoskeleton. *IEEE Transactions on Neural Systems and Rehabilitation Engineering*, 23(2), 277-286.
- Wang, W.-F., Lien, W.-C., Liu, C.-Y., & Yang, C.-Y. (2018). Study on tripping risks in fast walking through cadence-controlled gait analysis. *Journal of healthcare engineering*, 2018.
- Wang, X., Ma, Y., Hou, B. Y., & Lam, W.-K. (2017). Influence of gait speeds on contact forces of lower limbs. *Journal of healthcare engineering*, 2017.
- Waters, R. L., Lunsford, B. R., Perry, J., & Byrd, R. (1988). Energy-speed relationship of walking: standard tables. *Journal of Orthopaedic Research*, 6(2), 215-222.
- Webb, A., Banks, J., Phillips, C., Hudson, D., Taunton, D., & Turnock, S. (2011). Prediction of passive and active drag in swimming. *Procedia Engineering*, 13, 133-140.
- Wei, W., Wu, H., & Ma, H. (2019). An autoencoder and LSTM-based traffic flow prediction method. *Sensors*, 19(13), 2946.

- Weinhandl, J. T., Irmischer, B. S., & Sievert, Z. A. (2017). Effects of gait speed of femoroacetabular joint forces. *Applied bionics and biomechanics*, 2017.
- Westervelt, E. R., Grizzle, J. W., Chevallereau, C., Choi, J. H., & Morris, B. (2018). *Feedback control of dynamic bipedal robot locomotion*: CRC press.
- Wiering, M., & Van Otterlo, M. (2012). Reinforcement learning. *Adaptation, Learning, and Optimization*, 12.
- Wilson, A. D., & Bobick, A. F. (1999). Parametric hidden markov models for gesture recognition. *IEEE transactions on pattern analysis and machine intelligence*, 21(9), 884-900.
- Winter, D. A. (1991). *Biomechanics and motor control of human gait: normal, elderly and pathological*.
- Winter, D. A. (2009). *Biomechanics and motor control of human movement*: John Wiley & Sons.
- Witte, K., Ganter, N., Baumgart, C., & Peham, C. (2010). Applying a principal component analysis to movement coordination in sport. *Mathematical and Computer Modelling of Dynamical Systems*, 16(5), 477-488.
- Witten, I. H., Frank, E., Hall, M. A., & Pal, C. J. (2016). *Data Mining: Practical machine learning tools and techniques*: Morgan Kaufmann.
- Wolpaw, J. R., & McFarland, D. J. (2004). Control of a two-dimensional movement signal by a noninvasive brain-computer interface in humans. *Proceedings of the national academy of sciences*, 101(51), 17849-17854.
- Wolpaw, J. R., McFarland, D. J., Neat, G. W., & Forneris, C. A. (1991). An EEG-based brain-computer interface for cursor control. *Electroencephalography and clinical neurophysiology*, 78(3), 252-259.
- Wu, A. R., Simpson, C. S., van Asseldonk, E. H., van der Kooij, H., & Ijspeert, A. J. (2019). Mechanics of very slow human walking. *Scientific reports*, 9(1), 1-10.
- Wu, Y., Yuan, M., Dong, S., Lin, L., & Liu, Y. (2018). Remaining useful life estimation of engineered systems using vanilla LSTM neural networks. *Neurocomputing*, 275, 167-179.
- Xiao-wei, X. (2020). Study on the intelligent system of sports culture centers by combining machine learning with big data. *Personal and Ubiquitous Computing*, 24(1), 151-163.
- Xie, D., Zhang, L., & Bai, L. (2017). Deep learning in visual computing and signal processing. *Applied Computational Intelligence and Soft Computing*, 2017.
- Xie, J., Xu, J., Nie, C., & Nie, Q. (2015). *Prediction on Performance of Age Group Swimming Using Machine Learning*. Paper presented at the International Conference on High Performance Computing and Applications.
- Xie, J., Xu, J., Nie, C., & Nie, Q. (2017). Machine learning of swimming data via wisdom of crowd and regression analysis. *Mathematical Biosciences & Engineering*, 14(2), 511-527.
- Yamaguchi, G. T. (1990). Performing whole-body simulations of gait with 3-D, dynamic musculoskeletal models. In *Multiple Muscle Systems* (pp. 663-679): Springer.
- Yan, T., Cempini, M., Oddo, C. M., & Vitiello, N. (2015). Review of assistive strategies in powered lower-limb orthoses and exoskeletons. *Robotics and Autonomous Systems*, 64(Supplement C), 120-136. doi:<https://doi.org/10.1016/j.robot.2014.09.032>
- Yang, Y.-T., Yoshida, Y., Hortobágyi, T., & Suzuki, S. (2013). Interaction between thorax, lumbar, and pelvis movements in the transverse plane during gait at three velocities. *Journal of Applied Biomechanics*, 29(3), 261-269.
- Yoo, J.-H., Hwang, D., & Nixon, M. S. (2005). *Gender classification in human gait using support vector machine*. Paper presented at the ACIVS.

- Yoon, B.-J. (2009). Hidden Markov models and their applications in biological sequence analysis. *Current genomics*, *10*(6), 402-415.
- Yuwono, M., Su, S. W., Guo, Y., Moulton, B. D., & Nguyen, H. T. (2014). Unsupervised nonparametric method for gait analysis using a waist-worn inertial sensor. *Applied Soft Computing*, *14*, 72-80.
- Zabalza, J., Ren, J., Zheng, J., Zhao, H., Qing, C., Yang, Z., . . . Marshall, S. (2016). Novel segmented stacked autoencoder for effective dimensionality reduction and feature extraction in hyperspectral imaging. *Neurocomputing*, *185*, 1-10.
- Zajac, F. E., & Winters, J. M. (1990). Modeling musculoskeletal movement systems: joint and body segmental dynamics, musculoskeletal actuation, and neuromuscular control. In *Multiple muscle systems* (pp. 121-148): Springer.
- Zaroug, A., Lai, D. T., Mudie, K., & Begg, R. (2020). Lower Limb Kinematics Trajectory Prediction Using Long Short-Term Memory Neural Networks. *Frontiers in bioengineering and biotechnology*, *8*.
- Zaroug, A., Proud, J. K., Lai, D. T., Mudie, K., Billing, D., & Begg, R. (2019). Overview of Computational Intelligence (CI) Techniques for Powered Exoskeletons. In *Computational Intelligence in Sensor Networks* (pp. 353-383): Springer.
- Zeman, A. (2002). *Consciousness: a user's guide*: Yale University Press.
- Zeman, A. (2005). What in the world is consciousness? *Progress in brain research*, *150*, 1-10.
- Zhang, J., Fiers, P., Witte, K. A., Jackson, R. W., Poggensee, K. L., Atkeson, C. G., & Collins, S. H. (2017). Human-in-the-loop optimization of exoskeleton assistance during walking. *Science*, *356*(6344), 1280-1284.
- Zhang, M.-H., & Cheng, Q.-S. (2003). Gaussian mixture modelling to detect random walks in capital markets. *Mathematical and computer modelling*, *38*(5-6), 503-508.
- Zhang, M., Xie, S. Q., Li, X., Zhu, G., Meng, W., Huang, X., & Veale, A. J. (2017). Adaptive patient-cooperative control of a compliant ankle rehabilitation robot (CARR) with enhanced training safety. *IEEE Transactions on Industrial Electronics*, *65*(2), 1398-1407.
- Zhang, Y., & Gu, D. (2019). *A Deep Convolutional-Recurrent Neural Network for Freezing of Gait Detection in Patients with Parkinson's Disease*. Paper presented at the 2019 12th International Congress on Image and Signal Processing, BioMedical Engineering and Informatics (CISP-BMEI).
- Zhang, Y., & Ma, Y. (2019). Application of supervised machine learning algorithms in the classification of sagittal gait patterns of cerebral palsy children with spastic diplegia. *Computers in biology and medicine*, *106*, 33-39.
- Zhang, Y., Yang, Z., Lan, K., Liu, X., Zhang, Z., Li, P., . . . Pan, J. (2019). *Sleep stage classification using bidirectional lstm in wearable multi-sensor systems*. Paper presented at the IEEE INFOCOM 2019-IEEE Conference on Computer Communications Workshops (INFOCOM WKSHPS).
- Zhao, A., Qi, L., Dong, J., & Yu, H. (2018). Dual channel LSTM based multi-feature extraction in gait for diagnosis of Neurodegenerative diseases. *Knowledge-Based Systems*, *145*, 91-97.
- Zhao, C.-y., Zhang, X.-g., & Guo, Q. (2012). *The application of machine-learning on lower limb motion analysis in human exoskeleton system*. Paper presented at the International Conference on Social Robotics.
- Zhao, K., Teng, Z., Gong, N., Chen, F., & Zhao, P. (2019). *Clustering of Human Motion Trajectory for Lower Limb Rehabilitation Robot Design Based on Machine Learning*. Paper presented at the ASME International Mechanical Engineering Congress and Exposition.

- Zhou, H., & Hu, H. (2008). Human motion tracking for rehabilitation—A survey. *Biomedical Signal Processing and Control*, 3(1), 1-18.
- Zhu, F., Ye, F., Fu, Y., Liu, Q., & Shen, B. (2019). Electrocardiogram generation with a bidirectional LSTM-CNN generative adversarial network. *Scientific reports*, 9(1), 1-11.

**8 APPENDIX A**  
**(PUBLICATIONS)**

# Chapter 15

## Overview of Computational Intelligence (CI) Techniques for Powered Exoskeletons



Abdelrahman Zaroug, Jasmine K. Proud, Daniel T. H. Lai,  
Kurt Mudie, Dan Billing and Rezaul Begg

**Abstract** There is an emerging need to synchronise wearable function with user intention as many exoskeletons reported in current literature have limited capability to predict user intention. In order to achieve good synchronization, closed loop feedback is required. Overcoming these limitations necessitates an architecture composed of networked sensors and actuators with smart control algorithms to fuse sensor data and create smooth actuation. This review chapter discusses the growing need to deploy computational intelligence (CI) techniques as well as machine learning (ML) algorithms so that exoskeletons are able to predict the user intentions and consequently operate in parallel with human intention. A comprehensive review of major portable, active exoskeletons are provided for both upper and lower limbs with a focus on the need for smart algorithms integration to drive them. The application areas include rehabilitation and human performance augmentation.

**Keywords** Wearable Robotics · Exoskeletons · Computational Intelligence  
Machine Learning · Hidden Markov Model · Artificial Neural Networks  
Gaussian Mixture Model · Support Vector Machines

### 15.1 Introduction

Robots were designed to assist humans to complete repetitive or monotonous tasks, such as part assembly in factories. However, currently robots are moving toward

---

A. Zaroug (✉) · J. K. Proud · D. T. H. Lai · K. Mudie · R. Begg  
Institute of Sport, Exercise and Active Living (ISEAL), Victoria University,  
Melbourne, Australia  
e-mail: Abdelrahman.Zaroug@live.vu.edu.au

D. T. H. Lai  
College of Engineering and Science, Victoria University,  
Melbourne, Australia

D. Billing  
Defence Science and Technology Group, Melbourne, Australia

© Springer-Verlag GmbH Germany, part of Springer Nature 2019  
B. B. Mishra et al. (eds.), *Computational Intelligence in Sensor  
Networks*, Studies in Computational Intelligence 776,  
[https://doi.org/10.1007/978-3-662-57277-1\\_15](https://doi.org/10.1007/978-3-662-57277-1_15)

richer interaction with human operators. Instead of solely exchanging commands to/from the user, they are now becoming an extension of the human body, interacting through physical movement, sensory feedback and determining user intention. This has given rise to the term wearable robotics or robots worn by human operators. According to Carpino et al. [1], wearable robotics are a type of mechatronic system that are designed to assist the human body for either performance augmentation or for rehabilitation and assistance of physically challenged persons. Wearable technologies, i.e. smart watches, fitness trackers, health monitors, are becoming prolific in today's society and thus their purpose has moved away from the purely functional into a form of self-expression. This induces a heightened social awareness of wearable technologies and their purpose [2]. Poor form design can have an adverse effect on social inclusion, perception of ability and a user's self-confidence. Wearables design needs to balance form and function equally as assistive devices used outside of rehabilitation design show decreasing frequency of use due to physical and psychological discomfort of the users [3].

Wearable robotics can be grouped into three main categories; orthoses, prostheses and exoskeletons [4]. Orthoses, as well as exoskeletons, are defined as mechanical devices that are outfitted by a user, mimics the joints/limbs motion and is anthropomorphic in nature [5]. On the other hand, exoskeletons are used to describe devices used by an able-bodied wearer [6], and occasionally when they span multiple joints, for rehabilitation purposes [5]. Orthoses are devices designed for individuals with limb pathology [5, 6]. Finally, prostheses are artificial limbs predominantly designed for amputees and the device replaces the lost limb/joint function.

There is an emerging need to synchronize wearable function with user intention. In order to achieve good synchronization, closed loop feedback will be required. This will necessitate an architecture composed of networked sensors and actuators, i.e. Wireless Sensor Networks (WSN) [7]. In addition, smart control algorithms will be required to fuse sensor data and create smooth actuation [8]. Machine learning helps in categorising large datasets by observing their regularities and recognising their patterns. This class of algorithms would be integral to future wearable robotic designs.

Within the last decade several review papers in the literature have addressed exoskeleton research [1, 5, 6, 9] and established the need for this technology. This review chapter discusses the state-of-the-art portable, active exoskeletons for both upper and lower limbs of the human body with a focus on the need for smart algorithms to drive them. Active systems use computational techniques for user control, safety parameters and task orientated function. The application areas of these exoskeletons include rehabilitation and human performance augmentation. The literature in lower limb devices tends to be more abundant, than its upper limb counterpart due to it addressing the rudimentary task of walking assistance [9], having less degrees of freedom and greater real estate from the addition of exoskeleton components.

## 15.2 Exoskeletons Background

Research in human exoskeletons began in the late 1960s [5], and the first to be designed was the Nicholas Yagn lower limb exoskeleton [10]. This was designed in parallel to the lower limbs to augment running, though it was not manufactured or effectively demonstrated. From an operational perspective, exoskeletons as well as active orthoses act either in series or in parallel [11] to the human body. The former is meant to add length and displacement to the body, however, the latter is to support the limb by offering strength as well as endurance [6].

With regard to operational energy, exoskeletons can be sub-classified into active [12], passive [13, 14] and quasi-passive devices [15, 16]. Active devices are essentially devices that include an actuator, controller and a battery. Passive devices however, are exactly the opposite. They deliver assistance through the addition of power, provision of support or the transfer of loading, using energy conservation elements such as springs and dampers. Finally, quasi-passive devices are a hybrid between the active and passive mechanisms in such a way that the passive elements are used to store and release energy while the active elements are used to control the timing (when to release energy) as well as the quantity of released energy.

An active exoskeleton is an external, typically anthropomorphic, structure that provides supported or augmented movement to the wearer through a mechatronic system [17]. The creation of mechanical power is achieved through the use of actuators, creating movement that can at times be greater than what is biomimetically possible by the user. Due to this many exoskeletons have been developed for human performance augmentation, such as carrying heavy loads, improving endurance, reducing fatigue and performing repetitive tasks. The potential benefit of an anthropomorphic exoskeleton is a small footprint and unrestricted movement. However, exoskeletons do not yet work synergistically enough with the musculoskeletal system for human kinematics and kinetics to allow natural motion. The main challenge for the adoption of exoskeletons in industry is caused by issues such as discomfort, device weight, musculoskeletal alignment and kinematics and detection of human intention.

The majority of current active upper limb exoskeletons use electric motors with some using pneumatic actuation. Hydraulic and other actuation methods are rarely used for upper limb exoskeletons. The development of upper limb exoskeletons has been mainly for; power assist, movement of limbs for people with limited function, rehabilitation or assistive living; augmentation, amplifying the current capabilities of the human body or lifting external loads; and providing additional support to workers through postural controls or additional limb strength/control. Commonly used power transmission methods are gear and cable drives [17]. As for the lower limb exoskeletons, pneumatic, hydraulic, and electric motors have all been reported in the literature. However, currently electric motors are widely used in both rehabilitation as well as to enhance human performance, as they feature simpler design features and can adopt complex control methods.

The upper limb category includes exoskeletons that augment the hand, wrist, elbow and/or shoulder [17], while the lower limb encompasses the major joints; hips, knees and ankles.

### 15.2.1 Exoskeleton Structure

The degrees of freedom (DOF) of an exoskeleton are determined by the number of articulated joints in the structure. The human body has 244 DOF [18], a highly complex system to be accommodated in an exoskeleton. Designers aim to minimise complexity while still maintaining normal motion, this can be done through removing DOF, supporting a discrete segment of the movement cycle or under-actuating the system.

A balance needs to be found between the weight and size of the system, its reaction speed and force transmission. Traditional actuators such as electric motors, pneumatics and hydraulics still face major issues in terms of form factor, power-to-weight and control. The human body has multiple DOF for each of its joints and the addition of an external structure to the body can hinder or distort normal movement. Exoskeleton actuation systems fall into 4 categories: electric, hydraulic, pneumatic and other. While power transmission can occur through gears, cables, belt drives or rigid linkages [17].

A rigid frame requires precise alignment to the human joints, these being numerous, it can cause the system to become bulky. However, rigid-link systems allow for easy control and force transmission. A soft frame combats this issue but may cause undesired motion through the joints via unintended deformation in the frame or poor human-mechanical coupling, leading to inefficient force transmission. Cable driven systems are commonly used due to the space constraints and the ability to separate the actuator from the end effector. A Bowden cable is a flexible cable consisting of a plastic outer shell, an incompressible steel structure, a friction reducing inner lining and the inner cable. It is used as a push/pull mechanism for linear force transmission. The use of this type of force transmission reduces the weight of the system on the affected limb and allows the design to be scalable [19]. However, Bowden cables show significantly low efficiency in power transmission due to unstable friction between the inner and outer sheaths and positional accuracy loss [20, 21].

Issues arise with the ability to provide large forces through electrical actuators required to sustain and assist the motor movements of the wearer. Movement between joints have large velocity and acceleration peaks that can only be mimicked using powerful actuators, which are large and heavy thus using them would then hinder the movement due to reduced space between joints. Small, lightweight motors can only create sufficient forces through the addition of gearing systems which then add frictional forces to the creation of movement and impede performance. Electric motors require a secondary system of gears, belts or cables in order to transfer power and can induce additional complexity through low efficiency and joint misalignment.

Pneumatic Artificial Muscles (PAMs) show desirable characteristics such as a high power-to-weight ratio, linear contraction and flexibility in wearable applications. Their motion differs from air cylinders, where it simultaneously contracts its length as the soft chamber dilates [22]. Soft exoskeletons appear to be promising for use in wearable robotics due to their low cost, easy manufacturability and inherent biosafety. Soft exoskeleton actuation mechanisms use pneumatic or hydraulic systems to create limb forces.

Hydraulic and pneumatic actuators are limited to single plane motion, they require additional maintenance to other forms of actuation and require large pressure pumps. However, they provide benefits in terms of high power density and easy power transfer. Hydraulic systems suffer from low force generation due to the lack of rigid structure to transfer force to the distal joints.

### ***15.2.2 Exoskeletons Evaluation***

Testing of device affects on the wearer is within 3 categories: physiological parameters, biomechanical parameters, and wearability [23, 24]. Physiological tests measure the variation in baseline performance of human function whilst using the exoskeleton. Commonly performed physiological tests are muscle activity, muscle fatigue and oxygen consumption.

Muscle activity testing is performed via electromyography (EMG). EMG measures the electrical activity that causes skeletal muscle activation via electrodes placed on the skin. While testing of an upper limb exoskeleton may show a decrease in arm muscle activity, the external forces placed on the body by the addition of the device could cause an increase in muscle activity in a different part of the body and change the movement pattern of the wearer. This is due to the necessity for the weight of the exoskeleton to be deflected away from the user by transferring the force into the ground. Muscle fatigue however is subjective and measured against the users variation in stamina with and without the robotic intervention, while oxygen consumption is a more definitive test that compares the amount of oxygen consumed and carbon dioxide expelled to that of the users baseline.

Biomechanical testing involves measuring force loading, joint torque, compression and shear forces experienced by the user. This quantitative analysis shows the distribution of forces on the body caused by the exoskeleton and external loading. Similar dynamic mechanical tests can be used to analyse the performance of the exoskeletons function. Function tests include range of motion, static holding and dynamic lifting. All of the tested protocols are vital to understanding how the exoskeleton functions and affects the human wearer when performing movement, however for device uptake to be successful the major consideration for exoskeletons is wearability (user comfort).

In Radder et al. [3], there were key factors users identified as leading to consistent use of a device. It must be comfortable (compact, lightweight, portable), quickly initialized (donning, doffing, powering up) and only provide assistance-as-needed. Some other features were identified: the device needed to be hygienic and therefore washable [25], able to be submerged in water, battery life should last for a day of intermittent use, and provide modular support [3]. Feedback in the form of task performance was also important to users while health care professionals were also interested in force generation and joint kinematics [3].

## 15.3 Exoskeletons for Human Performance Augmentation

Over 40% of workers in the European Union suffer musculoskeletal disorders such as lower back, neck or shoulder pain annually, caused by physical work loads and repetitive movements [23]. The occurrence of reduced capacity, injury or disability in the workforce has led to research into technological interventions for prevention. Alongside mechanical processes and robotic automation, exoskeletons are now being explored for use in human performance augmentation in industrial, agricultural and military applications.

Robotic intervention is used for repetitive tasks that lead to user fatigue and allow users to remain in the work process for extended periods without suffering debilitating physical effects. The development of industrial exoskeletons is due to a humans ability to make fast adaptable decisions based on observation and where full automation via robotic intervention of these tasks is either prohibitively expensive or not possible. These exoskeletons are designed to support posture, hold, carry and support loads and perform dynamic lifting [23].

### 15.3.1 Upper Limb Devices

While the development of upper limb exoskeletons has been ongoing for many years and many exist in the current research spectrum, this area of technology has developed slowly and very few are available for use by the general population. The problem is that many of these devices have restricted portability because of their size, weight and poor mobility.

The majority of current upper limb exoskeletons use electric motors with some using pneumatic actuation. Hydraulic and other actuation methods are rarely used for upper limb exoskeletons. These exoskeletons are used for power assist, augmentation or lifting external loads. Commonly used power transmission methods are gear and cable drives [17].

Upper limb exoskeletons were originally developed to assist military personnel in improving endurance through assistance in heavy load carrying. These have now been developed with the purpose of assisting in the performance of specific tasks for workers in agriculture, manufacture and construction such as stooped work, load carrying and overhead work.

The Toyota Technological Institute Exoskeleton (TTI-Exo) is a multipurpose exoskeleton for power assistance [26]. It is a full body system with the upper limb section having 2 active DOF in shoulder and elbow flexion/extension and 1 passive DOF in shoulder rotation. Actuation is provided by harmonic drive brushless servo motors with integrated encoders. An encoder only, sensorless control approach using disturbance observer modules to estimate user-applied and task specific force variations is implemented. The use of this model means that robot dynamics and joint friction that can cause additional disturbances must be compensated for via

model-based dynamic and friction compensation algorithms. The suit was tested by 5 participants in laboratory experiments for power assistance and rehabilitation collecting EMG data. A reduction in muscle activity of up to 85% was observed when using the exoskeleton.

Ikerlans Orthosis (IKO) is a 5 DOF exoskeleton supporting shoulder, elbow and forearm motion for force amplification in the workplace with an additional 4 passive DOF to allow for movement of the structure around the body [27]. The upper limb is remotely actuated using a combination of electrical motors with Bowden cables and artificial muscles. For dynamics and control capability testing a 2 DOF section model was created for elbow flexion/extension and rotation. Position control is via a non-linear enhanced proportionalintegralderivative (PID) controller. Experimental results indicated that desired smooth motion is achieved with no variation when under load. The exoskeleton is capable of supporting 10kg loads.

Agrirobot is an exoskeleton to assist with agricultural harvesting of produce and load carrying [28]. It contains 10 DOF in a full body symmetrical suit, actively actuating using DC motors, at the joint, the shoulder, elbow, hip, knee and passively actuating the ankle. Agrirobot has multiple function modes that can be selected via voice command. There is an automatic movement pattern mode that functions for harvesting root crops and vine fruit, and a user controlled mode that follows a system of sensors to determine user intention. Encoders and gyroscopes detect joint positions while hall and pressure sensors detect user movements. The exoskeleton was tested for various harvesting situations by a single subject. The exoskeleton was able to adapt to these movements but created mobility restrictions in the back and shoulder due to the limited DOF.

### ***15.3.2 Lower Limb Devices***

BLEEX is a 7 DOF exoskeleton [1, 6, 9], 4 of which are active, those being hip flexion/extension, abduction/adduction and knee and ankle flexion/extension, the other 3 DOF are hip and ankle rotation and ankle inversion/eversion. It has been designed for military application load carrying and is capable of supporting 75 kg. Actuation is provided via bidirectional linear hydraulic cylinders. Control information is gathered from the exoskeleton rather than the user. The 8 actuated joints contain 8 encoders and 16 linear accelerometers to determine their angular acceleration and velocity. Additionally, it contains: single-axis force sensors at each actuator for force control, and an inclinometer for backpack orientation. A sensitivity amplification control strategy is used which changes the inverse dynamics in the sagittal plane depending on the gait phase, which is determined by the foot switches and load distribution sensors, that are for measuring ground contact and force distribution.

The Hybrid Assistive Leg (HAL), manufactured by Cyberdyne in Japan is the most investigated exoskeleton in the literature [29–34]. Different types of HAL have been

developed, single-leg, to full lower-limbs and also a full body exoskeleton. Hence, it is designed for healthy population to upgrade human capabilities, and also for individuals with impaired limbs. HAL 5 is a full body exoskeleton for performance augmentation and rehabilitation [1, 6]. It utilises direct drive at each of the joints with DC motors containing harmonic drives. The control system is made up of a number of sensory components; skin-surface EMG electrodes are placed at the posterior and anterior femur to detect user walking intent; potentiometers measure joint angles; gyroscopes, accelerometers, and ground reaction force sensors determine postural information. All of these sensors work together to determine user intent and control suit movement. It has been reported that HAL 5 increases the user's ability to lift loads by up to 40 kg and can almost double their leg press ability. There are few peer reviewed results of this system and there is a lengthy calibration process for each specific user.

The MIT exoskeleton uses a quasi-passive actuation system for backpack load carrying by transferring the load through a rigid link system to the ground [1, 5, 9, 35]. It provides augmentation at the hip, knee and ankle alongside a support system for load carrying on the back. Joint augmentation is provided via controlled release of springs with variable dampers during the negative power phase of each joint movement. Control strategies are determined by walking gait patterns. The walking gait phase that the user is positioned in is determined by a sensing system for joint angles, joint torques and ground reaction forces. Experimentation has shown that the exoskeleton is capable of transferring up to 90% of the carried load into the ground but indicated a 10% rise in metabolic cost when using it.

Finally, the K-SRD (Lockheed Martin) is an active lower extremity device that is computer controlled based on kinetic and kinematic user data. It has been designed to reduce user fatigue as well as stress on the lower back and legs during repetitive tasks that potentially involves lifting, pushing/pulling heavy loads, squatting, and walking over long distances through up or downhill with or without carrying loads. It has been reported [36], that the exoskeleton can potentially assist dismounted troops by reducing effort during physical tasks.

Lower limb devices are further along in their development with devices such as HAL-5 [34] available for workplace testing and components of it commercially available. Whereas the upper limb counterparts are still in research, development and prototyping. With all devices, there is minimal user validation testing reported. This could be due to a lack of testing standards around user validation protocols for exoskeletons [24]. The development of testing standards will allow for a clearer evaluation of exoskeletons function capabilities; especially the impact of the device on the human user.

Even with minimal user validation consistent challenges are apparent. Those being the limitation of movement and user discomfort due to poor form fitting and large weight of devices; and the value proposition of exoskeletons for multiple task cases of a single user, thus creating overly complicated systems. A narrow use-case (constrain activities of the human) may allow improved customisation and thereby a greater value proposition.

## 15.4 Exoskeletons for Rehabilitation and Assistance

The field of rehabilitation technology includes a wide breadth of research based interventions to treat the many issues that arise after accident or illness. Limb function is most commonly affected by stroke and as of 2009 there were 375,800 stroke survivors living in Australia with over a third of stroke victims (131,100) having difficulty gripping or holding objects [37]. As of 2009 there were 75,000 carers providing at home assistance for people with stroke and disability [37], many of these people receiving care would gain independence with the assistance of a mechatronic intervention. Additional causes of paralysis include traumatic injury to the spine, brain and motor neurons as well as neurological diseases [38].

With improvements in technology, the need for mechatronic interventions is increasing [37], with the purpose of improving quality of life, providing independence and restoring limb function to the user. However, developers of such devices have faced challenges due to problematic interaction between mechatronic devices and human users [39]. This is mainly due to biomechanical, mechanical and psychological factors [3]. For desired interaction to be possible, exoskeleton complexity needs to be reduced. Exoskeleton complexity is determined by the selection of the degrees of freedom for the joints and their arrangement, type of sensors and actuators used and the link lengths. Simplifying the exoskeleton to the requirements of the user can assure easier interaction.

### 15.4.1 Upper Limb Devices

Robotic assistance is used for repetitive tasks that lead to user fatigue and allow users to remain in the work process for extended periods without suffering physical effects. Robotic interventions for rehabilitation can reduce costs and increase the speed of recovery in some instances, through highly accurate and repeatable fine motor movements specific to the users requirements [40].

While many devices provide rehabilitation treatment, another important use is in-home assistance for activities of daily living (ADL). In Australia, 29.3% of people living with disability primarily having physical limitations with 42% experiencing physical impairments [41]. Physical disability is the 3rd largest primary disability group, after intellectual and psychiatric disabilities, and the number of people with limited physical function is increasing annually [41]. There are numerous causes of limb function loss, the foremost being stroke, spinal cord injury, head injury and multiple sclerosis. In stroke survivors hand function is most commonly affected. With the average person performing 1500 grasping tasks per day, stroke can severely affect independence and quality of life. More than 70% of patients post stroke require long term medical assistance and about 50% live with permanent impairment [42], however robot aided rehabilitation of the distal joints has been shown to improve the whole arm function [21].

Nycz et al. [21] has created a 4 DOF remotely actuated exoskeleton for finger flexion/extension with the purpose of assisting stroke survivors with grasping tasks and improve distal hand function. The systems actuation is due to linear force transmitted via Bowden cable to a spring sliding mechanism attached to the fingers. Closed loop position control via a hysteresis controller is used to compensate for positional hysteresis due to bending of the Bowden cable during actuation. While the positional control reduced the deviation in deflection at the fingertips it still showed an undesired difference in the corresponding positional change.

The Dinh et al. [43] soft arm exoskeleton, has been created for movement assistance of the elbow joint for flexion/extension. The system is comprised of a DC motor and Bowden cable force transmission. Joint position is monitored via flex sensors while cable tension is measured via load cells. The exoskeleton uses a 3 level hierarchical cascade control. The first level consists of active impedance control estimating the user's motion intention; the mid level controller compensates for positional deviation due to the Bowden cable slack and sets the actuator position according to arm position; the low level controls drive the actuators while compensating for the nonlinearity of the cables and provide the desired joint torque. The exoskeleton was tested on 3 subjects performing standardised range of motion (ROM) exercises under load to determine the accuracy, quality of movement and comparison of muscle activity via EMG. The controller was successful in providing the desired motion to the user and reducing muscle activity.

Mohammadi et al. [44] have developed a 3 DOF rehabilitation exoskeleton for physical upper limb limitations caused by spinal cord injury. It provides active flexion/extension of the elbow and wrist via geared DC motors and rigid links while allowing passive rotation of the forearm. The closed loop control system consists of sensor driven force signals and motion trigger commands supplied by the user. When the user resists the motion of the exoskeleton, motor velocity is reduced and once the velocity is below a set threshold the motor is stopped. The principle of this control method is to regulate the robots position by controlling the velocity of its links. Testing of 1 subject showed that the exoskeleton followed the desired trajectory of the user with a tracking error of less than 7% in terms of root-mean-square error index.

Robotic Upper Extremity Repetitive Trainer (RUPERT IV) is a 5 DOF exoskeleton for full arm therapy and rehabilitation [45]. It uses pneumatic muscle actuators to provide shoulder, elbow and wrist extension, forearm and humeral rotation. There are multiple control systems within this unit, an inner loop that works at the individual joint level and contains a PID feedback controller. Within 3 of the joints there is the addition of an iterative learning controller (ILC), in parallel with the PID controller. Due to the repetitive nature of the tasks, the use of the ILC improves the quality of movement by measuring errors and updating the control command. The outer loop that works at the functional task level, contains an open loop trajectory planning module to provide a smooth command signal to the inner loop. The exoskeleton was tested on 2 subjects and results showed that the control system was able to adapt and improve the quality of movement within a couple of trials.

### 15.4.2 Lower Limb Devices

These exoskeleton devices are intended to assist patients with weak limbs, mostly due to neurological disorders, such as stroke, paraplegia, hemiplegia, Cerebral Palsy and so forth, to walk again. These exoskeleton devices are strapped to the lower limbs and actuated using electrical actuators, controlled (e.g. on-board computer) with the aid of feedback sensors (e.g. encoders). Therefore, unlike treadmill-based rehabilitation robots in [46, 47], they require active engagement from the operator by perpetuating the torso balance using crutches and navigating through various surfaces. Few of them have been commercialised such as the ReWalk (Argo Medical Technologies, Israel), Ekso (Ekso Bionics, USA), and the Indego (Parker Hannifin, USA) rehabilitation exoskeletons.

The H2 is a 6 DOF robotic exoskeleton [48], designed for stroke survivors. It applies impedance control which uses force field control to direct the patient's walking trajectories through three actuated joints in each leg (hips, knees and ankles). Hence, the ankle drives prevent foot drop for paraplegic patients. It was designed for patients 1.50–1.95 m in height and up to 100 kg body weight. The 12 kg aluminium mechanical structure allows movements in the sagittal plane along with 20° in the frontal plane to allow turning through the hip joint. Brushless 100 W DC motors coupled with a harmonic drive are implemented at each joint. The research in [48], reports that this exoskeleton has been tested on small number of patients and requires personalised training for each users needs.

ReWalk is another wearable robotic exoskeleton for stroke survivors [49]. Manufactured by Argo Medical Technologies, it was the first to receive FDA (Food and Drug Administration) approval in the US to be used at home and in the community. Unlike the H2, the ReWalk exoskeleton is only actuated at the hips as well as the knees with a DC motors. For the control, users have to balance the trunk which consists of a tilt sensor that produces a pre-set hip and knee angle displacement, which eventually generates a step. A wireless pad controller is on the wrist for transition command control (e.g. sit-stand-sit transfers), and crutches must be used for balancing effect.

The Hybrid Assistive Leg (HAL) for rehabilitation purposes, relies on two types of control; a voluntary control system which uses bioelectrical signals, and a robotic autonomous control system that produces motor patterns according to the user's motion [29]. For the sensory feedback system, it utilises skin surface EMGs below the hips and above the knees on both the anterior as well as the posterior sides for bioelectrical signal detection.

For posture estimation, it utilises potentiometers, accelerometers, and gyroscopes, all mounted on the backpack. In [32], HAL was used to assist the knee flexion of hemiplegic patients whom EMG signals can still be detected at the knee flexor. Hinged from a model based control which calculates the knee flexion torque based on a compensating torque for gravity (static lower limb model), viscous torque, and finally the assistive torque for the knee joint. The exoskeleton was able to detect the user intention in the right knee of a 60 year old male participant. The study found

that HAL was able to reduce muscular activity, and it actively overcame the limiting motor functions caused by paralysis.

Produced by Parker Hannifin is the Indego exoskeleton, which was initially designed in Vanderbilt University for paraplegic patients [50]. The design features simplicity as the modular design facilitates portability, and compared to ReWalk and Ekso, there are no straps around the shoulders, which allows the patient to sit in a wheelchair while wearing the exoskeleton. With the aid of Functional Electrical Stimulation (FES) as a means to stimulate muscle activity, Indego uses a joint level controller which works in either Proportional Derivative (PD) mode or impedance control mode. Higher level control consists of a state machine that governs each individual controller and in turn allows changing between modes. Switching between each finite state is governed by the Centre of Pressure (CoP) relative to the forward heel, and that essentially allows transition between movements such as sit-to-stand or stand-to-sit.

REX exoskeleton by REX Bionics is another rehabilitation device for patients with mobility impairments as well as severe disabilities. Without the use of crutches, the device is designed to assist in overground walking, sit-to-stand and stair ascending. With the aid of linear actuators, the device is manually controlled using a joystick thus the system has no sensors to estimate user intention [1].

Finally, Wandercraft is an exoskeleton to assist paraplegic patients to walk again using 12 actuators. It is very similar to REX in terms of stability requirement, as paraplegic users are not required to use crutches. The study in [51], implemented the device in validating a stabilising controller inspired from bipedal robots using a decentralised controller. As the device has been recently released, there are few reviews on its actuators or controller types.

Similarly to human augmentation exoskeletons, lower limb device development exceeds that of upper limb devices. Commercially available upper limb exoskeletons are large, bulky, fixed devices used in musculoskeletal and neurological rehabilitation within hospitals and rehabilitation centres. The challenges faced in creating portable upper limb devices are the complexity of the tasks performed and the joint DOF. Whereas, the lower limb walking assist exoskeletons reviewed in this paper are more commonly available and used in medical and rehabilitation centres than upper limb devices. This enhanced level of development could be due to the narrow use case of these devices ie. They perform a single task, the walking gait, which is a consistent cyclical movement pattern. Narrowing the use case of a device leads to a less complex system and allows for more efficient and effective control strategies to be implemented.

## **15.5 Computational Intelligence (CI) and Machine Learning (ML) Frameworks and Applications**

Earlier successfully demonstrated exoskeletons [35, 48, 49, 52] have nonetheless experienced some limitations including; the lack of user intention prediction as well as the mandatory use of crutches for stability and direction [51]. Overcoming these

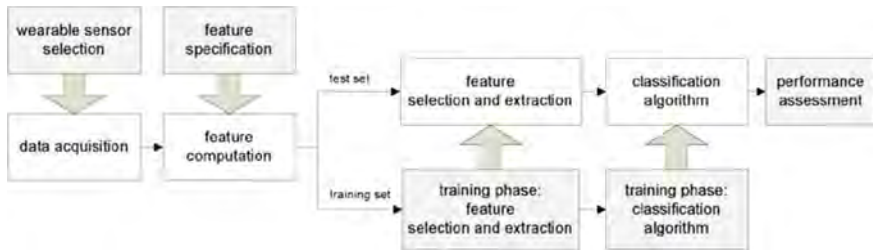


**Fig. 15.1** Computational Intelligence generic frameworks for user intention detection [60]

limitations requires smarter control algorithms. Hence, there is a growing need to deploy CI techniques as well as ML algorithms so that exoskeletons are able to predict the user intentions and consequently operate in line with human intention. CI techniques are a group of modelling methods that rely on a computer-based intelligent system. While ML algorithms are very similar, however they are data-driven and rather rely on pattern recognition [53].

The literature in lower limb devices research tends to be more abundant, as they tackle walking for most works, which is a rudimentary physical task [9]. Furthermore, lower limb devices are easier to design compared to its upper limb counterpart. Therefore, CI as well as ML implementations in lower limb exoskeletons tend to be more focused, especially in detection and prediction of walking gait phases. There are two main motives behind gait event detection which are; to study human patterns to evaluate walking after rehabilitation [54, 55], and to be used in therapeutic as well as assistive devices including; FES [56, 57], active orthosis [5], prosthesis [58], and exoskeletons [59]. Figure 15.1 depicts the workflow of a generic scheme meant to detect user intention. In the following sub-sections, detailed illustration of each component (e.g. wearable sensor selection, features extraction, etc.) will be discussed and their implementation into exoskeletons will be reviewed.

### 15.5.1 Wearable Sensor Selection

Without gait phase information, the exoskeleton will not be able to support the lower limbs accurately so that gait trajectories are calculated precisely and gait execution is generated correctly [59]. Kinematic data which are the movements caused by forces as well as kinetic data which are the forces that cause movements, are the most common data types used in the literature for gait detection [61]. This data offers a great deal of biomechanical information [61].

The choice of sensors used to measure the biomechanical data is a crucial element in gait events detection [60] and it varies according to the collection purpose. For example, the use of motion capture systems with force platforms is considered the benchmark and has been widely used in literature [62, 63] for experimental purposes

as well as for offline gait detection studies. However, the sensors are costly and are not suitable for outdoor use [54]. Therefore, for use in outdoor environments and for online gait detection, wearable sensors offers the best choice [64, 65]. Owing to the fact that they are light weight, non-invasive and can easily be attached to the body without altering the users normal locomotion [60].

The most used wearable sensors [66] for gait detection include gyroscopes [58, 67], accelerometers [68], Inertial Measurements Units (IMUs) [69], Force Sensitive Resistors (FSRs) [67], wireless pressure shoe insoles [70], encoders [54], and the electroencephalogram (EEG) as well as electromyography (EMG) [71, 72]. EMG measures the muscles electrical response to nerve stimulation and has been used as a method of exoskeleton control. Surface EMG uses electrodes placed on the skin and has the benefit of being non-invasive. Several works in the literature have considered the detection of muscles electric signals, called EMG signals, as a mean for the exoskeleton to comprehend human intentions, such as in Hybrid Assistive Limb (HAL) exoskeleton [73], and the NEUROExos [74]. In [75], a lower limb exoskeleton is developed with the use of EMG signals which are calibrated using pose sensors (Hall sensors, accelerometers, and floor contact sensors). Results have shown the possibility of measuring one muscle to represent a group of neighbouring muscles, however, this method was only successful at a specific joint motion and therefore further research is needed to see whether this works in other motions. Moreover, the device was only tested on healthy user, not the devices intended target user, hence, further investigation is needed. Conversely, in [76], with the aid of EMGs and other intelligent computational algorithms, the knee exoskeleton was able to predict human motor intent in real-time. The EMG signal was treated as a harmonic oscillator using the energy kernel method [77].

EMGs are very sensitive to electrode placement, noise from neighbouring muscles and the influence of human sweat. Hence, they are deemed unreliable for prolonged use, as they require calibration for inter-subject variability in rehabilitative devices [78]. Problems arise in its use for intended hand movement detection as the slender muscles controlling the individual finger overlap those of the arm [79] and precise electrode placement is needed. Whereas systems such as brain-computer interface perform better at capturing intended user movement.

Brain-Computer Interface (BCI) is a method of creating a pathway to communicate directly from the brain to a computer. Non-invasive BCI uses EEG to detect electrical activity in the brain via the placement of electrodes on the scalp. It allows the activation of an assistive device even when full limb paralysis is present. Non-invasive EEG BCI requires a number of electrodes to be worn on a tight-fitting cap with user specific programming and user training. This method requires substantial initialisation time and potentially could cause the user social discomfort. The reliability of these signals for lower limb exoskeleton is still being researched, such as in [72, 80], as the mobility sources are difficult to record from the brain cortex [81]. Hence, a new trend is to merge both EMG and EGG signals to enhance the detection accuracy of human intention as in [78].

Among all of the aforementioned sensors, IMU sensors offer the best choice for measuring position as they are multidimensional, non-invasive sensors and immune

to interference [60]. Moreover, they do not require external sources (e.g. electromagnetic signal) which could easily restrict their sensing range compared to optical tracking systems, electromagnetic transmitters, audio trackers and so forth [82]. They are commonly composed of three dimensional sub-sensors, including accelerometers and gyroscopes. Therefore, their main function falls into position and orientation tracking of the bodies onto which they are fixed. Nonetheless, they still lack accuracy at a large scale compared to inertial navigation systems (INSs) [83]. When implementing in exoskeletons, IMUs were found to be quickly initialised and practical [84, 85].

The latest developments in the area of micro-electro-mechanical systems (MEMs) has made IMUs more miniaturised and low in both cost as well as power consumption. As magnetic sensors have been integrated into IMUs, the entire earth offers abundant external magnetic source for their operation. The combination of magnetic and IMU sensors has shown a viable solution in studies that require three-dimensional position tracking such as in gait analysis and clinical studies. This is done by integrating the gyroscopic signal from a known starting point given by magnetometers and accelerometers. However, this results in an unbounded error which grows over time, due to low-frequency gyro bias drifts [82], which can be addressed using the Kalman Filter (KF). The KF is an optimal estimation algorithm used to extract measurements of what cannot be measured from what can be measured. It is an effective tool for multisensory fusion as well as filtering based on recursive Bayesian state estimation (Markov process). The Global Kalman Filter (GKF), helps in measuring all modules assuming they are related with each other [86], and therefore it ameliorates the accuracy of a multi-body systems such as in exoskeletons.

Classifying the data is a means of recognising the gait type (e.g. running vs. cycling) and the different combination of gait events taking place within that particular type. Generally, classifying focuses on processing the acquired data from the aforementioned sensors. The processing can be classified into two major categories; classification using machine learning which relies on pattern recognition as well as past events or experience from large sensor datasets, such as in [54, 67, 87], and algorithms that classify gait events using other methods, such as in [65, 68, 70].

### ***15.5.2 Machine Learning***

Gait data representation tends to be enormous in size and variability which may be tedious to understand and categorise. Machine learning helps in categorising large datasets by observing their regularities and recognising their patterns. This can be done through a number of machine learning algorithms which learn from past and present events and then adapt to the environment, regardless of human interventions [88]. Each of those algorithms have a different method of learning and classification such as Support Vector Machines (SVM) [62], decision trees, linear regression and neural nets [89]. Figure 15.2 shows the design process of typical machine learning.

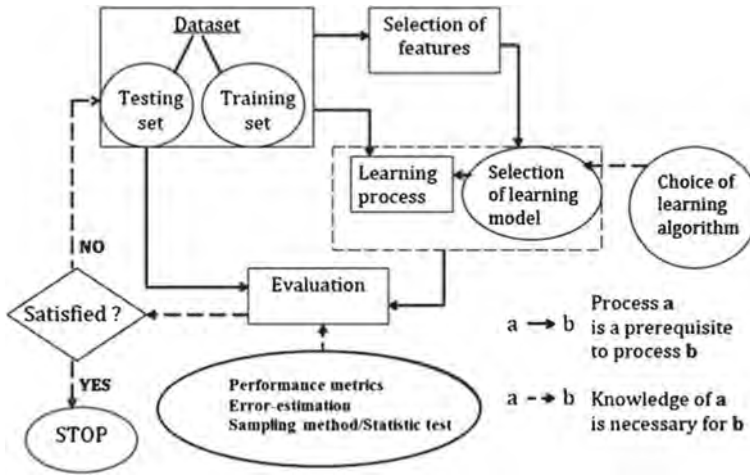


Fig. 15.2 General machine learning design process [88]

There are major elements common among all machine learning algorithms including datasets, features selection, model selection, and evaluation.

### 15.5.2.1 Dataset

Datasets are the starting point or input to the machine learning process. They are predominantly divided into two types; the training set and the testing set. The training set is data used to train the model, while the testing set approximates the model error rate. Due to irregularity or sometimes deficiency in datasets, this step might require a pre-processing afore getting into the learning algorithm, such as data normalization [90] and cleaning [91].

### 15.5.2.2 Feature Selection

Feature selection is sometimes considered as a pre-processing step or as a sub-algorithm computed within the machine learning model (e.g. hidden units in ANN) [92]. The objective is to clear the dataset from any redundant or irrelevant information. Therefore, it largely contributes to the accuracy of the learning model. It is beneficial in the case where the data size is multidimensional. It also expedites the process of learning because it only allows meaningful data to be considered [93]. However, precautions must be taken as crucial information might be discarded if poor feature selection is done. Common approaches of feature extraction are filters, wrappers, and embedded methods [92, 93].

Feature selection should not be confused with dimensionality reduction. Albeit, it seems counter-intuitive to discriminate between both terms, since feature selection ultimately leads to reduction in data dimension. In dimensionality reduction, the goal is to build new combinations of attributes or features and therefore it includes transformational techniques [94]. However, feature selection methods add or discard attributes without changing them, this means that it preserves the original-axis of this information [95]. Common dimensionality reduction techniques are; Principal Component Analysis (PCA) and Linear Discriminant Analysis (LDA).

### 15.5.2.3 Learning Model

The learning model is the mathematical framework for the selected learning algorithm [89]. The model selection largely depends on the model that offers the best description or prediction for the presented data [96]. It is how the algorithm models the problem and generates a classifier. A classifier is defined as a system that takes a vector of feature values and generates a single output vector. For example, in the following training set  $D$ :

$$D = \{d_1 = (x_1, y_1), d_2 = (x_2, y_2), d_n = (x_n, y_n)\} \quad (15.1)$$

The machine learning system then tries to find out the best possible mapping function between the input  $x_k$ , and its corresponding output  $y_k$ , until it reaches generalisation.

There are numerous machine learning models in the literature [97]. Nonetheless, the way they have been grouped is distinctive among authors. For example in [88], algorithms have been classified according to their mathematical model; learning style algorithms (e.g. supervised learning), algorithms that classify data based on similarities (e.g. SVM), and other measures. However, in [89, 93], algorithms were classified according to their interaction with input data; supervised learning, unsupervised learning, and reinforcement learning.

In supervised learning, the machine is presented with a set of input vectors along with its corresponding output/outcome vectors which are referred to as labelled training data. The machine is directly told which outputs are true for each set of inputs. However, for the unsupervised learning, there are no set of target values for each set of input vectors. The machine is not told what the correct answer is and is set to discover patterns in data and to group each similar data point using clustering techniques.

Reinforcement learning is a decision-making problem where the machine tries to seek out the appropriate actions in a given situation. The goal here is to get the most out of a reward, which is essentially a feedback mechanism or rather the reinforcement of the learning process [98]. Typically, the machine interacts with its environment by forming a sequential state, and all the past and current states have a direct impact on the reward. Consequently, the machine keeps on amending its learning model.

### 15.5.2.4 Evaluation Process

Designing a good classifier has never been a straightforward matter. Even when counting the number of incorrect classifications or rather the error rate, it turns out for most of the time the error rate does not manifest the entire picture [97, 99]. The main purpose of this step varies according to the performance criteria; however, the common goal is to measure the classifiers performance or what has been learned so far. Other goals are to compare different learning algorithms against different classifiers on a specific problem, compare different classifiers within the same learning algorithm, or to create a set of generic classifiers for a specific problem [93].

The most basic evaluation approach is to use results from a classified testing set (see Fig. 15.2), and from there correct classifications are counted, hence error rate is known. Other more accurate approaches include; sensitivity and specificity analysis [67, 100], cross-validation [101], Gmean, and cost functions [99].

## 15.5.3 Models Implemented in Exoskeletons

### 15.5.3.1 Hidden Markov Model (HMM)

The generation of natural analogue signals (e.g. speech samples, measured temperatures, etc.) can be characterised by signal models [102]. The most commonly used signal models are statistical models that are generally classified into deterministic models as well as stochastic models. For deterministic models, the models behavioural properties are known, such as sine wave and exponential function. However, for stochastic models, the signals behaviour is inconsistent. Hence, statistical models are the most efficient approach for describing the signals properties.

A stochastic process can be represented as a sequence of random variables

$$S = (S_1, S_2, \dots, S_N) \quad (15.2)$$

from a discrete or continuous domains [103]. Markov chain is a type of stochastic modelling. It defines a series of random variables, in which the current state depends on the past states. Hidden Markov Model (HMM) is a double stochastic process in which the first process (hidden) is the Markov property which describes how the system may transition from one state to another. The second stochastic process (observable) gives the statistical description of the emissions from each state (the sensor readings or the feature vectors constructed from them), in terms of either discrete probabilities or continuous probabilities represented in probability density functions (PDFs) [102, 103]. The major elements of HMM includes the following [102–104]:

1.  $N$ , is the number of hidden states in the model (Eq. 15.2). However, the actual state at time  $t$  is denoted as  $q_t$ , where  $t = 1, 2, \dots$
2.  $M$ , is the number of distinct observation symbol for each hidden state. Denoted as follows:

$$V = (v_1, v_2, \dots, v_M) \quad (15.3)$$

and the actual state at time  $t$  is denoted as  $O_t$ .

3.  $A = (a_{ij})$ , is the state transition probability matrix, where:

$$a_{ij} = P(q(t+1) = s_i | q_t = s_j), 1 \leq i, j \leq N \quad (15.4)$$

4.  $B = (b_j(v_k))$ , is the probability distribution of an observable hidden state  $j$ , where:

$$b_j(v_k) = P(O_t = v_k | q_t = s_j), 1 \leq j \leq N, 1 \leq k \leq M \quad (15.5)$$

5.  $\pi = (\pi_i)$ , is the initial state distribution, where:

$$\pi_i = P(Q_1 = s_i), 1 \leq i \leq N \quad (15.6)$$

Given the appropriate values of  $N$ ,  $M$ ,  $A$ ,  $B$  and, the HMM can be used as a generator to give an observation sequence

$$O = (O_1, O_2, O_3, O_T) \quad (15.7)$$

where,  $T$  is the number of observation in the sequence, and for simplicity, the following is the compact notation

$$\lambda = (A, B, \pi) \quad (15.8)$$

There are a number of other algorithms associated with HMM, that are concerned with computing the parameters mentioned in Eq. 15.8:

1. The forward-backward algorithm [105], which efficiently computes the observation sequence probability,  $O = (O_1 O_2 O_3 \dots O_T)$ .
2. The Viterbi algorithm [105], which finds the optimal state sequence  $Q = (Q_1, Q_2, \dots, Q_T)$  within the hidden part, given the observation sequence in 1.
3. The Expectation maximization technique [93] or the Baum-Welch algorithm [102], which obtain the maximum probabilities for the model parameters  $\lambda$ .

### 15.5.3.2 Applications of HMM in Exoskeletons

Examples of applications where HMM has been successfully implemented include areas of speech processing [102], bioinformatics [106], and gesture recognition [107].

It has also been implemented in the recognition of human physical activities, which became attractive in the area of healthcare monitoring [60] and other applications mentioned earlier.

In the area of wearable robotics, exoskeletons and biomechanics there have been few studies to implement HMM within gait phase detection using data obtained from wearable sensors. For example, in [67], HMM was able discriminate between two pathological gaits in typical developing children (TD) as well as children suffering from Hemiplegia (HC). The HMM was trained using a single-axis gyroscope embedded within an IMU on each foot.

Additionally, in [100], two HMMs were used to detect gait phases as well as walking and jogging activities, using gyroscopic data obtained from an IMU mounted on the navicular space of the left foot. Using data from shoe insoles HMM achieved 96% success on walking phase detection in [108]. A novel HMM distributed classifier based on Hierarchical Weighted Decision (HWD) [109] was introduced in [87] and the results showed high specificity and sensitivity values of more than 0.98. The HMM was also implemented in prosthetic devices. For example, the HMM was able to detect different steady-state gait phases of amputee walking using data acquired from seven IMUs mounted on different body segments in [58]. For the upper extremities in [110] an average accuracy of 94.63% was attained using HMM based on data from EMGs to classify six different static limb motions; hand open and close, pronation, supination, wrist flexion and extension.

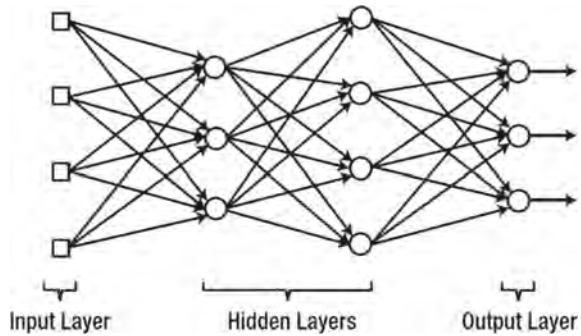
Like any machine learning algorithm, training is where the HMM learns about the nature of presented data. The standard methods for HMM training are the forward-backward or Baum-Welch algorithms [105]. However, if training is not done carefully it might become challenging for the model to come out with optimal representation of datasets during the testing phase. Insufficient training data was reported in [58] where there were only three users from which the same IMU data was used as a training set and test set. Likewise, in [67] the same training data of 10 TD and 10 HC were used during the test phase but with a different classifier, which resulted in low sensitivity and specificity values in non-walking tasks. However, unlike [100], the training phase was unsupervised.

Finally, in order for the HMM classification results to be validated, many studies compared the obtained results against threshold-based algorithms. In [67], HMM results were compared against FSR mounted on the foot and the algorithm found to be producing high sensitivity as well as specificity results. Also, in [100] HMM outperformed threshold results obtaining more than 94% and 98% for specificity and sensitivity analysis respectively, which is a good generalisation. In the prosthetic study, [58] compared the HMM performance to a rule-based algorithm, and the results were approximately similar (97% success rate).

### 15.5.3.3 Artificial Neural Networks (ANN)

Artificial Neural Networks (ANN) is a mathematical model that emulates the structure as well as the function of the biological Neural Networks. The work in

**Fig. 15.3** The general structure of ANN [111]



[111, 112] provides a comprehensive discussion on the ANN working principles. Figure 15.3 shows the general structure of ANN which consists of three major layers, the input layer which receives the input data, the hidden layers which process and classify the data, and finally the out player which obtain the classification result(s).

#### 15.5.3.4 Applications of ANN in Exoskeletons

To date there is a large opportunity to use ANN for gait analysis. Among these is Jung et al. [54] in which training as well as validation is conducted using supervised learning. The study compared two NN configurations namely; the multiple layer perceptron (MLP) and the nonlinear autoregressive with external inputs (NARX). Analysis was conducted offline using MATLAB as well as online using the exoskeleton Robin-H1 equipped with 2 IMUs, 4 absolute encoders, 4 incremental encoders, and 2 FSRs. Results showed that MLP as well as NARX obtained a very similar outcome of approximately 2% error rate and a superior performance to threshold method using FSRs. Also, [59] introduced and validated a gait recognition model using ANN or rather Multiple Layer Perceptron (MLP) for lower limb exoskeletons with only joint angular sensors. The study started by dividing the swing phase into three sub phases namely; initial phase, middle phase and the terminal swing. While the stance phase was divided into initial contact, loading response, mid-stance, terminal stance, and pre-swing. The study found that it is much easier to distinguish the range of motion between the knee and the hip joints during the stance phase and the swing phases. The Fisher's Linear Discriminant method was used as an offline data analysis to extract features which in turn informs the gait phase. However, to be used in an exoskeleton, MLP was adopted as an online analysis method to classify the data. Using cross-validation, MLP showed good performance with correct detection rate for sample points in the training or testing sets of 94.45% and correct detection rate for sample points in a single phase of 87.22%. Other work such as in [113], implemented deep convolutional NN, for gait recognition using imaging technique that converts the human body features automatically into silhouette image for identity purposes.

### 15.5.4 *Future Challenges and Prospects*

This section will highlight algorithms that are still under investigation, however, there is a good potential for these algorithms to be adopted into exoskeletons. Moreover, some of these algorithms are meshed with other ML algorithms so that they achieve optimum user prediction.

#### 15.5.4.1 **Gaussian Mixture Model (GMM)**

As the name implies, GMM is a combination of multivariate density functions. A full detailed analysis on GMM can be found in [114]. GMM applications include; forecast verification [115], market studies [116], physics [117], robotics [118], and biomechanics [119, 120].

In Allen et al. [115], GMM was used along with Bayesian adaptation to compensate for subject specific training in recognition of three postures (sitting, standing and lying) as well as five physical movements (sit to stand, stand to sit, lie to stand, stand to lie and walking). Thirty-two GMMs were trained from multiple users for each movement type using the Expectation Maximization algorithm, and then adopted to specific participants using the Bayesian adaptation. Data was self-collected at home (unsupervised pilot study) using a tri axial accelerometer from six healthy users, and it was divided into approximately 60–40% as a training and testing sets.

Adopting GMM improved the classification accuracy of time domain features (92.2%), which obtained better performance compared to frequency domain features (79.2%). However, as there was a single accelerometer there was challenges in distinguishing between sitting and standing. Also in [121], Infinite GMM (IGMM) was fused with a Parallel Praxile Filter (PPF) in order to attain real-time gait phase recognition, which is a vital tool for patients to identify their walking patterns and update the parameters used for clinical rehabilitation. Hence, the IGMM was used to classify walking gait phases based on Ground Contact Forces (GCF) acquired from a barometric sensor, while model parameters were estimated and updated using the PPF. With the aid of a Proportional-Integral-Defereential (PID) controller, a sparse Gaussian Process (GP) is used in [122] to learn the human trajectory through torque sensors installed on the knee joint. The study aimed at improving the Human Robot Interaction (HRI) mechanism by allowing the exoskeleton to track the joints angular motion. Data was collected while wearing the exoskeleton without operating the hydraulic actuators and then analysed offline using MATLAB. Results suggested the possibility of using GMM in intention recognition with physical HRI. For the upper extremity an implementation of both HMM and GMM (obtaining emission probabilities) was reported in [123] for object grasp and release tasks, using data from EMGs instrumented in a band around the forearm as well as a motion capture system. A comparison result between n-gram HMM and GMM with a different number of mixture components based on inter-subject training and testing yielded

mean accuracy of 75.96% with 5 mixtures attained using the unigram (i.e. a single sequence) HMM.

### 15.5.4.2 Support Vector Machines (SVM)

Support Vector Machines proposed by Valdimir Vapnik [124] are a powerful tool for pattern recognition and classification problems. Given its simplicity and easy implementation it requires few parameters to be tuned and it offers good generalisation in many data classification problems [125]. It is widely used for binary classification problems [62, 126, 127], where it finds the optimal separating hyperplane (see Fig. 15.4).

There are a number of applications where SVM is found to be contributing, amongst those are; face detection [128], text recognition [129], protein classification [130], and gait recognition [62, 126, 131–133].

In Nakano et al. [127], four types of SVM were used including; Linear SVM, Quadratic SVM, Cubic SVM, and Gaussian SVM to differentiate walking patterns between normal and patient users, using data obtained from a custom designed wireless gait sensor installed on 7 users (3 normal and 4 patients). The wireless gait sensor is a multi-dimensional kit, which combines 3 MEMS chips including; a single axis gyroscope, a dual axis gyroscope, and a 3-axis linear accelerometer. Linear, Quadratic, and Cubic SVM obtained high specificity and sensitivity values of 100 and 95.2% respectively, as well as 98% accuracy. While Gaussian attained 87.8% accuracy, 71.7% sensitivity, and 100% specificity. Also in Begg et al. [62], SVM was used to discriminate the walking patterns between elderly and young populations using basic spatial/temporal, kinetic and kinematic data obtained from a force platform as well as a 3D motion analysis system. With gait data obtained from 24 users (12 youths and 12 elderly), results suggested better performance was achieved when combining more than a single type of data.

That is, analysing the kinetic data alone obtained up to 83.3% of accuracy, while the combination of kinetic and kinematic data achieved up to 91.7% of accuracy. It was also found that not all features help in improving the classification accuracy. In Fig. 15.5, only 3 features were required to attain the optimum accuracy and accuracy started to decrease after inclusion of features.

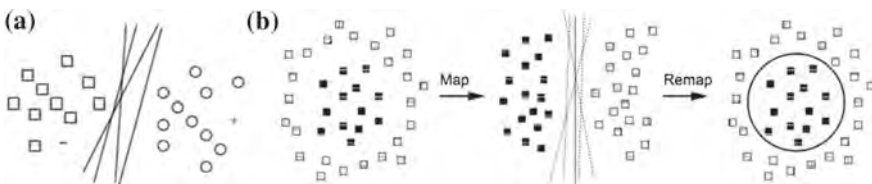
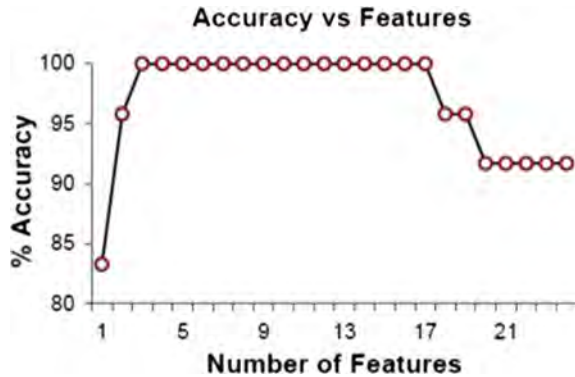


**Fig. 15.4** Linear (a) and non-linear (b) SVM to find optimum possible planes to divide the data into two classes [62]

**Fig. 15.5** The classification accuracy of SVM against the number of features in [62]



Overall, SVM is a powerful tool for binary discrimination problems, however, it is yet to be applied in active exoskeletons that are generally multiclass problems [134].

## 15.6 Summary

An ideal exoskeleton is an extension of the human body that attempts to assist movement. A major challenge in current exoskeleton designs is the need to synchronise user intention with exoskeleton function to achieve smooth interaction between the user and device. The fusion of intelligent machine learning algorithms into the exoskeletons controller has potential to improve the human machine interface and user experience. The goal of future research in the area is to develop exoskeletons that automatically adapt to the users environment or settings and learn from mistakes as well as user experience. These would boost user confidence while wearing the exoskeleton.

As research starts to focus on the feasibility of adopting machine learning techniques, it should be emphasised that each algorithm excels at a specific problem. For example, HMM has shown better performance in motions classification compared to SVM, GMM, and LDA in [60]. It offers a good advantage when intent transitions are prerequisite actions to each other, such as in the upper extremity, where approach is a prerequisite to grasp [102]. Unlike other classifiers which classify each input feature at each time independently, HMM considers the entire motion sequence over time. Hence, it is suitable to work with stochastic signals, such as EMGs [110, 123].

Comparing HMM to ANN, they outweigh each other from different perspectives. The HMM has a robust capacity in modelling the time series actions, while ANN is better in categorising the actions using spatial data [59]. In addition, HMM offers much better performance in classification of stochastic signals (EMG) compared to ANN [110]. However, HMM, ANN, and SVM are claimed to be computationally intensive and therefore unsuitable for rehabilitation training [121]. In conclusion, we

foresee that future exoskeleton control would need an intelligent learning framework to be developed that seamlessly integrates the different machine learning techniques discussed in this chapter.

**Acknowledgements** The authors gracefully acknowledge the funding of this research by the Defence Science and Technology Group (DSTGroup), Melbourne, Australia.

## References

1. Carpino, G., Accoto, D., Tagliamonte, N.L., Ghilardi, G., Guglielmelli, E.: Lower limb wearable robots for physiological gait restoration: state of the art and motivations. *Medic* **21**, 72–80 (2013)
2. Shinohara, K., Wobbrock, J.O.: Self-conscious or self-confident? A diary study conceptualizing the social accessibility of assistive technology. *ACM Trans. Accessible Comput.* **8** (2016)
3. Radder, B., Kottink, A., van der Vaart, N., Oosting, D., Buurke, J., Nijenhuis, S., Prange, G., Rietman, J.: User-centred input for a wearable soft-robotic glove supporting hand function in daily life. In: *IEEE International Conference on Rehabilitation Robotics (ICORR)*, pp. 502–507. IEEE (2015)
4. Pons, J.L.: *Wearable Robots: Biomechatronic Exoskeletons*. Wiley, New York (2008)
5. Dollar, A.M., Herr, H.: Lower extremity exoskeletons and active orthoses: challenges and state-of-the-art. *IEEE Trans. Robot.* **24**, 144–158 (2008)
6. Herr, H.: Exoskeletons and orthoses: classification, design challenges and future directions. *J. Neuroeng. Rehabil.* **6**, 21 (2009)
7. Akyildiz, I.F., Su, W., Sankarasubramaniam, Y., Cayirci, E.: Wireless sensor networks: a survey. *Comput. Netw.* **38**, 393–422 (2002)
8. Lai, D.T.H., Palaniswami, M., Begg, R.: *Healthcare Sensor Networks: Challenges Toward Practical Implementation*. CRC Press, Boca Raton (2011)
9. Yan, T., Cempini, M., Oddo, C.M., Vitiello, N.: Review of assistive strategies in powered lower-limb orthoses and exoskeletons. *Robot. Auton. Syst.* **64**, 120–136 (2015)
10. Yagn, N.: *Apparatus for facilitating walking*. Google Patents (1890)
11. Dick, G.J., Edwards, E.A.: *Human bipedal locomotion device*. Google Patents (1991)
12. Saccares, L., Sarakoglou, I., Tsagarakis, N.G.: iT-Knee: an exoskeleton with ideal torque transmission interface for ergonomic power augmentation. In: *IEEE/RSJ International Conference on Intelligent Robots and Systems (IROS)*, pp. 780–786. IEEE (2016)
13. Collins, S.H., Wiggin, M.B., Sawicki, G.S.: Reducing the energy cost of human walking using an unpowered exoskeleton. *Nature* **522**, 212–215 (2015)
14. Van Dijk, W., Van der Kooij, H., Hekman, E.: A passive exoskeleton with artificial tendons: design and experimental evaluation. In: *IEEE International Conference on Rehabilitation Robotics (ICORR)*, pp. 1–6. IEEE (2011)
15. Diller, S., Majidi, C., Collins, S.H.: A lightweight, low-power electroadhesive clutch and spring for exoskeleton actuation. In: *IEEE International Conference on Robotics and Automation (ICRA)*, pp. 682–689. IEEE (2016)
16. Dollar, A.M., Herr, H.: Design of a quasi-passive knee exoskeleton to assist running. In: *IEEE/RSJ International Conference on Intelligent Robots and Systems*, pp. 747–754. IEEE (2008)
17. Gopura, R.A.R.C., Bandara, D.S.V., Kiguchi, K., Mann, G.K.I.: Developments in hardware systems of active upper-limb exoskeleton robots: a review. *Robot. Auton. Syst.* **75**, 203–220 (2016)

18. Kuo, A.D.: A mechanical analysis of force distribution between redundant multiple degree-of-freedom actuators in the human: implications for the central nervous system. *Hum. Mov. Sci.* **13**, 635–663 (1994)
19. Yi, J., Shen, Z., Song, C., Wang, Z.: A soft robotic glove for hand motion assistance. In: IEEE International Conference on Real-time Computing and Robotics (RCAR), pp. 111–116. IEEE (2016)
20. Yun, Y., Agarwal, P., Fox, J., Madden, K.E., Deshpande, A.D.: Accurate torque control of finger joints with UT hand exoskeleton through Bowden cable SEA. In: 2016 IEEE/RSJ International Conference on Intelligent Robots and Systems (IROS), pp. 390–397 (2016)
21. Nycz, C.J., Btzer, T., Lambercy, O., Arata, J., Fischer, G.S., Gassert, R.: Design and characterization of a lightweight and fully portable remote actuation system for use with a hand exoskeleton. *IEEE Robot. Autom. Lett.* **1**, 976–983 (2016)
22. Yi, J., Shen, Z., Song, C., Wang, Z.: A soft robotic glove for hand motion assistance. In: 2016 IEEE International Conference on Real-time Computing and Robotics (RCAR), pp. 111–116 (2016)
23. de Michiel, P., Looze, T.B., Krause, F., Stadler, K.S., O’Sullivan, L.W.: Exoskeletons for industrial application and their potential effects on physical work load. *Ergonomics* **59**, 671–681 (2016)
24. Mudie, K.L., Boynton, A.C., Karakolis, T., O’Donovan, M.P., Kanagaki, G.B., Crowell, H.P., Begg, R.K., LaFiandra, M.E., Billing, D. C.: Consensus paper on testing and evaluation of military exoskeletons for the dismounted combatant. Under Review (2017)
25. Kang, B.B., Lee, H., In, H., Jeong, U., Chung, J., Cho, K. J.: Development of a polymer-based tendon-driven wearable robotic hand. In: IEEE International Conference on Robotics and Automation (ICRA), pp. 3750–3755. IEEE (2016)
26. Ugurlu, B., Nishimura, M., Hyodo, K., Kawanishi, M., Narikiyo, T.: Proof of concept for robot-aided upper limb rehabilitation using disturbance observers. *IEEE Trans. Hum. Mach. Syst.* **45**, 110–118 (2015)
27. Martinez, F., Retolaza, I., Pujana-Arrese, A., Cenitagoya, A., Basurko, J., Landaluze, J.: Design of a five actuated DoF upper limb exoskeleton oriented to workplace help. In: 2nd IEEE RAS & EMBS International Conference on Biomedical Robotics and Biomechanics, pp. 169–174 (2008)
28. Toyama, S., Yamamoto, G.: Wearable agrirobot. *J. Vibroeng.* **12**, 287–291 (2010)
29. Maeshima, S., Osawa, A., Nishio, D., Hirano, Y., Takeda, K., Kigawa, H., Sankai, Y.: Efficacy of a hybrid assistive limb in post-stroke hemiplegic patients: a preliminary report. *BMC Neurol.* **11**, 116 (2011)
30. Kawamoto, H., Kamibayashi, K., Nakata, Y., Yamawaki, K., Ariyasu, R., Sankai, Y., Sakane, M., Eguchi, K., Ochiai, N.: Pilot study of locomotion improvement using hybrid assistive limb in chronic stroke patients. *BMC Neurol.* **13**, 141 (2013)
31. Watanabe, H., Tanaka, N., Inuta, T., Saitou, H., Yanagi, H.: Locomotion improvement using a hybrid assistive limb in recovery phase stroke patients: a randomized controlled pilot study. *Arch. Phys. Med. Rehabil.* **95**, 2006–2012 (2014)
32. Kawamoto, H., Taal, S., Niniss, H., Hayashi, T., Kamibayashi, K., Eguchi, K., Sankai, Y.: Voluntary motion support control of Robot Suit HAL triggered by bioelectrical signal for hemiplegia. In: Annual International Conference of the IEEE Engineering in Medicine and Biology Society (EMBC), pp 462–466. IEEE (2010)
33. Suzuki, K., Kawamura, Y., Hayashi, T., Sakurai, T., Hasegawa, Y., Sankai, Y.: Intention-based walking support for paraplegia patient. In: IEEE International Conference on Systems Man and Cybernetics, pp. 2707–2713 (2005)
34. Sankai, Y.: HAL: hybrid assistive limb based on cybernetics. In: *Robotics Research*, pp. 25–34. Springer, Berlin (2010)
35. Walsh, C.J., Endo, K., Herr, H.: A quasi-passive leg exoskeleton for load-carrying augmentation. *Int. J. Humanoid Rob.* **4**, 487–506 (2007)
36. Martin, L.: University of Michigan study suggests soldiers could cover inclined terrain more easily using Lockheed Martins FORTIS K-SRD exoskeleton. Lockheed Martin (2017)

37. Australian Institute of Health Welfare: Stroke and Its Management in Australia: An Update, 37 edn., Canberra (2013)
38. Maciejasz, P., Eschweiler, J., Gerlach-Hahn, K., Jansen-Troy, A., Leonhardt, S.: A survey on robotic devices for upper limb rehabilitation. *J. Neuroeng. Rehabil.* **11**, 3 (2014)
39. Jarrass, N., Morel, G., Proietti, T., Roby-Brami, A., Crocher, V., Robertson, J., Sahbani, A.: Robotic exoskeletons: a perspective for the rehabilitation of arm coordination in stroke patients. *Front. Hum. Neurosci.* **8**, 947 (2014)
40. Yun, Y., Agarwal, P., Fox, J., Madden, K.E., Deshpande, A.D.: Accurate torque control of finger joints with UT hand exoskeleton through Bowden cable SEA. In: *IEEE/RSJ International Conference on Intelligent Robots and Systems (IROS)*, pp. 390–397. IEEE (2016)
41. Australian Institute of Health and Welfare (AIHW): Disability Support Services: Services Provided Under the National Disability Agreement 2015–16, vol. 140. Canberra (2017)
42. Popov, D., Gaponov, I., Ryu, J.H.: Portable exoskeleton glove with soft structure for hand assistance. In: *Activities of Daily Living. IEEE/ASME Transactions on Mechatronics*, vol. 22, issue 2, pp. 865–875 (2017)
43. Dinh, B.K., Xiloyannis, M., Antuvan, C.W., Cappello, L., Masia, L.: Hierarchical cascade controller for assistance modulation in a soft wearable arm exoskeleton. *IEEE Rob. Autom. Lett.* **2**, 1786–1793 (2017)
44. Mohammadi, E., Zohoor, H., Khadem, S.M.: Control system design of an active assistive exoskeletal robot for rehabilitation of elbow and wrist. In: *Second RSI/ISM International Conference on Robotics and Mechatronics (ICRoM)*, pp. 834–839. IEEE (2014)
45. Balasubramanian, S., Ruihua, W., Perez, M., Shepard, B., Koeneman, E., Koeneman, J., Jiping, H.: RUPERT: An exoskeleton robot for assisting rehabilitation of arm functions. *Virtual Rehabilitation, IEEE* (2008)
46. Veneman, J.F., Kruidhof, R., Hekman, E.E., Ekkelenkamp, R., Van Asseldonk, E.H., Van Der Kooij, H.: Design and evaluation of the LOPES exoskeleton robot for interactive gait rehabilitation. *IEEE Trans. Neural Syst. Rehabil. Eng.* **15**, 379–386 (2007)
47. Colombo, G., Joerg, M., Schreier, R., Dietz, V.: Treadmill training of paraplegic patients using a robotic orthosis. *J. Rehabil. Res. Dev.* **37**, 693 (2000)
48. Bortole, M., Venkatakrishnan, A., Zhu, F., Moreno, J.C., Francisco, G.E., Pons, J.L., Contreras-Vidal, J.L.: The H2 robotic exoskeleton for gait rehabilitation after stroke: early findings from a clinical study. *J. Neuroeng. Rehabil.* **12**, 54 (2015)
49. Esquenazi, A., Talaty, M., Packel, A., Saulino, M.: The ReWalk powered exoskeleton to restore ambulatory function to individuals with thoracic-level motor-complete spinal cord injury. *Am. J. Phys. Med. Rehabil.* **91**, 911–921 (2012)
50. Quintero, H.A., Farris, R.J., Goldfarb, M.: A method for the autonomous control of lower limb exoskeletons for persons with paraplegia. *J. Med. Devices* **6**, 041003 (2012)
51. Agrawal, A., Harib, O., Hereid, A., Finet, S., Masselin, M., Praly, L., Ames, A., Sreenath, K., Grizzle, J.: First steps towards translating HZD control of bipedal robots to decentralized control of exoskeletons. *IEEE Access* **5**, 9919–9934 (2017)
52. Chu, A., Kazerooni, H., Zoss, A.: On the biomimetic design of the berkeley lower extremity exoskeleton (BLEEX). In: *Proceedings of the 2005 IEEE International Conference on Robotics and Automation (ICRA)*, pp. 4345–4352. IEEE (2005)
53. Fukuda, S., De Baets, B.: A short review on the application of computational intelligence and machine learning in the bioenvironmental sciences. In: *2012 Joint 6th International Conference on Soft Computing and Intelligent Systems (SCIS) and 13th International Symposium on Advanced Intelligent Systems (ISIS)*, pp. 106–110. IEEE (2012)
54. Jung, J.-Y., Heo, W., Yang, H., Park, H.: A neural network-based gait phase classification method using sensors equipped on lower limb exoskeleton robots. *Sensors* **15**, 27738–27759 (2015)
55. Perry, J., Davids, J.R.: Gait analysis: normal and pathological function. *J. Pediatr. Orthop.* **12**, 815 (1992)
56. Rushton, D.: Functional electrical stimulation and rehabilitationan hypothesis. *Med. Eng. Phys.* **25**, 75–78 (2003)

57. Williamson, R., Andrews, B.J.: Gait event detection for FES using accelerometers and supervised machine learning. *IEEE Trans. Rehabil. Eng.* **8**, 312–319 (2000)
58. Gori, M., Kamnik, R., Ambroi, L., Vitiello, N., Lefeber, D., Pasquini, G., Muni, M.: Online phase detection using wearable sensors for walking with a robotic prosthesis. *Sensors* **14**, 2776–2794 (2014)
59. Liu, D.-X., Wu, X., Du, W., Wang, C., Xu, T.: Gait phase recognition for lower-limb exoskeleton with only joint angular sensors. *Sensors* **16**, 1579 (2016)
60. Mannini, A., Sabatini, A.M.: Machine learning methods for classifying human physical activity from on-body accelerometers. *Sensors* **10**, 1154–1175 (2010)
61. Rueterbories, J., Spaich, E.G., Larsen, B., Andersen, O.K.: Methods for gait event detection and analysis in ambulatory systems. *Med. Eng. Phys.* **32**, 545–552 (2010)
62. Begg, R., Kamruzzaman, J.: A machine learning approach for automated recognition of movement patterns using basic, kinetic and kinematic gait data. *J. Biomech.* **38**, 401–408 (2005)
63. O'Connor, C.M., Thorpe, S.K., O'Malley, M.J., Vaughan, C.L.: Automatic detection of gait events using kinematic data. *Gait Posture* **25**, 469–474 (2007)
64. Hanlon, M., Anderson, R.: Real-time gait event detection using wearable sensors. *Gait Posture* **30**, 523–527 (2009)
65. Preece, S.J., Kenney, L.P., Major, M.J., Dias, T., Lay, E., Fernandes, B.T.: Automatic identification of gait events using an instrumented sock. *J. Neuroeng. Rehabil.* **8**, 32 (2011)
66. Tao, W., Liu, T., Zheng, R., Feng, H.: Gait analysis using wearable sensors. *Sensors* **12**, 2255–2283 (2012)
67. Abaid, N., Cappa, P., Palermo, E., Petrarca, M., Porfiri, M.: Gait detection in children with and without hemiplegia using single-axis wearable gyroscopes. *PloS One* **8**, e73152 (2013)
68. González, R.C., López, A.M., Rodríguez-Uría, J., Alvarez, D., Alvarez, J.C.: Real-time gait event detection for normal subjects from lower trunk accelerations. *Gait Posture* **31**, 322–325 (2010)
69. Nogueira, S.L., Siqueira, A.A., Inoue, R.S., Terra, M.H.: Markov jump linear systems-based position estimation for lower limb exoskeletons. *Sensors* **14**, 1835–1849 (2014)
70. Bamberg, S.J.M., Benbasat, A.Y., Scarborough, D.M., Krebs, D.E., Paradiso, J.A.: Gait analysis using a shoe-integrated wireless sensor system. *IEEE Trans. Inf. Technol. Biomed.* **12**, 413–423 (2008)
71. Joshi, C.D., Lahiri, U., Thakor, N.V.: Classification of gait phases from lower limb EMG: application to exoskeleton orthosis. In: *IEEE Point-of-Care Healthcare Technologies (PHT)*, pp. 228–231. IEEE (2013)
72. Li, J., Chen, G., Thangavel, P., Yu, H., Thakor, N., Bezerianos, A., Sun, Y.: A robotic knee exoskeleton for walking assistance and connectivity topology exploration in EEG signal. In: *6th IEEE International Conference on Biomedical Robotics and Biomechatronics (BioRob)*, pp. 1068–1073. IEEE (2016)
73. Kawamoto, H., Sankai, Y.: Comfortable power assist control method for walking aid by HAL-3. In: *IEEE International Conference on Systems, Man and Cybernetics*, vol. 4. IEEE (2002)
74. Lenzi, T., De Rossi, S.M.M., Vitiello, N., Carrozza, M.C.: Intention-based EMG control for powered exoskeletons. *IEEE Trans. Biomed. Eng.* **59**, 2180–2190 (2012)
75. Fleischer, C., Reinicke, C., Hommel, G.: Predicting the intended motion with EMG signals for an exoskeleton orthosis controller. In: *IEEE/RSJ International Conference on Intelligent Robots and System (IROS)*, pp. 2029–2034. IEEE (2005)
76. Chen, X., Zeng, Y., Yin, Y.: Improving the transparency of an exoskeleton knee joint based on the understanding of motor intent using energy kernel method of EMG. *IEEE Trans. Neural Syst. Rehabil. Eng.* **25**, 577–588 (2017)
77. Chen, X., Yin, Y., Fan, Y.: EMG oscillator model-based energy kernel method for characterizing muscle intrinsic property under isometric contraction. *Chin. Sci. Bull.* **59**, 1556–1567 (2014)
78. Chen, G., Chan, C.K., Guo, Z., Yu, H.: A review of lower extremity assistive robotic exoskeletons in rehabilitation therapy. *Crit. Rev. Biomed. Eng.* **41**, 4–5 (2013)

79. Biggar, S., Yao, W.: Design and evaluation of a soft and wearable robotic glove for hand rehabilitation. *IEEE Trans. Neural Syst. Rehabil. Eng.* **24**, 1071–1080 (2016)
80. Wang, S., Wang, L., Meijneke, C., Van Asseldonk, E., Hoellinger, T., Cheron, G., Ivanenko, Y., La Scaleia, V., Sylos-Labini, F., Molinari, M.: Design and control of the MINDWALKER exoskeleton. *IEEE Trans. Neural Syst. Rehabil. Eng.* **23**, 277–286 (2015)
81. Petersen, T.H., Willerslev-Olsen, M., Conway, B.A., Nielsen, J.B.: The motor cortex drives the muscles during walking in human subjects. *J. Physiol.* **590**, 2443–2452 (2012)
82. Sabatini, A.M.: Estimating three-dimensional orientation of human body parts by inertial/magnetic sensing. *Sensors* **11**, 1489–1525 (2011)
83. Barbour, N., Schmidt, G.: Inertial sensor technology trends. *IEEE Sens. J.* **1**, 332–339 (2001)
84. Elliott, G., Marecki, A., Herr, H.: Design of a clutchspring knee exoskeleton for running. *J. Med. Devices* **8**, 031002 (2014)
85. Beravs, T., Reberek, P., Novak, D., Podobnik, J., Munih, M.: Development and validation of a wearable inertial measurement system for use with lower limb exoskeletons. In: 11th IEEE-RAS International Conference on Humanoid Robots (Humanoids), pp. 212–217. IEEE (2011)
86. Nogueira, S.L., Lambrecht, S., Inoue, R.S., Bortole, M., Montagnoli, A.N., Moreno, J.C., Rocon, E., Terra, M.H., Siqueira, A. A., Pons, J.L.: Global Kalman Filter approaches to estimate absolute angles of lower limb segments. *Biomed. Eng. Online* **16**, 58. BioMed. Central (2017)
87. Taborri, J., Rossi, S., Palermo, E., Patan, F., Cappa, P.: A novel HMM distributed classifier for the detection of gait phases by means of a wearable inertial sensor network. *Sensors* **14**, 16212–16234 (2014)
88. Mason, J.E., Traor, I., Woungang, I.: *Machine Learning Techniques for Gait Biometric Recognition: Using the Ground Reaction Force*. Springer, Berlin (2016)
89. Paluszek, M., Thomas, S.: *MATLAB Machine Learning*. Apress, USA (2017)
90. Karvanen, J.: The statistical basis of laboratory data normalization. *Drug Inf. J.* **37**, 101–107 (2003)
91. Chapman, A.D.: *Principles and Methods of Data Cleaning. Primary species and species-occurrence data* (2005)
92. Isabelle, G.: *Feature Extraction Foundations and Applications. Pattern Recognition*. Springer, Berlin (2006)
93. Bishop, C.M.: *Pattern Recognition and Machine Learning*. Springer, Berlin (2006)
94. Japkowicz, N., Shah, M.: *Evaluating Learning Algorithms: A Classification Perspective*. Cambridge University Press, Cambridge (2011)
95. Guyon, I., Elisseeff, A.: An introduction to variable and feature selection. *J. Mach. Learn. Res.* **3**, 1157–1182 (2003)
96. Guyon, I., Saffari, A., Dror, G., Cawley, G.: Model selection: beyond the bayesian/frequentist divide. *J. Mach. Learn. Res.* **11**, 61–87 (2010)
97. Witten, I.H., Frank, E., Hall, M.A., Pal, C.J.: *Data Mining: Practical Machine Learning Tools and Techniques*. Morgan Kaufmann, Cambridge (2016)
98. Wiering, M., Van Otterlo, M.: Reinforcement learning. *Adapt. Learn. Optim.* **12** (2012)
99. Kubat, M.: *An Introduction to Machine Learning*. Springer, Berlin (2015)
100. Mannini, A., Sabatini, A.M.: Gait phase detection and discrimination between walking/jogging activities using hidden Markov models applied to foot motion data from a gyroscope. *Gait Posture* **36**, 657–661 (2012)
101. Salvador, R., Radua, J., Canales-Rodríguez, E.J., Solanes, A., Sarr, S., Goikolea, J.M., Valiente, A., Mont, G.C., del Carmen Natividad, M., Guerrero-Pedraza, A.: Evaluation of machine learning algorithms and structural features for optimal MRI-based diagnostic prediction. *Psychosis PloS One* **12**, e0175683 (2017)
102. Dugad, R., Desai, U.B.: A tutorial on hidden Markov models *Signal Processing and Artificial Neural Networks Laboratory. Department of Electrical Engineering, Indian Institute of Technology, Bombay Technical Report* (1996)

103. Fink, G.A.: *Markov Models for Pattern Recognition: From Theory to Applications*. Springer Science & Business Media (2014)
104. Ching, W.-K., Huang, X., Ng, M.K., Siu, T.-K.: *Markov Chains Models, Algorithms and Applications*, 2nd edn. Springer, New York (2013)
105. Jurafsky, D., Martin, J.H.: *Speech and Language Processing*, vol. 3. Pearson, London (2014)
106. Yoon, B.-J.: Hidden Markov models and their applications in biological sequence analysis. *Curr. Genomics* **10**, 402–415 (2009)
107. Wilson, A.D., Bobick, A.F.: Parametric hidden markov models for gesture recognition. *IEEE Trans. Pattern Anal. Mach. Intell.* **21**, 884–900 (1999)
108. Crea, S., De Rossi, S.M., Donati, M., Reberek, P., Novak, D., Vitiello, N., Lenzi, T., Podobnik, J., Muni, M., Carrozza, M.C.: Development of gait segmentation methods for wearable foot pressure sensors. In: 2012 Annual International Conference of the IEEE Engineering in Medicine and Biology Society (EMBC), pp. 5018–5021. IEEE (2012)
109. Banos, O., Damas, M., Pomares, H., Rojas, F., Delgado-Marquez, B., Valenzuela, O.: Human activity recognition based on a sensor weighting hierarchical classifier. *Soft Comput.* **17**, 333–343 (2013)
110. Chan, A.D., Englehart, K.B.: Continuous myoelectric control for powered prostheses using hidden Markov models. *IEEE Trans. Biomed. Eng.* **52**, 121–124 (2005)
111. Kim, P.: *MATLAB Deep Learning With Machine Learning. Neural Networks and Artificial Intelligence*. Springer, Berlin (2017)
112. Da Silva, I.N., Spatti, D.H., Flauzino, R.A., Liboni, L.H.B., dos Reis Alves, S.F.: *Artificial Neural Networks: A Practical Course*. Springer, Berlin (2017)
113. Alotaibi, M., Mahmood, A.: Improved gait recognition based on specialized deep convolutional neural network. *Computer Vision and Image Understanding*. In: 2015 IEEE Applied Imagery Pattern Recognition Workshop (AIPR). IEEE (2015)
114. McLachlan, G., Peel, D.: *Finite Mixture Models*. Wiley, New York (2004)
115. Lakshmanan, V., Kain, J.S.: A Gaussian mixture model approach to forecast verification. *Weather Forecast.* **25**, 908–920 (2010)
116. Zhang, M.-H., Cheng, Q.-S.: Gaussian mixture modelling to detect random walks in capital markets. *Math. Comput. Model.* **38**, 503–508 (2003)
117. Stepanek, M., Kus, V., Franc, J.: Modification of Gaussian mixture models for data classification in high energy physics. *J. Phys. Conf. Ser.* **574**, 012150 (2015)
118. Park, S., Mustafa, S.K., Shimada, K.: Learning based robot control with sequential Gaussian process. In: 2013 IEEE Workshop on Robotic Intelligence in Informationally Structured Space (RiSS), pp. 120–127. IEEE (2013)
119. Allen, F.R., Ambikairajah, E., Lovell, N.H., Celler, B.G.: An adapted Gaussian mixture model approach to accelerometry-based movement classification using time-domain features. In: 28th Annual International Conference of the IEEE Engineering in Medicine and Biology Society, pp. 3600–3603. IEEE (2006)
120. Vögele, A.M., Zsoldos, R.R., Kürger, B., Licka, T.: Novel methods for surface EMG analysis and exploration based on multi-modal gaussian mixture models. *PloS One* **11**, 0157239 (2016)
121. Papavasileiou, I., Zhang, W., Han, S.: Real-time data-driven gait phase detection using infinite Gaussian mixture model and parallel particle filter. In: IEEE First International Conference on Connected Health: Applications, Systems and Engineering Technologies (CHASE), pp. 302–311. IEEE (2016)
122. Long, Y., Du, Z.-j., Dong, W., Wang, W.-d.: Human gait trajectory learning using online Gaussian process for assistive lower limb exoskeleton. In: *Wearable Sensors and Robots*, pp. 165–179. Springer, Berlin (2017)
123. Siu, H.C., Shah, J.A., Stirling, L.A.: Classification of anticipatory signals for grasp and release from surface electromyography. *Sensors* **16**, 1782 (2016)
124. Vapnik, V.: *The Nature of Statistical Learning Theory*. Springer Science & Business Media (2013)
125. Le Borgne, H., O’Connor, N.: Natural scene classification and retrieval using Ridgelet-based image signatures. In: *International Conference on Advanced Concepts for Intelligent Vision Systems*, pp. 116–122. Springer, Berlin (2005)

126. Begg, R.K., Palaniswami, M., Owen, B.: Support vector machines for automated gait classification. *IEEE Trans. Biomed. Eng.* **52**, 828–838 (2005)
127. Nakano, T., Nukala, B.T., Zupancic, S., Rodriguez, A., Lie, D.Y., Lopez, J., Nguyen, T.Q.: Gaits classification of normal vs. patients by wireless gait sensor and Support Vector Machine (SVM) classifier. In: *IEEE/ACIS 15th International Conference on Computer and Information Science (ICIS)* (2016)
128. Jee, H., Lee, K., Pan, S.: Eye and face detection using SVM. In: *Proceedings of the 2004 Intelligent Sensors, Sensor Networks and Information Processing Conference*, pp. 577–580, IEEE (2004)
129. Rajnoha, M., Burget, R., Dutta, M.K.: Offline handwritten text recognition using support vector machines. In: *4th International Conference on Signal Processing and Integrated Networks (SPIN)*, pp. 132–136 (2017)
130. Cai, C., Han, L., Ji, Z.L., Chen, X., Chen, Y.Z.: SVM-Prot: web-based support vector machine software for functional classification of a protein from its primary sequence. *Nucleic Acids Res.* **31**, 3692–3697 (2003)
131. Liu, X., Zhou, Z., Mai, J., Wang, Q.: Multi-class SVM based real-time recognition of sit-to-stand and stand-to-sit transitions for a bionic knee exoskeleton in transparent mode. In: *International Conference on Intelligent Robotics and Applications*, pp. 262–272. Springer, Berlin (2017)
132. Nukala, B.T., Shibuya, N., Rodriguez, A., Tsay, J., Lopez, J., Nguyen, T., Zupancic, S., Lie, D.Y.-C.: An efficient and robust fall detection system using wireless gait analysis sensor with artificial neural network (ANN) and support vector machine (SVM) algorithms. *Open J. Appl. Biosens.* **3**, 29–39 (2014)
133. Yoo, J.-H., Hwang, D., Nixon, M.S.: Gender classification in human gait using support vector machine. In: *ACIVS*, pp. 138–145. Springer, Berlin (2005)
134. Mai, J., Zhang, Z., Wang, Q.: A real-time intent recognition system based on SoC-FPGA for robotic transtibial prosthesis. In: *International Conference on Intelligent Robotics and Applications*. Springer, pp. 280–289. (2017)



# Lower Limb Kinematics Trajectory Prediction Using Long Short-Term Memory Neural Networks

Abdelrahman Zaroug<sup>1\*</sup>, Daniel T. H. Lai<sup>1,2</sup>, Kurt Mudie<sup>3</sup> and Rezaul Begg<sup>1\*</sup>

<sup>1</sup> Institute for Health and Sport, Victoria University, Melbourne, VIC, Australia, <sup>2</sup> College of Engineering and Science, Victoria University, Melbourne, VIC, Australia, <sup>3</sup> Defence Science and Technology Group, Melbourne, VIC, Australia

## OPEN ACCESS

### Edited by:

Matteo Zago,  
Politecnico di Milano, Italy

### Reviewed by:

Francesco Travascio,  
University of Miami, United States  
Nicola Francesco Lopomo,  
University of Brescia, Italy

### \*Correspondence:

Abdelrahman Zaroug  
abdelrahman.zaroug@live.vu.edu.au  
Rezaul Begg  
rezaul.begg@vu.edu.au

### Specialty section:

This article was submitted to  
Biomechanics,  
a section of the journal  
Frontiers in Bioengineering and  
Biotechnology

**Received:** 17 January 2020

**Accepted:** 31 March 2020

**Published:** 08 May 2020

### Citation:

Zaroug A, Lai DTH, Mudie K and  
Begg R (2020) Lower Limb  
Kinematics Trajectory Prediction  
Using Long Short-Term Memory  
Neural Networks.  
Front. Bioeng. Biotechnol. 8:362.  
doi: 10.3389/fbioe.2020.00362

This study determined whether the kinematics of lower limb trajectories during walking could be extrapolated using long short-term memory (LSTM) neural networks. It was hypothesised that LSTM auto encoders could reliably forecast multiple time-step trajectories of the lower limb kinematics, specifically linear acceleration (LA) and angular velocity (AV). Using 3D motion capture, lower limb position–time coordinates were sampled (100 Hz) from six male participants (age  $22 \pm 2$  years, height  $1.77 \pm 0.02$  m, body mass  $82 \pm 4$  kg) who walked for 10 min at 5 km/h on a 0% gradient motor-driven treadmill. These data were fed into an LSTM model with a sliding window of four kinematic variables with 25 samples or time steps: LA and AV for thigh and shank. The LSTM was tested to forecast five samples (i.e., time steps) of the four kinematic input variables. To attain generalisation, the model was trained on a dataset of 2,665 strides from five participants and evaluated on a test set of 1 stride from a sixth participant. The LSTM model learned the lower limb kinematic trajectories using the training samples and tested for generalisation across participants. The forecasting horizon suggested higher model reliability in predicting earlier future trajectories. The mean absolute error (MAE) was evaluated on each variable across the single tested stride, and for the five-sample forecast, it obtained  $0.047 \text{ m/s}^2$  thigh LA,  $0.047 \text{ m/s}^2$  shank LA,  $0.028 \text{ deg/s}$  thigh AV and  $0.024 \text{ deg/s}$  shank AV. All predicted trajectories were highly correlated with the measured trajectories, with correlation coefficients greater than 0.98. The motion prediction model may have a wide range of applications, such as mitigating the risk of falls or balance loss and improving the human–machine interface for wearable assistive devices.

**Keywords:** LSTM, neural networks, machine learning, forecasting, gait, walking

## INTRODUCTION

An increasingly useful application of machine learning (ML) is in predicting features of human actions. If it can be shown that algorithm inputs related to actual movement mechanics can predict a limb or limb segment's future trajectory, a range of apparently intractable problems in movement science could be solved. One such problem is how to anticipate movement characteristics that can

predict the risk of tripping, slipping or balance loss. Previous work has investigated balance control using wearable sensors to estimate the body's centre of mass (CoM) trajectory (Fuschillo et al., 2012). The Internet of things (IoT) has also created a new paradigm of algorithms and systems to predict and subsequently apply interventions to prevent falls (Rubenstein, 2006; Tao and Yun, 2017; Nait Aicha et al., 2018). Perhaps the most valuable motion-prediction application is in the design and control of wearable assistive devices, such as prostheses, bionics and exoskeletons, in which smart algorithms can ensure safer, more efficient integration of the assistive device with the user's natural limb and body motion (Lee et al., 2017; Rupal et al., 2017).

Previous computational methods have investigated motion trajectory prediction, using position-time inputs and their derivatives (velocity and acceleration). Lower limb trajectory prediction has been implemented in rehabilitation robotics (Duschau-Wicke et al., 2009). Using inverse dynamics, Wang et al. (2011) designed a model for foot trajectory generation using a predefined pelvic trajectory and line fitting 10 data points from a single gait cycle. Also using inverse dynamics, Ren et al. (2007) predicted all segment motions and ground reaction forces from the average forward velocity gait, double stance duration and gait cycle period. Another technique was implemented in the Lower Extremity Powered Exoskeleton (LOPES) device to emulate the trajectories from a healthy limb to the impaired limb (Vallery et al., 2008). Prediction of the lower limb joint angles future trajectory that effectively leads to foot events timing was also investigated in the works of Aertbeliën and De Schutter (2014) and Tanghe et al. (2019) using probabilistic principal component analysis (PPCA).

Recent methods implemented ML algorithms such as artificial neural networks (ANNs) to identify subject gait trajectories to recognise neurological as well as pathological gait patterns (Alaqtash et al., 2011; Horst et al., 2019). Artificial neural networks were also used to improve user intention detection in wearable assistive devices (Jung et al., 2015; Islam and Hsiao-Wecksler, 2016; Moon et al., 2019; Trigili et al., 2019). A variation of ANNs called generalised regression neural networks (GRNNs) was found to be capable of predicting lower limb joint angles (hip, knee and ankle) from the linear acceleration (LA) and angular velocity (AV) of foot and shank segments (Findlow et al., 2008), or from subject gait and anthropomorphic parameters (Luu et al., 2014). Recurrent neural networks (RNNs) and convolutional neural networks (CNNs), which are classes of ANNs, were able to classify human motions and activities (Murad and Pyun, 2017; Han et al., 2019).

Long short-term memory (LSTM) neural networks are a subclass of RNNs, and they have proven success in modelling a wide range of sequence problems, including human activity recognition (Ordóñez and Roggen, 2016), gait diagnosis (Zhao et al., 2018), falls prediction (Nait Aicha et al., 2018) and gait event detection (Kidziński et al., 2019). Long short-term memory autoencoder is an architecture of LSTM that has been implemented in an array of applications such as language translation (Ding et al., 2018) and in forecasting of video frames (Srivastava et al., 2015), weather (Gangopadhyay et al., 2018; Reddy et al., 2018; Poornima and Pushpalatha, 2019), traffic

flow (Park et al., 2018; Wei et al., 2019) and stock prices (Li et al., 2018).

Given the potential of lower limb trajectory prediction, no previous work was found that utilised ML techniques to predict future lower limb trajectories using simulated inertial measurement data, which could have a profound impact on human movement science. Simulated measurement data such as the kinematics output from inertial measurement units (IMUs; i.e., LA and AV) offer the opportunity to transcend a predictive model outside the laboratory settings. The aim of this work was to determine whether the kinematics of lower limb trajectories during walking could be reliably extrapolated using LSTM autoencoder neural networks. It was hypothesised that an LSTM autoencoder could reliably forecast multiple time-step trajectories of the lower limb kinematics.

## MATERIALS AND METHODS

### Collection Protocol

Ethics approval was granted by the Department of Defence and Veterans' Affairs Human Research Ethics Committee and Victoria University Human Research Ethics Committee (Protocol 852-17). All participants signed a consent form and volunteered freely to participate. Walking data were obtained from six male participants ( $22 \pm 2$  years old,  $1.77 \pm 0.02$  m in height,  $82 \pm 4$  kg in mass) who walked for 10 min at 5 km/h on a 0% gradient treadmill. A set of 25 retroreflective markers were attached to each participant in the form of clusters (Findlow et al., 2008). Each cluster comprised a group of individual markers that represent a single body segment (e.g., shank). That included left and right foot (three markers), left shank (four markers), right shank (five markers), left thigh (three markers), right thigh (four markers) and pelvis (three markers). The 3D position of each cluster was tracked using a 14-camera motion analysis system (Vicon Bonita, Version 2.8.2) at 150 Hz. Virtual markers were also established to calibrate the position and orientation of the lower body skeletal system (Garofolini, 2019). Three-dimensional ground reaction force and moment data were collected from a force-plate instrumented treadmill (Advanced Mechanical Technology, Inc., Watertown, MA, United States) at 1,500 Hz.

### Dataset Processing

Recorded 3D positional and force data were processed using Visual 3D (C-motion, Inc, Version 6) to obtain LA and AV. In Visual 3D (**Figure 1**), the data were firstly filtered using a low-pass digital filter with a 15-Hz cut-off frequency and normalised to mean 0 and standard deviation 1 using standard scores (z-scores), preserving the original data properties. Secondly, raw AV was obtained as the derivative of Euler/Cardan angles (C-motion, 2015), and the raw LA was generated by the double derivative of segment linear displacement using built-in pipeline commands (Hibbeler, 2007). These data (LA and AV) simulated the kinematic outputs from body-mounted IMUs widely used in wearable assistive devices, monitoring lower limb kinematics (Santhiranayagam et al., 2011; Lai et al., 2012), controlling powered actuators (Lee et al., 2017) and recognising human

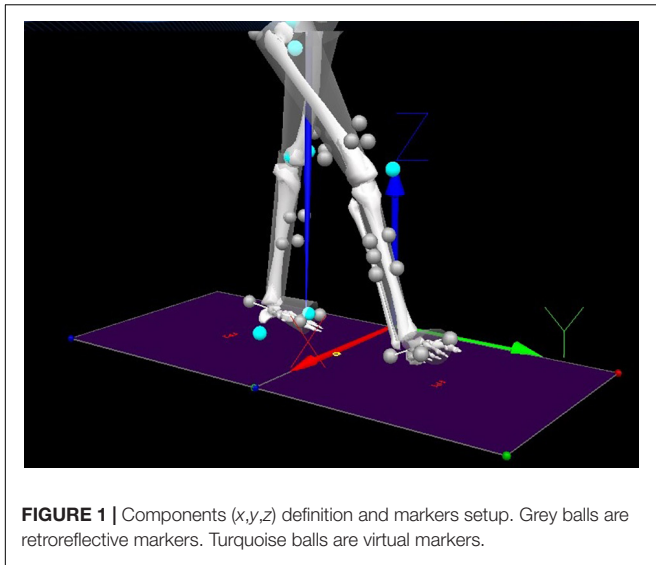


**FIGURE 1** | Components (x,y,z) definition and markers setup. Grey balls are retroreflective markers. Turquoise balls are virtual markers.

actions (Van Laerhoven and Cakmakci, 2000; Jimenez-Fabian and Verlinden, 2012; Koller et al., 2016).

As shown in **Figure 1**, the main direction of movements included the translation along the Y-axis (i.e., LA) and the rotation along the X-axis (i.e., AV), which were used for LSTM prediction, resulting in four predictor variables: (i)  $Y_1$  thigh LA, (ii)  $Y_2$  shank LA, (iii)  $X_3$  thigh AV and (iv)  $X_4$  shank AV. The thigh segment was defined as the reference frame to the shank, and the shank segment was defined as the reference frame to the thigh (**Figure 2**).

## Dataset Description

The data were divided into training and testing sets. The training set comprised 2,665 strides from five participants that included four kinematic feature variables ( $Y_1$ ,  $Y_2$ ,  $X_3$ ,  $X_4$ ) (N-columns) and 453,060 samples or time steps (M-rows) for each variable. To attain generalisation, a testing set was used that comprised of a single stride from the sixth participant with the four feature variables and 170 samples for each variable.

## Time Series Transformation to a Supervised Learning Problem

The inputs to the LSTM were four parallel feature variables and the outputs were the successive four parallel feature variables. Prior to feeding into the LSTM model, the  $M \times N$  training and testing datasets were transformed to a 3D dataset using a sliding window technique (Banos et al., 2014). The sliding window comprised of an input window, an output window and a sliding size. The input window consists of  $M$  samples and  $N$  features, so as the output window. The input window is the input data to the LSTM model, and the output window is the future prediction output from the LSTM model. The sliding size is how much of  $M$  samples that both the input and the output windows are sliding forward with (see **Figure 3**). The sliding size ( $M$  samples) was always equal to the output size.

## Recurrent Neural Networks

While multiple layer perceptrons (MLPs) consider all inputs as independent, RNNs are designed to work with time series data (Ordóñez and Roggen, 2016). RNNs are a class of ANN architecture designed specifically to model sequence problems and exploit the temporal correlations between input data samples (Elman, 1990; Murad and Pyun, 2017). It contains feedback connections between each of its units, which enables the network to relate all the previous inputs to its outputs (**Figure 4**).

The forward pass equations from the inputs to the outputs of the RNN are given as follows.

For the hidden units:

$$a_h^t = \sum_{i=1}^I w_{ih} x_i^t + \sum_{h'=1}^H w_{h'h} b_{h'}^{t-1} \quad (1)$$

and differentiable activation functions are then applied:

$$b_h^t = \theta_h(a_h^t) \quad (2)$$

The network input to output units:

$$a_k^t = \sum_{h=1}^H w_{hk} b_h^t \quad (3)$$

where

$a_h^t$  is the sum of inputs to unit  $h$  at time  $t$ ,  $b_h^t$  is the activation of unit  $h$  at time  $t$ ,  $\theta_h$  is the non-linear and differentiable activation function of unit  $h$ ,  $a_k^t$  is the sum of all inputs to output unit  $k$  at time  $t$ ,  $x_i^t$  is the input  $i$  at time  $t$ ,  $w_{ih}$  is the connection weights between input unit  $i$  and hidden unit  $h$ ,  $w_{h'h}$  is the connection weights between the previous hidden state  $h'$  and itself  $h$  and  $w_{hk}$  is the connection weights between the hidden state  $h$  and the output unit  $k$ . Bias was neglected for simplicity.

## LSTM Networks

As the input data propagates through the standard RNN's hidden connections to the output units, it either slowly attenuates or amplifies exponentially, referred to, respectively, as vanishing or exploding gradients (Bengio et al., 1994; Hochreiter et al., 2001). The problems with this approach are that the vanishing gradient prevents the network from learning long-term dependencies and the exploding gradient leads to weights oscillation. These difficulties have been addressed using gradient norm clipping to tackle the exploding gradient and a soft constraint to deal with the vanishing gradient (Pascanu et al., 2013). The LSTM design addresses these problems by maintaining a memory cell  $C$  (**Figure 5**) that enables the network to retain information over a longer period by using an explicit gating mechanism (Hochreiter and Schmidhuber, 1997; Graves, 2012; Karpathy et al., 2015).

Each LSTM cell has an input gate, forget gate, and output gate. The input gate dictates the information used to update the memory state, and the forget gate decides which information to discard or remove from the cell. The final gate specifies the information to output based on the cell input and memory. All gates are designed such that information is exchanged from inside and outside the block (**Figure 5**). Furthermore, each

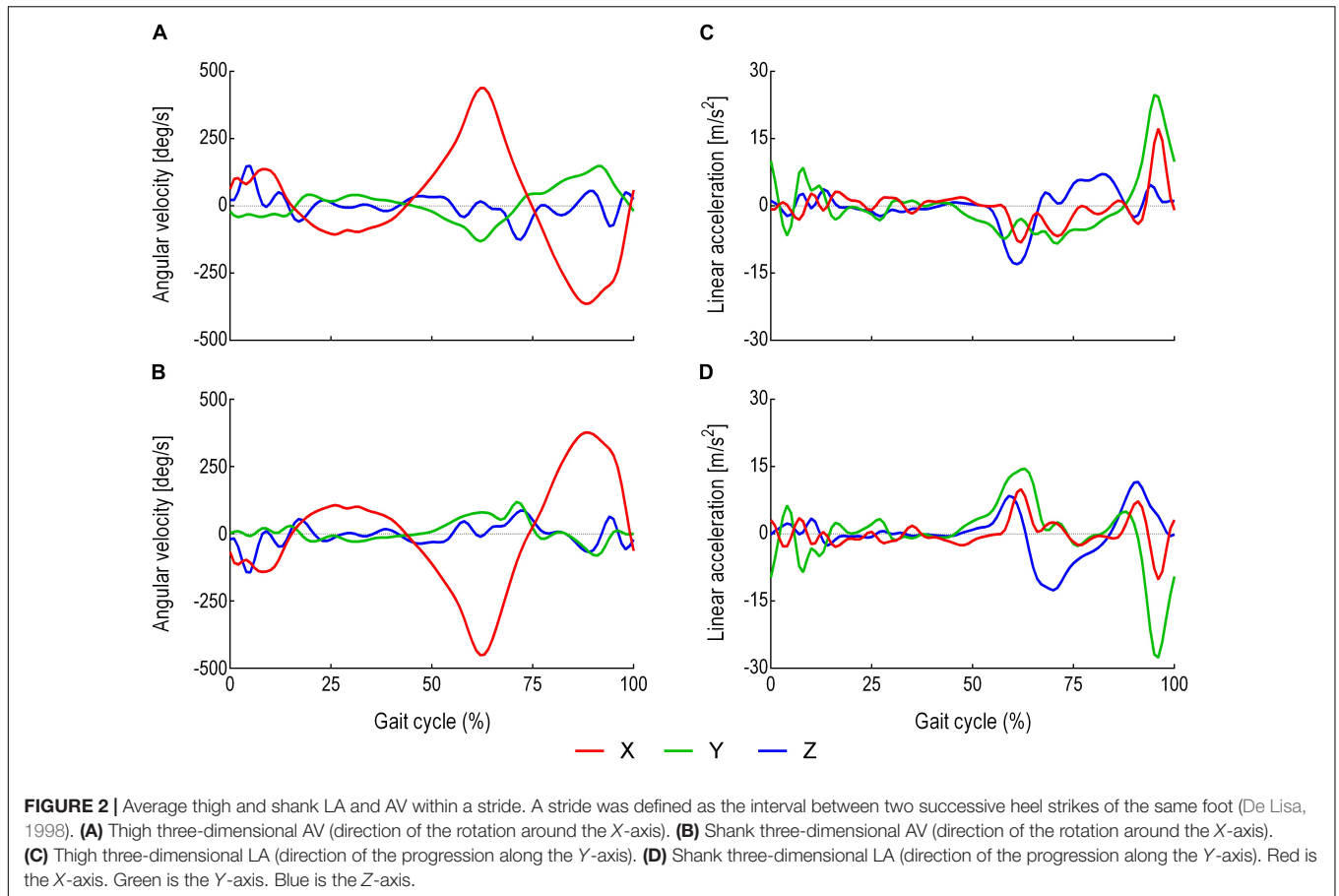


**FIGURE 2 |** Average thigh and shank LA and AV within a stride. A stride was defined as the interval between two successive heel strikes of the same foot (De Lisa, 1998). **(A)** Thigh three-dimensional AV (direction of the rotation around the X-axis). **(B)** Shank three-dimensional AV (direction of the rotation around the X-axis). **(C)** Thigh three-dimensional LA (direction of the progression along the Y-axis). **(D)** Shank three-dimensional LA (direction of the progression along the Y-axis). Red is the X-axis. Green is the Y-axis. Blue is the Z-axis.

memory block contains three peephole-weighted connections (dotted lines in **Figure 5**), which are the input weight  $w_{ci}$ , the output weight  $w_{co}$  and the memory state  $w_{c\phi}$ . The functions  $f$ ,  $g$  and  $h$  are usually tanh or logistic sigmoid activation functions (Graves, 2012). Below are the network equations (Graves, 2012) that govern the LSTM architecture used:

Input gates:

$$a_i^t = \sum_{i=1}^I w_{ii}x_i^t + \sum_{h=1}^H w_{hi}b_h^{t-1} + \sum_{c=1}^C w_{ci}s_c^{t-1} \quad (4)$$

$$b_i^t = f(a_i^t) \quad (5)$$

Forget gates:

$$a_\phi^t = \sum_{i=1}^I w_{i\phi}x_i^t + \sum_{h=1}^H w_{h\phi}b_h^{t-1} + \sum_{c=1}^C w_{c\phi}s_c^{t-1} \quad (6)$$

$$b_\phi^t = f(a_\phi^t) \quad (7)$$

Cells:

$$a_c^t = \sum_{i=1}^I w_{ic}x_i^t + \sum_{h=1}^H w_{hc}b_h^{t-1} \quad (8)$$

$$s_c^t = b_\phi^t s_c^{t-1} + b_i^t g(a_c^t) \quad (9)$$

Output gates:

$$a_o^t = \sum_{i=1}^I w_{io}x_i^t + \sum_{h=1}^H w_{ho}b_h^{t-1} + \sum_{c=1}^C w_{co}s_c^t \quad (10)$$

$$b_o^t = f(a_o^t) \quad (11)$$

Cell outputs:

$$b_c^t = b_o^t h(s_c^t) \quad (12)$$

where  $w_{ij}$  is the weight of the connection from unit  $i$  to unit  $j$ ;  $a_j^t$  is the network input to unit  $j$  at time  $t$ ;  $b_j^t$  is the activation of unit  $j$  at time  $t$ ;  $\iota$ ,  $\phi$ ,  $\omega$  respectively stand for the input gate, the forget gate and the output gate;  $C$  is the memory cell;  $w_{ci}$ ,  $w_{c\phi}$ ,  $w_{co}$  are peephole weights;  $s_c^t$  is the state of cell  $C$  at time  $t$ ;  $f$  is the input, output and forget gates activation function;  $g$  and  $h$  are the cell input and output activations, respectively;  $I$  is the number of inputs;  $H$  is the number of cells in the hidden layer; and index  $h$  is the cell outputs from other blocks in the hidden layer. Bias was neglected for simplicity.

### Design of the LSTM Model

The implemented model was based on the autoencoder LSTM, a neural network architecture composed of an encoder and a decoder (Ding et al., 2018). The encoder encodes the input variable length vector into a fixed length feature

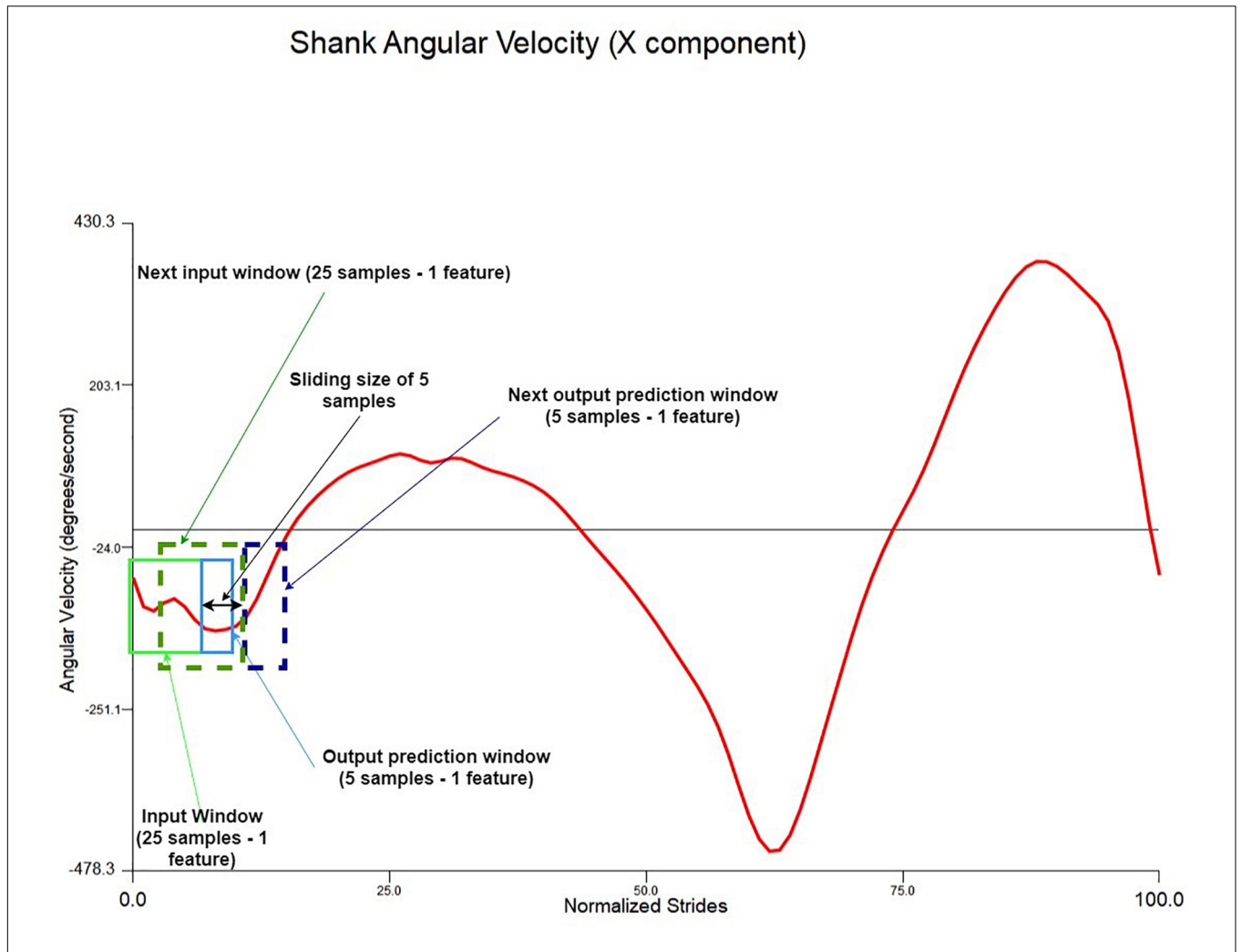


**FIGURE 3 |** Sliding window illustration example using the normalised shank angular velocity X-axis component (one feature). The window in this model is 25 samples and four features and the prediction outputs are five samples of four features.

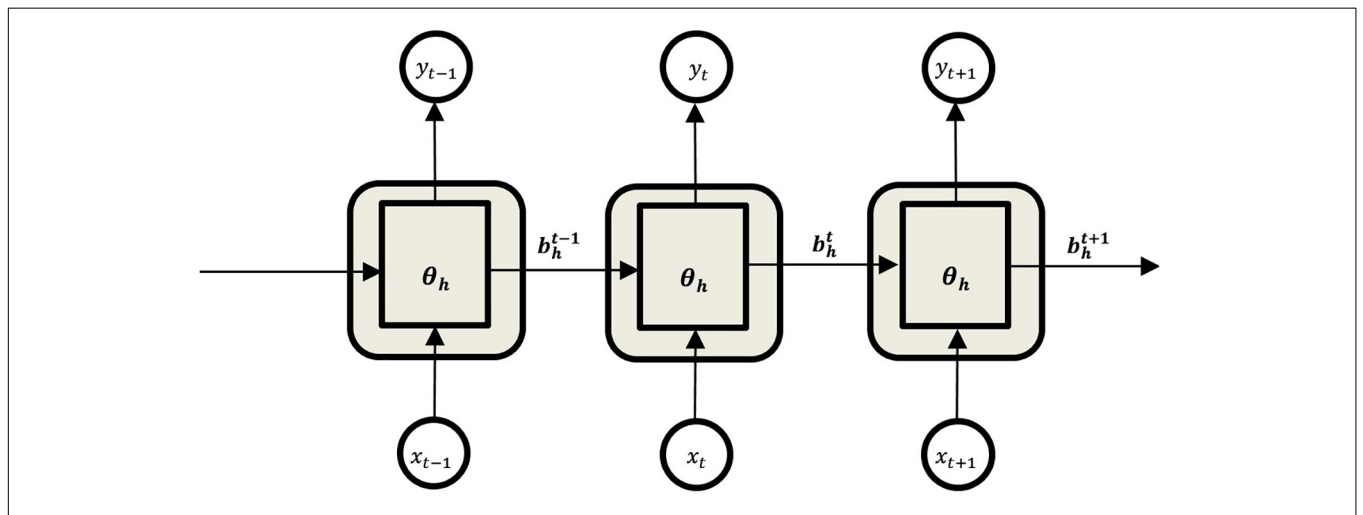


**FIGURE 4 |** Unfolded structure of the Recurrent Neural Network.

vector that captures the attributes of the variable length vector. The LSTM decoder decodes the encoded fixed length feature vector back into a variable length vector (Figure 6). The final layer is a fully connected dense (feedforward) mechanism for outputting predictions. The network weights and biases were updated at the end of each batch using an adaptive moment estimation (Adam) optimisation algorithm (Kingma and Ba, 2014) with mean absolute error (MAE) as an optimisation criterion. A single batch consists of 100 input/output windows. The activation for all LSTM layers was set to a rectified rectilinear unit (ReLU) activation function (Nair and Hinton, 2010). The LSTM autoencoder model was implemented in Google Colab as well as Amazon Web Services (AWS) using Python 3 (Libraries: Keras, Numpy, Pandas and Scikit learn).

### Evaluation Metrics

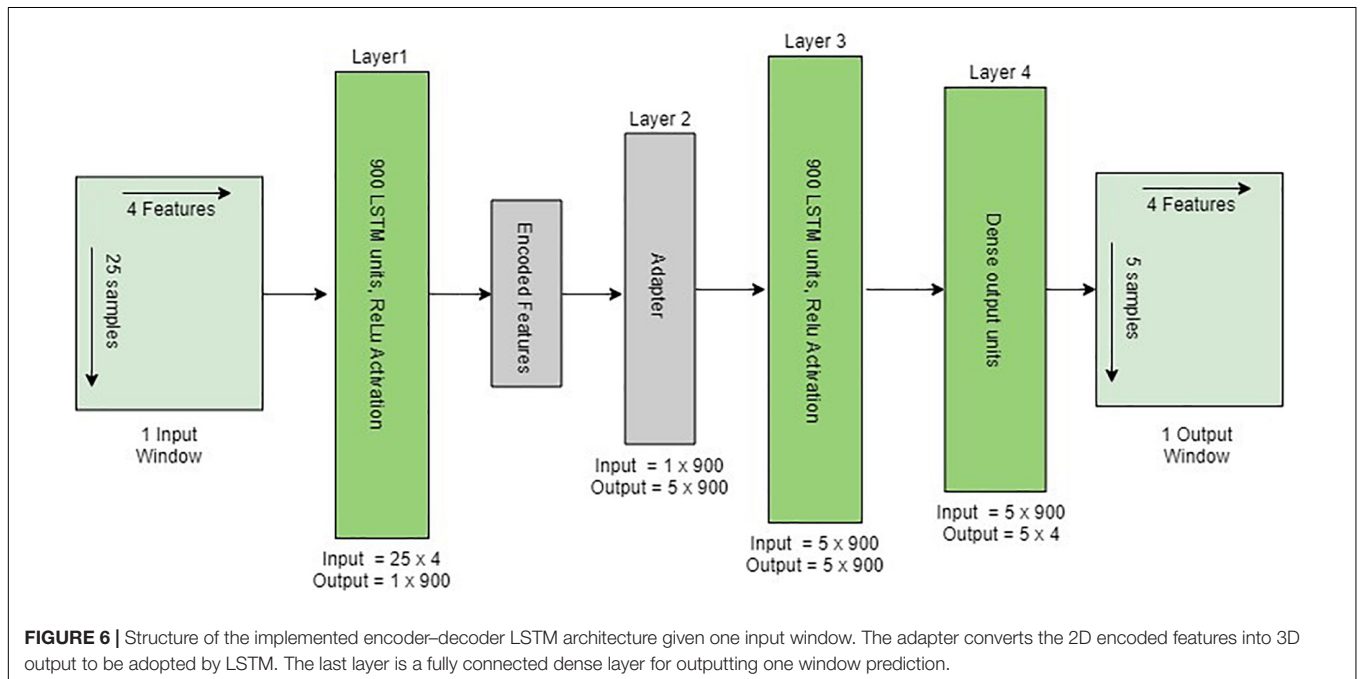
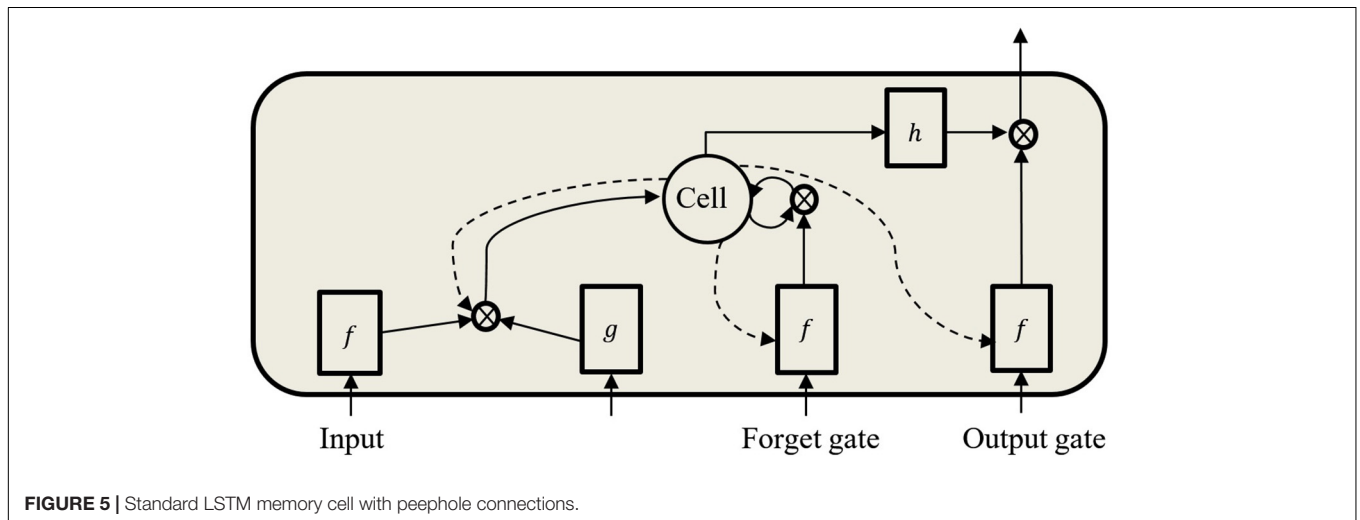
To evaluate the network quality, three parameters were considered to calculate how closely the network predicted variable trajectories  $\hat{y}_j (Y_1, Y_2, X_3, X_4)$  were to the actual variable trajectories  $y_j (Y_1, Y_2, X_3, X_4)$  across the  $n$  samples:

1. MAE given as:

$$MAE = \frac{1}{n} \sum_{j=1}^n |y_j - \hat{y}_j| \tag{13}$$

2. Mean squared error (MSE) given as:

$$MSE = \frac{1}{n} \sum_{j=1}^n (y_j - \hat{y}_j)^2 \tag{14}$$



3. Correlation coefficient (CC) given as:

$$P = \frac{\text{cov}(y, \hat{y})}{\text{std}(y) \times \text{std}(\hat{y})} \quad (15)$$

where  $\text{std}()$  is the standard deviation and  $\text{cov}(y, \hat{y})$  is the covariance between variables  $y$  and  $\hat{y}$ .

## RESULTS

Using the sparse grid search approach, the model's hyperparameters were tuned to determine the optimum model design (least MAE), including the number of epochs, batch size, layers and cells. The optimum model was then trained for 50 epochs (repetitions), and performance evaluated on the test set using MAE, MSE and the CC. The test set was a single stride that consisted of 170 samples. Initial 25 samples were used from the preceding cycle in order to start predicting the trajectories of the single stride.

### Model Performance With Different Input Window Sizes

The size of the input window was varied eight times at five sample intervals (5–40 samples) to demonstrate the optimum input window size (least error). The output sliding window was fixed to five samples prediction. The model performance is shown in **Figure 7** where the impact of each input window size on the prediction of each variable is computed.

### Model Performance With Five Samples Prediction

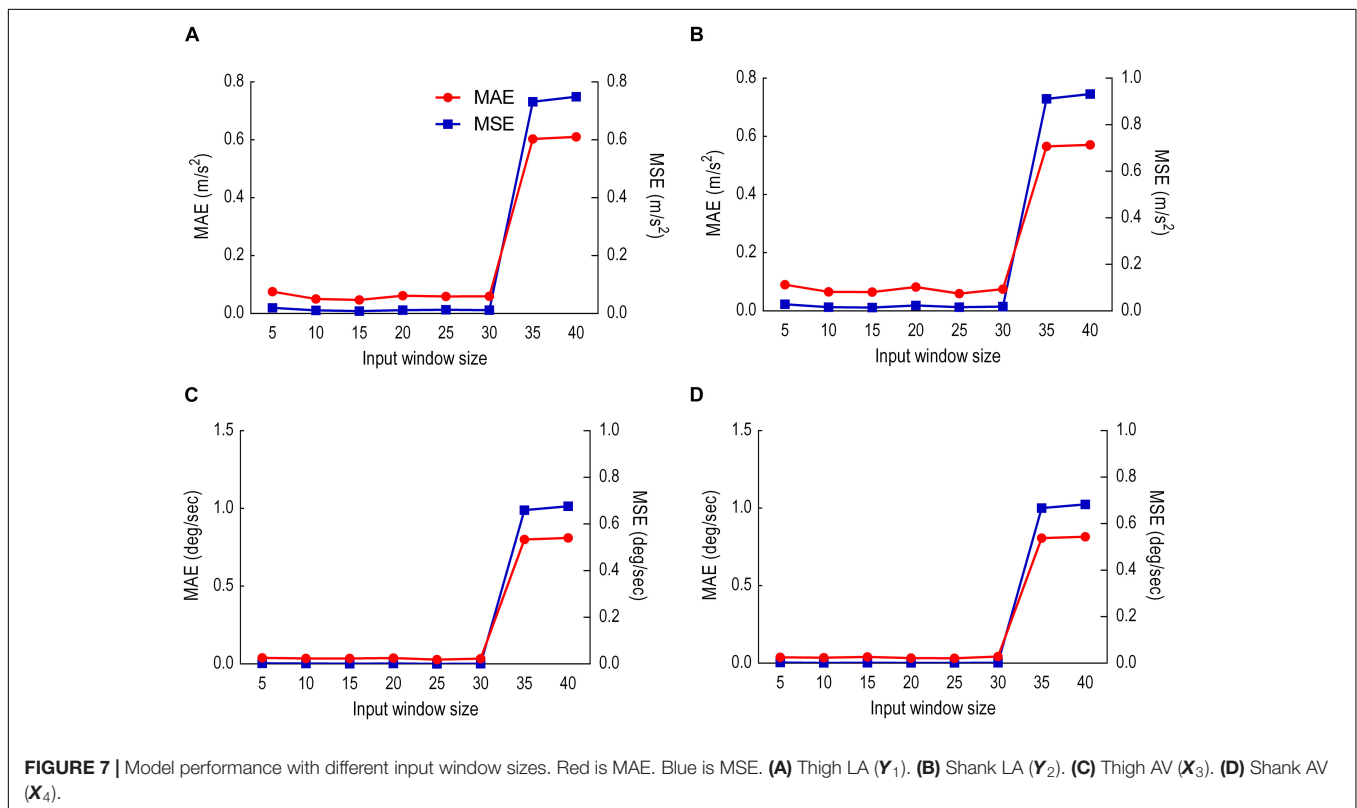
This sliding window comprised of 25 samples input and 5 samples prediction output. Results were given in two analyses: (i) predicted versus actual trajectories including the absolute error (AE) for each sample in the first output window (**Figure 8**) and for the whole gait cycle (**Figure 9**) and (ii) performance metrics (MAE, MSE and CC) for the first window of five samples (**Table 1**) and for all windows combined (**Table 2**).

### Model Performance With 10 Samples Prediction

This sliding window comprised of 25 samples input, 10 samples prediction output. **Figure 10** illustrates the results as predicted versus the actual trajectories including the AE for each sample in the first output window, whereas **Figure 11** displays the results for the whole gait cycle. Performance metrics (MAE, MSE and CC) for the first window of 10 samples are presented in **Table 3** and for all windows combined in **Table 4**.

## DISCUSSION

Our aim was to develop and evaluate an LSTM autoencoder model to predict the trajectories of four kinematic variables ( $Y_1$ ,  $Y_2$ ,  $X_3$ ,  $X_4$ ), simulating the output from wearable sensors (IMU). The predicted kinematic feature variables, LA and AV, for the shank and thigh were reliably predicted up to 10 samples or



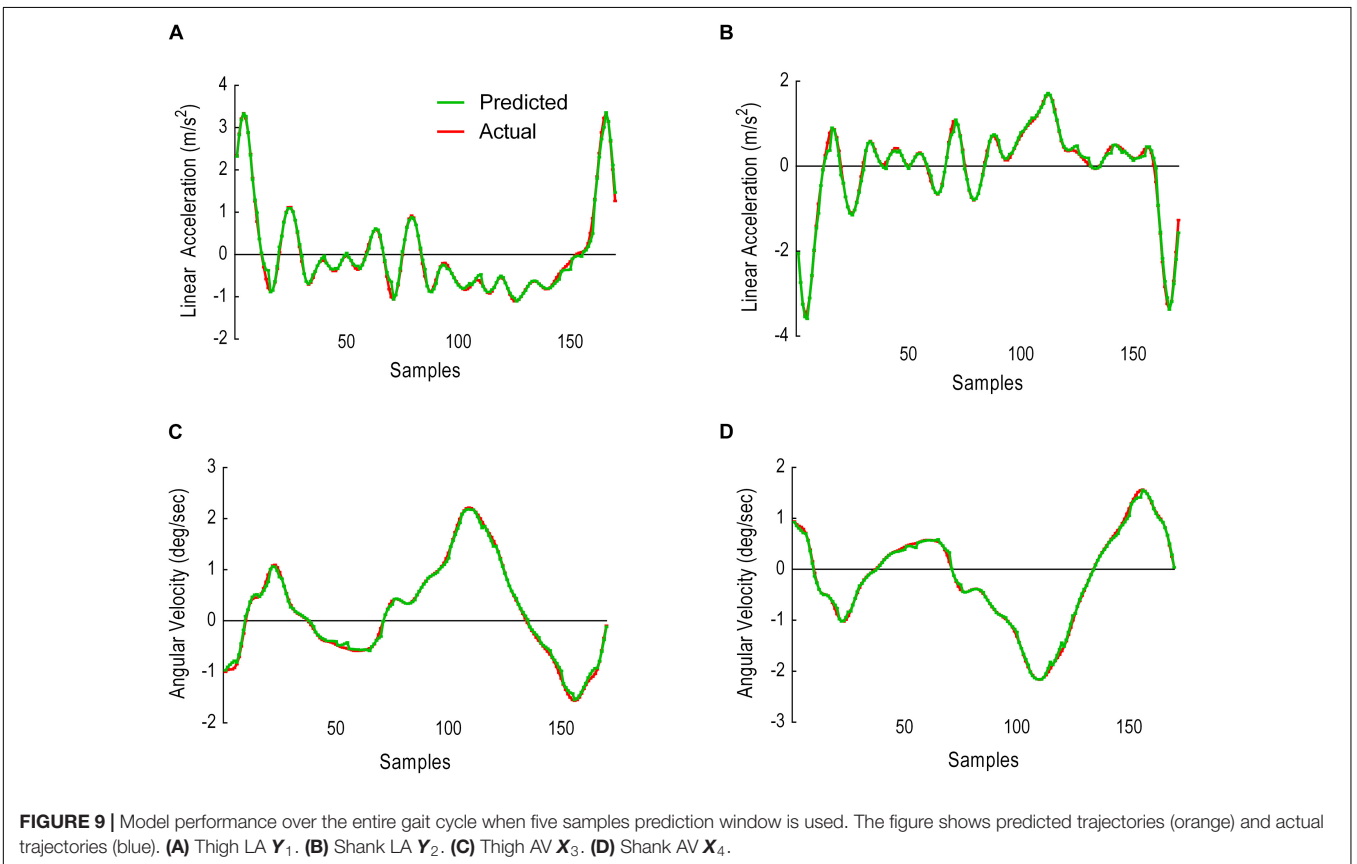
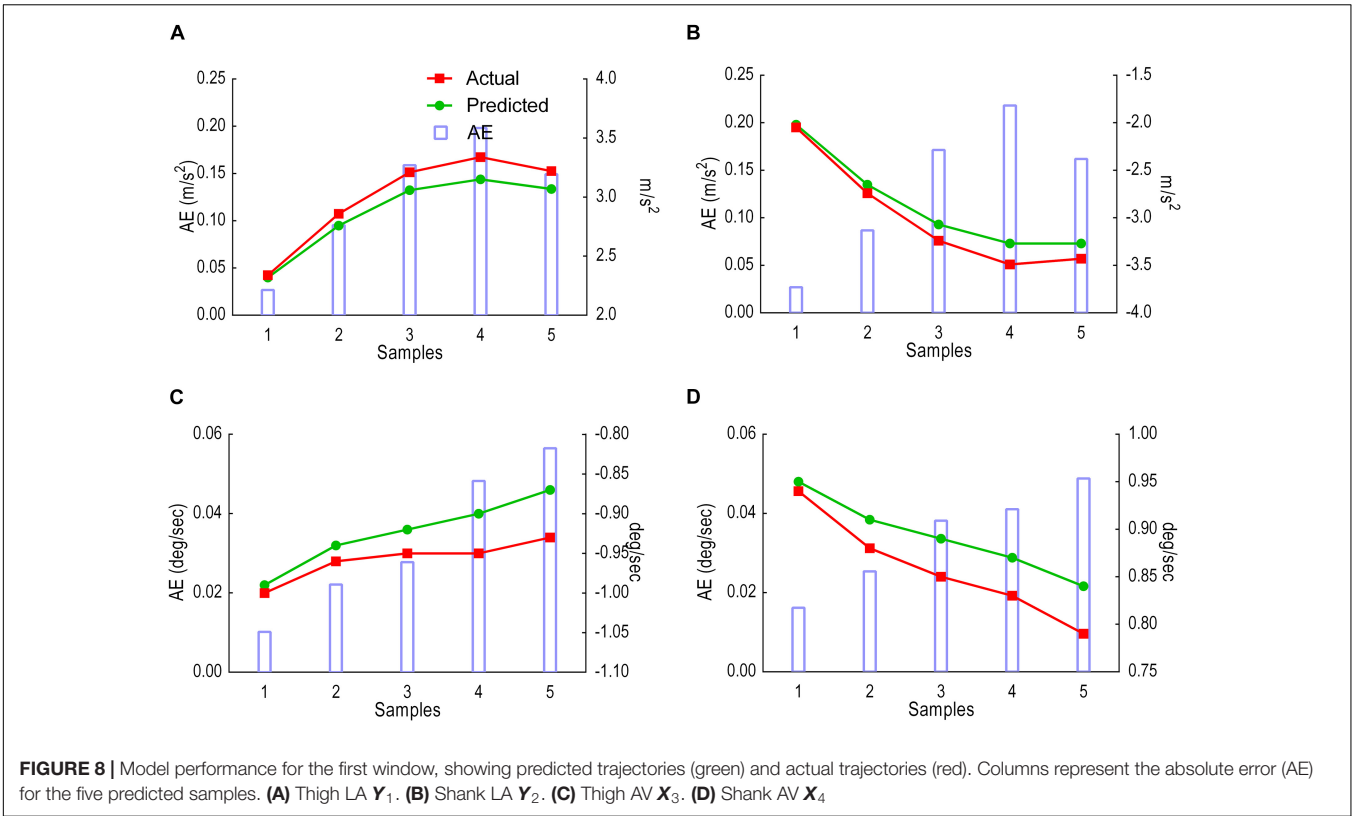


**TABLE 1** | Model performance for predicting the first five stride samples.

| Feature | MAE                    | MSE                    | CC   |
|---------|------------------------|------------------------|------|
| $Y_1$   | 0.125 m/s <sup>2</sup> | 0.019 m/s <sup>2</sup> | 0.99 |
| $Y_2$   | 0.133 m/s <sup>2</sup> | 0.022 m/s <sup>2</sup> | 0.99 |
| $X_3$   | 0.032 deg/s            | 0.001 deg/s            | 0.98 |
| $X_4$   | 0.033 deg/s            | 0.001 deg/s            | 0.99 |

**TABLE 2** | Model performance for predicting the complete stride using an input window size of 25 samples and an output window size of 5 samples.

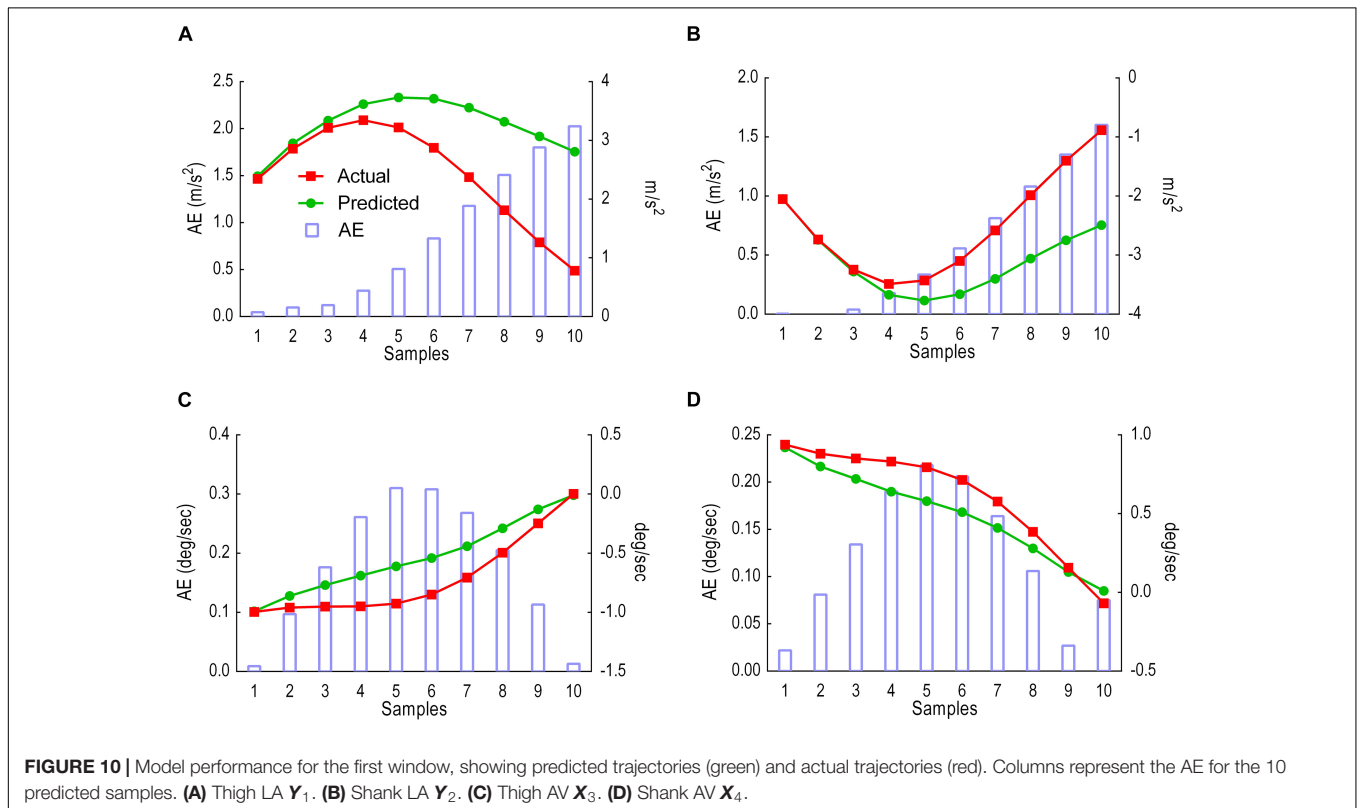
| Feature | MAE                    | MSE                    | CC   |
|---------|------------------------|------------------------|------|
| $Y_1$   | 0.047 m/s <sup>2</sup> | 0.006 m/s <sup>2</sup> | 0.99 |
| $Y_2$   | 0.047 m/s <sup>2</sup> | 0.006 m/s <sup>2</sup> | 0.99 |
| $X_3$   | 0.028 deg/s            | 0.001 deg/s            | 0.99 |
| $X_4$   | 0.024 deg/s            | 0.001 deg/s            | 0.99 |

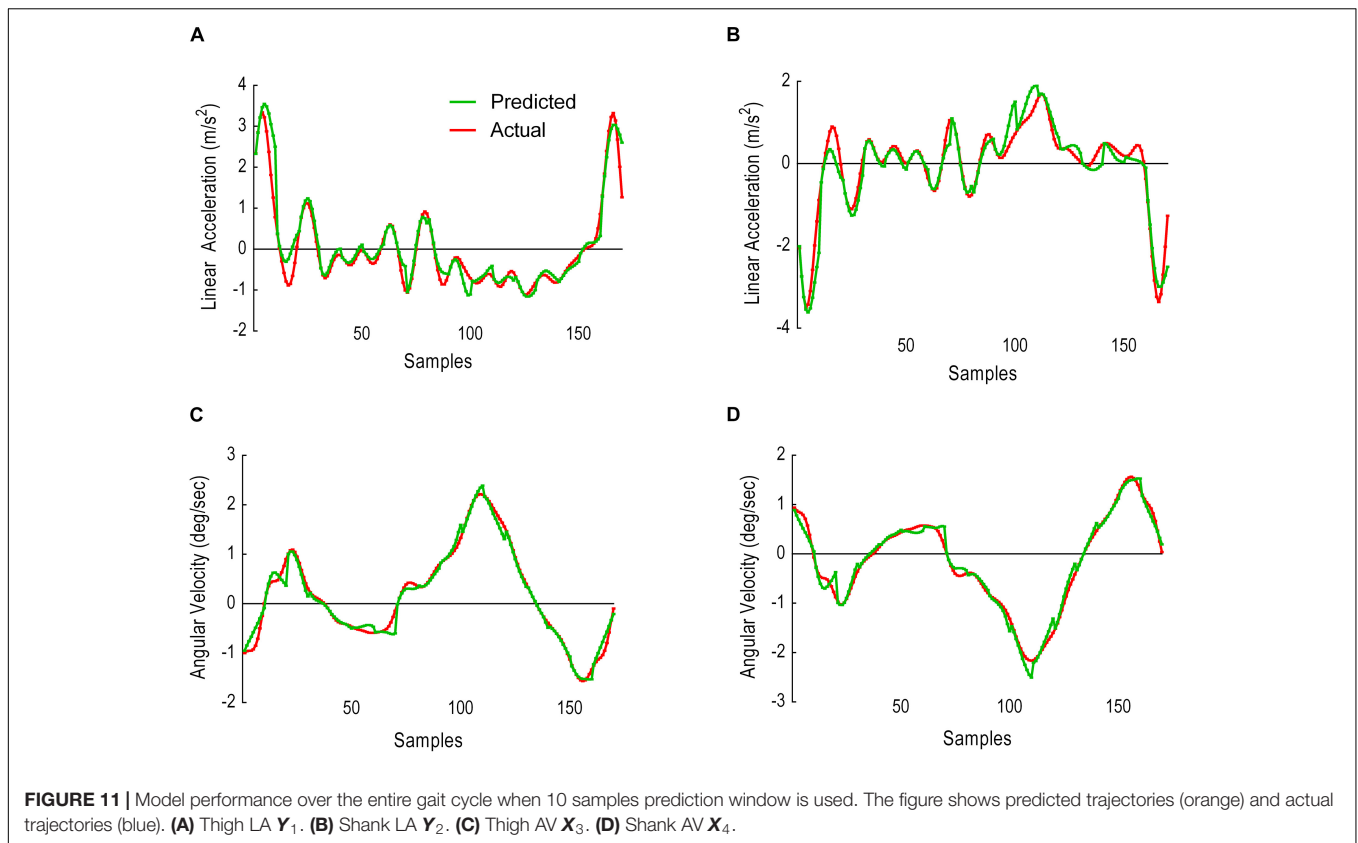
time steps, i.e., up to 60 ms in the future. A 60-ms prediction of future trajectories adds a feedforward term to an assistive device controller rather than being reactive and predominantly relying on feedback terms (i.e., sensory information; Tanghe et al., 2019). This enables the assistive device to adapt to changes in human gait, allowing smoother synchronisation with user intentions and minimising interruptions when the user changes their movement pattern (Elliott et al., 2014; Zhang et al., 2017; Ding et al., 2018; Zaroug et al., 2019). A known future trajectory might also monitor the risk of balance loss, tripping and falling, in which impending incidents can be remotely reported for early intervention (Begg and Kamruzzaman, 2006; Begg et al., 2007;

Nait Aicha et al., 2018; Hemmatpour et al., 2019; Naghavi et al., 2019). Since 60 ms falls in the range of slow (60–120 ms) and fast (10–50 ms) twitch motor units (Winter, 2009), this would enable wearable devices such as IMUs to alert (e.g., by audio/visual signal) an elderly user about an imminent risk of tripping and potentially gives them a chance to adjust their gait accordingly.

In contrast to the 1- to 2-s window for human activity recognition proposed by Banos et al. (2014), no window has previously been suggested for forecasting human movement trajectories (Banos et al., 2014). In addressing this limitation, the present project input and output sliding windows were tested to discover the optimum prediction model. The input window was varied from 5 to 40 samples, whereas the output window was fixed at 5 samples during each test. Results showed that both MAE and MSE increased after 25 samples for all variables except for the thigh LA  $Y_1$  in which 15 samples scored lowest. Due to the majority score, 25 samples were fixed, and the output window size manipulated between 5 and 10 samples. Prediction error MAE and MSE gradually increased across the first 5 and 10 sample prediction windows, indicating better prediction early in the stride cycle. This prediction horizon suggests that an output window exceeding five samples may not be sufficiently reliable for forecasting gait trajectories. LA-predicted trajectories began to deviate earlier than AV, possibly due to the double derivative generating a noisier signal.

Across the stride cycle, an output window of 5 samples showed better model performance (lower MAE scores) than the 10-sample output window, particularly when there is less noise in the predicted signal for all variables. Predictions of five samples





for all variables achieved high CC (0.99) and maintained below MAE 0.048 deg/s and 0.029 m/s<sup>2</sup>. These result parameters are different from those of earlier work (Findlow et al., 2008; Luu et al., 2014). The difference is in the type of predicted data (lower limb joint angles of the hips, knees and ankles) and in the type of output, which was not a forecast, but rather a prediction of joint angles from the LA and AV of the lower limb segments. Nonetheless, the work presented in this paper showed higher CC values than the earlier works (Findlow et al., 2008; Luu et al., 2014) at the intersubject test. Overall, the LSTM model was able

to learn the trajectories and generalise across participants. This generalisation is invaluable to adapt algorithm performance to a wider population in assistive devices, particularly when each user responds differently to the same device (Zhang et al., 2017).

This study was limited to the walking movement with a 60-ms prediction horizon and healthy participants walking at 5 km/h. The speed was imposed to report the feasibility of whether lower limb future trajectories are predictable. In future work, the model would be developed to accommodate a higher gait variance from more participants and other populations, such as female, older adults and individuals with gait disorders walking at their preferred as well as slower and faster speeds (Winter, 1991). More participants (i.e., stride examples) would potentially improve the model performance to predict trajectories above 60 ms and also provide a more comprehensive validation set, a strategy to find the optimum number of epochs and avoid model overfitting (Graves, 2013). The LSTM autoencoder can be made flexible by automating the input/output window size depending on the detected human activity, which revamps the LSTM capacity to recognise a wider range of human action transitions, such as slow to fast walking. Although LSTM autoencoders described here were able to learn and predict future data points, further research is needed to explore other LSTM architectures, such as bi-directional LSTM (Graves and Schmidhuber, 2005). Bi-directional LSTM can be useful in forward and backward modelling of sequential data, giving further insights into sequential pattern modelling (Liu and Guo, 2019; Zhang et al., 2019).

**TABLE 3 |** Model performance for predicting the first 10 stride samples.

| Feature | MAE                    | MSE                    | CC   |
|---------|------------------------|------------------------|------|
| $Y_1$   | 0.839 m/s <sup>2</sup> | 1.206 m/s <sup>2</sup> | 0.52 |
| $Y_2$   | 0.596 m/s <sup>2</sup> | 0.667 m/s <sup>2</sup> | 0.75 |
| $X_3$   | 0.176 deg/s            | 0.042 deg/s            | 0.94 |
| $X_4$   | 0.122 deg/s            | 0.019 deg/s            | 0.96 |

**TABLE 4 |** Model performance for predicting the complete stride using an input window size of 25 samples and an output window size of 10 samples.

| Feature | MAE                    | MSE                    | CC   |
|---------|------------------------|------------------------|------|
| $Y_1$   | 0.170 m/s <sup>2</sup> | 0.096 m/s <sup>2</sup> | 0.96 |
| $Y_2$   | 0.202 m/s <sup>2</sup> | 0.096 m/s <sup>2</sup> | 0.96 |
| $X_3$   | 0.079 deg/s            | 0.015 deg/s            | 0.98 |
| $X_4$   | 0.086 deg/s            | 0.014 deg/s            | 0.98 |

## CONCLUSION

This study confirmed the possibility of predicting the future trajectories of human lower limb kinematics during steady-state walking, i.e., thigh AV, shank AV, thigh LA and shank LA. An input window of 25 samples and an output window of 5 samples were found to be the optimum sliding window sizes for future trajectories prediction in LSTM. The LSTM model prediction horizon was better able to forecast the earlier sample trajectories and was also able to learn trajectories across different participants. Further work is required to systematically investigate the effects of tuning the model's hyperparameters, including layers and cells, optimisation algorithms and learning rate. Future work could focus on automating input/output window size and using predicted kinematics to identify discrete gait cycle events such as heel strike and toe-off (Kidziński et al., 2019). Long short-term memory methods for human movement prediction have applications to balance loss, falls prevention and controlling of assistive devices.

## DATA AVAILABILITY STATEMENT

The datasets generated for this study are available on request to the corresponding author.

## REFERENCES

- Aertbeliën, E., and De Schutter, J. (2014). "Learning a predictive model of human gait for the control of a lower-limb exoskeleton," in *Proceedings of the 5th IEEE RAS/EMBS International Conference on Biomedical Robotics and Biomechatronics* (Piscataway, NJ: IEEE). doi: 10.1109/TCYB.2020.2972582
- Alaqtash, M., Sarkodie-Gyan, T., Yu, H., Fuentes, O., Brower, R., and Abdelgawad, A. (2011). "Automatic classification of pathological gait patterns using ground reaction forces and machine learning algorithms," in *Proceedings of the 2011 Annual International Conference of the IEEE Engineering in Medicine and Biology Society* (Piscataway, NJ: IEEE). doi: 10.1109/IEMBS.2011.6090063
- Banos, O., Galvez, J.-M., Damas, M., Pomares, H., and Rojas, I. (2014). Window size impact in human activity recognition. *Sensors* 14, 6474–6499. doi: 10.3390/s140406474
- Begg, R., Best, R., Dell'Oro, L., and Taylor, S. (2007). Minimum foot clearance during walking: strategies for the minimisation of trip-related falls. *Gait Posture* 25, 191–198. doi: 10.1016/j.gaitpost.2006.03.008
- Begg, R., and Kamruzzaman, J. (2006). Neural networks for detection and classification of walking pattern changes due to ageing. *Aust. Phys. Eng. Sci. Med.* 29, 188–195. doi: 10.1007/bf03178892
- Bengio, Y., Simard, P., and Frasconi, P. (1994). Learning long-term dependencies with gradient descent is difficult. *IEEE Trans. Neural Netw.* 5, 157–166. doi: 10.1109/72.279181
- C-motion (2015). *Joint Velocity*. Available online at: [https://c-motion.com/v3dwiki/index.php/Joint\\_Velocity](https://c-motion.com/v3dwiki/index.php/Joint_Velocity) (accessed January 2020).
- Cho, K., Van Merriënboer, B., Gulcehre, C., Bahdanau, D., Bougares, F., Schwenk, H., et al. (2014). Learning phrase representations using RNN encoder-decoder for statistical machine translation. *arXiv [Preprint]*. doi: 10.3115/v1/D14-1179
- De Lisa, J. A. M. D. (1998). *Gait Analysis in Science and Rehabilitation*. Available online at: <https://ia800206.us.archive.org/6/items/gaitanalysisinsc00joel/gaitanalysisinsc00joel.pdf>
- Ding, Y., Kim, M., Kuindersma, S., and Walsh, C. J. (2018). Human-in-the-loop optimization of hip assistance with a soft exosuit during walking. *Sci. Robot.* 3:eaar5438. doi: 10.1126/scirobotics.aaar5438
- Duschau-Wicke, A., von Zitzewitz, J., Caprez, A., Lunenburger, L., and Riener, R. (2009). Path control: a method for patient-cooperative robot-aided gait rehabilitation. *IEEE Trans. Neural Syst. Rehabil. Eng.* 18, 38–48. doi: 10.1109/TNSRE.2009.2033061
- Elliott, G., Marecki, A., and Herr, H. (2014). Design of a clutch-spring knee exoskeleton for running. *J. Med. Dev.* 8:031002.
- Elman, J. L. (1990). Finding structure in time. *Cogn. Sci.* 14, 179–211.
- Findlow, A., Goulermas, J., Nester, C., Howard, D., and Kenney, L. (2008). Predicting lower limb joint kinematics using wearable motion sensors. *Gait Posture* 28, 120–126. doi: 10.1016/j.gaitpost.2007.11.001
- Fuschillo, V. L., Bagalà, F., Chiari, L., and Cappello, A. (2012). Accelerometry-based prediction of movement dynamics for balance monitoring. *Med. Biol. Eng. Comput.* 50, 925–936. doi: 10.1007/s11517-012-0940-6
- Gangopadhyay, T., Tan, S. Y., Huang, G., and Sarkar, S. (2018). "Temporal attention and stacked LSTMs for multivariate time series prediction," in *Proceedings of the 32nd Conference on Neural Information Processing Systems (NIPS 2018)*, Montréal.
- Garofolini, A. (2019). *Exploring Adaptability in Long-Distance Runners: Effect of Foot Strike Pattern on Lower Limb Neuro-Muscular-Skeletal Capacity*. Footscray VIC: Victoria University.
- Graves, A. (2012). *Supervised Sequence Labelling With Recurrent Neural Networks*. Available online at: <http://books.google.com/books> (accessed September 12, 2019).
- Graves, A. (2013). Generating sequences with recurrent neural networks. *arXiv [Preprint]*. Available online at: <https://arxiv.org/abs/1308.0850> (accessed September 12, 2019).
- Graves, A., and Schmidhuber, J. (2005). Framewise phoneme classification with bidirectional LSTM and other neural network architectures. *Neural Netw.* 18, 602–610. doi: 10.1016/j.neunet.2005.06.042
- Han, B.-K., Ryu, J.-K., and Kim, S.-C. (2019). Context-Aware winter sports based on multivariate sequence learning. *Sensors* 19:3296. doi: 10.3390/s19153296
- Hemmatpour, M., Ferrero, R., Montrucchio, B., and Rebaudengo, M. (2019). A review on fall prediction and prevention system for personal devices: evaluation and experimental results. *Adv. Hum. Comput. Interact.* 2019, 1–12.
- Hibbeler, R. C. (2007). *Engineering Mechanics Dynamics SI Units*. Singapore: Pearson Education South Asia.
- Hochreiter, S., Bengio, Y., Frasconi, P., and Schmidhuber, J. (2001). *Gradient Flow in Recurrent Nets: the Difficulty of Learning Long-Term Dependencies, A Field Guide to Dynamical Recurrent Neural Networks*. Piscataway, NJ: IEEE Press.

## ETHICS STATEMENT

The studies involving human participants were reviewed and approved by Associate Professor Deborah Zion Chair of Victoria University Human Research Ethics Committee. The patients/participants provided their written informed consent to participate in this study.

## AUTHOR CONTRIBUTIONS

AZ wrote the manuscript and coded the ML model. AZ, DL and RB contributed to research and ML model design and analysis. KM and RB designed the biomechanics experiment. KM and AZ collected and analysed the biomechanics data. All authors provided critical feedback on the manuscript and read and approved the final manuscript.

## FUNDING

This research is jointly funded by the Victoria University (VU) and the Defence Science and Technology Group (DST Group), Melbourne, Australia.

- Hochreiter, S., and Schmidhuber, J. (1997). Long short-term memory. *Neural Comput.* 9, 1735–1780.
- Horst, F., Lapuschkin, S., Samek, W., Müller, K.-R., and Schöllhorn, W. I. (2019). Explaining the unique nature of individual gait patterns with deep learning. *Sci. Rep.* 9:2391. doi: 10.1038/s41598-019-38748-8
- Islam, M., and Hsiao-Weckler, E. T. (2016). Detection of gait modes using an artificial neural network during walking with a powered ankle-foot orthosis. *J. Biophys.* 2016:7984157. doi: 10.1155/2016/7984157
- Jimenez-Fabian, R., and Verlinden, O. (2012). Review of control algorithms for robotic ankle systems in lower-limb orthoses, prostheses, and exoskeletons. *Med. Eng. Phys.* 34, 397–408. doi: 10.1016/j.medengphy.2011.11.018
- Jung, J.-Y., Heo, W., Yang, H., and Park, H. (2015). A neural network-based gait phase classification method using sensors equipped on lower limb exoskeleton robots. *Sensors* 15:27738. doi: 10.3390/s151127738
- Karpathy, A., Johnson, J., and Fei-Fei, L. (2015). Visualizing and understanding recurrent networks. *arXiv [Preprint]*. doi: 10.1142/9789813207813\_0025
- Kidziński, L., Delp, S., and Schwartz, M. (2019). Automatic real-time gait event detection in children using deep neural networks. *PLoS One* 14:e0211466. doi: 10.1371/journal.pone.0211466
- Kingma, D. P., and Ba, J. (2014). Adam: a method for stochastic optimization. *arXiv [Preprint]*. Available online at: <https://arxiv.org/abs/1412.6980> (accessed September 12, 2019).
- Koller, J. R., Gates, D. H., Ferris, D. P., and Remy, C. D. (2016). “Body-in-the-loop” optimization of assistive robotic devices: a validation study,” in *Proceedings of the 12th Conference Robotics: Science and Systems XII*. Available online at: <http://www.roboticsproceedings.org/rss12/index.html>
- Lai, D. T., Taylor, S. B., and Begg, R. K. (2012). Prediction of foot clearance parameters as a precursor to forecasting the risk of tripping and falling. *Hum. Mov. Sci.* 31, 271–283. doi: 10.1016/j.humov.2010.07.009
- Lee, G., Kim, J., Panizzolo, F., Zhou, Y., Baker, L., Galiana, I., et al. (2017). Reducing the metabolic cost of running with a tethered soft exosuit. *Sci. Robot.* 2:eaan6708.
- Li, H., Shen, Y., and Zhu, Y. (2018). “Stock price prediction using attention-based multi-input lstm,” *Proceedings of the Asian Conference on Machine Learning*, Nagoya.
- Liu, G., and Guo, J. (2019). Bidirectional LSTM with attention mechanism and convolutional layer for text classification. *Neurocomputing* 337, 325–338.
- Luu, T. P., Low, K., Qu, X., Lim, H., and Hoon, K. (2014). An individual-specific gait pattern prediction model based on generalized regression neural networks. *Gait Posture* 39, 443–448. doi: 10.1016/j.gaitpost.2013.08.028
- Moon, D.-H., Kim, D., and Hong, Y.-D. (2019). Development of a single leg knee exoskeleton and sensing knee center of rotation change for intention detection. *Sensors* 19:3960. doi: 10.3390/s19183960
- Murad, A., and Pyun, J.-Y. (2017). Deep recurrent neural networks for human activity recognition. *Sensors* 17:2556. doi: 10.1038/s41467-020-15086-2
- Naghavi, N., Miller, A., and Wade, E. (2019). Towards real-time prediction of freezing of gait in patients with parkinson’s disease: addressing the class imbalance problem. *Sensors* 19:3898. doi: 10.3390/s19183898
- Nair, V., and Hinton, G. E. (2010). “Rectified linear units improve restricted boltzmann machines,” in *Proceedings of the 27th International Conference on Machine Learning (ICML-10)*. Haifa.
- Nait Aicha, A., Englebienne, G., van Schooten, K., Pijnappels, M., and Kröse, B. (2018). Deep learning to predict falls in older adults based on daily-life trunk accelerometry. *Sensors* 18:1654. doi: 10.3390/s18051654
- Ordóñez, F., and Roggen, D. (2016). Deep convolutional and lstm recurrent neural networks for multimodal wearable activity recognition. *Sensors* 16:115. doi: 10.3390/s16010115
- Park, S. H., Kim, B., Kang, C. M., Chung, C. C., and Choi, J. W. (2018). “Sequence-to-sequence prediction of vehicle trajectory via LSTM encoder-decoder architecture,” in *Proceedings of the 2018 IEEE Intelligent Vehicles Symposium (IV)* (Piscataway, NJ: IEEE).
- Pascanu, R., Mikolov, T., and Bengio, Y. (2013). “On the difficulty of training recurrent neural networks,” in *Proceedings of the International Conference on Machine Learning*, Long Beach.
- Poornima, S., and Pushpalatha, M. (2019). Prediction of rainfall using intensified lstm based recurrent neural network with weighted linear units. *Atmosphere* 10:668.
- Reddy, V., Yedavalli, P., Mohanty, S., and Nakhat, U. (2018). *Deep Air: Forecasting Air Pollution in Beijing, China*. Available online at: [https://www.ischool.berkeley.edu/sites/default/files/sproject\\_attachments/deep-air-forecasting\\_final.pdf](https://www.ischool.berkeley.edu/sites/default/files/sproject_attachments/deep-air-forecasting_final.pdf) (accessed September 12, 2019).
- Ren, L., Jones, R. K., and Howard, D. (2007). Predictive modelling of human walking over a complete gait cycle. *J. Biomech.* 40, 1567–1574. doi: 10.1016/j.jbiomech.2006.07.017
- Rubenstein, L. Z. (2006). Falls in older people: epidemiology, risk factors and strategies for prevention. *Age Ageing* 35(Suppl. 2), ii37–ii41. doi: 10.1093/ageing/af084
- Rupal, B. S., Rafique, S., Singla, A., Singla, E., Isaksson, M., and Virk, G. S. (2017). Lower-limb exoskeletons: research trends and regulatory guidelines in medical and non-medical applications. *Int. J. Adv. Robot. Syst.* 14:1729881417743554.
- Santhiranayagam, B. K., Lai, D., Shilton, A., Begg, R., and Palaniswami, M. (2011). “Regression models for estimating gait parameters using inertial sensors,” in *Proceedings of the 2011 Seventh International Conference on Intelligent Sensors, Sensor Networks and Information Processing* (Piscataway, NJ: IEEE).
- Srivastava, N., Mansimov, E., and Salakhudinov, R. (2015). Unsupervised learning of video representations using lstms. *Proceedings of the International Conference on Machine Learning*, Long Beach.
- Tanghe, K., De Groote, F., Lefeber, D., De Schutter, J., and Aertbeliën, E. (2019). “Gait trajectory and event prediction from state estimation for exoskeletons during gait,” in *Proceedings of the IEEE Transactions on Neural Systems and Rehabilitation Engineering* (Piscataway, NJ: IEEE). doi: 10.1109/TNSRE.2019.2950309
- Tao, X., and Yun, Z. (2017). Fall prediction based on biomechanics equilibrium using Kinect. *Int. J. Distrib. Sensor Netw.* 13:1550147717703257.
- Trigili, E., Grazi, L., Crea, S., Accogli, A., Carpaneto, J., Micera, S., et al. (2019). Detection of movement onset using EMG signals for upper-limb exoskeletons in reaching tasks. *J. Neuroeng. Rehabil.* 16:45. doi: 10.1186/s12984-019-0512-1
- Vallery, H., Van Asseldonk, E. H., Buss, M., and Van Der Kooij, H. (2008). Reference trajectory generation for rehabilitation robots: complementary limb motion estimation. *IEEE Trans. Neural Syst. Rehabil. Eng.* 17, 23–30. doi: 10.1109/TNSRE.2008.2008278
- Van Laerhoven, K., and Cakmakci, O. (2000). “What shall we teach our pants? Digest of papers,” in *Proceedings of the Fourth International Symposium on Wearable Computers* (Piscataway, NJ: IEEE).
- Wang, P., Low, K., and McGregor, A. (2011). “A subject-based motion generation model with adjustable walking pattern for a gait robotic trainer: NaTure-gaits,” in *Proceedings of the 2011 IEEE/RSJ International Conference on Intelligent Robots and Systems* (Piscataway, NJ: IEEE).
- Wei, W., Wu, H., and Ma, H. (2019). An autoencoder and LSTM-based traffic flow prediction method. *Sensors* 19:2946. doi: 10.3390/s19132946
- Winter, D. A. (1991). *Biomechanics and Motor Control of Human Gait: Normal, Elderly and Pathological*. Waterloo, ON: University of Waterloo Press.
- Winter, D. A. (2009). *Biomechanics and Motor Control of Human Movement*. Hoboken, NJ: John Wiley & Sons.
- Zaroug, A., Proud, J. K., Lai, D. T., Mudie, K., Billing, D., and Begg, R. (2019). “Overview of Computational Intelligence (CI) techniques for powered exoskeletons,” in *Proceedings of the Computational Intelligence in Sensor Networks*. (Berlin: Springer), 353–383.
- Zhang, J., Fiers, P., Witte, K. A., Jackson, R. W., Poggensee, K. L., Atkeson, C. G., et al. (2017). Human-in-the-loop optimization of exoskeleton assistance during walking. *Science* 356, 1280–1284. doi: 10.1126/science.aal5054
- Zhang, Y., Yang, Z., Lan, K., Liu, X., Zhang, Z., Li, P., et al. (2019). “Sleep stage classification using bidirectional lstm in wearable multi-sensor systems,” in *Proceedings of the IEEE INFOCOM 2019-IEEE Conference on Computer Communications Workshops (INFOCOM WKSHPS)* (Piscataway, NJ: IEEE).
- Zhao, A., Qi, L., Dong, J., and Yu, H. (2018). Dual channel LSTM based multi-feature extraction in gait for diagnosis of Neurodegenerative diseases. *Knowledge Based Syst.* 145, 91–97.

**Conflict of Interest:** The authors declare that the research was conducted in the absence of any commercial or financial relationships that could be construed as a potential conflict of interest.

Copyright © 2020 Zaroug, Lai, Mudie and Begg. This is an open-access article distributed under the terms of the Creative Commons Attribution License (CC BY). The use, distribution or reproduction in other forums is permitted, provided the original author(s) and the copyright owner(s) are credited and that the original publication in this journal is cited, in accordance with accepted academic practice. No use, distribution or reproduction is permitted which does not comply with these terms.

**9 APPENDIX B**  
**(PARTICIPANT**  
**FORMS)**

## CONSENT FORM

**Title** **A Machine Learning Model for the Prediction of User Gait Intention in Exoskeletons**

I, ..... give my consent to participate in the project mentioned above on the following basis:

I have had explained to me the aims of this research project, how it will be conducted and my role in it.

I understand the risks involved as described in the Participant Information Sheet.

I am cooperating in this project on condition that:

- The information I provide will be kept confidential.
- The information will be used for this project and in future related projects.
- The research results will be made available to me at my request and any published reports of this study will preserve my anonymity.

I understand that:

- There is no obligation to take part in this study.
- I am free to withdraw at any time.

I have been given a copy of the participant information sheet and consent form, signed by me and by one of the principal investigators, as listed on the information sheet, to keep.

\_\_\_\_\_ Signature of participant

\_\_\_\_\_ Name in full

\_\_\_\_\_ Date

\_\_\_\_\_ Signature of Research Investigator

\_\_\_\_\_ Name in full

\_\_\_\_\_ Date

Should you have any complaints or concerns about the manner in which this project is conducted, please do not hesitate to contact the researchers in person, or you may prefer to contact Victoria University Human Research Ethics Committee at the following address:

Ethics Secretary, Victoria University Human Research Ethics Committee,

Office for Research, Victoria University, PO Box 14428, Melbourne, VIC, 8001, email [researchethics@vu.edu.au](mailto:researchethics@vu.edu.au) or phone (03) 9919 4781 or 4461.

## PARTICIPANT INFORMATION SHEET

|                                  |   |  |
|----------------------------------|---|--|
| <b>Title</b>                     | <b>A Machine Learning Model for the Prediction of User Gait Intention in Exoskeletons</b> |  |
| <b>Principal Investigator(s)</b> | Prof. Rezaul Begg   | <a href="mailto:rezaul.begg@vu.edu.au">rezaul.begg@vu.edu.au</a><br>Ph. 0399191116                         |
|                                  | A/Prof. Daniel Lai  | <a href="mailto:daniel.lai@vu.edu.au">daniel.lai@vu.edu.au</a><br>Ph. 0399194425                           |
|                                  | Dr. Kurt Mudie  | <a href="mailto:kurt.mudie@dst.defence.gov.au">kurt.mudie@dst.defence.gov.au</a><br>Ph. 0396267642         |
| <b>Student Investigator(s)</b>   | Mr. Abdelrahman Zaroug  | <a href="mailto:abdelrahman.zaroug@live.vu.edu.au">abdelrahman.zaroug@live.vu.edu.au</a><br>Ph. 0412076074 |

This Participant Information Sheet tells you about the research project. It explains the processes involved with taking part. Knowing what is involved will help you decide if you want to take part in the research. Please read this information carefully. Ask questions about anything that you don't understand or want to know more about.

Participation in this research is entirely voluntary; there is no obligation to take part in the study, and if you choose not to participate there will be no detriment to your career or future health care.

If you decide to take part in the research project, you will be asked to sign the Consent Form. You will be given a copy of this Participant Information and Consent Form to keep.

### **Brief description of the study**

**Background:** Exoskeletons are mechanical devices that are outfitted by a user, mimics the joint's or limb's motion, anthropomorphic in nature and designed to improve user performance and reduce injury risk. However, a major challenge in current exoskeletons is the need to synchronise user intention with exoskeleton function to achieve smooth interaction between the user and device. In order to achieve good synchronisation and create smooth actuation, feedback is required along with intelligent control algorithm, known as Machine Learning (ML) algorithms.

**Aim:** The aim of this research is to develop ML algorithms for future walking event prediction using human movement data.

**Method:** Inertial Measurement Units (IMUs) in conjunction with motion tracking system and instrumented treadmill will be used to collect lower limbs biomechanical data. These data will be used to develop, train and test ML algorithms to predict key events such as heel contact and toe off during walking.

**Significance:** The fusion of ML algorithms into an exoskeleton has the potential to improve the human machine interface and user experience. A compliant exoskeleton with intelligent machine learning algorithm could allow the device to automatically adjust to the users' environment or task requirements as well as learn from errors and user interactions. These

would boost the user safety (preventing falls and injury), confidence, create a smooth interaction while wearing the exoskeleton and improve the overall performance of the exoskeleton.

### **What does participation in this research involve?**

Participation will be required in one of two studies. Both studies will have similar trials, however, data collected from both studies will be processed differently. Participants will be required to arrive at VU Biomechanics lab for testing on a date and time arranged by the research investigators. You will be asked to wear a tight fitting upper garment, shorts and comfortable shoes to allow markers visibility and to ensure normal everyday walking. Prior to testing height and mass will be measured and a screening questionnaire and consent form completed for one of the two studies.

A typical session will take approximately 2-3 hours, including marker/IMU attachment, practice trial(s), rest intervals and data collection. You will be given rest breaks between conditions. There will be familiarisation and practice trial(s).

All testing will take place in the Biomechanics laboratory PB301 at Victoria University (Footscray Park Campus).

### **Study 1/2**

**Background:** Walking trials will be performed without an exoskeleton on a force plate embedded treadmill with lower body motion recorded using IMUs and a 13 camera motion analysis system (Vicon Bonita). Vicon Bonita is a standard three dimensional (3D) motion capture camera system that utilizes retroreflective passive markers to be tracked in a 3D space. The IMUs will be tracking the orientation and acceleration of the feet, shanks, thighs and trunk. The IMU devices utilize a built-in and battery powered accelerometer, gyrometer and magnetometer sensors. Data from IMUs will be synchronized and transmitted with Vicon cameras using built-in low energy Bluetooth.

**Experiment setup:** Markers will be placed laterally on four different body segments including feet (3 markers), shanks (3 markers left/4 markers right), thighs (4 markers right/5 markers left) and trunk or upper back (3 markers). Each group of markers (cluster) that represent a body segment will be placed on a rubber pad attached to the skin (only for thighs and shanks) using double sided tape. Upper back clusters will be attached to the upper body garment. The IMUs will be placed at the same sites as the markers using the company (IMeasureYou) supplied velcro straps.

**Testing protocols:** You will be required to complete 5 minutes of walking on an instrumented treadmill (AMTI) at three speeds as follows;

- a) Preferred speed (Normal).
- b) 10% faster than preferred (Fast).
- c) 10% slower than preferred (Slow).

### **Benefits**

No direct benefits to the participant are expected from participation. However, participants may receive an educational benefit from being exposed to the scientific experimental research process.

### **Risks of participating**

There are risks associated with participation but a range of safeguards have been put in place to minimize these risks:

1. Risk of physical injury during testing activities:
  - Participants will be healthy with no current injury, and the skills necessary to complete the tasks in a competent manner.

- The level of physical exertion will be no greater than that normally encountered during trade training or exercises.
  - Participants will be excluded from the study if they possess a pre-existing injury that is likely to place them at an unacceptable degree of injury risk as a result of participation in the study.
  - In the event that a participant is injured during the study, they will be afforded the standard level of care. This includes calling a medical practitioner or ambulance using the telephone in the laboratory and the Western Hospital is a short distance away. The participant will also be advised to see a medical practitioner for assessment.
  - Only those participants deemed acceptably low risk will be accepted into the study. All risks will be minimised by following standard exercise laboratory procedures.
  - All exercise testing procedures will be attended by the student research investigator and the exercise protocol will involve only low intensity exercise (walking), thus considerably reducing the potential risks.
2. The equipment used for data collection may harm the participant:
    - All equipment used to collect data from the participant will involve non-invasive measurement techniques and thus any risk of injury are very unlikely.
  3. Usability and acceptability:
    - Usability and acceptability of data will be agreed upon through consent form.
  4. Use of data and privacy:
    - All data will be de-identified and treated as confidential and only made available to members of the research team on a need to know basis. Information linking participant names to participant codes will only be accessed by the research investigators. This information will be destroyed after 5 years in accordance with Australian Code for the Responsible Conduct of Research.

### **Withdrawal from the research**

You will be provided a 24 hour cooling off period after providing consent and if you no longer wish to continue, you are free to notify the research team that you wish to withdraw. You may do this at any time during the study without any detriment to your career or future health care. Your individual data will also be removed from further analysis if you choose to withdraw, however, if you participate through to completion your de-identified data will be retained for further analysis.

### **Privacy and confidentiality**

The lab space (PB301) will be closed during testing and will only be accessible to researchers involved. No images or videos of participants will be collected, and it is not possible to identify a participant from the 3D marker recordings. Participants will have the freedom to choose the gender of the person attaching the markers/IMUs. An experienced female researcher (Mrs: Jasmine Proud) will be available to assist with marker/IMUs placement.

To make sure your privacy is maintained all data will be de-identified and treated as confidential. Your data will only be available to members of the research team on a need to know basis. Information linking your name to your code will only be accessed by the above investigators. This information will be destroyed after 5 years from the publication of reports arising from the study, in accordance with Australian Code for the Responsible Conduct of Research.

**Other relevant human research ethics considerations**

This project will be carried out according to the National Statement on Ethical Conduct in Human Research (2007). This statement has been developed to protect the interests of people who agree to participate in human research studies.

**Dissemination of research findings**

The results of this research will be reported through conference presentations and open literature publications. In any publication and/or presentation, information will be provided in such a way that you cannot be identified, except with your permission. Only de-identified and/or group data and statistical summaries will be presented in publicly released reports. If you wish to access your individual data you will be provided with a copy on request.

**Who is organising and funding this research?**

This research program is conducted by the Program in Assistive Technology Innovation (PATI) funded by Victoria University and DSTGroup. PATI is a collaboration between Defence Science and Technology (DSTGroup), Victoria University and The University of Melbourne, a partnership recognised as the leading resource for research and expertise on skin-out devices which enhance mobility by reducing and transferring mechanical load and/or reducing physiological work rate.

No member of the research team will receive a financial benefit from your involvement in this project.

**Concerns or complaints**

Should you have any complaints or concerns about the manner in which this project is conducted, please do not hesitate to contact either the researchers (see first page) or the Victoria University Human Research Ethics Committee at the following address:

Ethics Secretary, Victoria University Human Research Ethics Committee, Office for Research, Victoria University, PO Box 14428, Melbourne, VIC, 8001, email [researchethics@vu.edu.au](mailto:researchethics@vu.edu.au) or phone (03) 9919 4781 or 4461.

# ADULT PRE-EXERCISE SCREENING TOOL

This screening tool does not provide advice on a particular matter, nor does it substitute for advice from an appropriately qualified medical professional. No warranty of safety should result from its use. The screening system in no way guarantees against injury or death. No responsibility or liability whatsoever can be accepted by Exercise and Sports Science Australia, Fitness Australia or Sports Medicine Australia for any loss, damage or injury that may arise from any person acting on any statement or information contained in this tool.

Name: \_\_\_\_\_

Date of Birth: \_\_\_\_\_ Male  Female  Date: \_\_\_\_\_

## STAGE 1 (COMPULSORY)

AIM: to identify those individuals with a known disease, or signs or symptoms of disease, who may be at a higher risk of an adverse event during physical activity/exercise. This stage is self administered and self evaluated.

Please circle response

|    |  |     |    |
|----|--|-----|----|
| 1. | Has your doctor ever told you that you have a heart condition or have you ever suffered a stroke?  | Yes | No |
| 2. | Do you ever experience unexplained pains in your chest at rest or during physical activity/exercise?   | Yes | No |
| 3. | Do you ever feel faint or have spells of dizziness during physical activity/exercise that causes you to lose balance?                                | Yes | No |
| 4. | Have you had an asthma attack requiring immediate medical attention at any time over the last 12 months?   | Yes | No |
| 5. | If you have diabetes (type I or type II) have you had trouble controlling your blood glucose in the last 3 months?                                   | Yes | No |
| 6. | Do you have any diagnosed muscle, bone or joint problems that you have been told could be made worse by participating in physical activity/exercise? | Yes | No |
| 7. | Do you have any other medical condition(s) that may make it dangerous for you to participate in physical activity/exercise?                          | Yes | No |

IF YOU ANSWERED 'YES' to any of the 7 questions, please seek guidance from your GP or appropriate allied health professional prior to undertaking physical activity/exercise

IF YOU ANSWERED 'NO' to all of the 7 questions, and you have no other concerns about your health, you may proceed to undertake light-moderate intensity physical activity/exercise

I believe that to the best of my knowledge, all of the information I have supplied within this tool is correct.

Signature \_\_\_\_\_ Date \_\_\_\_\_